UNIVERSIDAD DE CALDAS
FACULTY OF EXACT AND NATURAL SCIENCES
MASTER IN EARTH SCIENCES

Structural architecture of Buriticá gold deposit, Colombia - insights from hydrothermal alteration geochemistry and implications for regional exploration.

Marcelo Arango Trujillo

Manizales, Colombia

March, 2023

Structural architecture of Buriticá gold deposit, Colombia - insights from hydrothermal alteration geochemistry and implications for regional exploration.

Marcelo Arango Trujillo

A thesis submitted in partial fulfillment of
the requirements for the degree of:
Master in Earth Sciences

Director:
M.Sc. Andrés Naranjo Sierra

Codirector:
Ph.D. Brett K. Davis

Universidad de Caldas
Faculty of Exact and Natural Sciences
Master in Earth Sciences
Manizales, Colombia
2023

Dedicatory

This work is dedicated to my daughter Penélope

who has been and will be the biggest

reason to keep forward.

Acknowledgments

First, I’d like to express sincere acknowledgements to Carlos Rios and Andrés Naranjo for giving me the opportunity to improve my passionate skills for structural geology during the time exploring Buriticá deposit and even nowadays in the industry.

The project’s supervision by Brett Davis and Andrés Naranjo is much appreciated, for all the long online meetings, field visits, advice throughout the different courses of the program, perfecting my writing abilities and enhance the document. These guys are humble human beings who share the same passion for knowledge sharing and rocks in general.

Additionally, thanks to Zijin-Continental Gold for allowing me to perform this study and for providing me support with the information, time and expenses that this research required. To all the exploration and mine geology colleagues who helped me with information, logistics and contributions to the manuscript. Special thanks to Leo Luo, Luz Tamayo, Cristian Ruiz, Pilar Zuluaga, Sonia Gonzalez, Jorge Pelaez, Diego Henao, Paola Corredor, Jhonatan Giraldo, Carolina Perez, Carolina Osorio and all the local field collaborators who helped me guide in the steep mountains and carry rock samples.

Finally, thanks to Richard M. Tosdal and Cesar García for the detailed review, feedback and improvement of this thesis.

Note

" Last but not least, I wanna thank me

I wanna thank me for believing in me

I wanna thank me for doing all this hard work

I wanna thank me for having no days off

I wanna thank me for, for never quitting

I wanna thank me for always being a giver

And tryna give more than I receive

I wanna thank me for tryna do more right than wrong

I wanna thank me for just being me at all times "

- *Snoop Dogg*

Abstract

The development of hydrothermal ore systems is strongly influenced by deformation within brittle and ductile regimes. Localization of mineralization is ruled by permeability enhancement processes and structural architecture that involves fault damage zones, fault intersections, stress field orientations and magnitudes, fluid pressure, and host-rock properties. Constant permeability generation favors multiple fluid flux injections and enrichment of the mineralized systems, and is particularly efficient in deep penetrative fault-related pathways.

The work presented here aimed to define the structural and geological framework of the Buriticá gold deposit in Colombia, through assessment of gold grade controls, distribution of host-rock units and gold pathfinders, vein and alteration development, and the geometric and overprinting relationships of veins with non-mineralized structures and intrusive events.

The review of deposit-scale geochemical datasets has been essential to resolving the 3D distribution of elements and alteration assemblages. In combination with documentation of host-rock structures and overprinting relationships, this has been a critical element to establishing the structurally-controlled permeability network responsible for development of the Buriticá hydrothermal system.

Finally, the work aimed to determine the deposit-scale geological history and provide guidance on the implications for exploration procedures. The approach has been accomplished by using techniques that included logging and sampling, surface and underground mapping, petrography of host-rocks and veins, lithogeochemistry classifications, XRD, geochronology and 3-D modelling.

The Buriticá gold deposit is a fault-controlled hydrothermal ore system, bounded by long-lived penetrative faults that provided permeable channels for fluid flux and multiple vein-fill stages. At the orebody- and deposit-scale, mineralized structures developed as fault-hosted extension veins with subsequent shearing. The sericite halo alteration assemblage controls the Au grade distribution in Yaraguá and Veta Sur mineralized systems and host-rocks, overprinting early-formed and typical hydrothermal alteration assemblages of a porphyry Cu deposit. Lithogeochemical assessment has identified the calc-alkaline affinity of the Buriticá

Intrusive Complex (BIC), as well as the direct relationship between Au grade and sericite alteration intensity. Geochronology results place the BIC within the Miocene-aged Middle Cauca belt, reporting an U-Pb age on zircon of 7.7 ± 0.1 Ma. The accommodation of strain in fault damage zones, mineralized and non-mineralized structure intersections, and formation of dilation zones such jogs and second-order extension veins, were key for development of high Au grade volumes.

Keywords: (Buriticá, permeability, gold, fault control, Middle Cauca belt, Colombia).

Table of Contents

List of figures

List of tables

List of abbreviations

Abbreviation	Description
°C	Degree Celsius
Å	Ångström
Au	Gold
BIC	Buriticá Intrusive Complex
BMZ	Broad Mineralized Zone
BSE	Backscatter electron
CAB	Calc-alkaline Basalt
Cb	Carbonate
CBM	Carbonate Base Metal
CCOP	Colombian-Caribbean Ocean Plateau
Chl	Chlorite
CL	Cathodoluminescence
Cpy	Chalcopyrite
CTN	Centena vein
E-MORB	Enriched Mid-Ocean Ridge Basalt
Eq	Equivalent
EQ	Epithermal quartz
g	Gram
GA	Gallery
Gn	Galena
Hb	Hornblende
IAT	Island Arc Tholeiite
ICDD	International Centre for Diffraction Data
ICP-AES	Inductively Coupled Plasma Atomic Emission Spectroscopy
ICP-MS	Inductively Coupled Plasma Mass Spectrometry
km	Kilometer
LPM	Low-grade porphyry mineralization
m	Meter
m.a.s.l	Meters above sea level
Ma	Million years
mL	Milliliter
Moz	Million ounces
MSWD	Mean Square Weighted Deviation
MU	Murcielagos vein
nm	Nanometer
N-MORB	Normal Mid-Ocean Ridge Basalt
OIA	Oceanic Island Alkali Basalt
OIT	Oceanic Island Tholeiite
ORG	Ocean Ridge Granite

Abbreviation	Description
PCI	Poor crystallized illite
Plg	Plagioclase
PLOCO	Provincia Litósferica Oceánica Occidental
Po	Pyrrhotite
ppm	Parts per million
Px	Pyroxene
Py	Pyrite
QS	Quartz-sulphide
Qz	Quartz
RL	Real level
SA	San Antonio vein
Sec Bt	Secondary biotite
Ser	Sericite
SJU	San José de Urama
Sph	Sphalerite
Stb	Stibnite
Syn-COLG	Syn-Collision Granites
UTM	Universal Transverse Mercator
VAG	Volcanic Arc granites
VS	Veta Sur
WGS	World Geodetic System
WPG	Within-Plate Granites
WPI	Well crystallized illite
wt.%	Weight percent
XRD	X-ray diffraction
YR	Yaraguá
ZJCNL	Zijin Continental Gold
μm	Micrometer
σ1/σ2/σ3	Sigma 1/Sigma 2/Sigma 3 = Principal structural stresses

1. Introduction

Gold mining in Colombia has been ongoing since the pre-Colombian era before the Spanish Conquest (Rodriguez & Warden, 1993). Currently, gold deposits in Colombia have been categorized into several types, including porphyry Cu-Au, porphyry Au, transitional porphyry-epithermal Cu-Au, orogenic Au, and placer Au (Sillitoe et al., 1982; Sillitoe, 2008). Many of these deposits are linked to Miocene and Pliocene magmatism derived from the subduction of the Nazca plate beneath the South American plate (Cediel et al., 2003; Stern, 2004). The country-scale trend of these Miocene-aged rocks extends throughout the Colombian Andes, from the southern part comprising the Piedrancha Batholith and Cuembí Stock, to the northern portion with the Vetas – California plutonic units. Distribution of these igneous bodies is mainly in the eastern flank of Western Cordillera and western flank of Central Cordillera, always being proximal to the strong N-S structurally controlled Cauca basin. In addition, isolated Miocene and Pliocene plutons are found within Central Cordillera, Santander Massif and Quetame Massif in Eastern Cordillera (Leal-Mejía, 2011). Petrochemical data and U-Pb (zircon) ages for intrusions and coeval volcanic rocks from the Western and Central Cordilleras define a calk-alkaline affinity, metaluminous (I-type) and medium-to high-K, further demonstrating that these clusters are limited arc segments that migrated in time and space, from south to north and west to east (Leal-Mejía, 2011).

The Buriticá gold deposit is one of the most important representations of gold mineralization along the Miocene metallogenic Middle Cauca belt. It is located in Buriticá town, 90 km from Medellin city, Colombia (Figure 1). Buriticá gold deposit was first owned by Continental Gold in 2007, being subsequently 100 % acquired by Zijin Mining Group in 2020. A total of 356.053 m of assayed drill core and 9.294 m of underground samples have then allowed the estimation of indicated and inferred resources of 16.02 Mt at 11 g/t AuEq (5.67 Moz) and 21.87 Mt at 9.2 g/t AuEq (6.46 Moz), respectively (ZJCNL internal report, 2021).

Previous geological work at Buriticá gold deposit has played a significant role in influencing the current research project. The Buriticá gold deposit has been considered as a low- to intermediate-sulphidation epithermal gold deposit, hosted by the 7.41 ± 0.40 Ma ($^{40}Ar/^{39}Ar$ on hornblende) (Lesage, 2011) aged Buriticá andesite porphyry that has intruded the Cretaceous Cañasgordas Group (Alvarez, 1971). Gold mineralization related with proximal sericite-adularia and propylitic alterations, has been dated at 7.74 ± 0.08 Ma ($^{40}Ar/^{39}Ar$ on sericite) (Lesage, 2011). Also, fluid inclusion and sulfur isotope data showed a magmatic origin, which was a mix between a hot (>300°C) and saline fluid (average 5.5 wt.% NaCl equiv.) with a cool (250°C) and less saline meteoric fluid (average 3.6 wt.% NaCl equiv.) (Lesage, 2011). Additionally, another study by Aerne & Kretz (2014) differentiated two phases and trends of magma intrusions and documented the gold-fertility and magmatic-hydrothermal fluid genesis that were crucial to the mineralization. Fluid inclusion analysis in defined mineralization stages indicated temperature ranges of 315 – 380 °C for pre-ore, 270 – 330 °C for stage 1-ore (pyrite, chalcopyrite, galena, tetrahedrite, sphalerite, gold, silver and quartz), and 250 – 330 °C for stage 2-ore (pyrite, sphalerite, gold and quartz). The main processes considered critical for Au precipitation were boiling and fluid desulphidation from magmatic derived gold-bearing fluids with variable pressure conditions (Aerne & Kretz, 2014). Since these previous studies, substantial new data and exposures have become available, which provide important sources for advancing the understanding of Buriticá deposit. A logical outcome of the current project is the refinement of parameters used for exploration at the district- and regional-scale.

Due to the proximity of Buriticá to the Cauca-Romeral fault system in the eastern flank of Western Cordillera, a structural geological control to deposit formation and architecture is evident at the deposit-scale. This is dominantly a product of the major faults playing roles as deposit-scale flow pathways for mineralizing fluids, and as sites of deposition and accumulation of mineralization (Cowan, 2020). These structures include the Tonusco Fault (Álvarez & González, 1978 and González, 2001), the Diatrema Fault and the Sierra Fault (named in this work), which have predominantly N strikes with dextral movements, which is consistent with the kinematics of the Cauca-Romeral Fault System (Ego et al., 1995). The geologic units in the area are mostly represented by Cretaceous volcanic, sedimentary, and intrusive rocks, formed by, and in, active mantle plumes in the oceans as well as island arcs (Kerr et al., 2003; Greene et al., 2010), which were later accreted into the continental margin (White et al., 2003; Whattam & Stern, 2015).

The western Veta Sur and eastern Yaraguá fault-vein systems are the most important mineralized volumes at Buriticá. These structures are nearly vertical, striking 50° – 70° and 85° – 95° for Veta Sur and Yaraguá systems, respectively. The Veta Sur system is hosted in basalts, volcanic breccias and mudstones (Barroso Formation), while the Yaraguá system is hosted in diorites, and intrusive and magmatic/hydrothermal breccias; it is in this system where the Buriticá Intrusive Complex (BIC) hosts mineralization.

This study focuses on the definition of the structural setting of the Buriticá gold deposit and on the key controlling factors that define the tectonic and magmatic evolution of the host rocks. Parameters related to mineralogy, alteration, geochemistry, lithology, faults, precious metal distribution, deposit-scale alteration and geochemical distributions, data from assayed drill cores, underground/surface sampling and mapping, airborne geophysics and geochronological data were incorporated to propose alteration and structural 3D models of the Buriticá gold deposit. Furthermore, this study identifies and addresses controls on mineralization styles, gold grade control in the main mineralized structures, principal fluid-flow pathways, gold pathfinders, brittle and ductile deformation relationships, and fault architecture at the deposit-scale. Ultimately, the information gained from the above research results provide insights into the structural, hydrothermal, and magmatic setting of Buriticá gold deposit. In turn, this supplies an approach for regional exploration and vectoring to porphyry-epithermal gold deposits in the Buriticá mining district, as well as the metal-rich Miocene metallogenic middle Cauca belt.

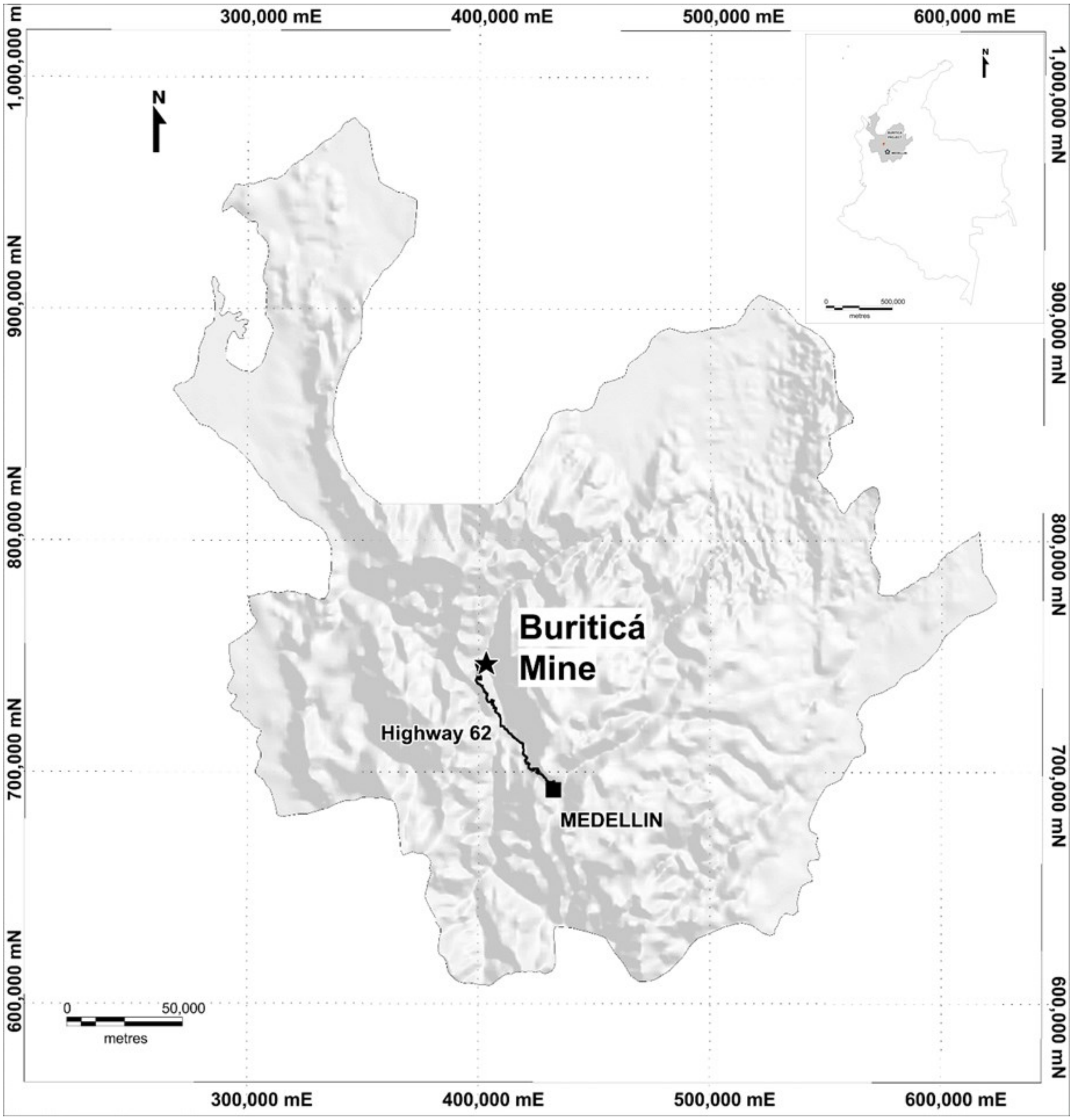

Figure 1. Location map of Buriticá gold deposit in Antioquia department. WGS 84 18 N projection.

1.1. Objectives

1.1.1. General

To define the structural architecture of Buriticá gold deposit, Colombia.

1.1.2. Specific

- To generate a detailed structural geological framework of Buriticá gold deposit and a 3D model of permeability pathways through incorporation of geochemistry with fault architecture.

- To establish a geological history of Buriticá that incorporates structural evolution, fluid migration, vein development, and intrusive episodes that are consistent with geochronological data and with the individual geological histories of significant veins.

- To record gold pathfinders related to Buriticá deposit and to make an informed classification of the deposit style for Buriticá. In addition, to develop a roadmap for pragmatic ongoing exploration in Colombia.

- To establish a geological history for several principal veins including review of highly mineralized veins (e.g., Yaraguá, Veta Sur) and veins lacking mineralization, and incorporate geochronology into the vein history.

- To establish overprinting and geometric relationship between 1st, 2nd and 3rd order fault structures, including assessment of roles played by host lithologies and ductile structures, and to define the disposition of geologic units that are consistent with structural architecture.

- To identify ductile structures and assess their roles with relation to fault development and permeability and definition of particular controls for gold grade through detailed study of key veins.

2. Geological Framework

In Colombia, the Northern Andean block comprises three major mountain ranges: Western, Central and Eastern cordilleras. The Western Cordillera was formed during consecutive oceanic terrane accretions, while the Central and Eastern Cordilleras are composed of Precambrian and Paleozoic continental units that are covered by sedimentary rocks (Toussaint & Restrepo, 1989). The Buriticá gold deposit is located in the eastern flank of Western cordillera and is hosted within the Cañasgordas terrane, west of a major fault known as the Cauca-Romeral Fault System. Its general origin is associated with Late Miocene arc-magmatism (Andesita de Buriticá) along the Middle Cauca Belt, in turn related to the subduction of the Nazca plate under the South American plate (Figure 3).

2.1. Regional Geology-Tectonic Evolution

Colombian Western Cordillera has a complex history of collision, accretion, faulting, magmatism, and subduction (Cediel, et al., 1983; Toussaint & Restrepo, 1988; Kerr et al., 1997; Cediel et al., 2003; Kennan & Pindell, 2009; Shaw, Leal-Mejía & Melgarejo, 2019). The Western Andean Territory (TAOC in Spanish) was defined by Toussaint & Restrepo (1988) as extending from the thrust fault suture to the east (Romeral Fault System) westwards to the Dabeiba Suture (Figure 2). Mafic and ultramafic igneous rocks associated with marine sediments, and low-medium grade metamorphic rocks, are found on the eastern limit of Western Cordillera and have been divided into the Dagua Group for the southernmost units, Diabasic Group for the center zone and Cañasgordas Group to the north zone. Western Colombian geology comprises large-scale groups of units bounded, and in contact, by faults, known as terranes (Figure 2). The Calima and Cuna terranes principally make up the Western Cordillera, and are products of the following history of accretion: the Calima oceanic terrane accreted to the Tahami terrane during the Early Cretaceous; these two terranes were then accreted to the Chibcha terrane (Central Cordillera) in the Late Cretaceous to Paleocene (Figure 2); The Cuna terrane was subsequently accreted to the Calima terrane in the Miocene, producing the current morphology of the Colombian Andes (Toussaint & Restrepo, 1990).

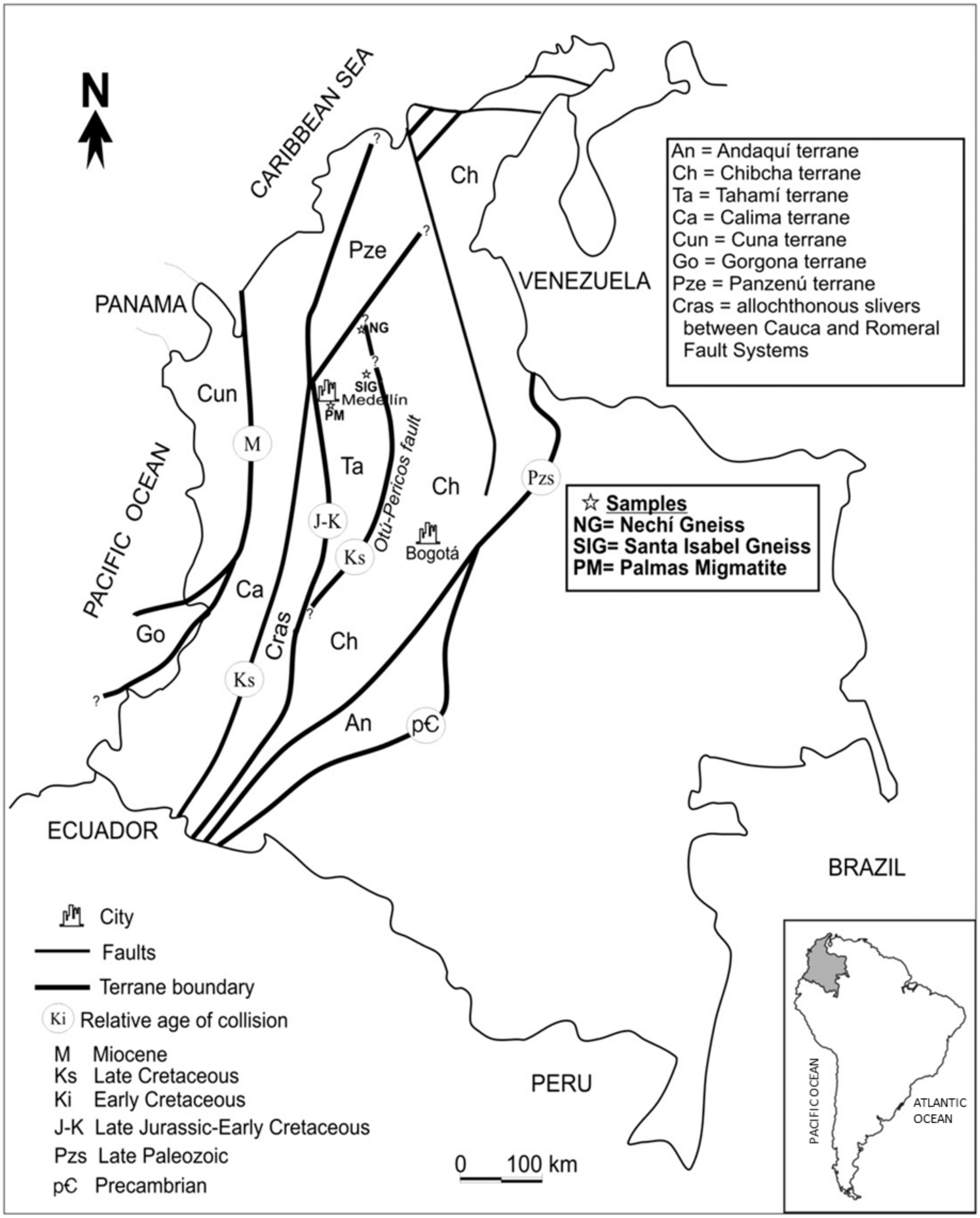

Figure 2. Terranes of Colombia. Modified from Restrepo et al. (2011) after Restrepo & Toussaint (1988) and Ordóñez-Carmona & Pimentel (2002).

The Western Cordillera comprises mainly Late Jurassic to Cretaceous age volcanic rocks with oceanic affinity (Vinasco, 2019). They were formed from either an oceanic plateau or islands arcs associated with a plume (Nivia, 1996; Villagómez et al., 2011; Guiral-Vega, et al., 2015; Spikings et al., 2015), which migrated eastwards until colliding with the South American plate in the Late Cretaceous (Spikings, 2015). It has been suggested that sections of these allochthonous terranes have been accreted, obducted and subducted in the northwest of the South American continental margin. Several names have been given to these terranes by various authors, including:

- Calima Terrane (Toussaint & Restrepo, 1988).
- Western Cretaceous Oceanic Lithospheric Province, PLOCO in Spanish (Nivia, 1996).
- Colombian-Caribbean Ocean Plateau, CCOP (Kerr, et al. 1997).
- Western Cordillera Complex (Moreno-Sanchez & Pardo-Trujillo, 2003).
- Caribe Terrane (Gómez Tapias et al., 2017).

The basement is composed of 1) mafic to ultramafic plutonic rocks intercalated with mafic volcanic rocks and marine sediments (the Barroso Formation; Weber et al., 2015), and 2) meta-sedimentary rocks covering part of the basement grouped in the Penderisco Formation (Álvarez & González, 1978).

Several works have concluded that the Western Cordillera has a Cretaceous oceanic basement, based on marine fossils that yielded Middle Albian to Coniacian age (Etayo, 1980; Geoestudios, 2005). Additional support for the contention of Cretaceous basement by other authors and techniques is given in Table 1.

Rock units of Buriticá and rock units of the Western Cordillera, including those at Buriticá, have been incorporated into the Cañasgordas and Dagua zones. The Buriticá terrane is located to the north and is bounded to the NE by the Montelibano Fault, to the SE by the Romeral Fault, to the SW by the Dabeiba Fault and to the NW by the Sinú lineament (Figure 2). This regional structural architecture suggests an accretion process on the northwestern margin of South America from the Middle Albian to the Maastrichtian (Etayo et al., 1983).

Following the accretion process, the Barroso-Sabanalarga magmatic arc was formed (Rodríguez & Zapata, 2014) as a consequence of the subduction of the Farallones plate with east vergence beneath the South American plate. This led to magmatism with tholeiitic to calk-alkaline characteristics (Rodríguez & Arango, 2013), resulting in tonalitic rock bodies of 100.9 ± 0.85 Ma (Buriticá tonalite, Weber et al., 2015) up to 91.1 ± Ma 6.4 (Santa Fe Batholith/Sabanalarga Batholith, Göebel & Stibane, 1979) (Table 1).

The current named Western Cordillera basement collided and was accreted through different terranes and times from the Late Cretaceous to Cenozoic, along the Cauca-Romeral Fault System. The latter played the role of suture and was formed in the Permian – Triassic during Pangea's rupture characterized by several phases before and during the Andean Orogeny. Currently, the fault system is defined by dextral, oblique, and reverse faults, and represents most of the contacts between the continental and oceanic basements. There are also mylonitized shear zones that have deformed Cretaceous aged units, including meta-sedimentary, volcanic-sedimentary rock, and ultramafic rocks (Vinasco, 2019).

Uplift of the Central Cordillera began in the Paleocene, thus sourcing sediments for accumulation in the Western Cordillera during the Eocene. In the Oligocene, the Andean Orogeny commenced while the uplift process of the Central Cordillera continued. At the same time, the uplift of the Western Cordillera was coeval with the Panama-Chocó Block accretion, which reactivated the Cauca-Romeral Fault System (Kerr et al., 1997; Vinasco, 2019; Zapata & Rodríguez, 2020). Adjustment of the plates occurred in the Late Miocene, as the Farallones Plate rift developed and the Cocos and Nazca Plates were formed, resulting in arc volcanism (Combia Formation) and hypo-abyssal porphyritic intrusions bodies throughout the Colombian Pacific margin (Toussaint & Restrepo, 1987; Taboada et al., 2000; Marín-Cerón et al, 2019). Magmatism may have started in a west position at 13 Ma and migrated eastwards in the Middle Miocene (León et al., 2019). According to Leal, Shaw and Melgarejo (2019) these porphyritic bodies can be grouped into six (6) segments according to their ages and spatial distribution: Piedrancha-Cuembí, Cauca-Patía Alto, Farallones-El Cerro, Middle Cauca (Buriticá, 7.41 ± 0.4 Ma; Marmato, 6.58 ± 0.07 Ma; Nuevo Chaquiro, 10.9 ± 0.2 Ma), Cajamarca-Salento (Colosa, 7.4 ± 0.2 Ma) and Río Dulce. (Figure 3).

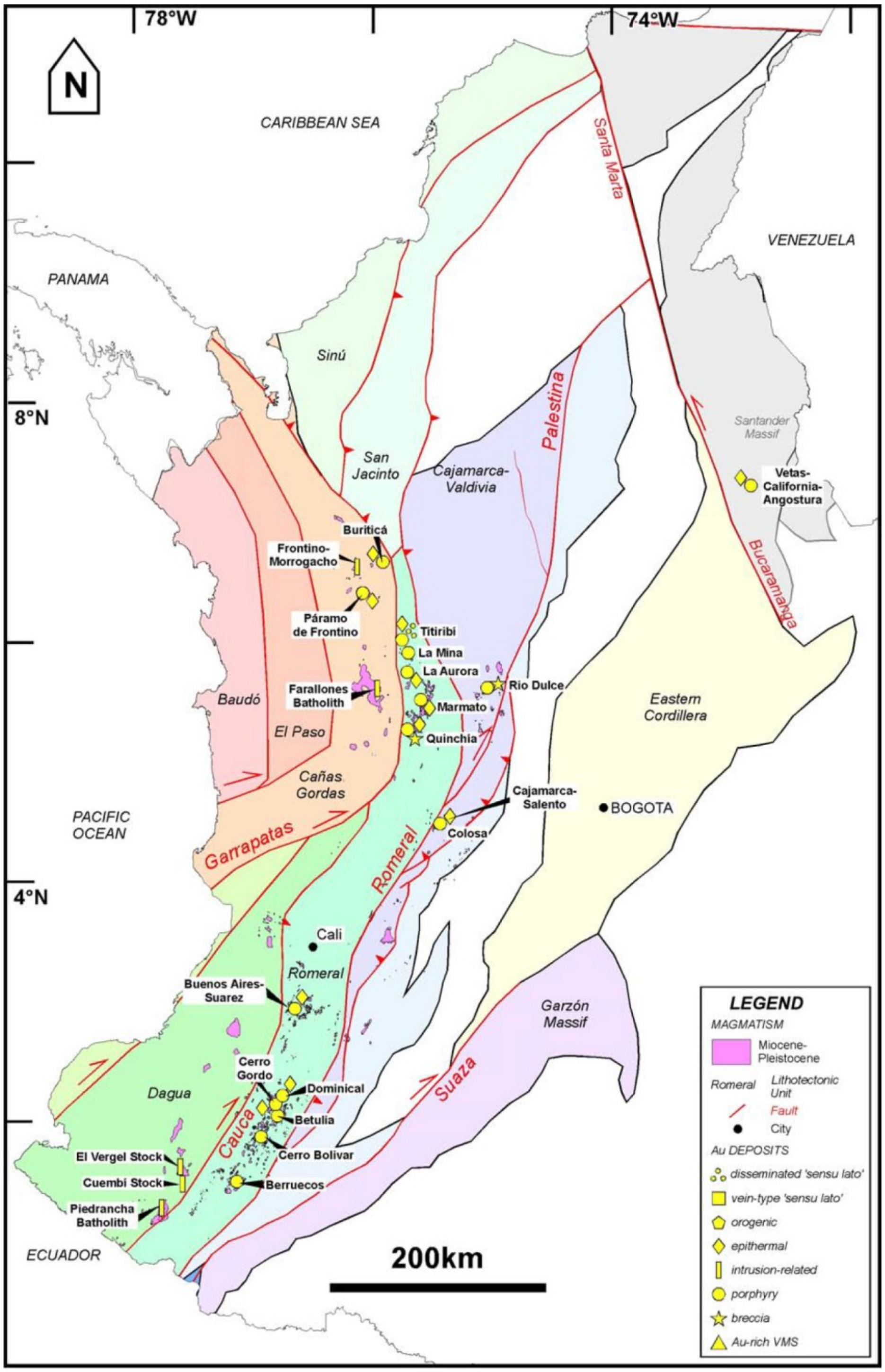

Figure 3. Miocene to Pleistocene magmatism, terranes and gold occurrences in the Colombian Andes. Taken from Cediel et al. (2003) and adapted from Leal-Mejía (2011).

Table 1. Age constraints summary compilation of rock formations in the Buriticá zone.

Unit	Age	Method	Localization	Author	Comments
BIC[1]	7.44 ± 0.075 Ma	U-Pb		Correa et al., 2018	Magmatism
BIC	7.41 ± 0.40 Ma	Ar-Ar		Lesage, 2011	Magmatism
BIC	7.74 ± 0.08 Ma	Ar-Ar		Lesage, 2011	Hydrothermal Alteration
BIC	11.8 ± 1.1 Ma	K-Ar		Leal, 2011	Magmatism
Buriticá Tonalite	91.1 ± 6.4 Ma	K-Ar		Göbel and Stibane, 1979	
Buriticá Tonalite	100.9 ± 0.85 Ma	U-Pb		Weber et al., 2015	
Santa Fe Batholith	92 ± 2 Ma	Ar-Ar	Peñitas Pinguro	Vinasco, 2001	
Santa Fe Batholith	98 ± 9.1 Ma	Sm-Nd		Weber, 2011	
Santa Fe Batholith	81.66 ± 0.65 Ma	U-Pb		Correa et al., 2018	
Sabanalarga Batholith	97 ± 10 Ma	K-Ar	West flank of Central Cordillera	González, Restrepo, Toussaint and Linares, 1978	
Sabanalarga Batholith	98 ± 3.5 Ma	K-Ar	Liborina-Sabanalarga	González & Londoño, 1998	
Barroso Formation	84.2 ± 1.4 Ma	Ar-Ar		Geoestudios, 2005	
Barroso Formation	92 Ma	K-Ar		Toussaint & Restrepo, 1976	Hornblende in gabbro

[1] BIC: Buriticá Intrusive Complex

Unit	Age	Method	Localization	Author	Comments
Barroso Formation	105 ± 10 Ma	K-Ar	1.138.680 1.155.395	Toussaint & Restrepo, 1978	Eastern outcrops of Barroso Fm
Barroso Formation	Upper Campanian	Fossils		Correa et al., 2018	*Nostoceras cf. Pauper*
	Campanian - Maastrichtian			Geoestudios, 2005	*Globigerinella escheri Rugoglobigerina sp.*
	Turonian-Coniacian			Mejía, 1984	Radiolaria
	Aptian – Albian			Etayo, 1980	*Ptychoceras sp. Metahamites sp.*
Diabasas de San José de Urama	155.1 ± 11.2 Ma	Ar-Ar		Rodríguez & Arango, 2012	

2.2. Local Geology

The local geology framework of the Buriticá gold deposit has been refined through detailed mapping and logging during exploration campaigns by Zijin-Continental Gold as well as through ongoing mine operations by the same company. Buriticá vein systems are hosted primarily in the Barroso Formation to the west and the Buriticá Intrusive Complex (BIC) to the east, both units with an important deformation related to faults including the Tonusco, Diatrema, Sierra, West and La Mina faults. Relatively larger volumes of igneous rock units are also exposed in the area, represented by the Sabanalarga and Santa Fe Batholiths, and the Buriticá Tonalite (Nivia & Gómez 2005).

2.2.1 Composition

The Barroso Formation represents one of the oldest rocks surrounding Buriticá, comprising intercalated sedimentary and volcanic rocks that belong to the Cañasgordas Group (Álvarez, 1971). The volcanic rocks are basalts, hyaloclastites, andesites, tuffs and breccias with textural variations from aphanitic to porphyritic. (Álvarez, 1983; Mejia, 1984; Rodríguez &

Arango, 2013). Sea-floor alteration of primary mafic minerals is common throughout the entire volcanic unit and is related mostly to epidote, quartz and/or calcite veining, and zeolites that fill vesicles. Mineralization is characterized by pyrrhotite, and lesser pyrite and chalcopyrite.

The sedimentary rocks of the Barroso Formation comprise intercalations of black mudstones, graywackes, siliceous limestones and fine conglomerates. These are commonly found in concordant contact with the volcanic units and display lenticular/boudinage shapes in the contact planes. Sedimentary rocks are generally dark brown to black colored with intense fracturing and covered on the surface by thin crusts of calcite-pyrite (Álvarez & González, 1978). These rocks are made up of amorphous silica with organic matter and iron oxides; the presence of calcite veins is common (Álvarez & González, 1978). The eastern limit of this unit is the Sabanalarga Fault, a component of the Cauca-Romeral Fault System (Figure 6). To the west of this unit and at deposit-scale, the Sierra Fault acted as a control for magmatic-hydrothermal breccia development and deformation of both sedimentary and volcanic rocks (Figure 4). The sedimentary package of the Barroso Formation is formally named the Penderisco Formation, with two members, the Nutibara and Urrao members (Álvarez, 1983). These have organic beds in which fossil fragments were found and yielded ages of Aptian – Albian (Etayo, 1980), Turonian – Coniacian (Mejía, 1984), Campanian – Maastrichtian (Feininger & Castro, 1972; Moreno & Pardo, 2003), and Upper Campanian (Correa et al., 2018), indicating that the beginning of the deposition and volcanism of the Barroso – Sabanalarga arc occurred in the Early Cretaceous.

The Buriticá Intrusive Complex (BIC) defines a set of intrusive pulses and covers an area of 2.5 km^2, truncated to the east by the steep Tonusco Fault (Figure 4), while the contact to the west with the Barroso Formation and the Buriticá Tonalite is intrusive (Mejía, 1984). Furthermore, the Diatrema Fault developed high-strain deformed zones through this unit as well. The rocks are represented by dioritic to basaltic compositions with porphyritic textures, phenocrysts of plagioclase, hornblende, augite and biotite. Locally, the rocks display equigranular and fine-grained textures with small mafic xenoliths (Lesage, 2011; Correa et al., 2018).

The plug-shaped BIC has been dated at 7.41 ± 0.40 Ma by $^{40}Ar/^{39}Ar$ on hornblende (Lesage, 2011) and 7.44 ± 0.075 Ma by U-Pb on zircons (Correa et al., 2018), and represents the eastern host lithology to the Yaraguá System specifically (Figure 4). It is a body located between the town of Buriticá and the Pinguro village, named as Buriticá Andesite (Álvarez & González, 1978) and later as Andesite Stock of Buriticá (Leal-Mejía, 2011).

Propylitic alteration in the BIC overprints potassic alteration and this relationship dominates much of the bodies, with the exception of sericite alteration, which is more related to the mineralized structures and breccia zones within the BIC (Lesage, 2011). The latter, firstly described as dikes within the BIC, displays angular clasts of altered andesite that are embedded in a fine-grained matrix associated with high pressure volatile-driven explosions as a consequence of volcanism (Feininger & Castro 1965). Classified as an intrusive breccia, it is termed the Yaraguá Breccia, linked with the BIC intrusion, and displaying transitional contacts (Lesage, 2011). The Yaraguá Breccia is mainly matrix-supported, polymictic (basalt, chert, diorite, and andesite), with subangular to sub-rounded morphologies. Cretaceous age plutonic rocks, from west to east, comprise the Buriticá Tonalite, and the Santa Fe and Sabanalarga Batholiths. These N-S elongate bodies comprise mafic rocks, associated with subduction and plume originated magmas (Weber et al., 2015). The Buriticá Tonalite is well exposed to the southwest of Buriticá town, in the El Oso quarry, its composition being defined as dioritic to quartz-dioritic. This likely corresponds to an apophysis of the Sabanalarga Batholith, which is correlative with porphyritic units found along the Cauca River, and which led (Álvarez & González, 1978) to propose a Middle Pliocene age. However, K-Ar geochronological analysis yielded a Late Cretaceous age of 91.1 ± 6.4 Ma (Göbel & Stibane, 1979), and additional data from U-Pb in zircons gave an age of 100.9 ± 0.85 Ma (Weber et al., 2015). These ages are very similar to those obtained for the Santa Fe Batholith and Sabanalarga Batholith (Table 1).

The Santa Fe and Sabanalarga Batholiths are proximal to the Buriticá gold deposit but do not represent principal mineralization-hosting units at the deposit-scale. The Santa Fe Batholith is comprised of mafic plutonic rocks, elongate in a north-south direction orientation, syntectonic with the Cauca-Romeral Fault System suture and located west of it (Nivia et al., 1996). Its compositions vary from gabbroic, tonalitic to quartz-dioritic and gabbro-dioritic (Nivia & Gómez, 2005; Vinasco & Cordani, 2012; Weber et al., 2015). Several age dating methods have been applied to the Santa Fe Batholith, with Ar-Ar isotope analysis yielding results of 92 ± 2 Ma (Vinasco, 2001), Sm-Nd dating indicating an age of 98 ± 9.1 Ma (Weber, et al., 2011) and ages by U-Pb being 81.66 ± 0.65 Ma (Correa et al., 2018) (Table 1). The range of ages is interpreted as reflecting the period from crystallization to reheating of the body, suggesting a younger formation than the Sabanalarga Batholith (Zapata et al., 2017). Furthermore, the Santa Fe Batholith origin is in a shallow crust and corresponds to melting of mafic rocks (Weber et al., 2015). The contact with the Barroso Formation is intrusive and faulted (Nivia & Gómez, 2005).

The Sabanalarga Batholith is an elongate body with a N-S orientation. It is exposed from north of the Ituango town to south of the Anzá town, between the west flank of the Central Cordillera and the eastern flank of the Western Cordillera (Hall et al., 1975), and limited to the west by Cretaceous metabasalts and greenschists of the Valdivia Group (Zapata et al., 2017). It is comprised to the north by hornblende diorites and to the south by monzodiorites, diorites, quartz-diorites and tonalites (Álvarez, 1983). Radiometric ages of K-Ar in biotite yielded an age of 97 ± 10 Ma and 98 ± 3.5 Ma in hornblende, which correspond to the Albian – Cenomanian (González & Londoño, 1998). It is characterized by two magmatic pulses, with gabbros and diorites of subalkaline affinity comprising the initial one, and quartz-diorites and tonalites the second one, both sharing a common magmatic arc environment between the transition zone of the continental and oceanic crust (Rodríguez et al., 2012; Guiral-Vega et al., 2015). The entire rock unit is affected by the Cauca-Almaguer and Sabanalarga Faults, the contact with the Barroso Formation is discordant and intrusive in some places, indicating that it is a younger formation (Álvarez, 1983; Mejía, 1984). The contact with the rocks of the Valdivia Group to the east, generates a contact halo characterized by andalusite schists and hornfels (Correa et al., 2018).

The San José de Urama Diabase is located between the Santa Fe Batholith and Buriticá Tonalite, being bounded to the west by the Tonusco Fault, which locally puts it in contact with the BIC. Intrusive contacts are also present with the Buriticá Tonalite and BIC (Zapata et al., 2017). The San José de Urama Diabase is represented by a set of lava flows, dikes, dolerite sills and pillow basalts with ophitic, subophitic and intergranular textures that can be correlated with the effusive phases of the Barroso Formation (Mejía & Salazar, 1989), and constitute tectonic blocks emplaced from northwest to southeast between the N-S trending Cauca-Almaguer Fault and Dabeiba-Pueblo Rico Fault (Rodriguez, Zapata, & Gómez, 2012). The fact that is intruded by the Buriticá Tonalite and Buriticá Intrusive Complex (BIC) indicates an age of formation earlier than the Upper Cretaceous. In addition, according to whole rock Ar-Ar dating, the age corresponds to 155.1 ± 11.2 Ma, belonging to the Upper Jurassic-Lower Cretaceous limit (Rodríguez & Arango, 2013).

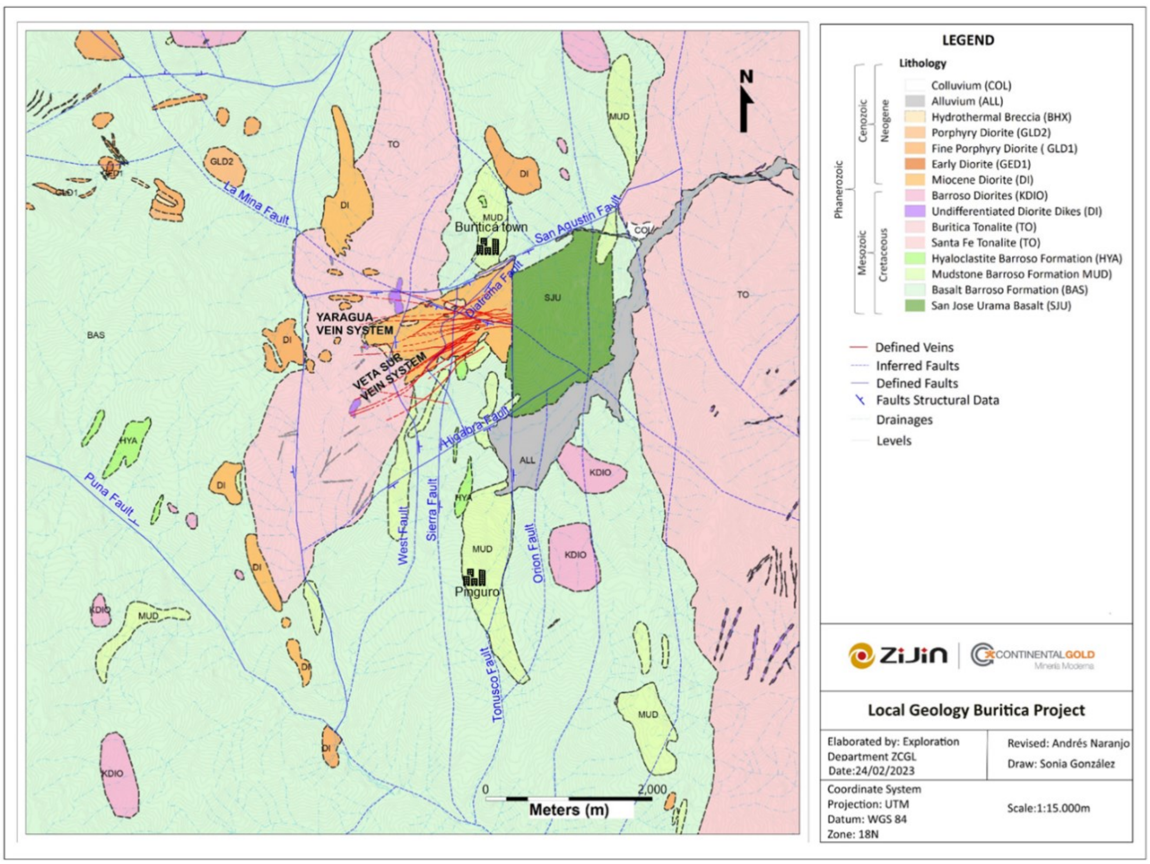

Figure 4. Geological map of Buriticá zone, Miocene diorite represents the BIC. WGS 84 18 N projection.

2.2.2 Alteration

There are several types of hydrothermal alteration in Buriticá gold deposit. These alteration assemblages conform to weak potassic alteration, chlorite-rich propylitic alteration, adularia-sericite and distal epidote-rich propylitic alteration associated with gold mineralization, and distal propylitic alteration (Lesage, 2011).

The oldest alteration assemblage corresponds to weak potassic alteration found in the andesitic rocks of the first intrusive pulses of BIC and in the Buriticá Tonalite (Lesage, 2011). The mineral assemblage is secondary biotite, orthoclase, magnetite and quartz in thin veinlets (Lesage, 2011).

Subsequently, the chlorite-rich propylitic alteration occurs as replacement of mafic minerals, including common actinolite replacement of plagioclase, and minor contributions of epidote and carbonates (Lesage, 2011). Abundant disseminated magnetite associated with pyrite and chalcopyrite can also be found. Minor pyrrhotite is associated with this alteration but it is not coeval with magnetite (Lesage, 2011). These two mineral assemblages are not related with the gold and base metals mineralization, rather occurring at a larger-scale in the BIC and the Buriticá Tonalite. The chlorite-rich propylitic alteration overprints the potassic alteration (Lesage, 2011).

Alteration associated with gold mineralization is characterized by proximal adularia-sericite and distal epidote-rich propylitic alteration, representing chemical gradients in the mineralized structures (Lesage, 2011). Overprinting relationships indicate that the propylitic alteration slightly precedes the adularia-sericite alteration (Lesage, 2011). As mentioned above, these alteration assemblages are restricted to the mineralized structures hosted by the BIC and the Yaraguá Breccia. Finally, these two alteration stages overprint the potassic and propylitic alteration (Lesage, 2011).

The adularia-sericite alteration is fault-vein controlled and manifests as 1 – 3 m width halos in some cases. This style of alteration comprises the main assemblage in the Yaraguá Breccia and BIC, which exhibits a strong geometric control imposed by the vein and fault structures.

The mineral assemblage defined for this alteration is sericite, adularia, quartz, calcite, ankerite, pyrite, and clays phases including kaolinite and illite (Lesage, 2011). Adularia can only be found in intensely altered zones, while sericite is more common even in less altered zones (Lesage, 2011). Where there is intense adularia-sericite alteration, the primary texture has been totally obliterated, later filled by quartz and carbonates (Lesage, 2011). Clays such as dickite, kaolinite and volkonskoite have been identified in surface surveys in the Yaraguá Breccia, indicating supergene origin (Lesage, 2011).

The distal propylitic alteration has an association of epidote, chlorite, calcite and pyrite, is pervasive and has replaced mafic minerals. Magnetite is absent and concentrations of chlorite are lower than epidote (Lesage, 2011).

2.2.3 Mineralization

Buriticá gold deposit mineralized structures are represented by several sets of steeply to moderately dipping fault-vein systems striking 85° – 95° (Yaraguá), 50° – 70° (Veta Sur) and 110° (Centena). These different structures are characterized by quartz, calcite, sulphides and sulfosalts, which include pyrite, galena, sphalerite, chalcopyrite, stibnite, pyrrhotite, tetrahedrite/tennantite and native gold (Lesage, 2011). In addition, fault damage zones and main fault intersections represent volumes of mineralized rock. ZJCNL internally recognizes it as Low Porphyry Mineralized zones (LPM).

Mineral paragenetic relationships define three stages of mineralization (Figure 5) (Lesage, 2011):

- Stage 1 is defined by banded quartz-base metal sulphide (pyrite-sphalerite-chalcopyrite-galena) with trace amounts of gold hosted in quartz or within sulphide minerals.
- Stage 2 displays a decrease in proportion of sulphides, resulting only in pyrite and minor light-yellow sphalerite, but an increase in quartz abundance and grain size, and displaying vuggy and crustiform textures. Gold is close to the boundary with Stage 1.

- Stage 3 displays calcite-rich brecciation localized and overprinted Stage 1 assemblage. Quartz, galena, light-yellow sphalerite and pyrite have well developed intergrowth textures, confirming coeval crystallization. Stibnite and tetrahedrite/tennantite are characteristic for this stage, as well as a fine-grained calcite matrix with breccia fragments of stage 1-2 sulphides. Microcrystalline bands of calcite and gold-galena intergrowths typically mark Stage 3.

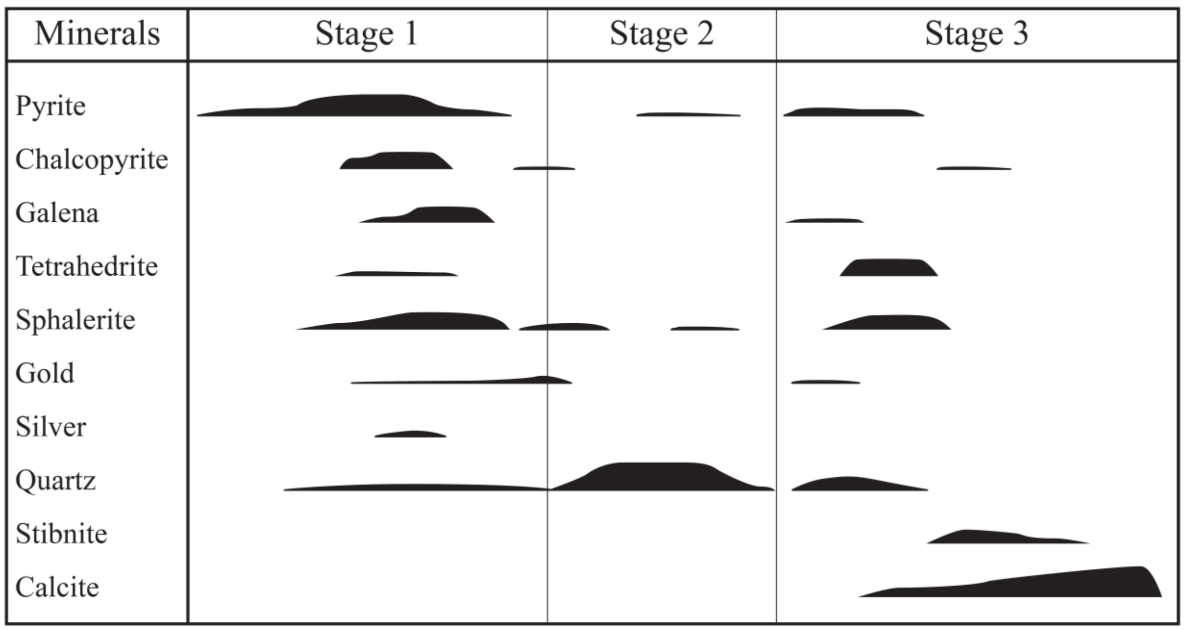

Figure 5. Mineralized fault-vein paragenesis. Taken from Lesage, (2011).

2.3. Structural geology

The tectonic setting of the Buriticá gold deposit is strongly influenced by two major fault systems, the Cauca-Romeral Fault System and the La Mina Fault (Figures 4, 26, 62). The Cauca-Romeral fault system, east of Buriticá, comprises mainly striking N faults, whereas the La Mina Fault strikes NW.

Both of the fault systems have been high strain deformation structures related with the suture zone and the accretions processes (De Souza et al., 1984; McCourt et al., 1984) that took place in the Early Tertiary. Regional-scale faults associated with these systems include the Sabanalarga Fault, Cauca-Almaguer Fault, Tonusco Fault and Puná Fault (Figures 4, 6). Locally, the Tonusco Fault is the eastern-most deformation structure, running N-S and hosting dextral strike-slip kinematics (Ego et al., 1995). To the west, the Diatrema Fault also strikes N-S but dips nearly 45° to the east. Farther westward, the steep dipping Sierra Fault accommodated dextral kinematics as well. The geometric relationships between the vertical and inclined structures have been crucial for localizing mineralization in the Buriticá gold deposit (i.e., Tonusco Fault, Diatrema Fault, Sierra Fault, La Mina Fault). Exploration drilling and mapping programs have outlined these structures and their geometric and crosscutting relationships, including the Tonusco Fault, Diatrema Fault, Sierra Fault and La Mina Fault, which have deformed the mineralized structures host rocks both with brittle and ductile deformation; the latter will be discussed in next chapters.

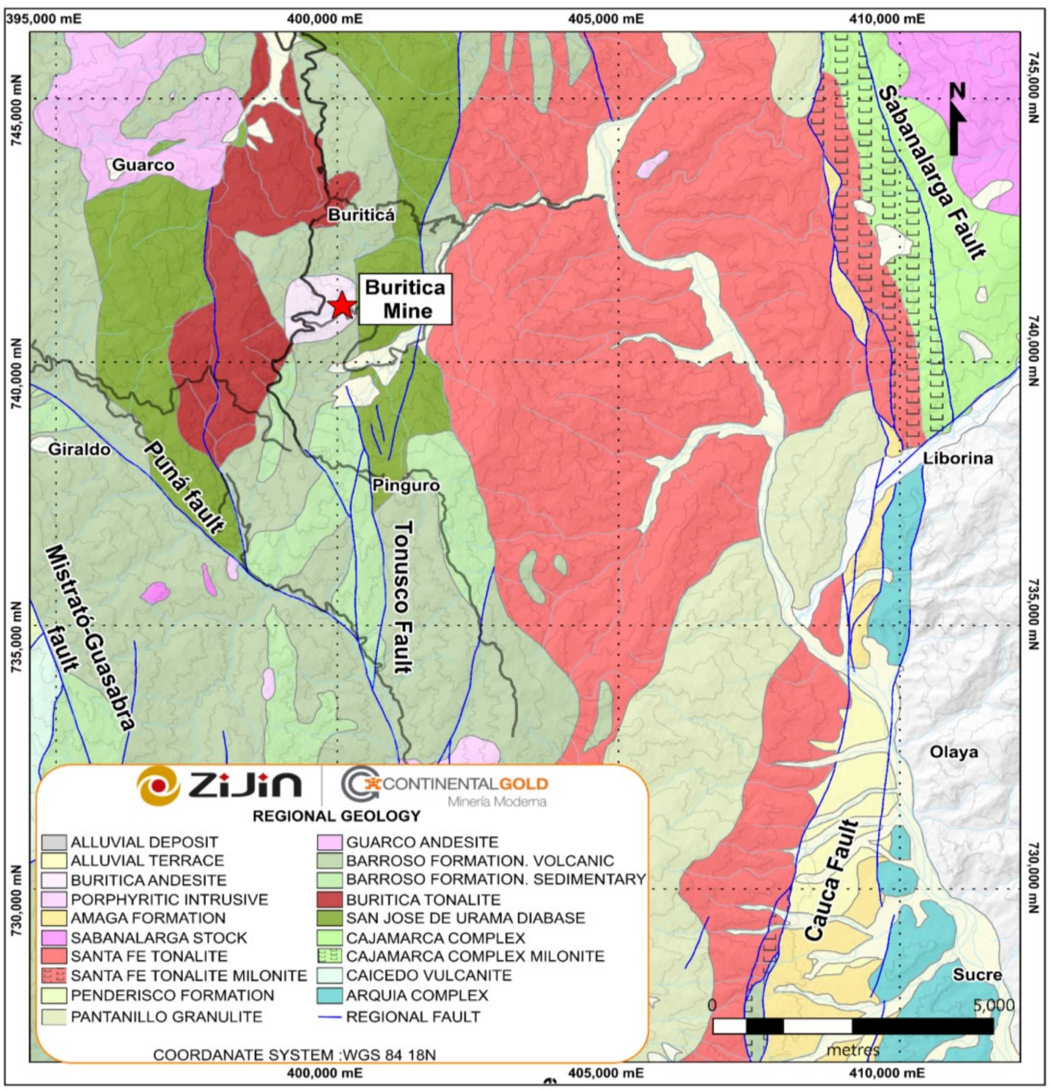

Figure 6. Regional geologic map of the zone showing principal faults. Modified after Correa et al., (2018).

3. Theoretical Framework

3.1. Porphyry deposits

Porphyry deposits get their name from the typical porphyritic texture of the plug-like intrusions that are genetically related to ore. These magmatic-hydrothermal deposits have variable contents of sulphide and oxide minerals, sourced from magmas and later precipitated at elevated temperatures (Seedorff et al., 2005). Texturally, fine-grained groundmass is characteristic of porphyries, as well as the low ore grades mostly found as thin veins or disseminated within the hydrothermally altered rock (e.g., Titley, 1966; Lowell & Guilbert, 1970). Porphyry deposits may vary in regards of host rock, magmatic composition, structural styles, resulting in a wide variability of occurrences (Gustafson & Hunt, 1975; Gustafson, 1978; Einaudi, 1982a). Hydrothermal porphyry systems evolve during spatial-time scales ranging from <1 mm to >10 km and up to 5 million years duration (Seedorff et al., 2005). Historically, the first known magmatic-hydrothermal deposits that exhibited features that would be defined as porphyry occurrences in current-day terminology were Cu rich and defined as disseminated Cu deposits. The formal use of the term porphyry was done until 1918, when it was made by Emmons.

Magmatic arcs that have formed along subduction zones show a strong correlation with porphyry deposit formation and distribution (Sillitoe, 1972, 1976) (Figure 7). Extensive distribution in both space and time results useful to determine earth and tectonics evolution, mostly associated with active magmatic-volcanic zones (Figure 7) (Meyer, 1981). The main metal content is used to classify these types of deposits, being porphyry Cu, porphyry Mo, porphyry Au, Porphyry W and porphyry Sn the major ones (Seedorff et al., 2005). Rock compositions include the whole range of modern volcanic rocks, but SiO_2 contents of 55 to 78 wt. percent are common (Seedorff et al., 2005). Globally, porphyry deposit distribution outlines the Phanerozoic orogenic belts including those in North America, the Andes, and Southwest Pacific (Figure 7). However, current known distribution is a function of preservation and exposure of deposits, since depth of formation occurs close to surface (1 –

6 km) with subsequent erosion, tectonism and burial (Figure 9) (Staude & Barton, 2001) being destructive, especially for relatively older deposits.

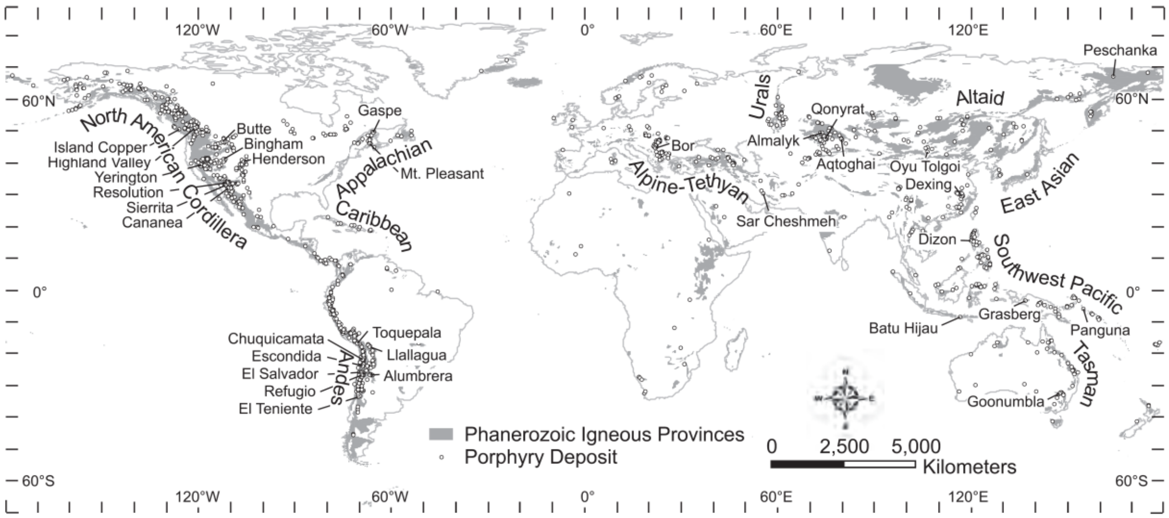

Figure 7. Distribution of porphyry deposits displaying the spatial relationship between igneous provinces and porphyry deposit discoveries. Taken from Seedorff et al., (2005).

3.1.1 Hydrothermal alteration

Hydrothermal processes in host rocks of porphyry deposits form the different types of alteration assemblages, which are principally controlled by wall-rock and fluid compositions (fluid-to-rock ratio) and pressure-temperature conditions. The latter forms variable types of gangue and sulphide minerals as wall-rock alteration occurs. Porphyry sizes (Cu > Mo ~ Au > Sn > W) also play a key role in the volume of rock affected by alteration, resulting in a great mass transfer activity (redistribution, concentration, or depletion) between hydrothermal fluids and host rock (Seedorff et al., 2005). Primary mineralogy of the intermediate composition of porphyry rocks consists of phenocrysts of plagioclase, biotite, hornblende, K-feldspar and quartz, which are subsequent converted to other phases through hydrothermal alteration. These minerals experimentally suggest magma conditions such water content and temperature of emplacement of > 4 wt. percent and ~ 675° to 700°C, respectively (Naney, 1983; Dilles, 1987).

Based on aluminosilicate rock compositions, chemical reactions responsible for the different alteration types are grouped as follows (Figure 9): volatile addition (propylitic alteration); hydrolysis (sericite, advanced argillic, and intermediate argillic alteration); alkali exchange (e.g., potassic and sodic-calcic alteration); addition of silica (silicic alteration) (Seedorff et al., 2005). Primary textures formed in the magma environment are replaced by the different alteration types, hence the degree of preservation depends on the intensity of each alteration. Sericite alteration is known for the conventional fine-grained K mica, but can also occur with quartz when K-feldspar is present and display characteristic alteration envelopes of variable intensity that may overlap if vein density is high (Figure 8) (Gustafson & Hunt, 1975; Titley, 1982b). Progressive hydrogen metasomatism and base-cation leaching are characterized by sericite and advanced argillic alteration in shallow environments (Stoffregen, 1987). Typical evolution of fluids is from high to low temperature, resulting in many ore and alteration minerals (Hemley et al., 1992; Redmond et al., 2004). Porphyry hydrothermal systems operate with temperatures of ~ 750° – 600°C in magma environments, to low temperatures of < 200°C in the exposed portions of some porphyry systems (Wilson et al., 1980; Ulrich et al., 2001). External fluids also make part during the evolution of a hydrothermal system and include saline formation waters (Dilles et al., 1992, 1995; Battles & Barton, 1995) and dilute meteoric waters (Sheppard et al., 1971; Selby et al., 2000).

3.1.2 Veins, Crosscutting relationships and Deformation

Veins form throughout the life of porphyry magmatic-hydrothermal systems and record the different process during ore deposition. Quartz vein genesis is related to pressure, in which hydrostatic conditions are the dominants parameters (Fournier, 1999). Abundant quartz veins are thought to be formed due to change from lithostatic to hydrostatic pressures as retrograde solubility occurs at pressures of < 800 bars (Rusk & Reed, 2002; Redmond et al., 2004). Since veins are prominent and key features within porphyry deposits, which Seedorff et al., (2005) divided in three structural style members: (1) disseminated style characterized by thin veinlets mineralization (Titley, 1982b); (2) the lode style (Einaudi, 1977b; 1982a); and (3) the breccia style (Sillitoe, 1985; Skewes & Stern, 1996). Low- to intermediate-sulphidation epithermal deposits with late veins and lodes with sericite envelopes are not included in any of these end members (Seedorff et al., 2005).

Classification of veins was first described by Gustafson & Hunt (1975), defining A, B and D type veins occurring at porphyry deposits in El Salvador (Figure 8). Early biotite (EB) and C veins were then added (Quiroga, 1995). Additionally, M veins occurrence in Island Copper, British Columbia, were added to the list (Figure 8) (Arancibia & Clark, 1996).

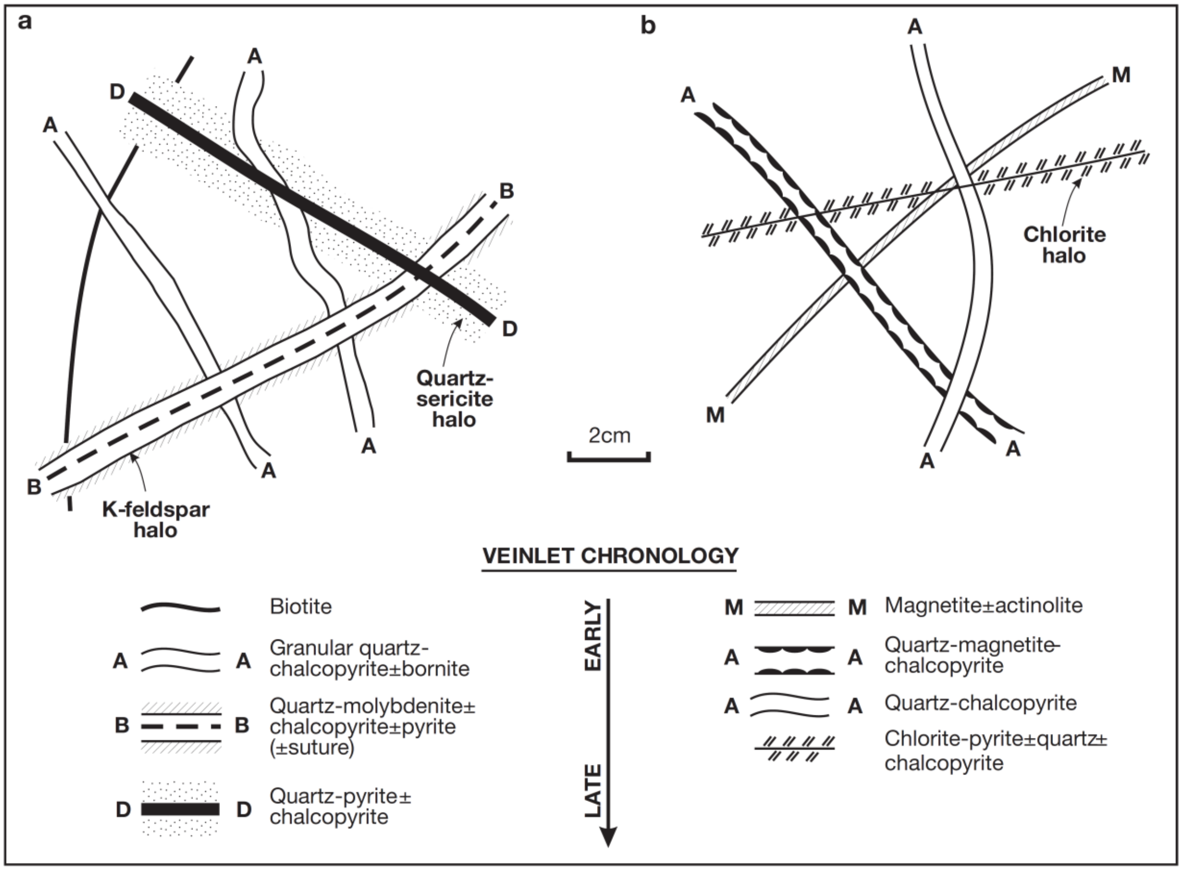

Figure 8. Schematic chronology of typical veinlet sequences in a. porphyry Cu-Mo deposits and b. porphyry Cu-Au deposits associated with calc-alkaline intrusions. Nomenclature follows Gustafson & Hunt (1975; A, B, and D types) and Arancibia & Clark (1996; M type). Taken from Sillitoe (2010).

Wall-rock alteration halos/selvages are usually symmetric on both sides of veins, as consequence of variable compositions of the vein fluids and reaction with the wall-rock. Mineral assemblages along halos may occur as single minerals or zoned patterns (Meyer & Hemley, 1967). Classification of veins can be based on several criteria comprising texture, mineralogy, vein infill, morphology, orientation and alteration envelope (Sedorff et al., 2005). Veins with sericite alteration halos are classified in greisen veins (Williams & Forrester, 1995); veins with sericite envelopes (Gustafson & Hunt, 1975); and base metal veins (Meyer et al., 1968). A common feature within these three vein type are the sericite alteration envelopes, with white mica, pyrite and quartz as principal distinct minerals. Porphyry Cu deposits often evidence these veins (veins with sericite envelopes and base metal veins) as systematically oriented fractures occurring and transitioning above and away from the bulk-tonnage orebodies (Gustafson & Hunt, 1975).

The relative ages of hydrothermal alteration and mineralization events can be reliably assessed through detailed documentation of veins offsetting other veins (Seedorff et al., 2005). Reopening of veins with subsequent precipitation also gives information about cross-cutting relationships but care must be taken (Meyer & Hemley, 1967). The typical case in which porphyry vein types are developed through decreasing temperature changes, then high temperature veins would cut the lower temperature veins, and this would indicate a normal crosscutting relationship (Seedorff & Einaudi, 2004a). Relationships between veins and porphyries can be used to classify the intrusive pulses; these are pre-mineral if all type of veins cut it; intra-mineral (inter-mineral) if it cuts and is cut by some veins, and post-mineral if it cuts every type of veins (Figure 9) (Sillitoe, 2000).

The different intrusions stages and their levels of exposure are in reference to the paleosurface, which is morphologically variable and changing during the evolution of hydrothermal systems (Sillitoe, 1994). The bottom reference for porphyry deposits at depth are the granitic cupulas, commonly found with equigranular to porphyritic textures (Emmons, 1927), from which porphyry stocks and dikes emanate towards the surface (Figure 9) (Dilles et al., 2000a). Post-mineral deformation is an important component for the degree of exposure of hydrothermal systems, including different type of faults. Strike-slip faults mostly develop lateral movements, hence the rate of exposure for greater depths of the system is low (McInnes et al., 1999; Tomlinson et al., 2001). Particular porphyry Cu deposits in Chile have been attributed to deformation by arc-parallel strike-slip faults and moderately dismemberment can occur due to progressive deformation (Lindsay et al., 1995; Tomlinson & Blanco, 1997a; Richards et al., 2001). Reverse and thrust faults duplicate sections and generate fault-bend folds in the hanging walls, however exposure of the systems is not considerable (Suppe, 1983). Consequently, normal faults relatively display the highest levels of exposure for hydrothermal systems, as deeper structural levels are uncovered in the footwall block (Houston, 2001).

3.1.3 Linkage between Porphyry and Epithermal deposits

Relationships between porphyry and epithermal deposits have been studied during the last two decades, discussing whether or not the different sulphidation styles represent an expression of deeper porphyry systems (Seedorff et al., 2005). High-sulphidation deposits are thought to be part of porphyry deposits, but low- to intermediate-sulphidation are not linked (Figure 9) (Sillitoe & Hedenquist, 2003). The sulphide type and assemblage results useful to frame the sulphidation state and referring to veins as formed late or in distal zones (Einaudi et al., 2003). Base metal rich intermediate-sulphidation epithermal deposits tend to occur at structural levels similar to those of porphyry intrusions, and basically represent the lateral and late equivalents of a porphyry system, rather than the tops (Jensen & Barton, 2000). Characteristically, evidence of intermediate-sulphidation epithermal manifestations are located next to high-temperature altered zones belonging to mineralized porphyry system (Seedorff et al., 2005).

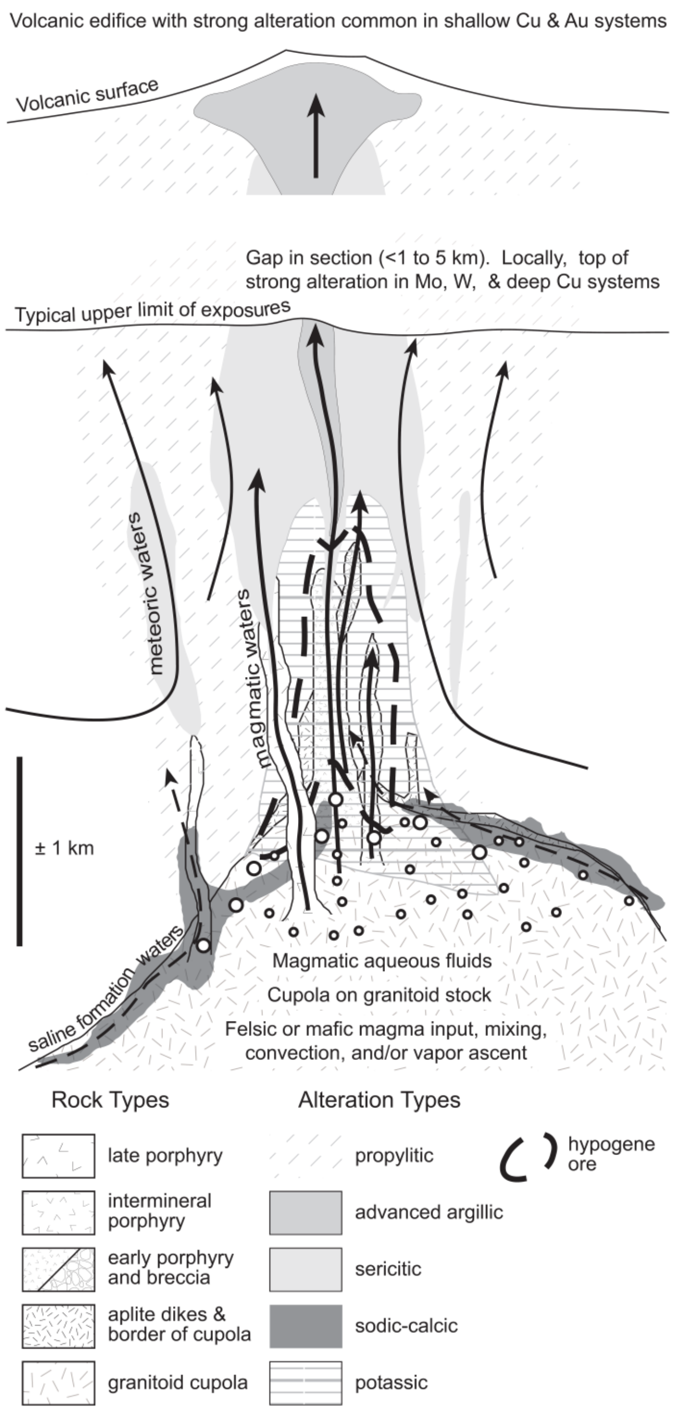

Figure 9. Porphyry deposit cross section displaying most prominent features including rock types and timing relationships, hydrothermal alterations, fluid flow pathways, and igneous bodies emplacement at shallow depths. Paleosurfaces and volcanic edifice are annotated regarding the levels of exposure by post-mineral deformation and high-sulphidation occurrence zone, respectively. Taken from Seedorff et al., (2005).

3.2. Permeability and fluid flux in Fault-Controlled Hydrothermal Systems

The lateral extent of fault-related ore deposits in vein arrays and hydrothermal alteration envelopes can range to more than several tens of meters away from the principal faults and shear zones. Low permeability host-rocks are the common feature associated with these fault-controlled deposits, in which ore formation involves large fluxes of overpressured fluids that depend on fracture generation rates and permeability enhancement to finally accommodate space for fluids.

The most recent and comprehensive review of permeability and fluid flux in fault-dominated hydrothermal systems is the seminal work of Cox (2020). This review covered permeability enhancement including failure types, geometry and kinematics of structures, fluid pressure conditions in high fluid flux zones, injection-driven failure style and its evolution of permeability over the life of the hydrothermal systems. All these factors are pertinent to the structural-hydrothermal evolution of the Buriticá mineral system and are considered in the following sections.

3.2.1 Failure Processes and Fracture-Controlled Permeability Enhancement

Hydrothermal ore deposits typically exhibit deformation control on their formation, commonly as mineralization localized in structures such as extension vein arrays, fault zones, or ductile shear zones. Examples of deposits with similar features are Butte, Montana (Bateman, 1958; Meyer et al., 1968; Houston & Dilles, 2013), and Porgera, Papua New Guinea (Munroe, 1995), these are hosted by multiple and variables structures of extensional vein arrays and faults.

Macroscopically brittle failure occurs by three different modes, 1) pure extension fracturing, 2) shear failure and 3) hybrid extensional shear failure (Figure 10). Extension fractures form perpendicular to the orientation of the minimum principal stress, σ_3, and hence form within the plane containing the maximum principal stress σ_1 (Lawn, 1993). These extension veins may be sealed by hydrothermal fluids, providing characteristics of stress field orientation during mineralizing events. The latter as a function of the tectonic settings; Figure 11 illustrates the compressive, extensional and strike-slip environments. Particularly, planar brittle shear fractures refer to faults related with the second failure type, in which displacement is relatively accommodated parallel to the failure surface. In this case the intersection of structures (Figure 11) results in nonplanar zones that are important for permeability enhancement and its anisotropy, flow localization and the geometry of ore shoots.

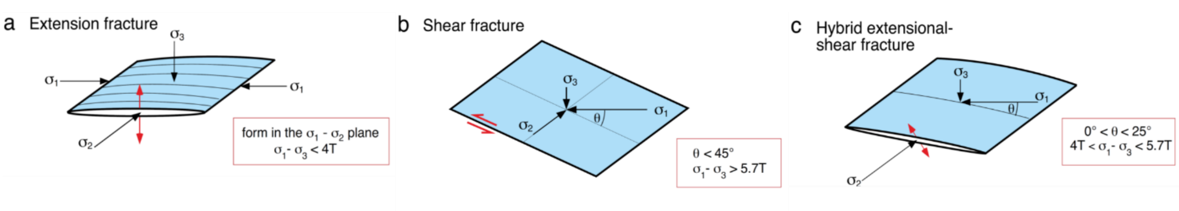

Figure 10. Stress field orientation for brittle failure types (a) extension fractures, (b) shear fractures, and (c) hybrid extensional shear fractures. Maximum principal stress σ_1, medium σ_2 and minimum σ_3 stresses are shown. Shear sense and opening directions are indicated by red arrows. Taken from Cox, (2020).

The third and last type of fracture failure is the hybrid extensional shear fracture, which has characteristic displacement both parallel and perpendicular to the fracture surface (Secor, 1965; Ramsey & Chester, 2004). Despite these being less common than other failure types, they can be found in combinations of extension veins and faults, likely forming under the same stress field where σ_2 is oriented parallel to the fault-vein intersection line, and the slip direction is in the fault plane and perpendicular to the fault-vein intersection (Figure 10) (Cox et al., 2001; Blenkinsop, 2008).

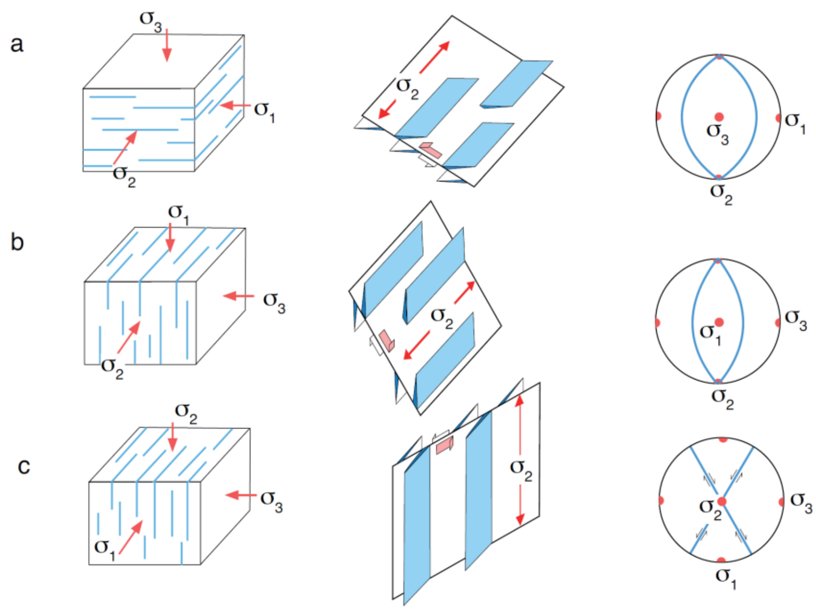

Figure 11. Geometric relationships for fault and extension fracture (veins) intersections in (a) contractional, (b) extensional, and (c) strike-slip regimes, with principal stresses and shear sense indicated. Stereoplots indicate orientations of principal stresses (red dots) and conjugate fault orientations (blue great circles). Poles to extension veins coincide with σ_3. Taken from Cox, (2020).

Shear fractures display two different rupture tip terminations that play significant roles for high fluid flux zones. Mode II is defined by terminations that are perpendicular to the slip direction whereas mode III is defined by parallelism between slip direction and terminations (Figure 12). These are mostly failure processes occurring in the seismogenic domain. As depth increases, the different modes of structures behave in different ways due to changes in temperature and pressure, principally ruled by the crust temperature gradient. Brittle-viscous transition structures are more related to orogenic lode gold systems, ranging temperatures around 350°C (Robert & Poulsen, 2001). However, these initially developed structures may be later overprinted by brittle shear failure (fault-fill veins) and extension failure events (extension veins) (e.g., Nguyen et al., 1998), and it is a diagnostic indicator of an evolving hydrothermal system into a low differential stress during the mineralizing event. The processes that drive fluid flux in the brittle-viscous transition zone and below the seismogenic regime are microscale fracturing, fluid pressurization and stress states.

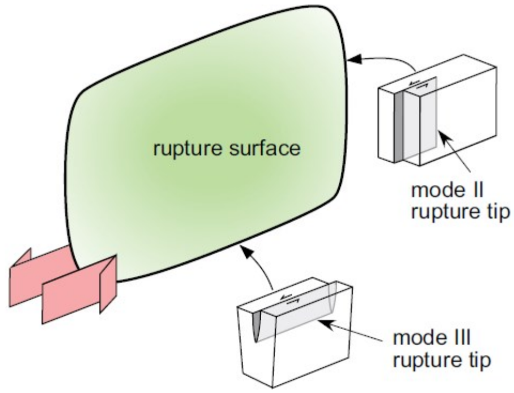

Figure 12. Illustration for mode II and mode III terminations of a fault rupture surface. Taken from Cox, (2020).

As described above, permeability enhancement involves several important and high influence factors including fluid pressurization, stress states and orientation, failure types and modes, geometry of associated structures, and deformation regime domains. A key point is that fracture-controlled permeability at all scales in hydrothermal systems is short-lived in comparison with the timescales of deposit formation due to rapid fracture sealing and compaction of fault damage products (Cox, 2005). Therefore, repeated generation of permeability through failure episodes is required to maintain high fluid fluxes for an ore deposit to form, as well as fast rupture events to avoid recovery of cohesive strength in between failures. Significantly, permeability evolution at all scales is controlled by competition between repeated episodes of permeability enhancement and a variety of permeability destruction processes (Cox et al., 2001; Sibson, 2001).

3.2.2 Dynamics of Permeability Enhancement and Fluid Flow in Overpressured, High Fluid Flux Regimes: Injection-Driven Failure Sequences

- Coupled fluid flow and seismic dynamics during fluid injection into low-permeability rock.

In low permeability rocks that host overpressured faults with high fluid flux regimes, the fault rupture episodes and consequent permeability enhancement is driven by fluid pressurization after injection of overpressured fluids, resulting in swarm seismicity (Cox, 2016). Some examples for injection-driven swarm in currently active hydrothermal systems are Hakone caldera (Yukutake et al., 2011), Long Valley caldera (Hill & Prejean, 2005; Shelly et al., 2015), Yellowstone caldera (Shelly et al., 2013a), and Mount Rainier (Shelly et al., 2013b). This process is characterized by consecutive low-magnitude ruptures with relatively insignificant initial mainshocks, occurring over periods ranging from several years to many decades.

Tens of thousands of slips events can occur during swarm seismicity events, leading to development of permeability enhancement. During rupture events of injection-driven swarms, in a natural setting, magnitudes may reach up to 2.5 to 4 Mw with their associated cumulative net slip (few centimeters) in areas less than 1 km2. The latter is analogous with the dimensions of fault-hosted hydrothermal ore deposits, in which seismicity activates fault segments and adjacent damage zones.

The onset of a swarm seismicity occurs adjacent to the injection site, and seismicity front migrates along the active fault network, thus enhancing permeability progressively (Figure 13) (Shapiro, 2015). Naturally, the most common flow has an upward component, however migration can vary along strike or even downward in complexes fault zones. That migration anisotropy turns out to be important for localizing jogs, fault bends and branch lines of fault splays in rupture zones (Yukutake et al., 2011), and to determine geometry and distribution of high fluid flux pathways. Hypocenter clusters are more likely to be located along well-defined fault zones, nevertheless diffuse seismicity occurs adjacently and is associated with low-displacement rupture damage zones with a respective lower permeability enhancement.

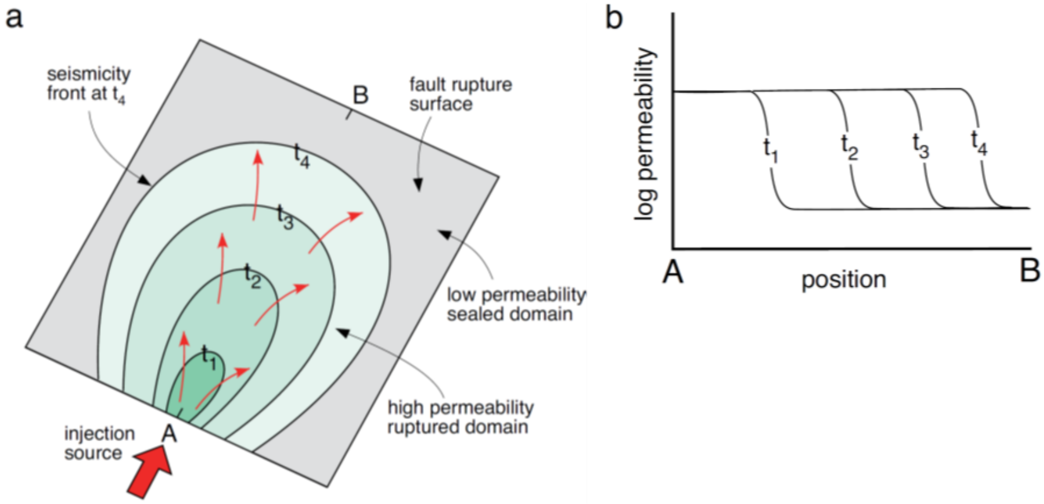

Figure 13. a. Swarm seismicity front migration during time of permeability enhancement, generated by overpressured fluids injection. b. Schematic illustration of evolution of permeability distribution from time t_1 to t_4 along A-B (in a). Taken from Cox, (2020).

- Implications of injection-driven swarm seismicity for behavior of fracture-controlled hydrothermal systems.

Permeability enhancement is provided by injection-driven swarm sequences, both natural and experimental, with volumes of activated zones that are dimensionally equivalent to some fault-related ore deposits (Sibson, 1996). So, genesis of hydrothermal deposits in overpressured settings is thought to occur during consecutive microseismic slip failure and high fluid flux events.

Bursts of recurrent swarms help propagate every rupture front at the same time the fluid pressure migrates through faults, while joining adjacent damage zones or misoriented faults if complex network exists (Figure 14). Regarding lode-hosting faults, a net slip of approximately 100 m during high fluid flux and with swarm sequences of microseismic magnitude (i.e., Mw <2.5) slip events, is expected to occur over periods of 104 years (Cox, 2016).

In conclusion, the way injection-driven swarm seismicity occurs provides insights about dynamics, timescales, rupture sizes and frequencies, flow rates, fluid volumes, and styles of high fluid flux fault systems. Furthermore, it allows for refinement of the classic fault-valve model (Sibson, 1981).

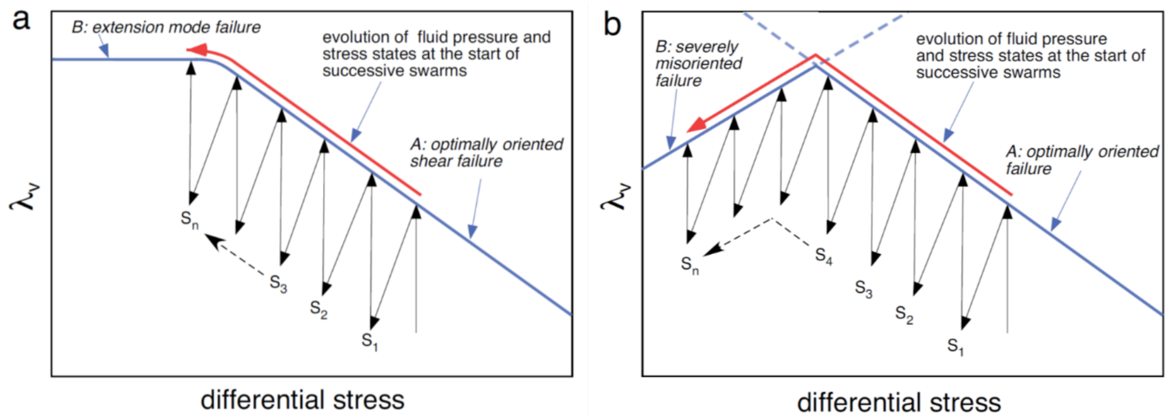

Figure 14. a. Failure mode diagram illustrating evolution of overall fluid pressures and stress states during successive earthquake swarms (S_1 to S_n) in one fault zone. b. Schematic failure mode diagram displaying the evolution of stress and fluid pressure states during successive swarms in a network of hydraulically connected faults. Taken from Cox, (2020).

3.2.3 Geometric and Kinematic Controls on Location, Geometry, and Styles of Fracture-Related Permeability Enhancement in Faults

Fault surfaces are mostly non-planar along the rupture and displacement zones, and irregularities and asperities can develop at all scales. Consequently, in some parts of the fault zone, dilation and permeability increase occurs during slip events. In addition, if wall-rock damage is generated during ruptures, it helps generate sites for permeability-control even more. The latter results in heterogeneous permeability distribution along and in damage zones, with geometric relationships that depending on kinematics and scale, lead to high fluid flux pathways and hydraulic connectivity controlling factors in connection with fluid reservoirs. Subsequently, the permeability-hydraulic connection remains dependent of the fault's geometry, associated structures, stress field orientations, kinematics, and hydraulic-linking structures with the highest importance, described as follows:

- Simple, subplanar fault segments.

In planar fault segments, the most common damage products are fault gouge and wear breccias, which represent higher permeability than the adjacent rocks. Despite the permeability enhancement as rupture occurs in planar surfaces, rapid hydrothermal sealing and granular compaction ends up with decrease of permeability and porosity, even more if slip is very localized and less than few millimeters thick (Sibson, 2003). It is very important to notice that intense off-fault fracture damage represents a high permeability generator when principal fault slip planes remain with low permeability, resulting in a flow control through damage zones structures such as extension veins (Figure 15) (Cox, 1995; Nguyen et al., 1998).

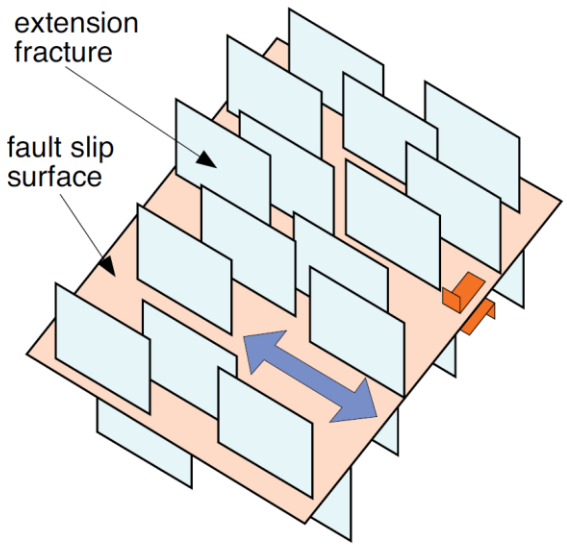

Figure 15. Setting of extensional veins and low permeability fault slip surface providing a high-permeability pathway. The direction of highest hydraulic connectivity within the sidewall fracture array is indicated by a blue arrow. Taken from Cox (2020).

- Fault termination zones.

As displacement decreases towards the tip of a fault, deformation is accommodated in the surrounding wall rock and results in several types of related structures, depending on the rupture tip mode. Mode II rupture tips (Figure 12) generate features termed extension wing veins that splay from the termination zones. Also known as wing cracks or horsetails (Figure 16a), these structures are strictly connected to the fault slip surface in a low near-field differential stress environment (e.g., McGrath & Davison, 1995). Fractures and breccia bodies commonly form in low σ_3 stress and dilational zones at fault tips, generating important hydraulic connectivity parallel to the fault plane and perpendicular to the fault slip direction. The evolution and growth of a fault involves continuous increase in fault slip during consecutive events, this indicates that damage zones are constantly cut by newly generated structures formed in each rupture slip episode (Figure 17) (Reches & Lockner, 1994).

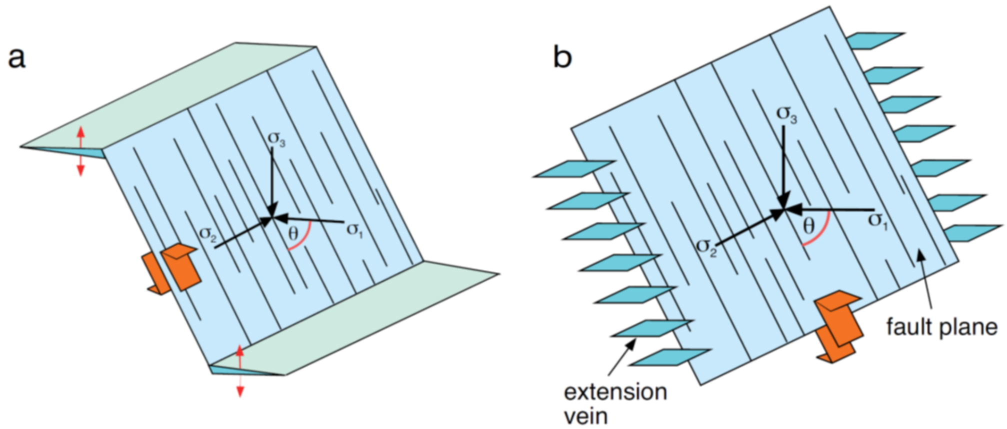

Figure 16. a. Geometry of wing cracks or veins formed at a mode II rupture tip. b. En-echelon fracture arrays related to mode III rupture tip. Modified after Cox (2020).

The mode III rupture tip results in the formation of en echelon vein arrays (Figure 16b), accompanied by local fault displacement and moderate fracture density that control hydraulic flow approximately parallel to the fault slip direction. Evidence of these different structure types in fault terminations is only possible when the fault rupture surface has been static in the same place during successive fault slip episodes after the formation of the tip damage zones. However, these terminal damage zones are still recognizable after fault growth by their asymmetric development in a single side of a fault (Figure 17).

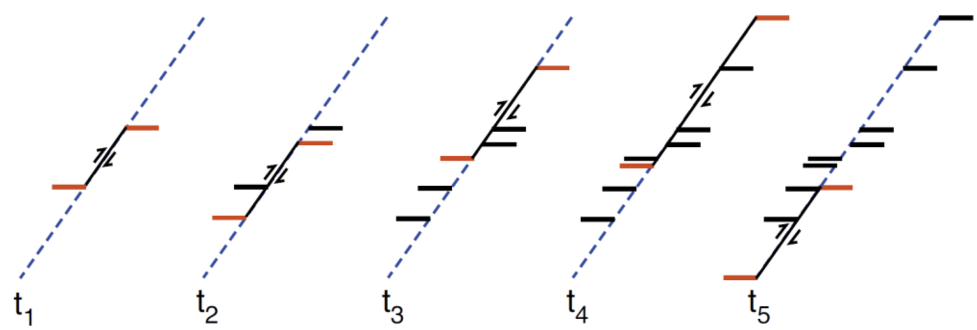

Figure 17. Schematic wing veins distribution over different times and slip surfaces (bold lines). Taken from Cox (2020).

- Fault bends.

Increase in length and displacement of faults occurs by linking initially disconnected shorter fault segments. Fault bends are changes in the orientation of a fault; they tend to form at a high angle to the fault slip direction and are related to extensional or contractional damage zone types depending on the propagation rupture direction (Figure 18). In such conditions, permeability enhancement and hydraulic connectivity occur along the bend elongation (Figure 18).

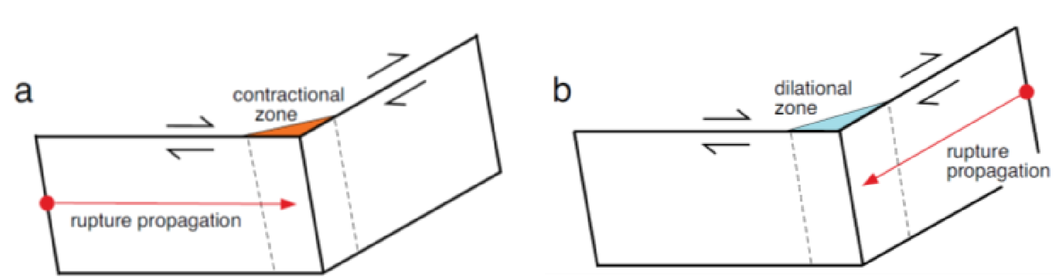

Figure 18. a. Contractional bend deformation in dextral strike-slip fault and rupture propagation from left to right. b. Dilational bend deformation in dextral strike-slip fault and rupture propagation from right to left. Taken from Cox (2020).

- Segment linkages.

In fault-related hydrothermal systems, connection between two approximately parallel fault segments are key factors for localizing permeability enhancement, fluid flow and ore shoots. There are two linkages types according to fault tip types modes, the ones between mode II fault tips referred to as fault jogs (Sibson, 1989, 2001), and between mode III fault tips termed relays (Walsh et al., 1999, 2018). Development of these types of linkages are multi-scale, since faults usually comprise nearly planar segments that are linked by stepovers with complex extension and shear arrays that transfer displacement from one side of the stepover to other. As increasing net slip in the main faults, evolution of linkages goes from a “soft-linkage” stage to a “hard-linkage” stage, depending on the connection of the fracture networks between faults. Jogs are hard-linked structures (Figure 19) that in high fluid flux and brittle deformation settings, leads to regeneration of permeability during successive rupture and slip events.

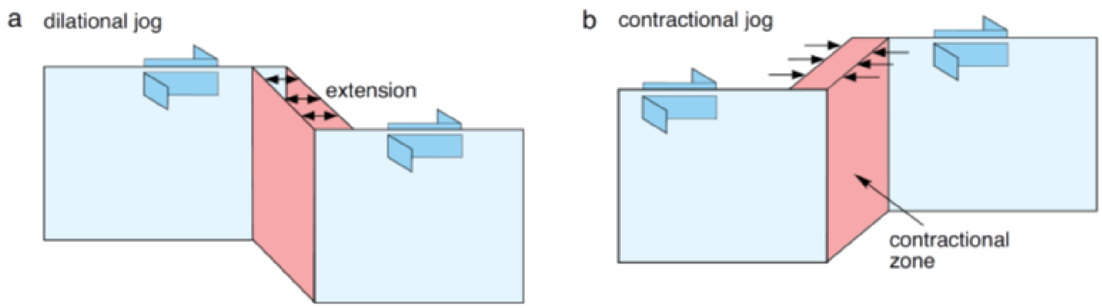

Figure 19. Geometry of (a) dilational jogs and (b) contractional jogs in a dextral strike-slip regime. Jogs display the direction of the highest hydraulic connectivity along the long axis and perpendicular to the slip direction. Taken from Cox (2020).

Fault kinematic and stress field orientation define whether jog types are contractional or dilational. The dilational jogs are commonly found in rhombic shapes and vein infill in zones with similar oriented veins or faults, also marked by maximum elongation parallel to σ_2 (Figure 20). Therefore, strongest hydraulic connectivity is along plunging axes of jogs for normal and reverse faults whereas strike-slip faults develop steep to vertical hydraulic connectivity (Figure 20).

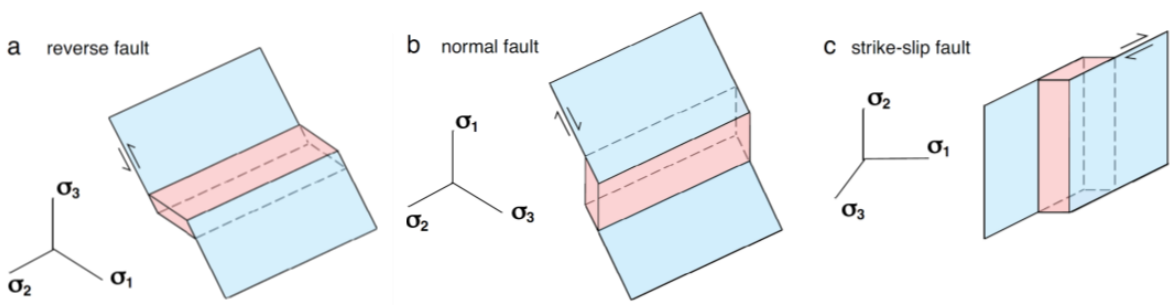

Figure 20. Geometry of dilational jogs in (a) reverse faults, (b) normal faults, and (c) strike-slip faults. Taken from Cox (2020).

Mode III fault tips linkages correspond to relays. These features form stepover zones elongated parallel to the fault slip direction (Figure 21). In extensional environments, relays have been marked as high fluid flux zones in shallow geothermal systems (Curewitz & Karson, 1997; Rowland & Simmons, 2012; Faulds & Hinze, 2015). As with jogs, relays evolve through the same stages as slip is accumulated. Underlying faults grow and link the other fault segment to generate a single breached relay (Walsh et al., 2018) (Figure 21a).

Importantly, high fluid flux is not associated with this stage and permeability can instead be higher outside relays (Leckenby et al., 2005). Repeated slip results in the linkage of faults, localizing fractures through brittle deformation within the relay and thus generating an important hydraulic connectivity zone. Within the strike-slip regime, gently plunging relays control hydraulic connectivity in a sub-horizontal way (Walsh et al., 1999, 2018).

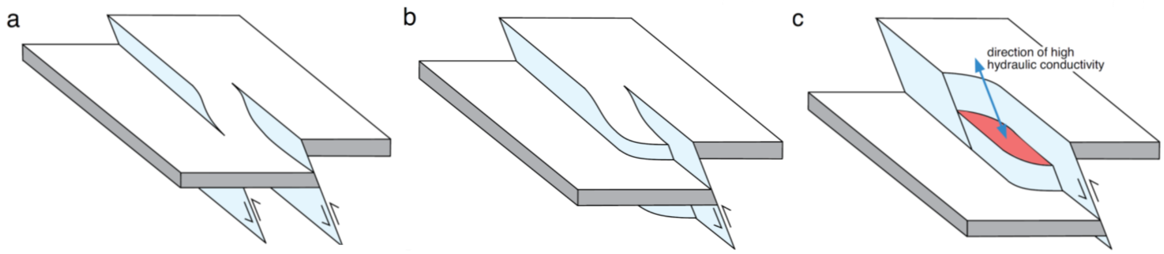

Figure 21. Overlapping reverse faults and linking fault relays. a. Unbreached relay at the soft linkage stage. b. Singly breached relay. c. Doubly breached relay. Taken from Cox (2020).

Jogs and relays function as fluid conduits and their connection to other permeable structures is critical for fluid flow. Therefore, if these structures are connected to an overpressured fluid source, development of high fluid pressures in the upper terminations can induce hydraulic fracture and subsequently drive propagation of permeability damage zones in planar fault segments (Figure 22-b). It is significant to note that bends, jogs and relays are characteristic transient structures, so the permeability enhancement is also transient. Successive rupture events destroy these structures by abrasion and fragmentation processes as faults accommodate every slip episode and mature (Wesnousky, 1988; Sterling et al., 1996, Walsh et al., 1999, Walsh et al., 2018).

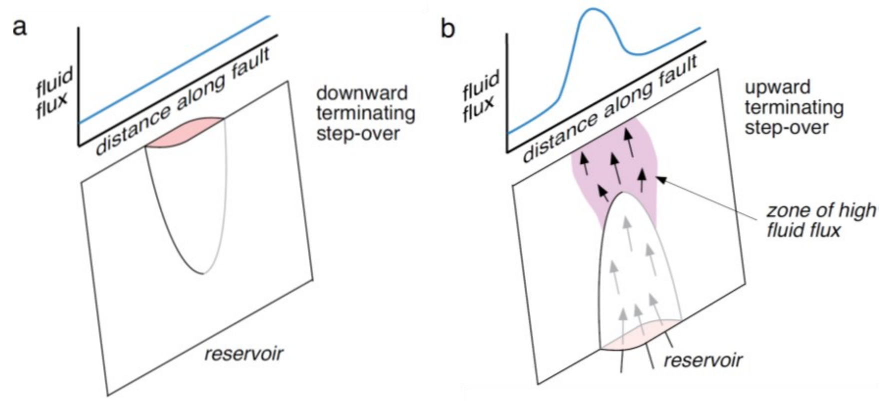

Figure 22. a. Doubly breached downward terminating step-over without connection to an overpressured fluid reservoir. b. Doubly breached upward terminating step-over that is connected to a deeper overpressured reservoir in which fluid-driven failure occurs by the fluid pressurization in the upward terminating zone. Taken from Cox (2020).

- Fault splays and intersections.

Branch lines on fault splays are structures formed in the intersection of mode II fault tips, characterized by linear to gently curved morphologies where a fault splits into two lower-displacement faults (Yielding, 2016). Fault splay formation is related to faults hosting the same kinematics, resulting in branch lines nearly perpendicular to the fault slip direction (Figure 23). In mode III fault tip, branch lines are parallel to the slip direction, thereby lower permeability enhancement is expected under these conditions. An intermediate setting between mode II and mode III fault splay branch lines generates important dilational fracture damage, leading to high hydraulic connectivity through variable angles and slip directions (Yielding, 2016).

A relatively common fault interaction is where a fault crosses another and the intersection line plays the role as a permeability conduit, such as occurs with conjugate faults (Yielding, 2016). In active geothermal systems, fault intersections are interpreted to localize permeability and flow (Faulds & Hinze, 2015). If coactive and permeable faults control different fluid types, fluid mixing may occur in the intersection zones to generate significant ore deposits.

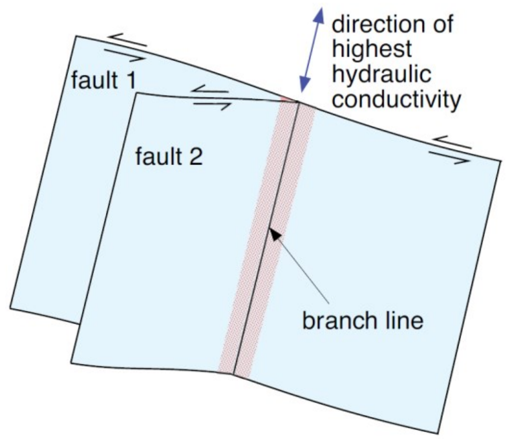

Figure 23. Mode II branch line on splay with permeability control (pink zone). Taken form Cox, (2020).

- Role of competence contrasts in localizing permeability enhancement.

In fault zones, remarkably high permeability sites are influenced by lithological heterogeneity (e.g., mechanical stratigraphy) and by mechanical anisotropy (e.g., preexisting layering and foliation) (Cox, 2005). If rheologically strong layers are present, they will localize brittle deformation and thus permeability enhancement. Such settings of faults and competent layers directly influence the distribution of dilatant jogs (Figure 24) that form zones of enhanced permeability that are elongate parallel to the intersection of the fault with the competent layer (Reid et al., 1975; Cox, 2005).

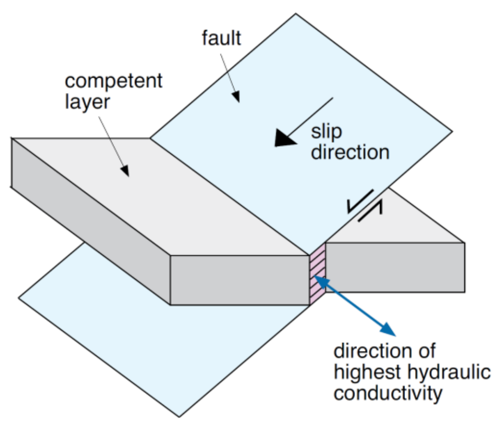

Figure 24. Fault deflection in the directions of σ_1 - σ_2 during development of dilatant jog. Taken from Cox, (2020).

Permeability enhancement is also developed when σ_1 is inclined moderately to the boundary of a competent layer that results in a shear stress component parallel to the boundary. Development of laminated bedding-parallel veins is associated with layer-parallel slip in interbedded competent and incompetent rocks during folding and flexural deformation events (Cox et al., 1991). Furthermore, lenses that undergo ductile shear also provide significant enhancement permeability as vein development will localize within and around competent and rheologically competent lenses.

- Effects of hydrothermal alteration on mechanical behavior and permeability enhancement.

Hydrothermal alteration changes the mechanical properties of host-rocks during high fluid flux episodes and along fluid pathways, which manifests as fracture localization and permeability enhancement. Munroe (1995) identified controls on fracturing and vein formation in Porguera Au deposit (Papua Nueva Guinea) as silicification of pelitic rocks that resulted in an important competence increase, thus enhancing permeability significantly in the early stages of the ore formation. The controls of alteration on rock deformation has also been documented in orogenic Au systems as these parameters can influence whether brittle or ductile failure occurs, resulting in variations from low to high permeability. For example, (e.g., Nguyen et al., 1998) noted that early potassic alteration and hydration in mafic host rocks led to a relatively more viscous deformation in shear zones rather than through brittle failure. Paragenetically late sodic alteration overprinted and replaced potassic assemblages, forming relatively more competent albite-quartz-bearing assemblages that were more likely to localize brittle shear failure and related extension vein arrays.

4. Methodology

In order to address the aims of the study, a summary of the research methodology is presented as follows:

4.1. Logging and sampling

Logging and sampling methods were carried out in the core shed at the Buriticá mine, during the exploration drilling programs from 2019 to 2021 (56,000 m), with sample sources including drill core and underground/surface outcrops. Special emphasis was taken on key core intervals through faults and for veins both proximal and distal to major structures, as well as lithological contacts and alteration intensity. Due to a confidentiality agreement, exact location of some data will not be presented.

4.2. Surface-underground mapping

Surface and underground mapping was conducted according to exploration programs during 2019 – 2021. Characterization considered mainly the principal structures and lithologies, sequence of vein formation, and morphologies of structures It also assessed the overprinting and geometric relationships of mineralized and unmineralized structures. Various examples of mapping carried out are displayed in Appendix 4. Due to a confidentiality agreement, exact location of some data will not be presented.

4.3. Petrography

Petrographic descriptions and analysis of 17 doubly polished thin sections (50 – 120 µm) were carried out with an emphasis in crystalline textures, primary and secondary mineral assemblages, alteration controls and overprinting relationships. The samples were chosen from the main host lithologies at the deposit-scale. Ore and gangue mineral distinction was carried out by optical microscopy in reflected and transmitted light. Thin section descriptions are provided in Appendix 1.

4.4. Lithogeochemistry

Whole-rock chemical analysis (major and trace elements) was conducted at ALS-Lab, Perú, by four-acid digestion combined with Inductively Coupled Plasma Mass Spectrometry (ICP-MS) and Inductively Coupled Plasma Atomic Mass Spectroscopy (ICP-AES), previous sample preparation at ALS-Lab, Colombia. Sampling was carried out from drill cores, surface and underground rock exposures. The analytical procedure included digestion of a prepared sample (nominal weight 0.25g) with 1.5mL concentrated nitric and perchloric acids, followed by concentrated hydrofluoric acid. The mixture was heated at 185°C until incipient dryness, leached with 50% hydrochloric acid and diluted to volume with weak HCl. The final solution was then analyzed by ICP-MS and ICP-AES, with results corrected for spectral inter-element interferences (www.alsglobal.com/geochemistry).

Zijin-Continental Gold's widespread 400.000 m assay data set was reviewed for geochemical interpretations, metal distribution and zonation, and characterization of sericite alteration intensity, by using the ioGAS™ multivariate data analysis software. Interpretations and their spatial constraints were incorporated within the structural architecture of the deposit. (Limitations regarding the petrogenetic diagram interpretations are recognized since cation oxide data is calculated by the software and based on averages).

4.5. X-ray diffraction

Five clay-altered samples were prepared and XRD analysis was carried out at the Inclay Laboratory in Bogotá. Analysis utilized a Miniflex 6G-C multipurpose Powder Diffractometer with a Cu tube (λ=1.54056 Å), with measurements in powder, natural, ethylene glycol and calcined treatments with a 2θ geometry and Bragg-Brentano configuration (Appendix 2). Qualitative analysis was performed based on the different treatments profiles and compared with the PDF-2 diffraction database of the International Centre for Diffraction Data (ICDD). This procedure is fully outlined in Rietveld (1969).

4.6. Geochronology

Intrusive rock units from the BIC were selected to constrain the age of the magmatic events. Samples were submitted and subsequently dated (see appendix 3). U-Pb zircon dating was conducted at the Isotope Geology Sernageomin Laboratory, in Santiago, Chile. Dating utilized laser-ablation using a 193 nm excimer laser (Photon-Machines Analyte G2) with a single collector, magnetic sector mass spectrometer (Thermo Fisher Scientific Element XR), and ensuing the zircon U-Pb conventional dating method. The whole processes of sample preparation can be found in www.sernageomin.cl. It involved crushing, heavy minerals concentration, zircon epoxy mounting, polishing, cathodolumiscence images, BSE images, LA-ICP-MS and data reduction. See appendix 3 for detailed information.

4.7. 3-D modeling

With the use of the Leapfrog Geo™ geological modeling software, the different structures and geological units were drawn. The entire assay data sets were reviewed for distribution of elements in 3D and in conjunction with features such as gold grade tenor, fault architecture, structure order, mineralogy, host lithologies and sericite alteration intensity.

5. Results

5.1. Structures

Underground and surface mapping, logging and photologging provided the zones of deformation at the deposit-scale. Photo-logging of 347 km of drillholes, resulted in 88.5% of intact rock, and 11.5% of deformed rock (Figure 25). The locations of deformation zones were recorded in the 3D mine grid, giving them geospatial context. The cartographic points and intervals of core were then modelled, and subsequently constrained with mineralized structures and host rock lithologies in 3D.

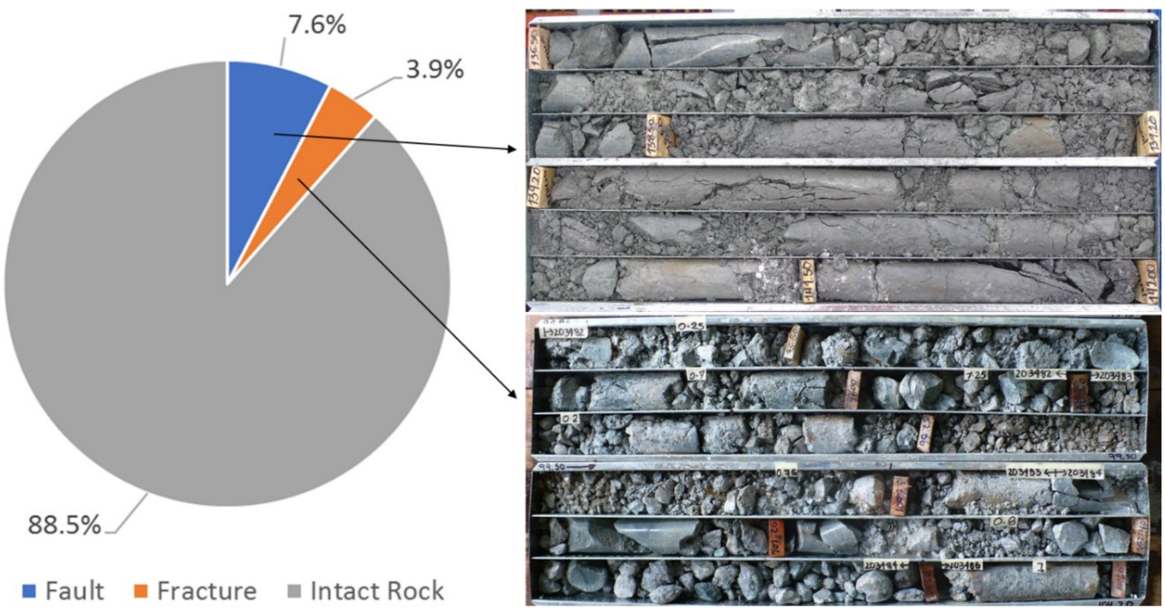

Figure 25. Pie chart showing proportions of deformed and intact rock, based on the photologging survey.

The Buriticá gold deposit displays an array of structures in several directions, including both mineralized and non-mineralized. The main first-order deformation structures correspond from east to west as follows: Higabra, Tonusco, Diatrema, Sierra, La Mina, San Agustin, and West faults (Table 2) (Figure 26, 27, 28, 29, 30).

Table 2. Characteristics of the Buriticá gold deposit structures.

Structure	Scale	Macro-morphology	If planar, interpreted strike	If planar, interpreted dip	Number of inferred movements	Movement sense	Associated with mineralization?	If mineralized, where?	Mineralization continuity	Mineralization style	Characteristics of veining	Does it terminate against other faults? If yes, which ones?	Hydrothermal breccias association	Comments
Higabra Fault	Regional	Planar?	NE-SW	Subvertical		Right Lateral	No					West Fault		
Tonusco Fault	Regional	Braided, anastomosing	N-S	Subvertical	Multiple	Right Lateral	Yes, contact area of intrusives and San Jose de Urama rocks	On W side of N-S strands comprising W margin of fault zone	Discontinuous	Shears	Qz, Th, Cb	N-S strands	Yes	Mylonites
Diatrema Fault	Regional	Braided	NNE	45 to the east	Multiple	Dextral - Reverse	Yes, high permeability	Both walls	Discontinuous	Extension vein hosted, shears	Sph , Ga, Py, Cpy	Tonusco	No	Mylonites
West Fault	Local	Planar?	N-S	Subvertical?								N-S strands		
San Augustin Fault	Regional	Multi-strand	NE-SW	Subvertical		Right Lateral ?	No					West Fault?		
Sierra Fault	Regional	Planar	NNE-SSW	Subvertical	Multiple	Right Lateral	Yes, LPM301	W-E sides	Discontinuous	Hydrothermal breccia, vein hosted	Cb, Py, Sph	San Agustin? Higabra?	Yes	Mylonites. NNE-SSW trend containing other mineral occurrences e.g., Venus, Cimarrona?
Puná Fault	Regional	Multi-strand	NW-SE	Subvertical	Multiple	Left Lateral						N-S strands to the south		Same trend as La Mina Fault

Structure	Scale	Macro-morphology	If planar, interpreted strike	If planar, interpreted dip	Number of inferred movements	Movement sense	Associated with mineralization?	If mineralized, where?	Mineralization continuity	Mineralization style	Characteristics of veining	Does it terminate against other faults? If yes, which ones?	Hydrothermal breccias association	Comments
La Mina Fault	Regional	Multi-strand	NW-SE	Subvertical		Left Lateral	Yes	Along the strike (Centena)	Discontinuous	Shears	Stage II >> Stage I	Tonusco (SE area)	Yes	NW-SE Buriticá structural Corridor, trend containing other mineral occurrences e.g., Poseidon, Medusa, Perseus, Orion, Electra Sur.
Centena	Regional	Braided	NW-SE	Subvertical	Multiple	Left Lateral	Yes	Along the strike	Continuous	Extension vein hosted, shears	Stage II>>Stage I	Diatrema, Tonusco		Same trend as La Mina Fault
San Antonio	Local		W-E	Subvertical			Yes	Along the strike	Continuous	Extension vein hosted, shears		Tonusco to the east. Sierra fault to the W	No	
Murcielagos	Local		W-E	Subvertical, Ramping	Multiple	Dextral-Reverse	Yes	Along the strike	Continuous	Extension vein hosted, shears		Tonusco to the east. Sierra fault to the W	No	

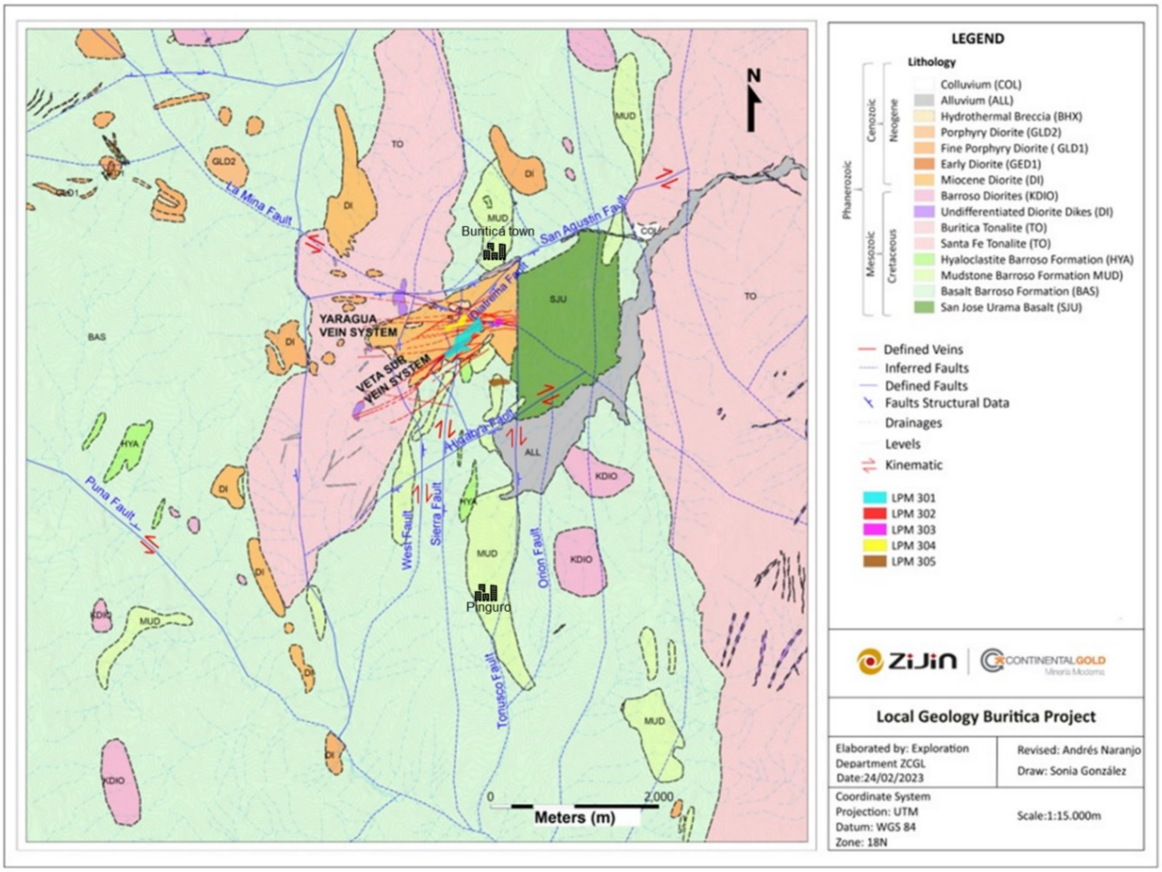

Figure 26. Map of Buriticá gold deposit with faults and apparent movements at district-scale.

The most important faults involved in the architecture of the Buriticá Gold deposit are:

- Tonusco Fault: N-S oriented structure running through the entire deposit and marking the limit of the mineralization to the east. It extends for about 60 km on strike and 900 m at depth. Deformation textures indicate a history comprising ductile and brittle events dominated by dextral kinematics.

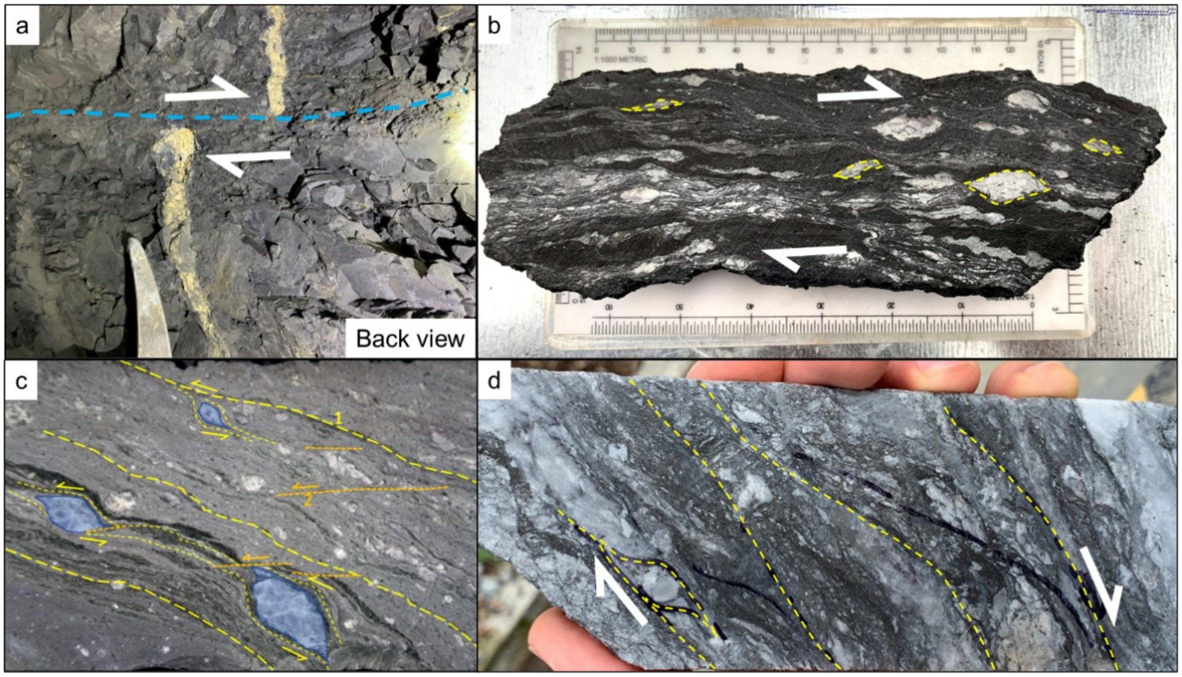

Figure 27. a. Displaced mineralized structure exposed in the back of a working. Blue dashed line represents the fault trace. The photo is turned up-side-down for perspective proposes. b-c-d. Core samples displaying high strain deformation and mylonitic textures with kinematic indicators defined by the asymmetric porphyroclasts.

- Diatrema Fault: Inclined structure dipping to the east. It terminates in the Tonusco Fault and has some subparallel fault planes above the main fault trace. Mineralized structures displaced by the Diatrema Fault record about 1 – 2 m offset with mainly E-block going up. Mylonites are present along this fault.

Figure 28. Damage zone of the Diatrema Fault in Yaraguá mine 1385 level. Multiple brittle events (dashed lines) are visible accompanied by strong sericite alteration. View is looking west and to a crosscut wall. Rock bolt for scale.

- Sierra Fault: Subvertical and N-S striking structure in the Veta Sur system. It deforms the interbedded volcanics and sedimentary package of Barroso Formation with a dextral sense, as well as control for hydrothermal breccia emplacement.

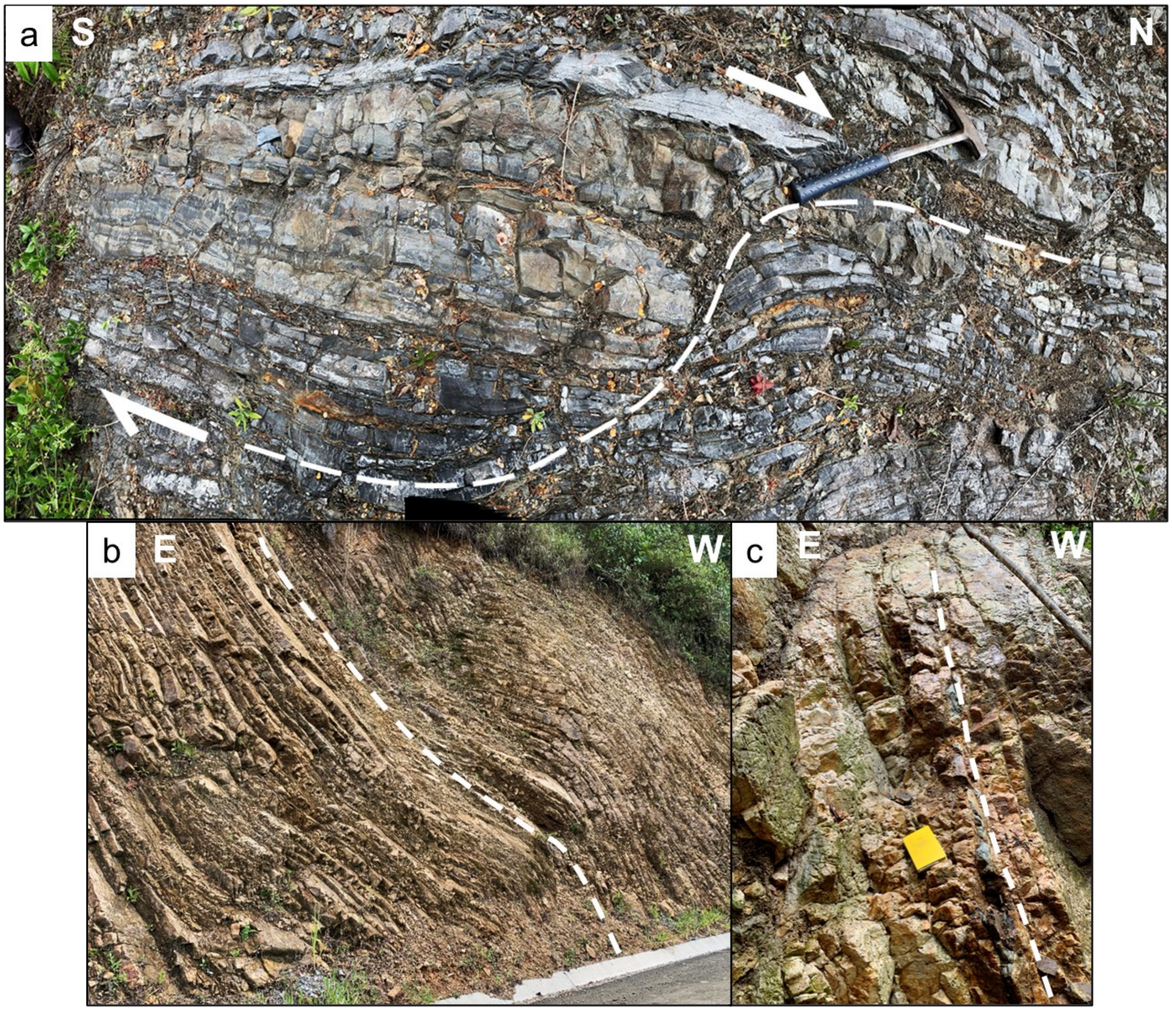

Figure 29. a. Sedimentary layering displaying right lateral movement with nearly vertical planes. View looking down the outcrop in the ground. b. Roadcut view looking south at the sedimentary package of Barroso formation, tilted, and faulted by the Sierra Fault. c. Development of mylonitic zones along the bedding planes. South side of La Mina creek.

- La Mina Fault: This fault, with a NW-SE trend, parallel to regional-scale faults and some mineralized structures (Centena). It displays a left-lateral movement. Additionally, when it intersects the Sierra Fault, hydrothermal breccias are controlled down the interception line dip/plunge.

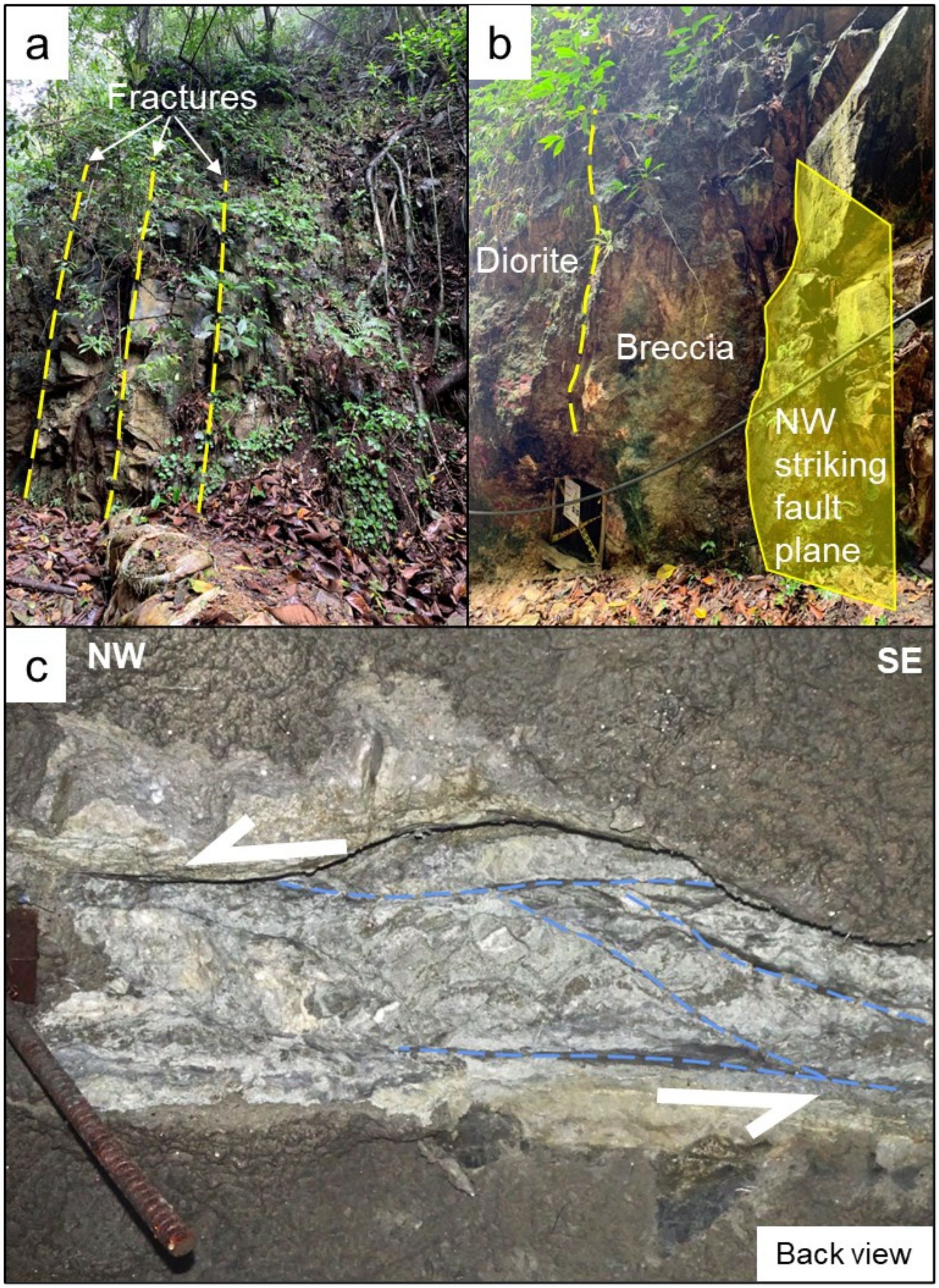

Figure 30. a. Close-spaced vertical fractures controlling hydrothermal breccia emplacement in la Mina Creek. View looking eastwards. b. Subparallel W-E oriented faults (dashed-lines) controlling the geometry of breccias when they intersect NW striking faults. Artisanal adit in the lower left for scale. c. Kinematic indicators exposed in the Centena mineralized structure displaying left lateral movement accommodated by subordinate internal structures, YR_GA_9734W. Bolt as scale.

Documentation and measurement of different types of structures during logging of oriented drill cores and mapping campaigns returned a data set of nearly 20.000 points, which was analyzed through stereography. The Veta Sur and Yaraguá systems are well distinguished in stereonets (Figure 31) and rose diagrams (Figure 32, 33), constraining the NE-SW and W-E mineralized trends, respectively.

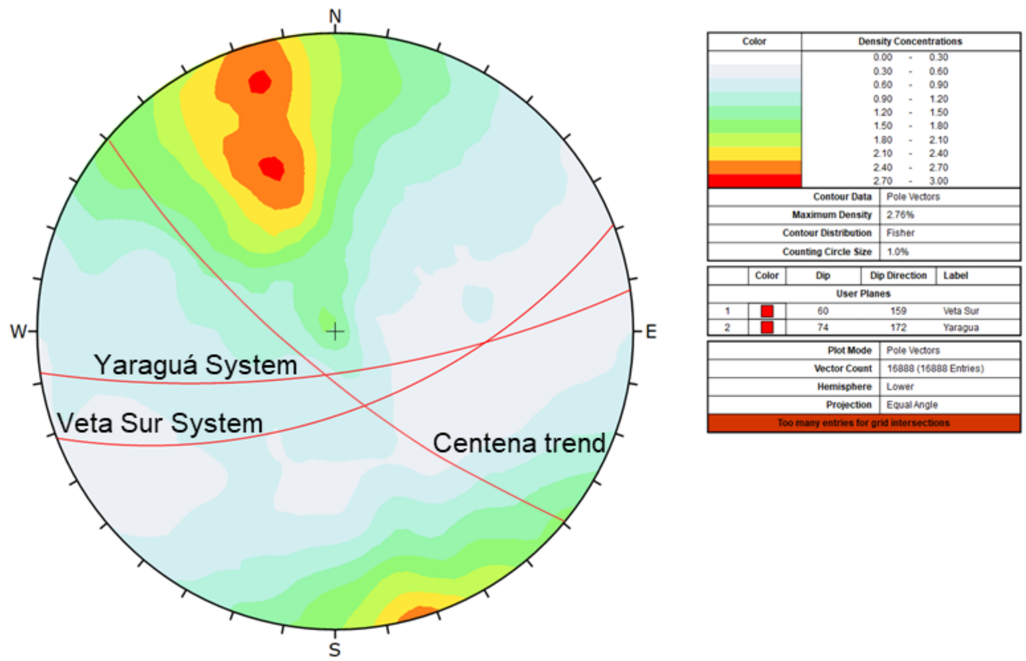

Figure 31. Stereonets of mineralized structures data showing both systems and their orientations, with dip values greater than 70° and almost all of them to the south. The Centena (NW-SE) trend has lower data density but is still visible among the entire data. Equal angle projection and lower hemisphere.

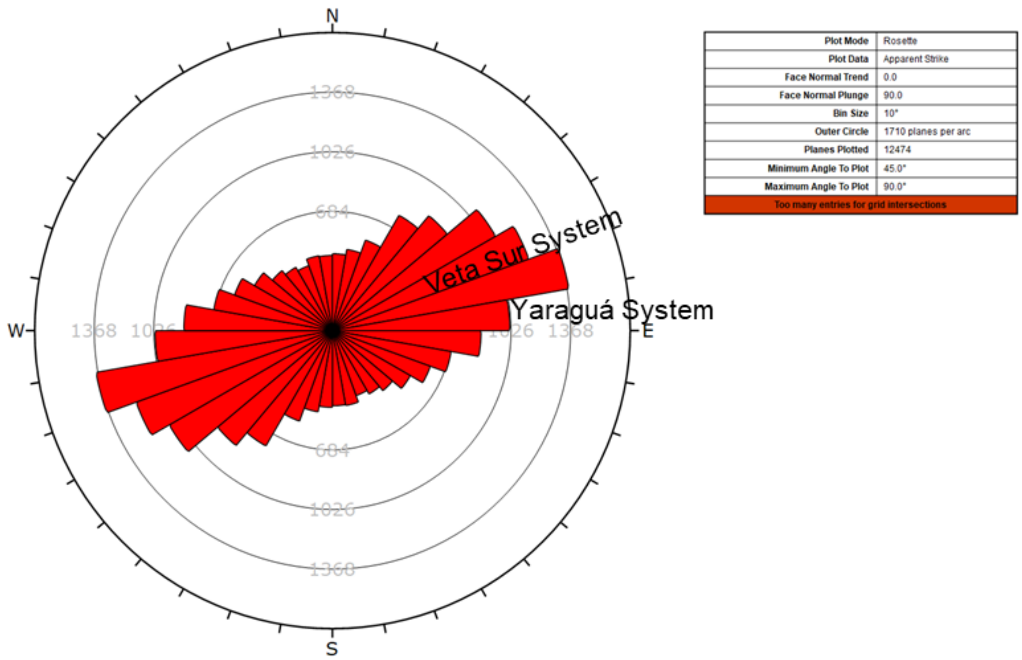

Figure 32. Rossete diagram of strike for mineralized structures that displays the different mineralized systems, each one in its respective trend and associated data density.

Faults were often recorded as “veins-bands”, which is the reason for data of mineralized structures being higher than faults. However, fault data demonstrates the different trends described above (Figure 34).

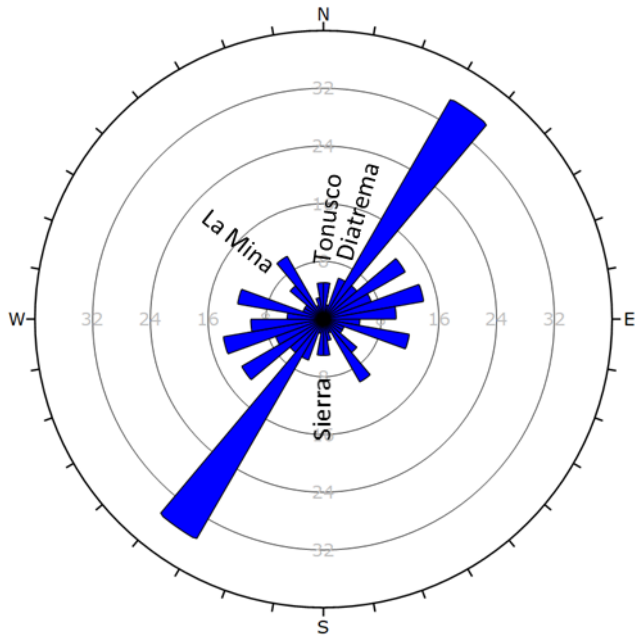

Plot Mode	Rosette
Plot Data	Apparent Strike
Face Normal Trend	0.0
Face Normal Plunge	90.0
Bin Size	10°
Outer Circle	40 planes per arc
Planes Plotted	147
Minimum Angle To Plot	45.0°
Maximum Angle To Plot	90.0°

Figure 33. Stereonet diagram with fault measurements data displaying principal deformation structures at Buriticá gold deposit.

A close follow-up of the orientation of the sedimentary rocks belonging to the Barroso Formation that are exposed in the surroundings of Buriticá gold deposit, exhibit a large-scale antiform structure. The axial plane strikes NE-SW, and the western and eastern limbs dip respectively to the northwest and southeast (Figure 34-a). East dipping limb has low support data due to minor exploration in the area whereas the NW striking beds are associated to La Mina Fault trend. Additionally, limbs show evidence for refolding processes plus faulting (Figure 34-b, 35-a, b).

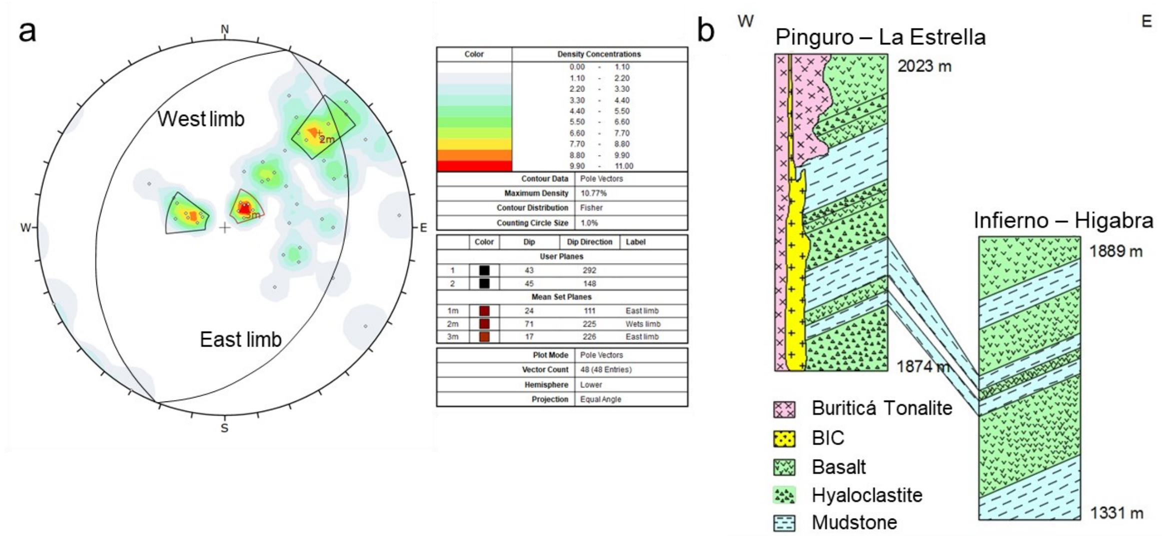

Figure 34. a. Antiform structure data (contoured poles to bedding) representation in stereonets, with limbs having opposing dip directions and an axial plane running N 15 – 20° E. Equal angle stereographic projection, lower hemisphere. b. Stratigraphic column of west limb of the antiform, showing displacement between sedimentary guide layers, all package dipping west.

Recorded mineralized structures during underground mapping and sampling, display several geometries and cross-cutting relationships. Mostly, a near vertical dip of the first-order veins typical of both mineralized systems is evidenced, with high density of extension veins (second-order structures) splaying off the larger ones and occurring in a single block (Figure 35-c, d). The geometric relationships between different order veins result in hanging-wall up movements with shearing evidence as well, and dextral sense regarding the strike component (Figure 26, 35). Texturally, different order structures have banded mineralization with sheared selvages and controlled sericite alteration halos (Figure 35-d, 36-b). Thickness of the first-order veins usually changes along strike and down dip, forming variable structures including jogs and linkages (Figure 36). Low angle but same striking veins between the vertical structures also occur, Cassandra vein a clear example of the latter (Figure 36-b, c, d, 58).

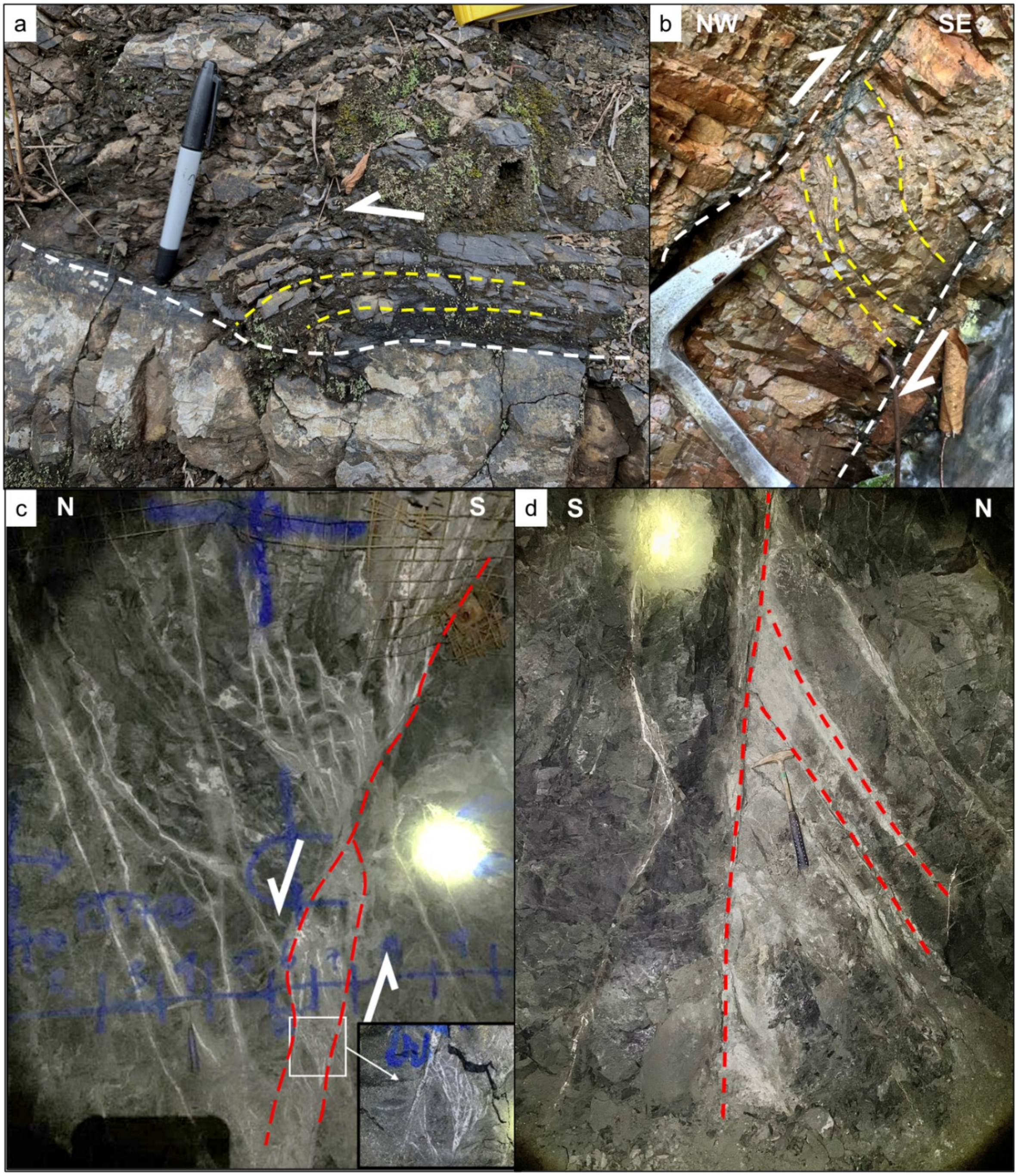

Figure 35. a.b. Surface outcrop of Barroso Fm. sedimentary package accommodating deformation along primarily layering and bedding planes (white dashed lines). Road from Pinguro to La Estrella. c. Ore gallery face view showing extension vein array occurring only in the hanging-wall of the main mineralized structure with composite mineral infill. d. Second-order veins splaying of the vertical first-order structures, with strong sericite alteration associated and controlled. Crosscut wall looking west.

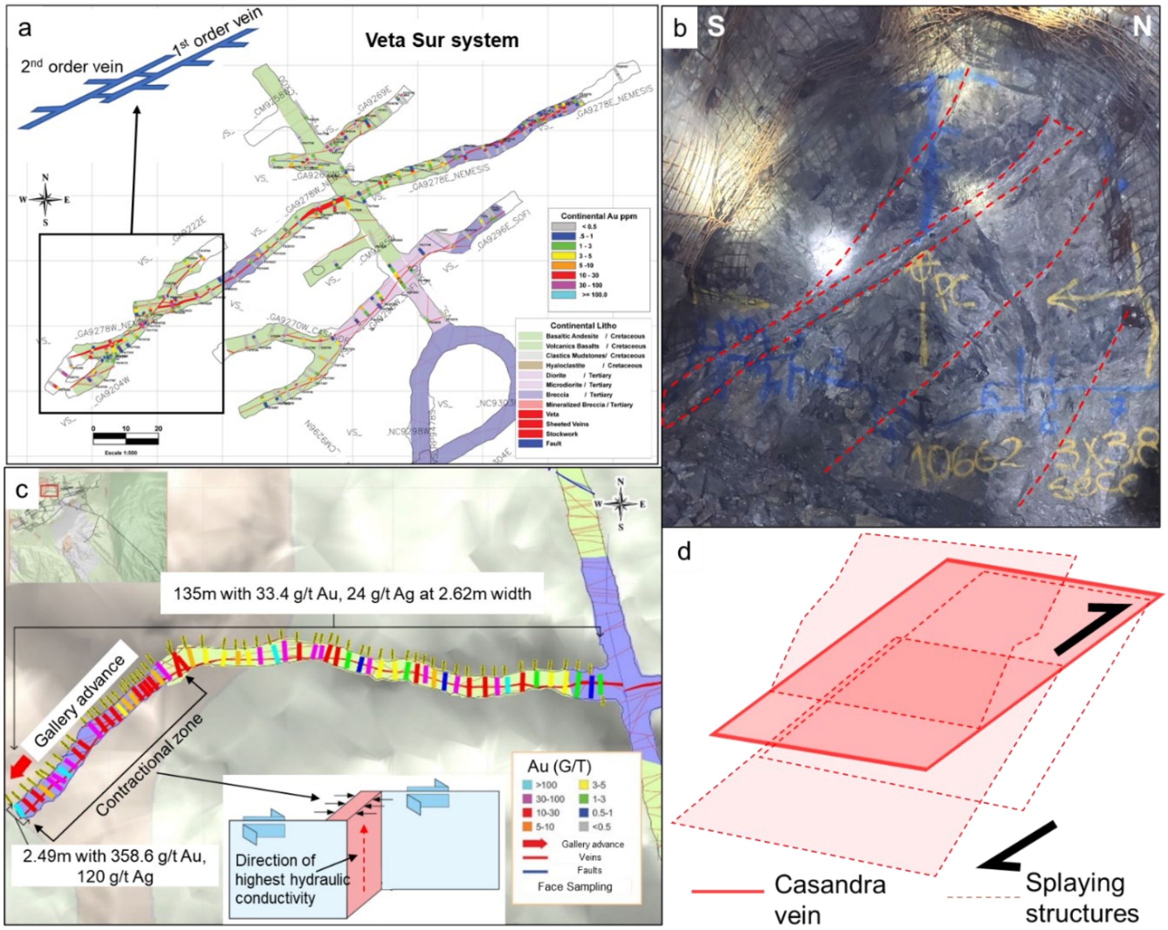

Figure 36. a. Underground development in the Veta Sur vein system displaying the typical behavior between different order structures. b. Face view of the gently dipping Cassandra vein splaying thinner shear veins on both hanging and foot walls. c. Map of the Cassandra vein showing Au-Ag grades values for the entire gallery and by face sample. W-E bounding faults with dextral kinematics form the illustrated schematic contractional jog (Modified after Cox, 2020). d. 3D representation of the Cassandra vein and associated features that define movement sense and grade control locally.

Mylonitic structures from some faults comprise the oldest recognizable contributors to the structural architecture of Buriticá gold deposit, including Diatrema Fault and Tonusco Fault (Figure 37-a). These large mylonitic zones are overprinted by brittle cataclastic deformation in all locations where mylonite was identified (Figure 27). Ductile deformed rocks are now expressed as remnants, appearing as discontinuous zones within, or adjacent to the zones of posterior cataclasite development. At deposit-scale, these structures represent a suite of interlinked high strain zones that localized the development of relatively younger lower strain cataclasite-bearing faults (Figure 37-a, 58).

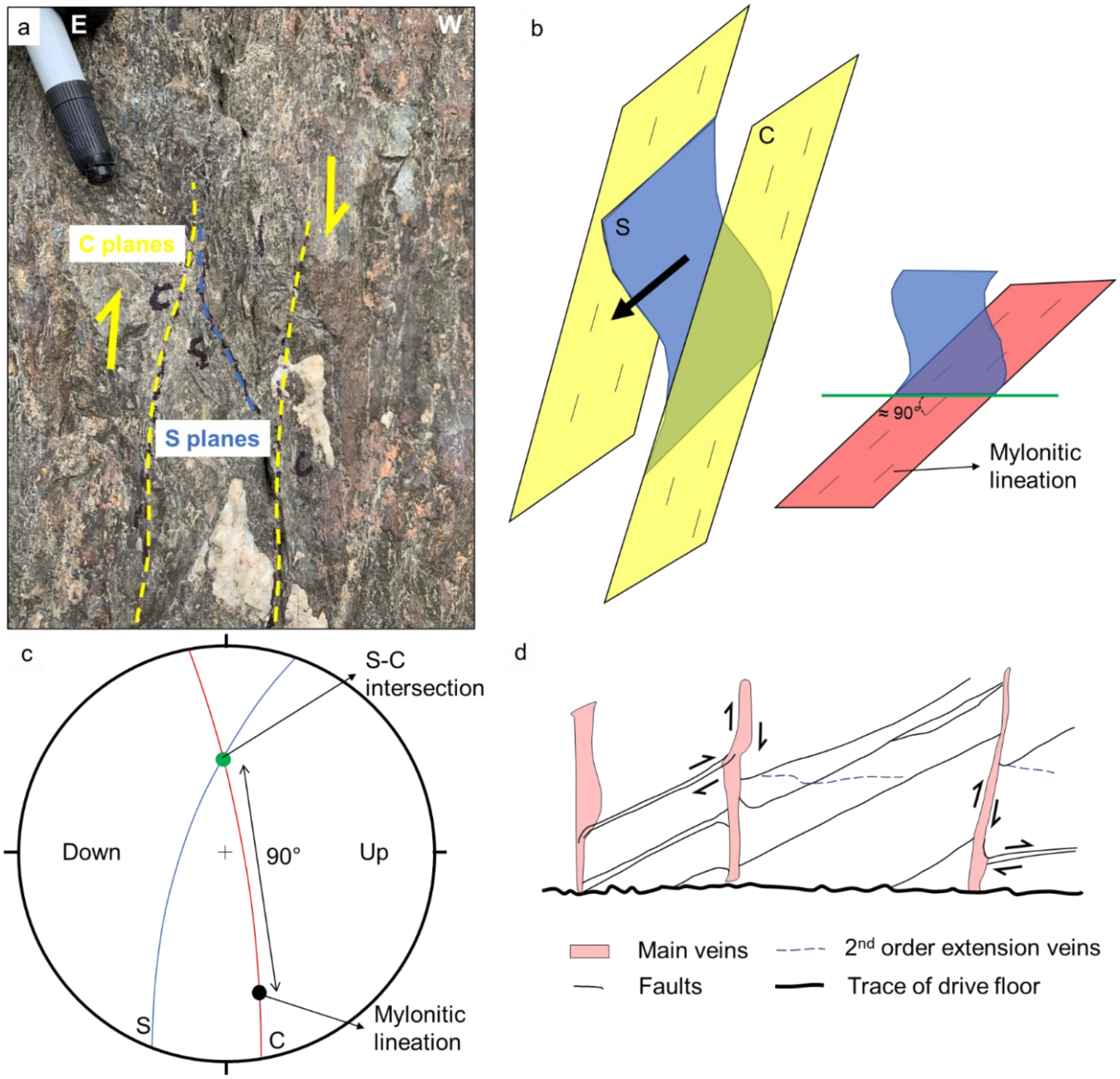

Figure 37. a. Outcrop of deformed basalt with S-C structures in a zone of mylonitic strain, Tonusco Fault. b. Spatial relationship between S-C plane and mylonitic lineation, being high angle intersection. c. Stereographic representation of features at the Tonusco Fault exposure, including movement sense (East-side-up). d. Crosscut wall mapping and documentation of overprinting relationships between all types of structures, especially at development-scale.

5.2. Petrography

From the 17 thin sections analyzed, 6 corresponded to the main host lithologic units at the deposit-scale (Figure 38), and 11 were part of the main mineralized structures (Figure 40). The BIC rocks are principally holocrystalline diorites, medium to fine grain size, with phaneritic and porphyritic textures. Alteration occurrences are variable, including chloritic, sericite, propylitic, potassic. Overprinting relationships show that sericite alteration is the major superimposed event over the remaining alterations assemblages. Opaque minerals are present in all lithologies (e.g., Hydrothermal breccias, diorites, basalts, mudstones, and hyaloclastites) and correspond to disseminated sulphides in general.

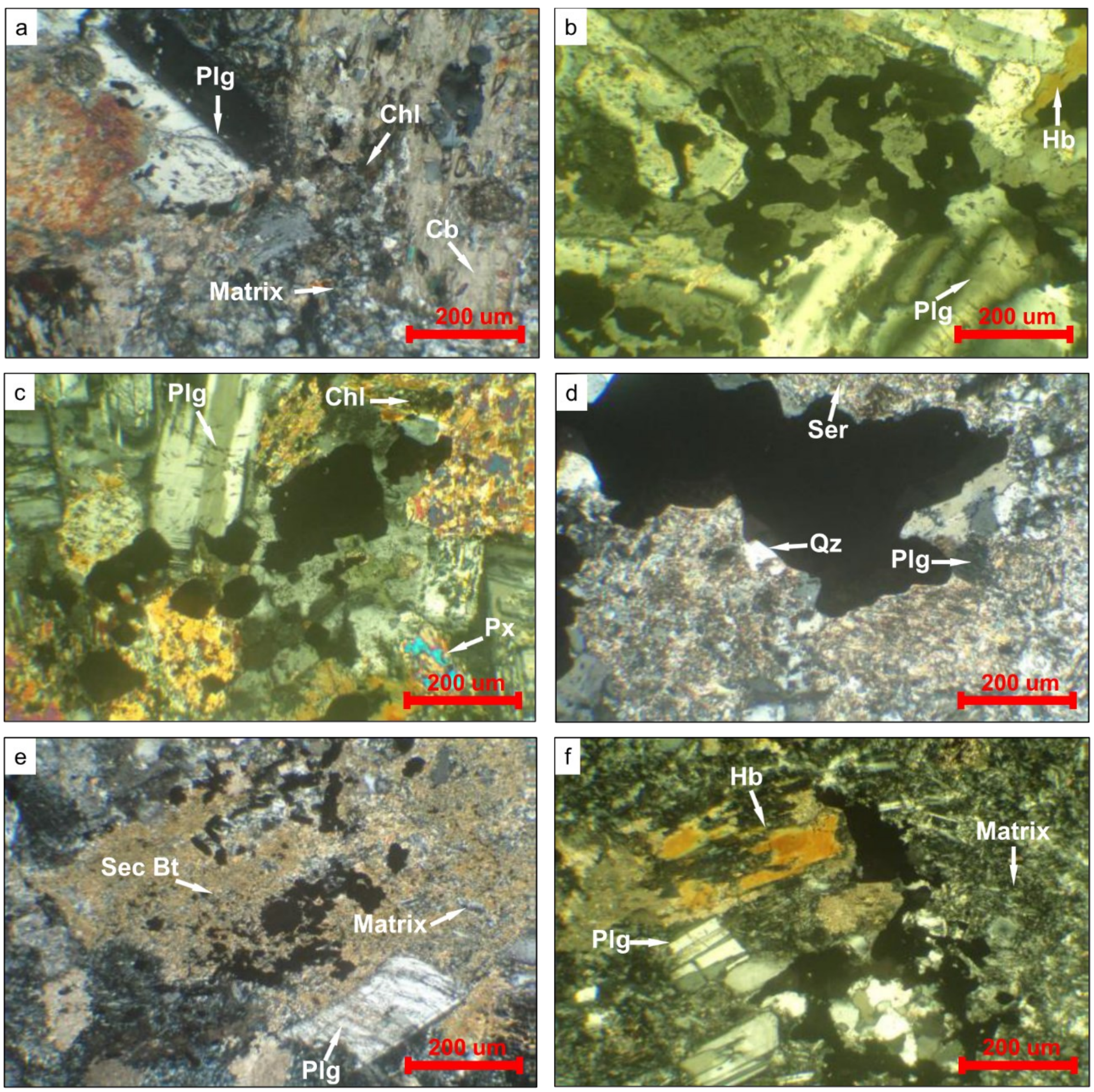

Figure 38. Different hosting lithologies at Buriticá gold deposit in thin section (Cross-polarized transmitted light microphotographs). a. Porphyritic diorite with epidote-actinolite alteration, overprinted by sericite and carbonates. Plagioclase phenocrysts embedded in an altered matrix. Mafic minerals are converted into calcite and chlorite (BUUY152). b. Phaneritic texture of plagioclase and hornblende crystals, and magnetite as opaque. Actinolite replaced hornblende, associated with disseminated epidote (BUUY339D01). c. Holocrystalline pyroxene diorite with chlorite alteration, plagioclase and augite type clinopyroxene crystals. Opaque minerals correspond to magnetite with chalcopyrite inclusions (BUUY249). d. Hydrothermal breccia with strong sericite alteration and relicts of plagioclase, pyrite is in a disseminated style (BUUY455). e. Hyaloclastite with brecciated texture, volcanic clasts and plagioclase in a fine grained matrix, overprinted by chlorite alteration. Sulphides are mostly located in the matrix (BUUY455). f. Quartz-diorite with hornblende and plagioclase disseminated crystals, in a partially sericite-calcite-chlorite altered matrix (GBUS003). Abbreviations: Cb = carbonate. Chl = chlorite, Hb = hornblende, Matrix = matrix, Plg = plagioclase, Px = pyroxene, Qz = quartz, Sec Bt = secondary biotite, Ser = sericite.

Buriticá mineralized structures display extensional textures with subsequent deformation along the strike, generating composite vein systems with several types of mineralogic associations related to the different mineralizing infill stages (Figure 5). In general, principal veins display textures including banded, crustiform, colloform, comb, crustiform-colloform and brecciated (Figure 39). Primary formed textures are superimposed by both successive infill stages and shearing, resulting in a variable distribution of events in a single vein (i.e., Cassandra jog) (Figure 35-c, 36-b, c). In addition, given the deformational related origin of LPMs, common features in relation with vein textures and arrays are shared, such as high density of millimetric thick veins, stockwork, truncated crosscutting relationships, sericite alteration and gangue infill types (Figure 39-d, g). Shear veins are likely to bifurcate mostly along strike, exploiting early formed weakness or other veins (Figure 35-c, 36-b).

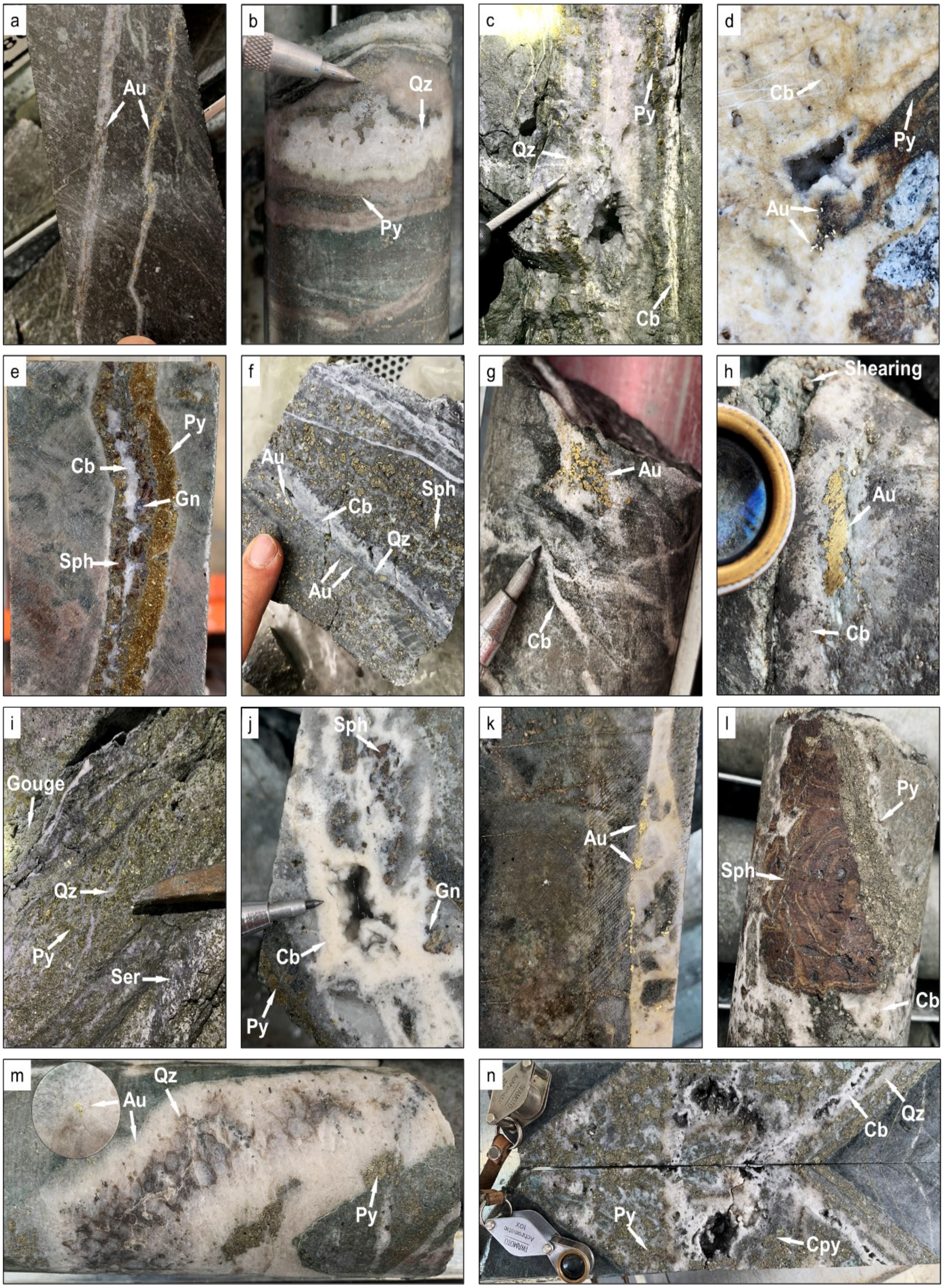

Figure 39. a. Visible gold in sinuous quartz vein. b. Colloform texture with quartz and pyrite. c. Comb texture defined by quartz vein with pyrite bands and sheared selvages. d. Visible gold in contact with

pyrite and calcite. e. Base metal sulphides in vein with banded texture. f. Cassandra vein hand sample with visible gold hosted in quartz, also banded texture inside and sheared boundaries. g. Calcite vein stockwork with visible gold in a LPM zone. h. Brittle deformed vein with visible gold hosted in quartz. i. Outcrop of Cassandra vein with various textures styles, including banded and sheared. j. Common vugs occurrence in high vein density zones. k. High-grade vein with abundant visible gold and hosted in diorite. l. Massive and zoned sphalerite crystal in principal vein. m. Crustiform bands of quartz with pyrite and gold crystals. n. Core sample of massive vein cut in half, displaying the typical banded textures and ore minerals. Abbreviations: Au = native gold, Cb = carbonate, Cpy = chalcopyrite, Gn = galena, Py = pyrite, Qz = quartz, Ser = sericite, Sph = sphalerite.

The metallographic analysis of mineralized structures confirms the different stages defined by (Lesage, 2011), and mineralization is comprised by pyrite, sphalerite, galena, chalcopyrite, pyrrhotite, stibnite and tetrahedrite-tennantite, mainly hosted by quartz and calcium carbonate (Figure 39, 40,). Native gold is within pyrite and sphalerite, and free in quartz and carbonate associated with stage 1 and 3, respectively (Figure 39, 40). Chalcopyrite disease texture is widespread in most of the veins (Figure 40-d). Stibnite, typical of stage 3 (Lesage, 2011), is identified at the outer bands of veins and with quartz plus carbonate (Figure 40-e).

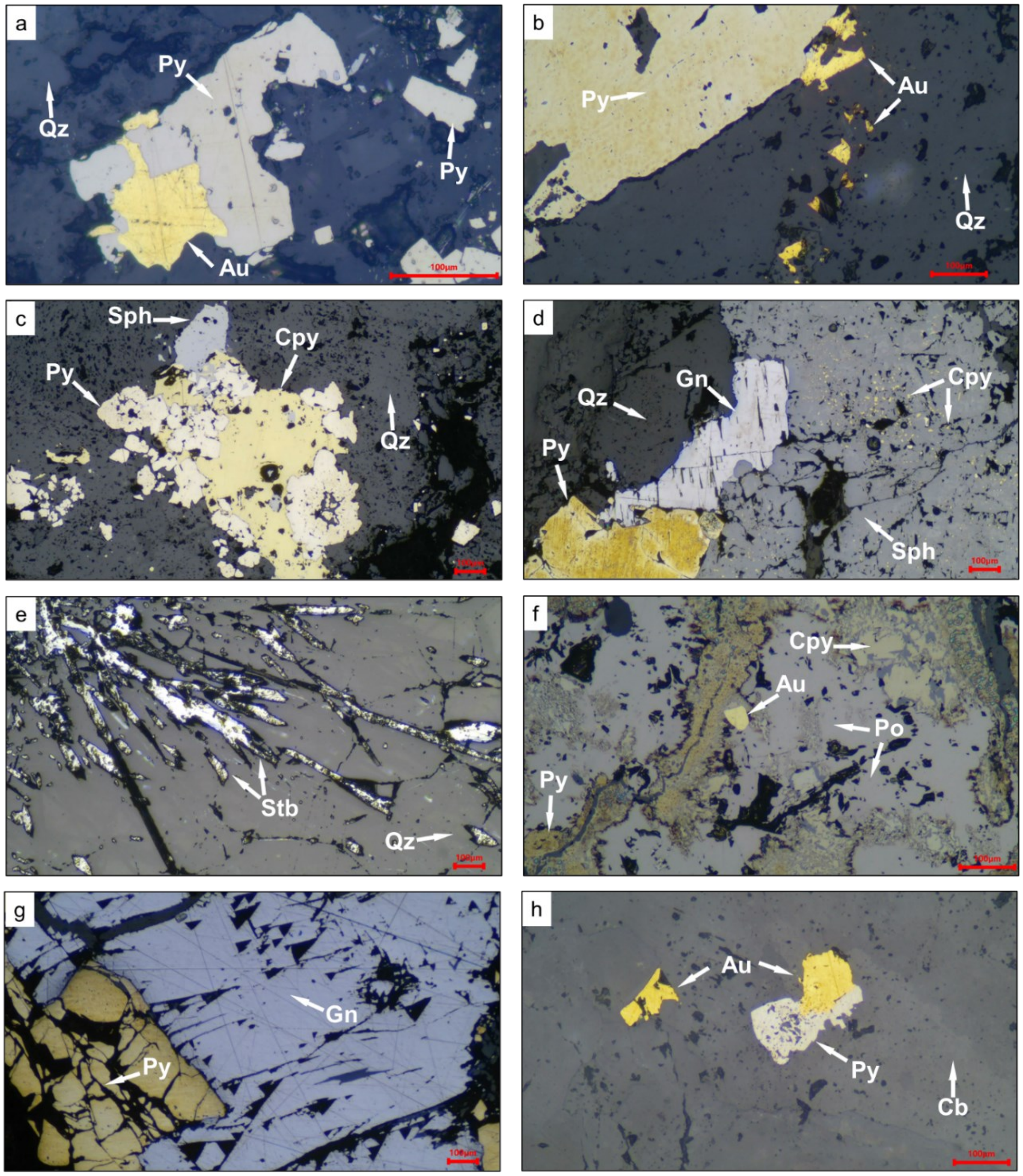

Figure 40. Overall sulphide minerals recorded in mineralized structures (Plane-polarized reflected light microphotographs). a. Native gold in quartz and in contact with pyrite (NEMESIS-2). b. Native gold crystals hosted in quartz (MU_01). c. Association of pyrite, chalcopyrite, and sphalerite minerals in quartz (NEMESIS-2). d. Relative larger sphalerite crystal with chalcopyrite disease texture in Centena vein, also sulphide minerals such galena and pyrite (CTN_01). e. Acicular and radial habit of stibnite crystals (MU_03). f. Pyrrhotite-chalcopyrite relationships with gold inclusions (NEMESIS). g. Well-shaped galena crystal in contact with moderately fractured pyrite (SA_03). h. Native gold hosted in quartz and carbonate, part of the gentle dipping Cassandra vein (Cassandra). Abbreviations: Au = native gold, Cb = carbonate, Cpy = chalcopyrite, Gn = galena, Po = pyrrhotite, Py = pyrite, Qz = quartz, Sph = sphalerite, Stb =stibnite.

Deformation at the microscopic scale is evidenced by moderate fracturing of the banded mineralization, particularly in pyrite. Brittle behavior of this mineral results in fractures at a high angle to the long axis of the grains, this being a consequence of ongoing deformation after growth (Figure 41). The latter defines permeability enhancement activity that has resulted in new mineral infill of pyrite plus quartz.

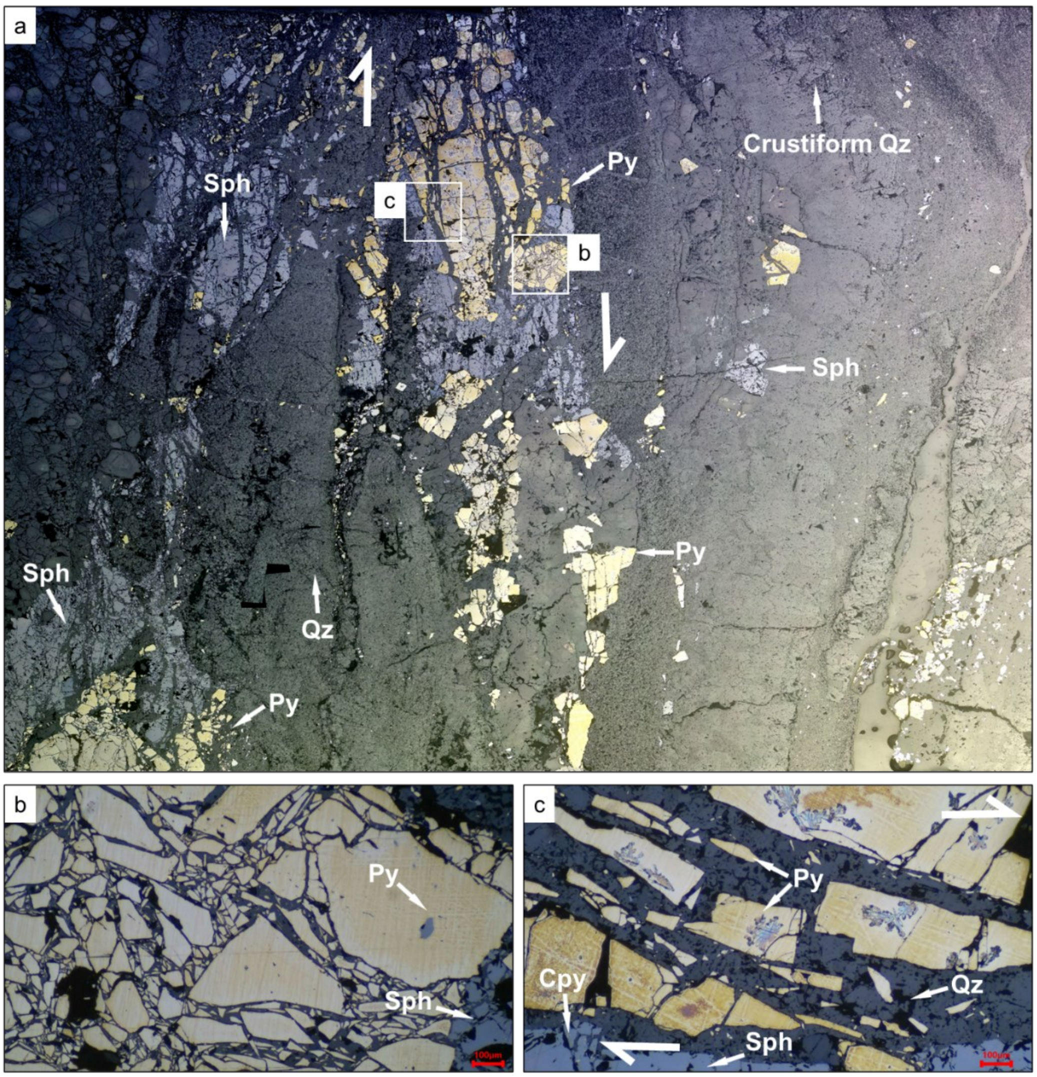

Figure 41. San Antonio vein and recorded deformation features at microscopic-scale (SA_01) (Plane-polarized reflected light microphotographs). a. Panorama view of whole thin section, displaying typical banded and crustiform textures, with subsequent brittle deformation. Arrows define apparent sense of movement bases on pyrite crystals asymmetry. White squares are insets for “b” and “c” microphotographs. b. Moderately brittle deformed pyrite crystal with quartz infill. c. High angle fractures to the long axis of pyrite crystals. Arrows define apparent sense of movement. Abbreviations: Cpy = chalcopyrite, Py = pyrite, Qz = quartz, Sph = sphalerite.

5.3. Lithogeochemistry

The geochemistry database comprised all the assayed drillholes and surface/underground samples. Main rock units, which include Barroso Formation, Buriticá Tonalite and BIC, were analyzed through immobile elements for rock classification purposes and tectonic discrimination. Barroso Formation comprised two members: sedimentary and volcanic. Volcanic breccias and basalts with sea floor alteration corresponded to 6,680 samples, while the sedimentary package of dark and grey mudstones covered 1,523 samples. The BIC incorporated both diorites and magmatic-hydrothermal breccias mainly located in the Yaraguá vein system, those were 9,345 points within the database. Finally, medium- to coarse-grained tonalite of the Buriticá Tonalite unit to the west were associated with 1,974 samples. Different hydrothermal alterations are widespread in every sample included in this analysis, being of variable intensity. Nevertheless, petrogenetic diagrams were used with the least altered rocks possible.

The relative ages of the host rock formation were analogously observed through the Ce Vs La binary diagram. The already known Cretaceous aged Barroso Formation plots under Ce < 25 ppm – La <12 ppm in Figure 42. Buriticá Tonalite plots in the same space of the Barroso Formation, as well as the BIC, giving Cretaceous and Tertiary ages respectively (Figure 42). The Sc Vs Ce plot correlates in Figure 43, constraining the geologic units as a function of the Sc values. Volcanic rocks of the Barroso Formation and Buriticá Tonalite are well defined below Ce < 25 ppm and 0 – 55 Sc ppm.

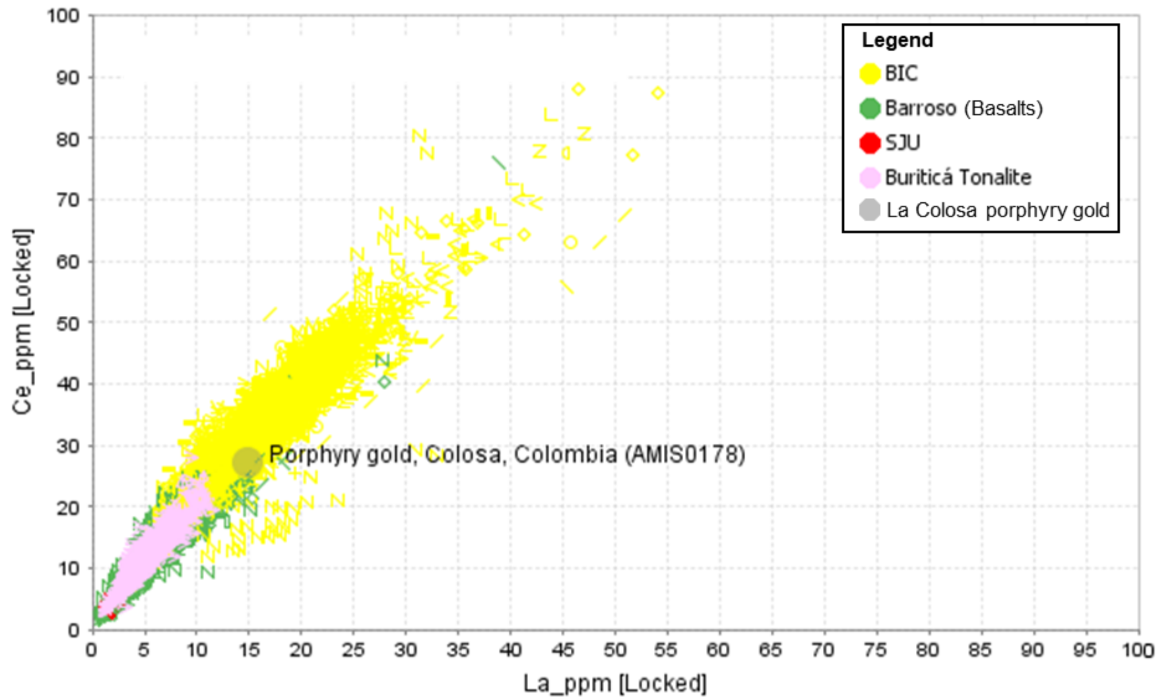

Figure 42. La Vs Ce plot showing different rock and host formations of the Buriticá gold deposit. For comparison, the La Colosa porphyry gold is shown as the gray dot (ioGAS).

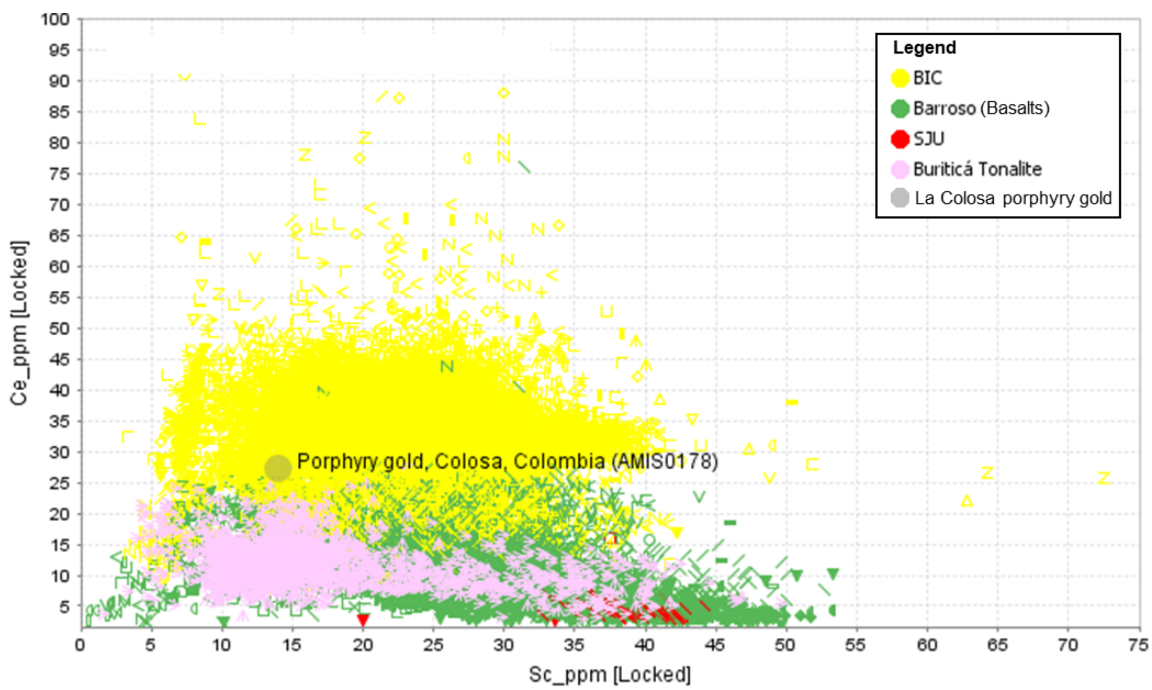

Figure 43. Binary plot of Sc Vs Ce displaying the well-defined distribution of the different geologic units. For comparison, the La Colosa porphyry gold deposit plots in the same field of the BIC.

Samples from the Barroso Formation and its volcanic member are defined by a high content of Ni and Cr (Figure 44), showing an enrichment trend. Values higher than Cr 400 ppm and Ni 250 ppm refer to the San José de Urama unit, which comprises relatively more primitive and basalt-related rocks cropping out east of the Tonusco Fault. The Buriticá Tonalite and BIC are mostly below Cr 350 ppm, whereas data plotted over this value is associated with basaltic fragments in igneous and brecciated bodies.

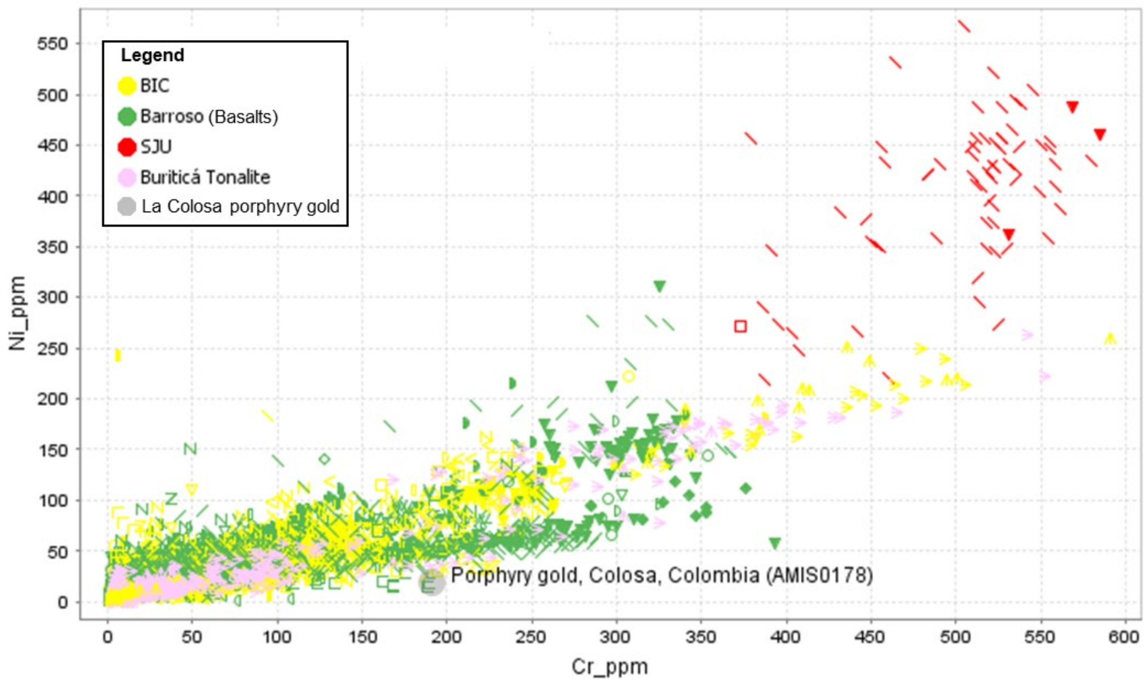

Figure 44. Cr and Ni constrained with the principal rock formations involved in the Buriticá deposit. Most of them are scattered mainly in Cr content and similar Ni. The values plotting in the top right of the diagram are from the San José de Urama unit (SJU).

Geochemistry of the magmatic rocks shows the Buriticá Tonalite to be scattered in both fields (tholeiitic and calc-alkaline affinities), whereas the BIC plots only in the calc-alkaline field, similar to the average node of La Colosa porphyry gold (Figures 45, 46; AFM, Cabanis & Lecolle, 1989).

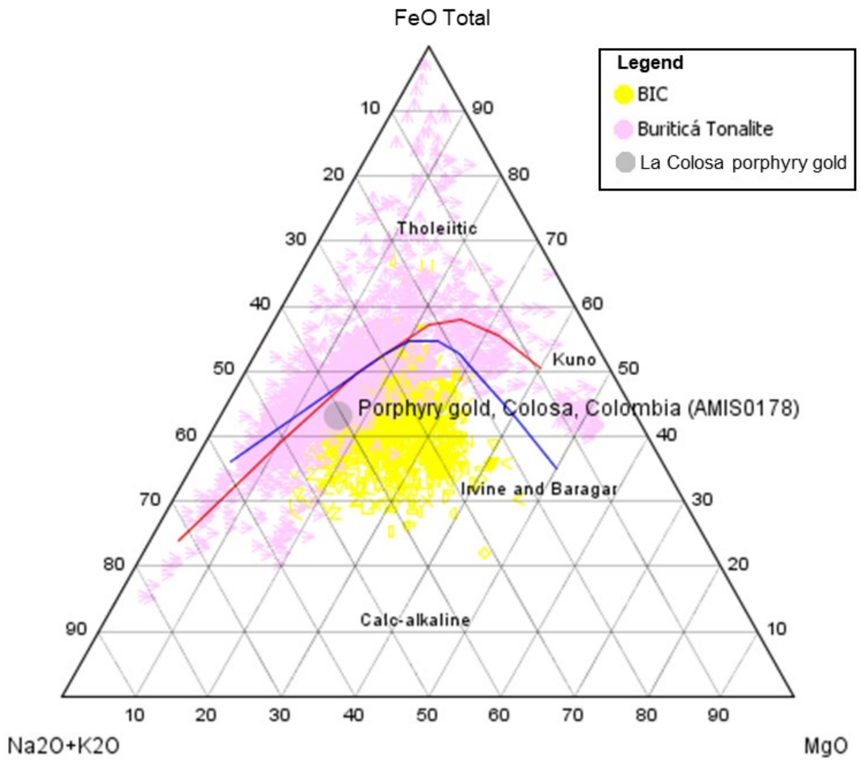

Figure 45. AFM diagram for geochemical affinity. The Buriticá Tonalite is widespread in tholeiitic and calc-alkaline fields while the BIC (least altered rocks) plots in the calc-alkaline affinity as well as the La Colosa porphyry gold deposit node. Major oxide data was averaged through an ioGAS™ conversion.

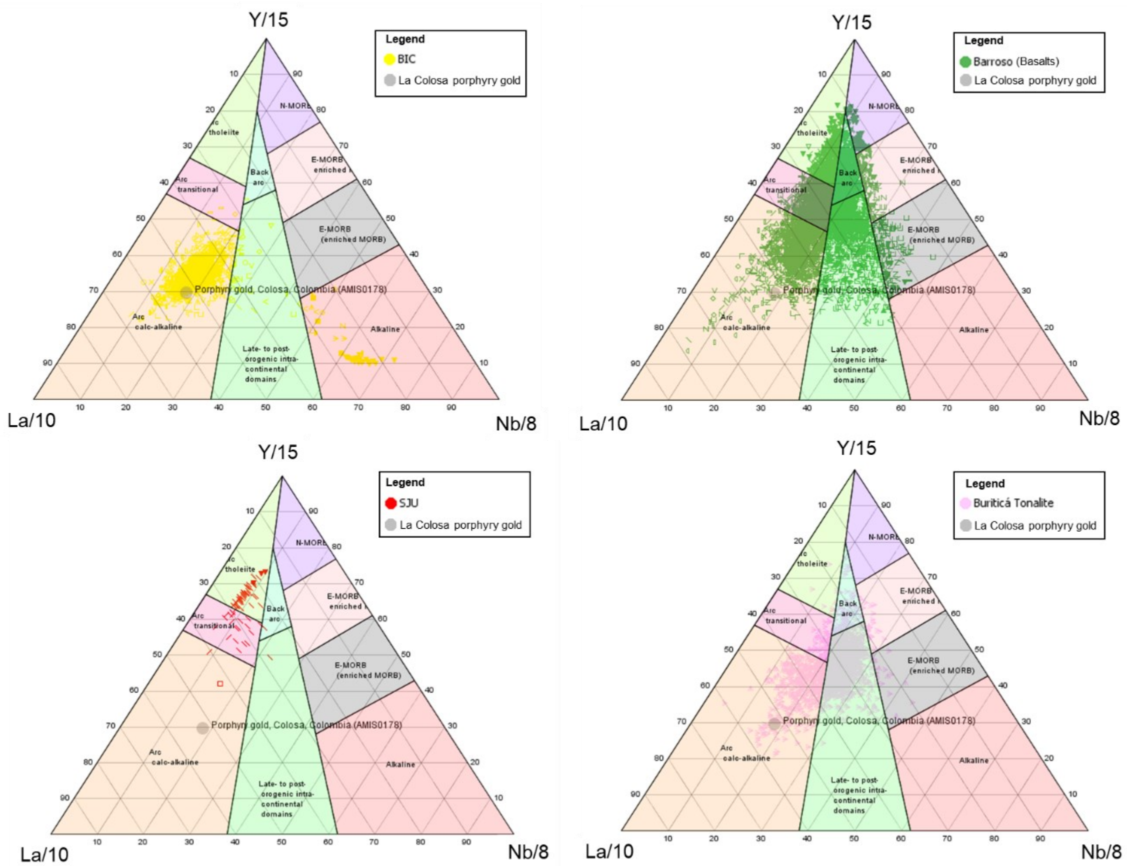

Figure 46. Tectonic classification of mafic igneous rocks. The BIC plots in the arc calc-alkaline domain; basalts from San Jose de Urama plot from transitional to tholeiite arc, Barroso Formation plots in several fields, E-MORB, N-MORB, back and arc tholeiite fields; the Buriticá Tonalite is scattered between arc calc-alkaline and late- to post-orogenic intracontinental fields (Cabanis & Lecolle, 1989).

Additional tectonic discrimination diagrams define the calc-alkaline affinity for the BIC, and the basaltic-andesitic associated rocks. The Barroso Formation volcanic rocks plot in the field of Island Arc Tholeiite (Figure 47; Hastie et., al 2007; Mullen, 1983, Pearce et al., 1984).

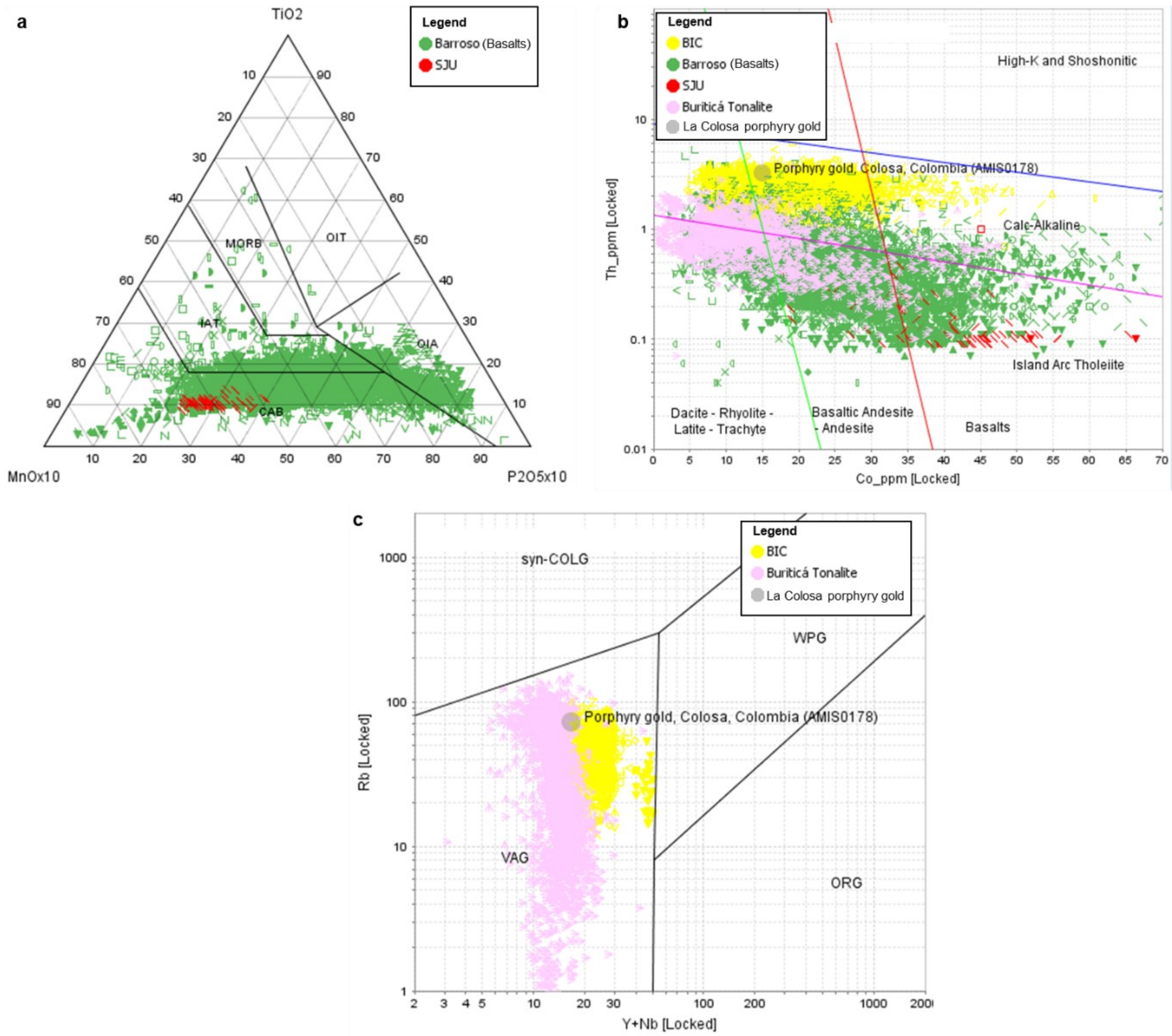

Figure 47. a. Basaltic andesites and basalts of oceanic regions diagram (Mullen, 1983). The BIC and Barroso Formation are defined in the Island Arc Calc-Alkaline field and Island Arc Tholeiite, respectively. b. Co-Th diagram (Hastie et al, 2007) discriminating affinity of rocks (least altered) from the Buriticá gold deposit and host rock formations. La Colosa gold deposit node is plotted within the same field of BIC. c. In the Y+Nb - Rb plot (Pearce et., 1984), the intrusive igneous bodies are restricted to the VAG field (volcanic arc granites), correlated with the calc-alkaline definitions of previous discrimination diagrams.

5.3.1 Hydrothermal alteration

Based on core logging, surface and underground mapping, Buriticá gold deposit records several hydrothermal alteration types which are typical of a porphyry copper deposit (Figure 48, 58). Propylitic (chlorite + epidote + calcite ± actinolite) alteration is the most extensive assemblage which covers the entire BIC and Barroso Formation at deposit-scale. It occurs as replacement of mafic minerals and mostly in a disseminated style (Figure 38-f, 48-e). Evidence of overprint on potassic alteration is common, resulting in embedded blocks of secondary biotite mainly within the BIC (Figure 48-b). Potassic (secondary biotite + magnetite ± K-feldspar) alteration is overprinted by all the remaining alteration assemblages (Figure 48-f). The style is pervasive and more related to the BIC unit. Chloritic (chlorite alone) alteration is similar in distribution and style as of propylitic alteration (Figure 48-f). Sodic-calcic (albite + actinolite ± epidote) is not very characteristic but is present in the diorites of the BIC. The mineral assemblage and style are reflected particularly in veinlets (Figure 48-a). Regarding the volcanic rocks (basalts, hyaloclastites) of the Barroso Formation, early formed sea-floor alteration is observed with a disseminated style and in rims of pillow lavas (Figure 48-c, l). Sericite (illite + muscovite) alteration is associated with the late stages of hydrothermal alteration of the deposit and importantly as the one related to the Au mineralizing events. Intensities range from moderate to pervasive which result in partly obliterated primary textures, both in hydrothermal breccias and along vein halos (Figure 48-d, g, h, i, 50).

Lithogeochemically, hydrothermal alteration and intensities were also assessed through the trace elements analysis of 411.609 samples. In the Ca-K-Na plot, the entire data for Buriticá deposit, including all Au ranges and host rocks, defines a greater population of rocks with weak or no alteration, and a smaller population related with strong alteration (Figure 49), with a trend (white dashed line) through the contoured zone.

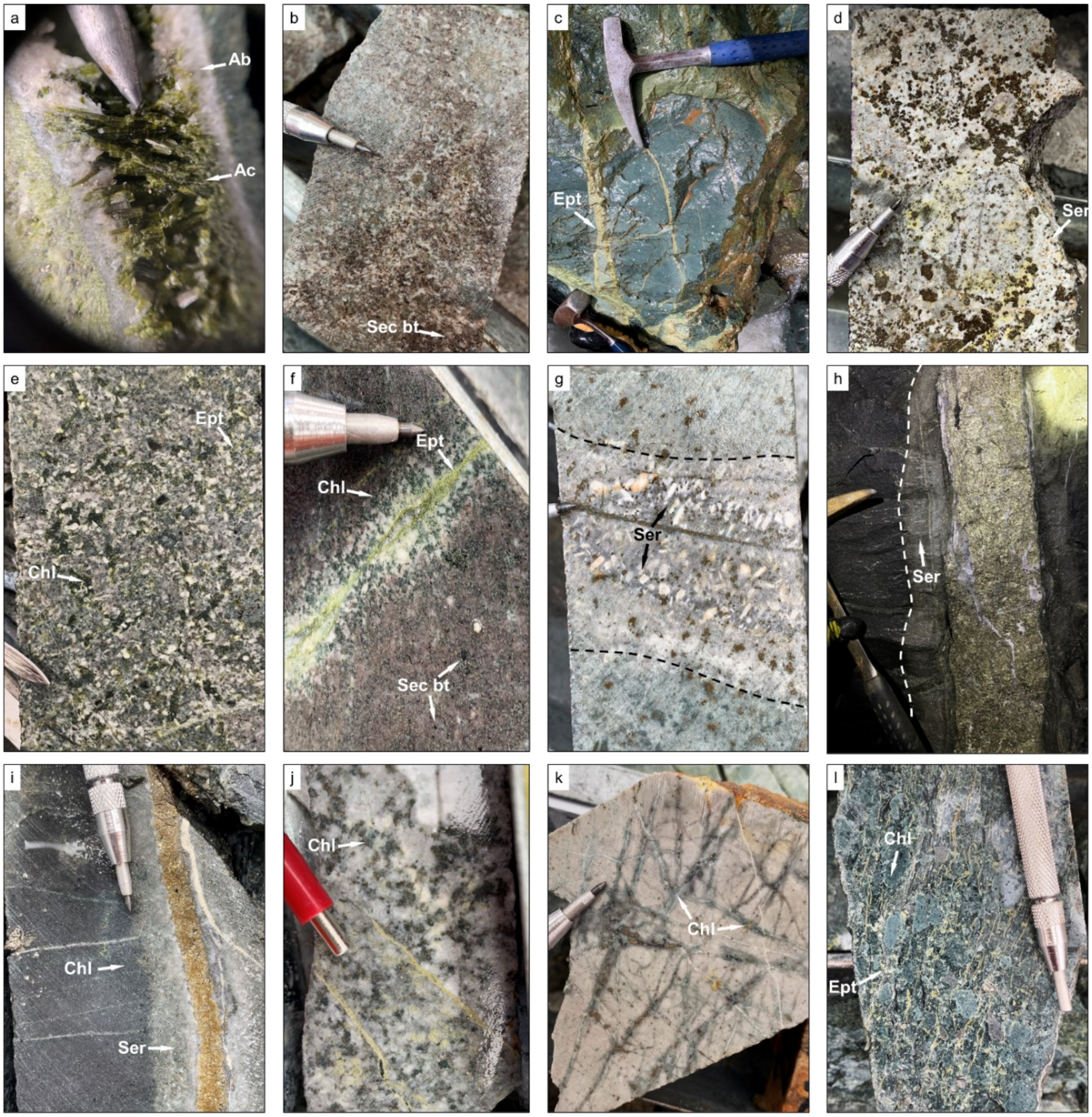

Figure 48. a. Vein of actinolite with albite halo. b. Potassic alteration (secondary biotite) with chlorite overprint in diorite. c. Pillow lava basalt with altered rims. d. Strong sericite alteration in hydrothermal breccia. e. Typical chlorite-epidote alteration in the BIC rocks. f. Chlorite-epidote veinlet overprinting potassic altered diorite. g. Sericite-pyrite halo commonly found along the mineralized structures. h. Face view of a vein cutting through diorite and with sericite halo. i. Overprinting relationships between chlorite and sericite vein related alteration. j. Coarse grained tonalite with chlorite and epidote alteration. k. Bleached mudstone with chlorite veinlets and strong alteration. l. Sea floor alteration in hyaloclastite form the Barroso formation. Abbreviations: Ab = albite, Ac = actinolite, Chl = chlorite, Ept = epidote, Sec Bt = secondary biotite, Ser = sericite.

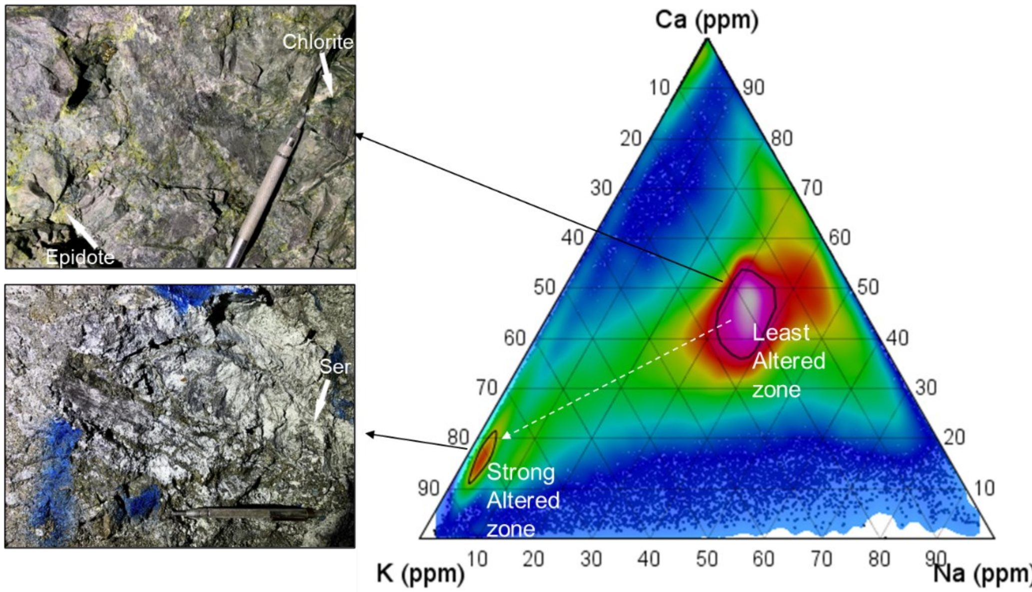

Figure 49. Ca-K-Na ternary plot of all Au ppm ranges, alteration intensity is contoured according to the point density. Chlorite-epidote and sericite alteration examples from drift walls are shown at left.

By looking at the data now filtered by > 0,5 Au ppm, the contoured zones tend to concentrate towards the K apex, forming three main different populations: weak, moderate and strong sericite alteration intensities (Figure 50). The weak population reaches 50% of K and Ca, and 40% of Na. The moderate population is defined by 50 – 80% of K, 5 – 25% Na and 60% Ca. The strong population mostly comprises high content of K (65 –95%), range of Ca from 5 to 35%, and very low Na not surpassing ± 5%. Sericite + carbonates population corresponds to a field near the Ca apex (70 – 100%) and K (0 – 30%).

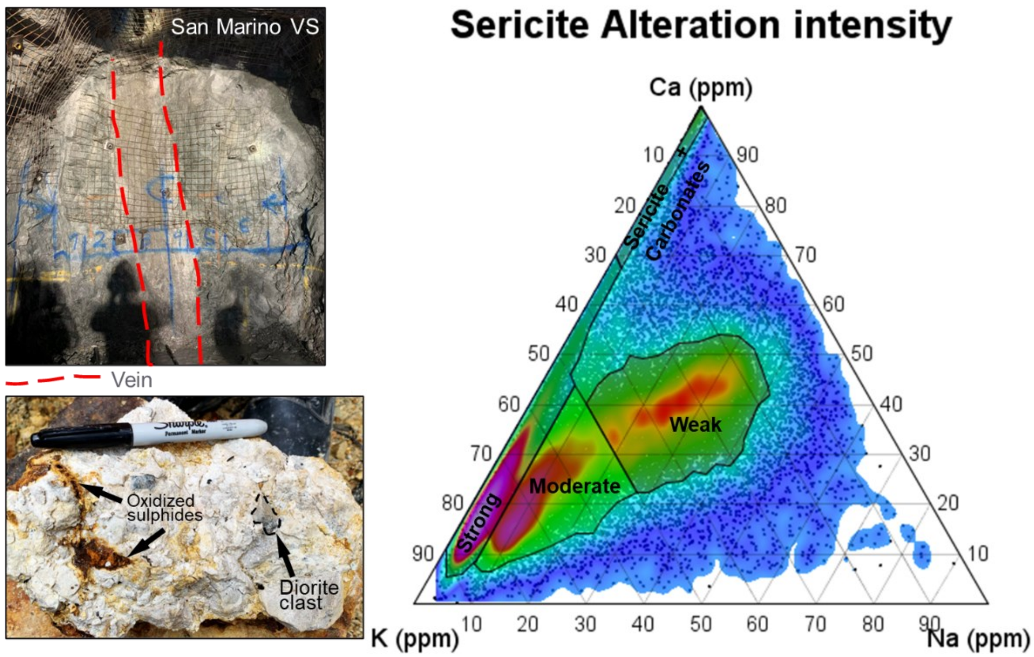

Figure 50. Ca-K-Na ternary plot of Au ppm ranges up to 0.5 ppm, point density contours highlight the different sericite alteration intensities. Sericite alteration stages I and II are shown at left. Upper photo is from an ore gallery face view with controlled sericite alteration along the mineralized structure and the lower one shows hydrothermal breccia bodies in the Veta Sur system.

After defining the fields of sericite alteration intensities, they were constrained with Au values distribution as follows (Figure 51): 0 – 5 Au ppm intervals are in the weak, moderate and strong zones, 5 – 30 Au ppm displays an increase in point density towards the moderate and strong zone, and > 30 Au ppm interval distribution has an affinity for strong alteration zone and sericite + carbonates zone.

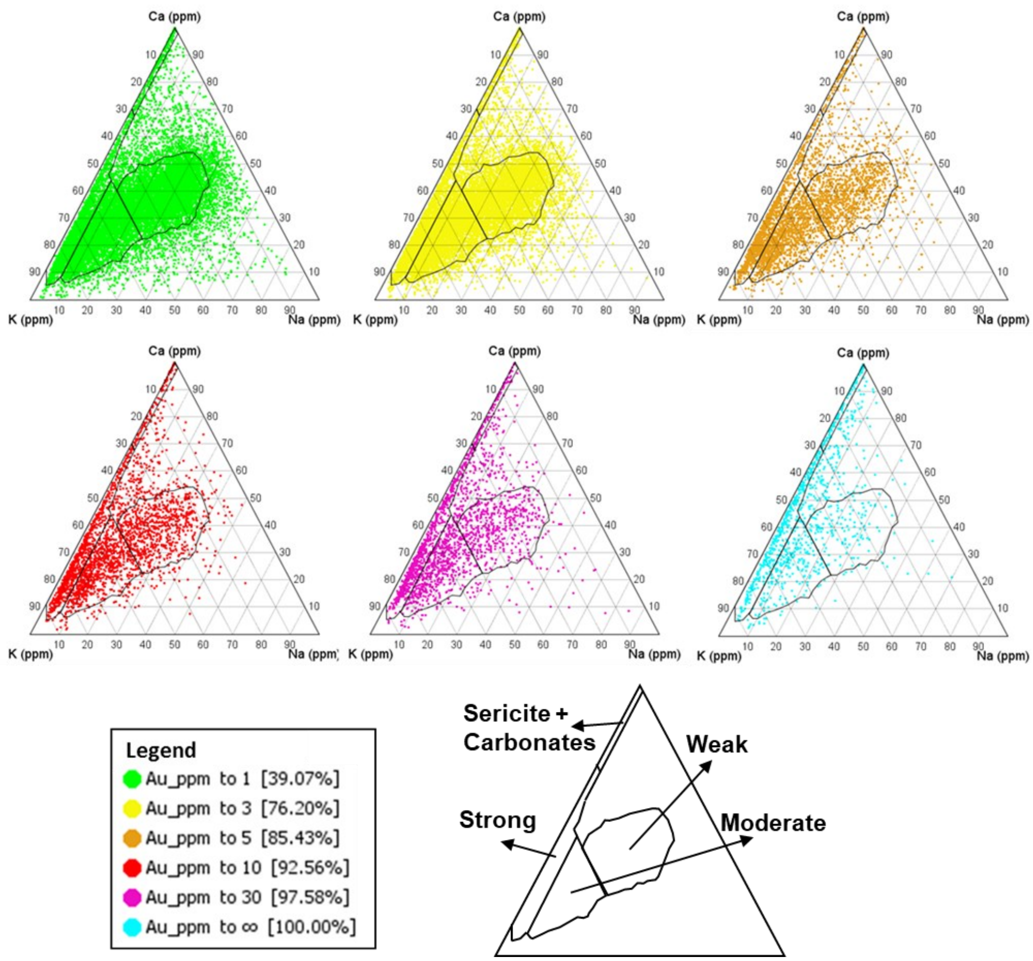

Figure 51. Ca-K-Na ternary plots with defined sericite alteration intensities zones associated with gold grade intervals in Buriticá deposit.

The K/Al versus Na/Al molar ratio plot also outlined the sericite alteration, in which fresh rock plot between 0.2 to 0.5 Na/Al and 0.1 to 0.4 K/Al. Moderate and strong sericite populations plot close to the Muscovite node and remain in the same field without much scattering. Contour distributions differentiated two populations of sericite alteration, consistent with the sericite alteration related to mineralized structures and the other one occurring in hydrothermal breccias (Figure 52). Furthermore, sericite + carbonate points plot in a very thin interval of Na/Al, but following the trend of moderate to strong intensities (Figure 52).

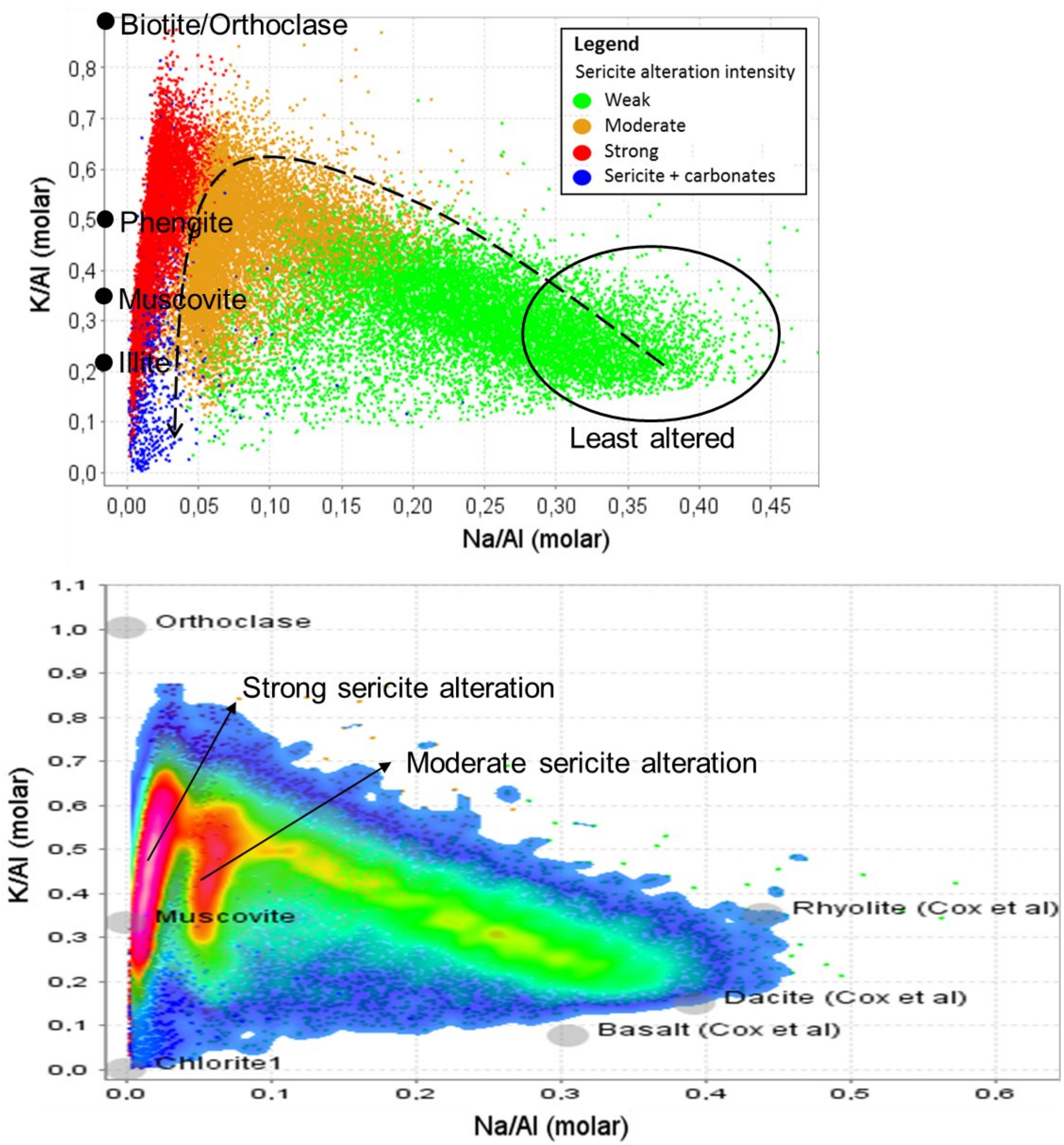

Figure 52. Na/Al versus K/Al molar ratios plot, dashed black arrow represents the alteration evolution trend. Alteration mineral nodes in the K/Al axis represent other alteration types.

The mineral association with pyrite and anhydrite was defined through a Ca-Fe-S ternary diagram, where the different sericite alteration intensities plot scattered but generally near the Fe and S apexes. Population near and towards the Fe apex indicates the magnetite-biotite mineral assemblages. Weak alteration comprises from 10 – 50% Ca, 0 – 40% S and 30 – 70% Fe. For moderate and strong intensities, the values ranges are tighter for Ca 0 – 35%, Fe 30

– 80% and S 15 – 65% (Figure 53-a). The Sericite + Carbonates points are widespread along Ca values and similar Fe and S intervals (Figure 53-a). In an attempt to differentiate K content in potassic and sericite alterations, figure 53-b displays a partial relationship for least altered rocks to the one with minor K content.

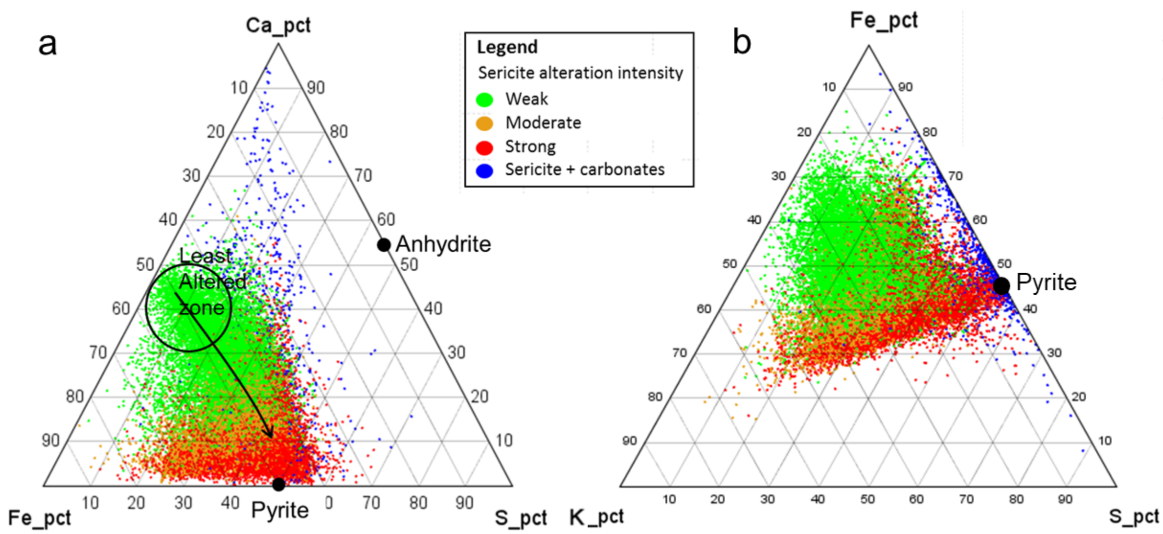

Figure 53. a. Ca-Fe-S ternary diagram displaying pyrite and anhydrite nodes constrained with sericite alteration intensities. b. K-Fe-S ternary diagram. (Differentiation of K content in potassic and sericitic alteration).

The spatial distribution for each sericite alteration intensity range is shown through deposit-scale plan views (Figures 54, 57) and sections (Figures 55, 56). Moderate to strong sericite alteration in Veta Sur and Yaraguá mineralized systems is controlled by steep faults and respective intersections. LPM301 and LPM304 are in tight relationship with the Diatrema and Sierra Faults, while LPM302 is associated with the Tonusco Fault (Figure 54, 55). Strong sericite alteration reaches greater depths in Veta Sur system than in Yaraguá (Figure 55, 56). The foot-wall and hanging-wall of the Diatrema Fault represents zones of moderate to strong sericite alteration, depending on the mineralized system and intersection with other deformation structures. The latter accommodated zones of gold accumulations related with intense sericite alteration (Figure 55, 56).

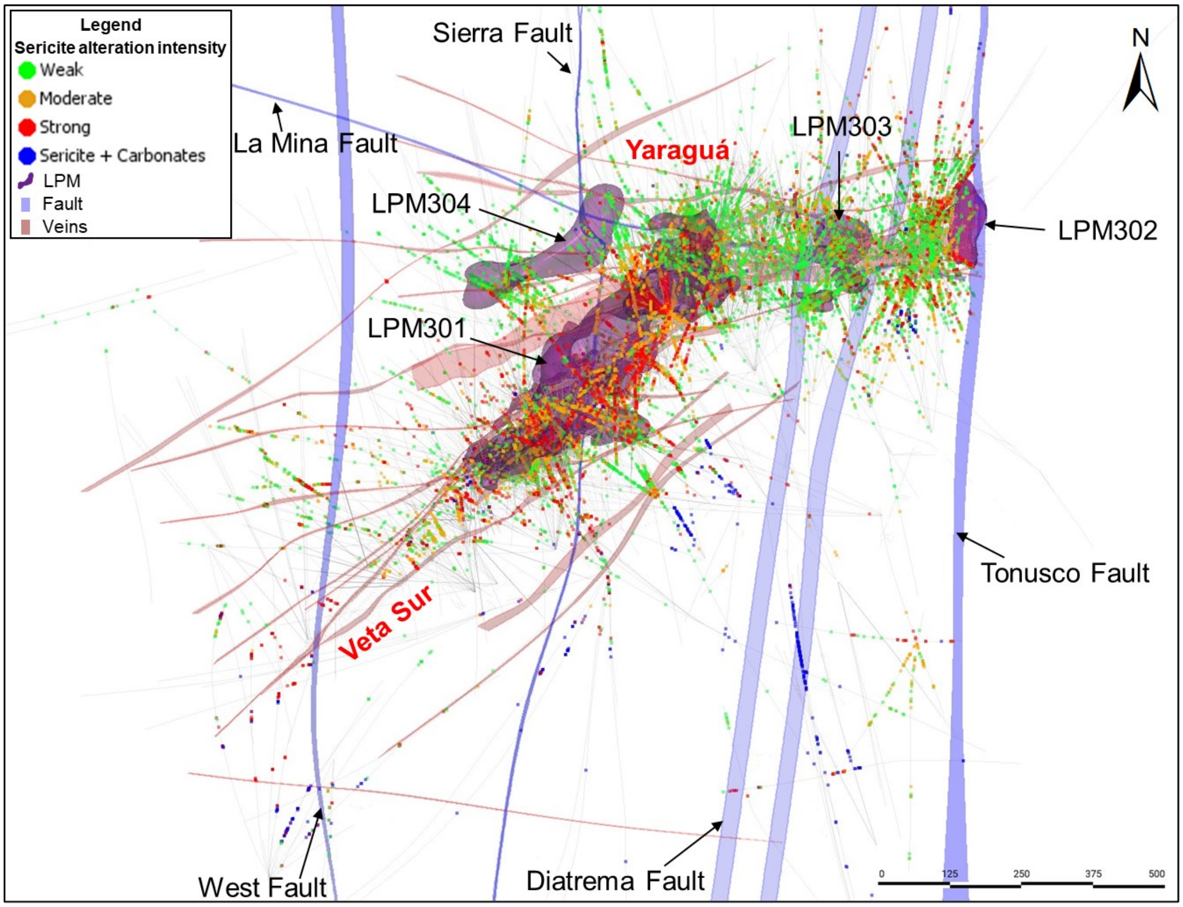

Figure 54. Plan view of mineralized structures (Veins), LPMs and structural geology in conjunction with sericite alteration.

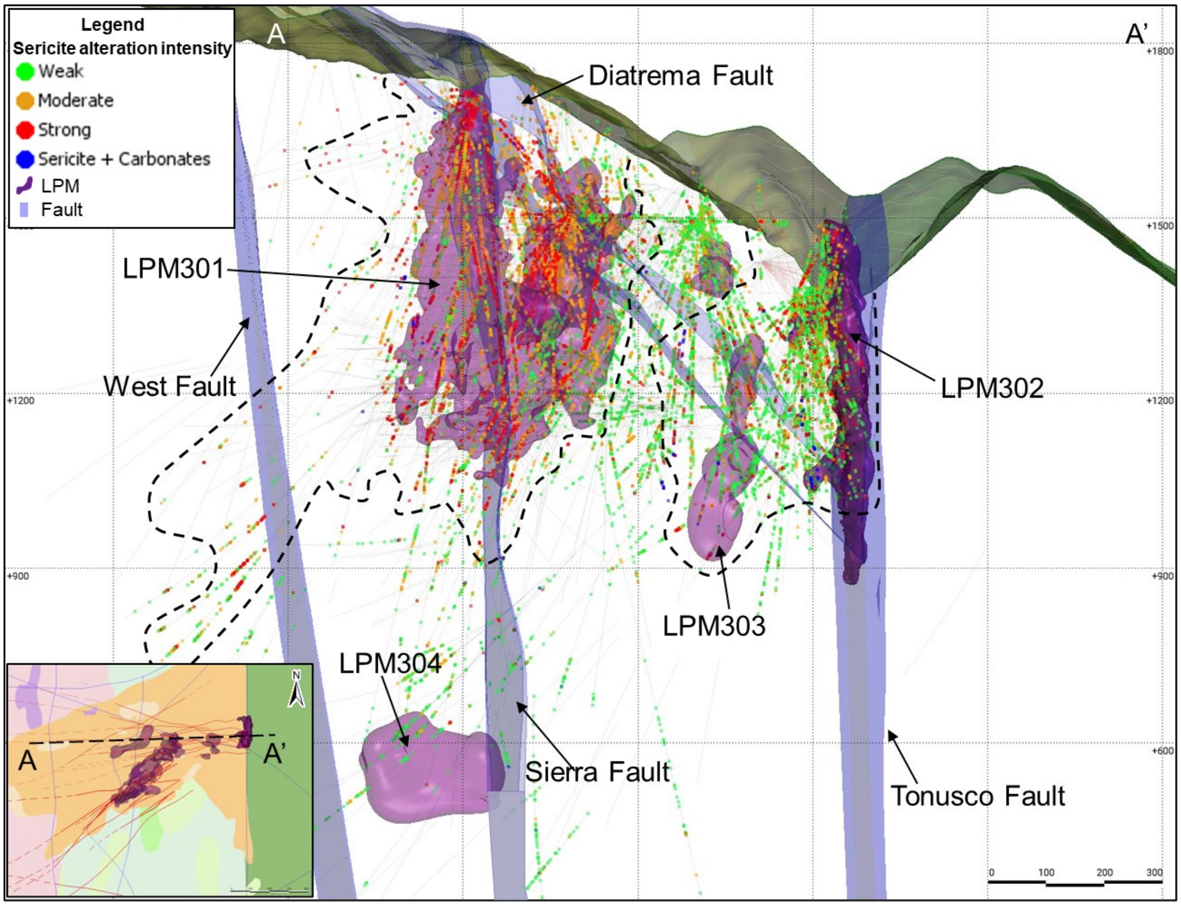

Figure 55. Section view looking north and displaying the fault architecture with its relationship to LPMs and moderate to strong sericite altered zones (black dashed contour lines). Section line along the Yaraguá vein system, 100 m wide.

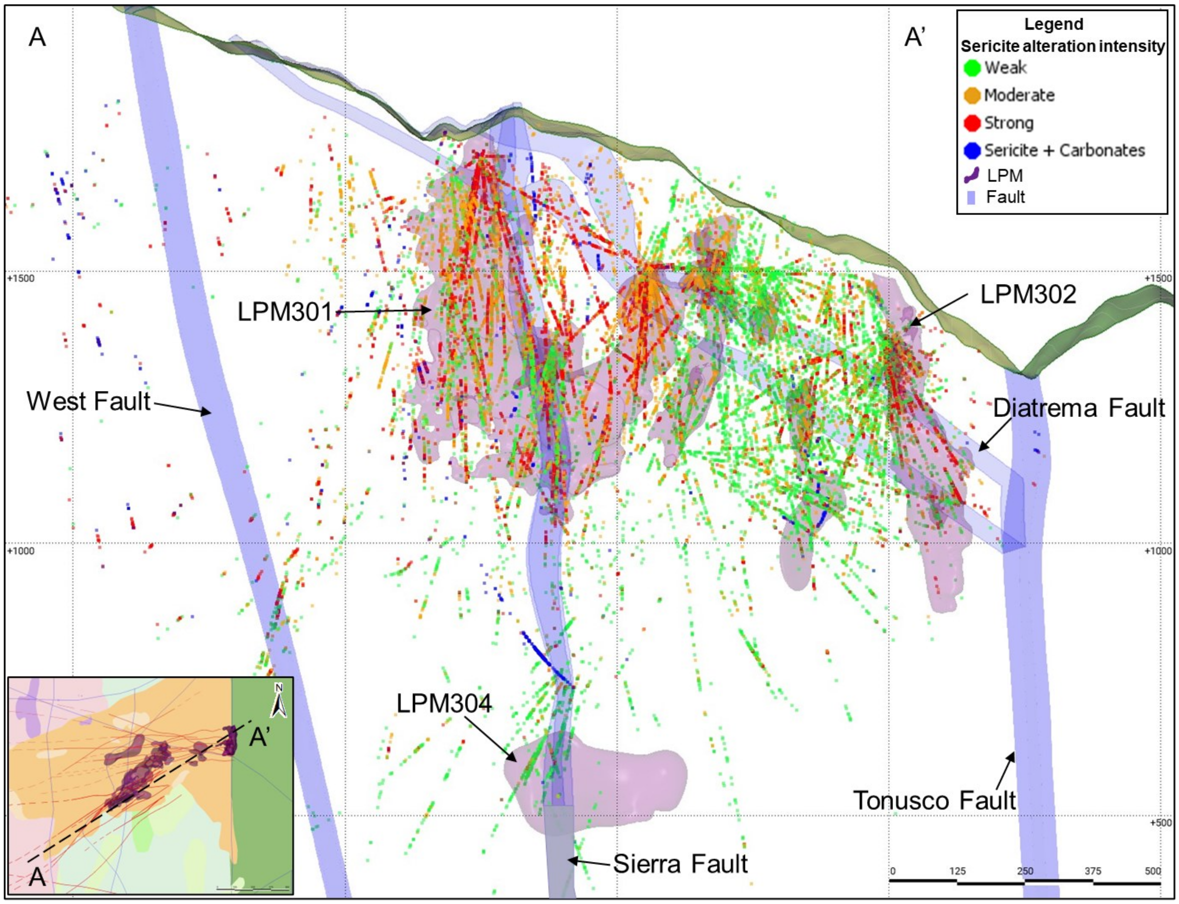

Figure 56. Section view looking northwest and displaying fault architecture with its relationship to LPMs and moderate to strong sericite altered zones. Section line along Veta Sur vein system, 100 m wide.

There were logged 400 km of drillcore through photographs, focusing on the intervals in which any intensity of sericite alteration occurred, the result was then constrained with defined sericite alteration intensities obtained from geochemical procedures (Figure 57). Both methods indicated the same zones and match well. Importantly, even some areas that could not be defined through geochemistry by the unavailability of ICP data, were recognized during photologging.

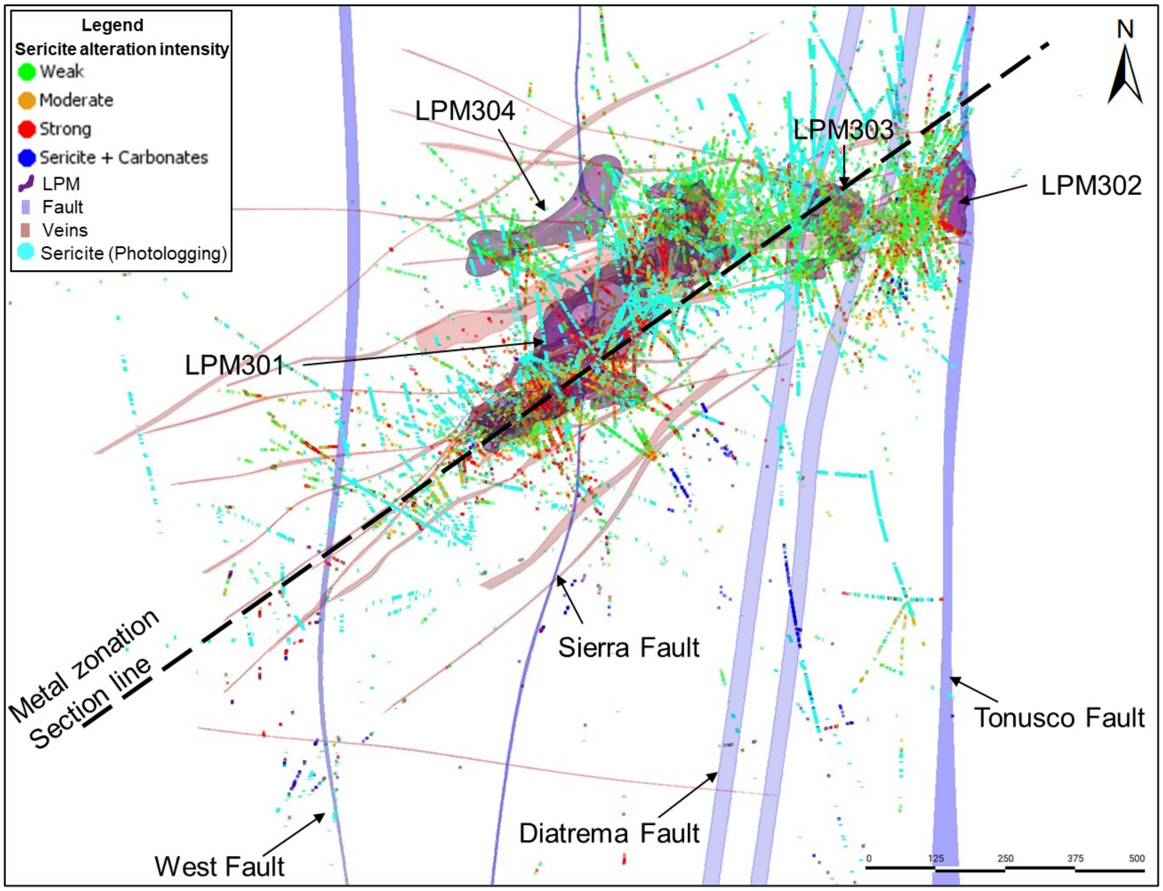

Figure 57. Comparison between sericite alteration characterization from photologging and geochemical mapping methodologies.

The different hydrothermal alteration types in Buriticá gold deposit were identified at all scales and then constrained with the structural architecture at district-scale (Figure 58). It basically resulted in a large propylitic alteration envelope with overprinting sericite alteration on the remaining ones such potassic and sodic-calcic. Volumes of sericite altered rock corresponded to vein halos, hydrothermal breccias, as well as zones of fault intersections (Figure 30-b, 54, 58). Upper part of both Yaraguá and Veta Sur vein systems showed minor intermediate argillic alteration. The easternmost Tonusco Fault played the role of a hard boundary to mineralization, hence for gold related sericite alteration (Figure 59).

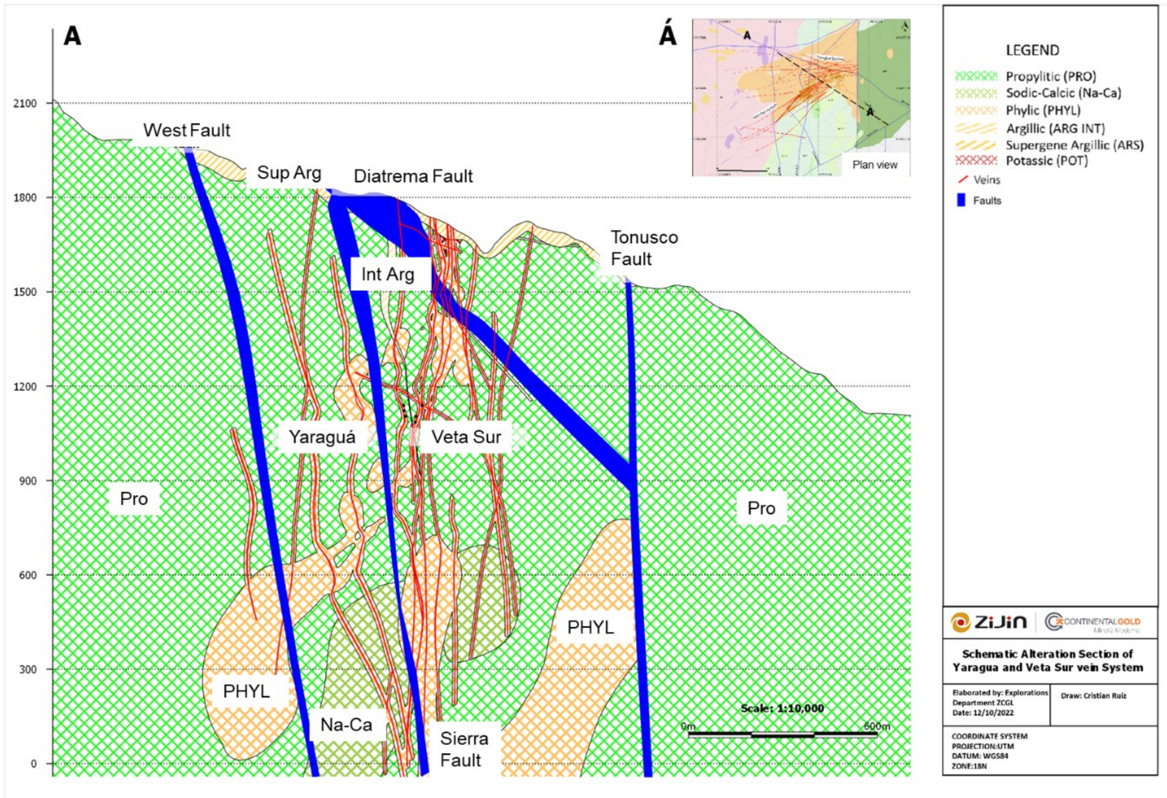

Figure 58. Hydrothermal alteration model for Buriticá gold deposit shown in a section looking northeast. A large volume of rock consists of propylitic alteration while sericite (phyllic in the legend) is only related to the mineralized structures and in between stacked-vertical faults.

As part of the geochemistry assessment, metal zonation and distribution were reviewed and sourced from drillhole assays. Figure 59 illustrates the metal zoning of the key and pathfinder elements applied for Buriticá deposit characteristics, in which a distinct vertical zonation was evidenced. In general, Au and Ag occurrence were from 1,700 to 600 m.a.s.l (Figure 59-a, b). Base metal content (Zn) was associated to the BIC and Yaraguá system, higher values above 1,000 m.a.s.l (Figure 59-c). Te and Bi elements represented the same pattern of Au (Figure 59-d, e). K had the strongest positive correlation with the LPM areas, Sierra Fault and the sericite altered and emplacement-controlled hydrothermal breccias (Figure 59-f). For porphyry related elements, Figure 59-h marked the higher Cu values related to the low Au grade potassic altered zone. Mo contents are localized within the BIC but are not correlated with any other metal (Figure 59-i).

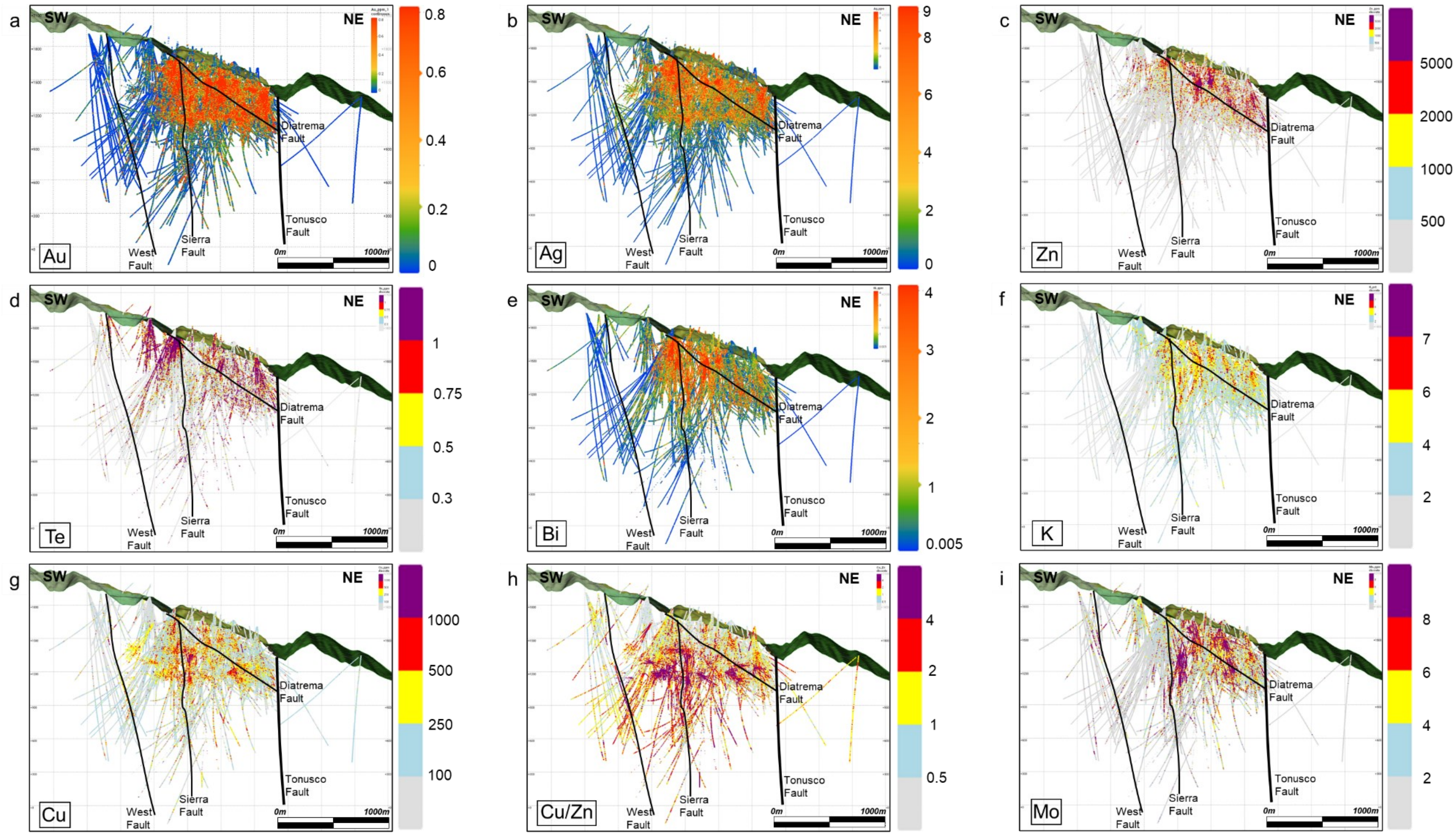

Figure 59. Cross section displaying diamond drill core assays with metal content distribution and zonation. Sample locations are constant for all figures. All values in ppm. Faults are represented by thicker black lines. Section line in Figure 57. a. Au. b. Ag. c. Zn. d. Te. e. Bi. f. K. g. Cu. h. Cu/Zn. i. Mo.

5.4. X-Ray Diffraction

Sampling was carried in the front of an active mine development working at Yaraguá mine (VS_1435RL_GA9136E). Each sample was taken at a specific distance from the mineralized structure according to the type and intensity of alteration. The front was represented by a 78/355 dipping structure, 0.3 m wide, with pyrite, sphalerite, galena, quartz and calcium carbonate. The host-rock was basalt with propylitic alteration, mostly disseminated. Sericite alteration was controlled along the mineralized structure, with strong and pervasive intensity. Chlorite, kaolinite and illite were the identified minerals in the whole sampled section. Based on the distance from the vein and its alteration type, clay minerals occur differently as follows: The mineralized structure is characterized by illite, moving 0.25 m away, there were kaolinite, chlorite and minor illite. Further away (> 0.8 m) the same minerals were identified, but in different proportions. The furthest zone from the mineralized structure is defined only by chlorite and kaolinite. According to the previous mineral qualification, clays phases and their paragenesis were defined and constrained, as a function of the distance from the mineralized structure (Figure 60). In addition, the crystallinity index also showed a marked trend for each mineral, also as a function of distance from the mineralized structure.

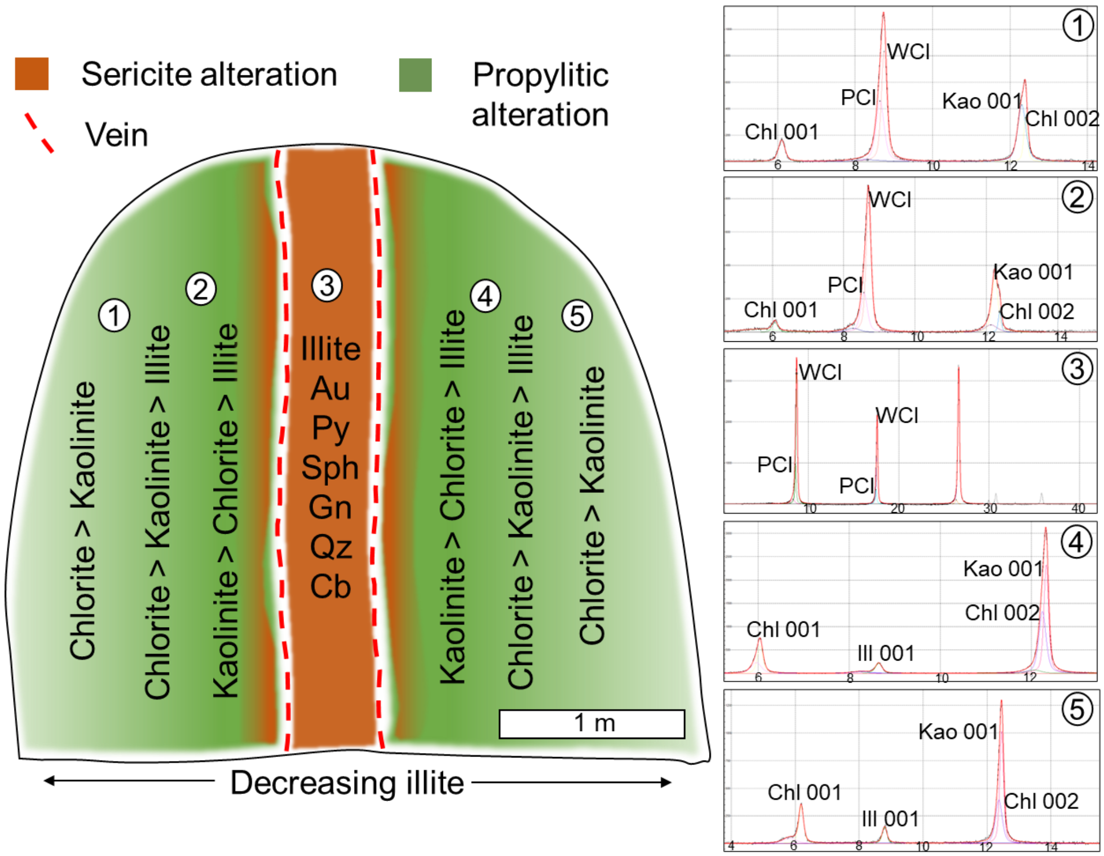

Figure 60. Schematic illustration of clay minerals paragenesis as a function of distance from the mineralized structure. Deconvoluted XRD diffractograms with natural treatment, displaying the different clay minerals occurring in the face sampling. 2θ geometry and Bragg-Brentano configuration. Abbreviations: Chl = chlorite, Ill = illite, Kao = kaolinite, PCI = poor crystallized illite, WCI = well crystallized illite.

5.5. Geochronology

Eleven samples from the Buriticá gold deposit were selected for radiometric age dating through the U-Pb, Ar/Ar methods, using zircon and sericite/biotite respectively (Table 3). Only three samples were suitable for the analysis using the U-Pb system (Figure 61), the remaining samples for Ar/Ar method could not be dated due to very small sericite crystal grain size. The analysis was conducted to date the crystallization ages of the rocks of the Buriticá Intrusive Complex (BIC), as well as the ages of the main hydrothermal alteration events. The zircon standard used was GJ-1 from Jackson et al., 2004.

Table 3. Summary of samples for geochronology at Buriticá gold deposit.

Sample	Label	mFrom	mTo	Dating method		Rock	Age	MSWD
BUSY291	2	1269.5	1275	U-Pb on Zr	Zr edge shooting	Pyroxene diorite	7.7 ± 0.1 Ma	1.2
BUSY390	3	248.8	250.3	Ar/Ar on Ser	Step heating	Murcielagos		
BUUY152	4	155.2	161.1	U-Pb on Zr	Zr edge shooting	Porphyry diorite	7.6 ± 0.1 Ma	1.6
BUUY339D 01	5	338.2	344.4	U-Pb on Zr	Zr edge shooting	Pyroxene diorite	7.7 ± 0.1 Ma	1.7
BUUY339D 04	6	210.3	211.8	Ar/Ar on Ser	Step heating	Murcielagos		
BUUY434	7	106.7	107.8	Ar/Ar on Ser	Step heating	Centena		
BUUY439	8	98.8	99.6	Ar/Ar on Ser	Step heating	Centena		
RPS_1611	9	0	1	Ar/Ar on Ser	Step heating	Martina		
GBUS003	10	681.1	691.4	U-Pb on Zr	Zr edge shooting	Tertiary dike		
SA_9679E	11	0	1	Ar/Ar on Ser	Step heating	San Antonio		
BUUY249D 01	12	350.7	372.0	U-Pb on Zr	Zr edge shooting	Pyroxene diorite		

Results of U-Pb dating returned ages of magmatic crystallization of ~ 7.7 ± 0.1 Ma, defining a Miocene age of the dioritic rocks that belong to the BIC and these included samples BUSY291, BUUY339D01 and BUUY152 (Figure 61, 62). The overall composition of the dated samples corresponds to dioritic, phaneritic to porphyritic textures and slight variations of proportions of rock forming minerals. Hydrothermal alteration is associated with the alteration of primary mafic minerals to chlorite, actinolite and epidote. Overprinting of sericite and calcite is also a key feature. Mineralization consists of pyrite and chalcopyrite in veinlets and disseminated styles.

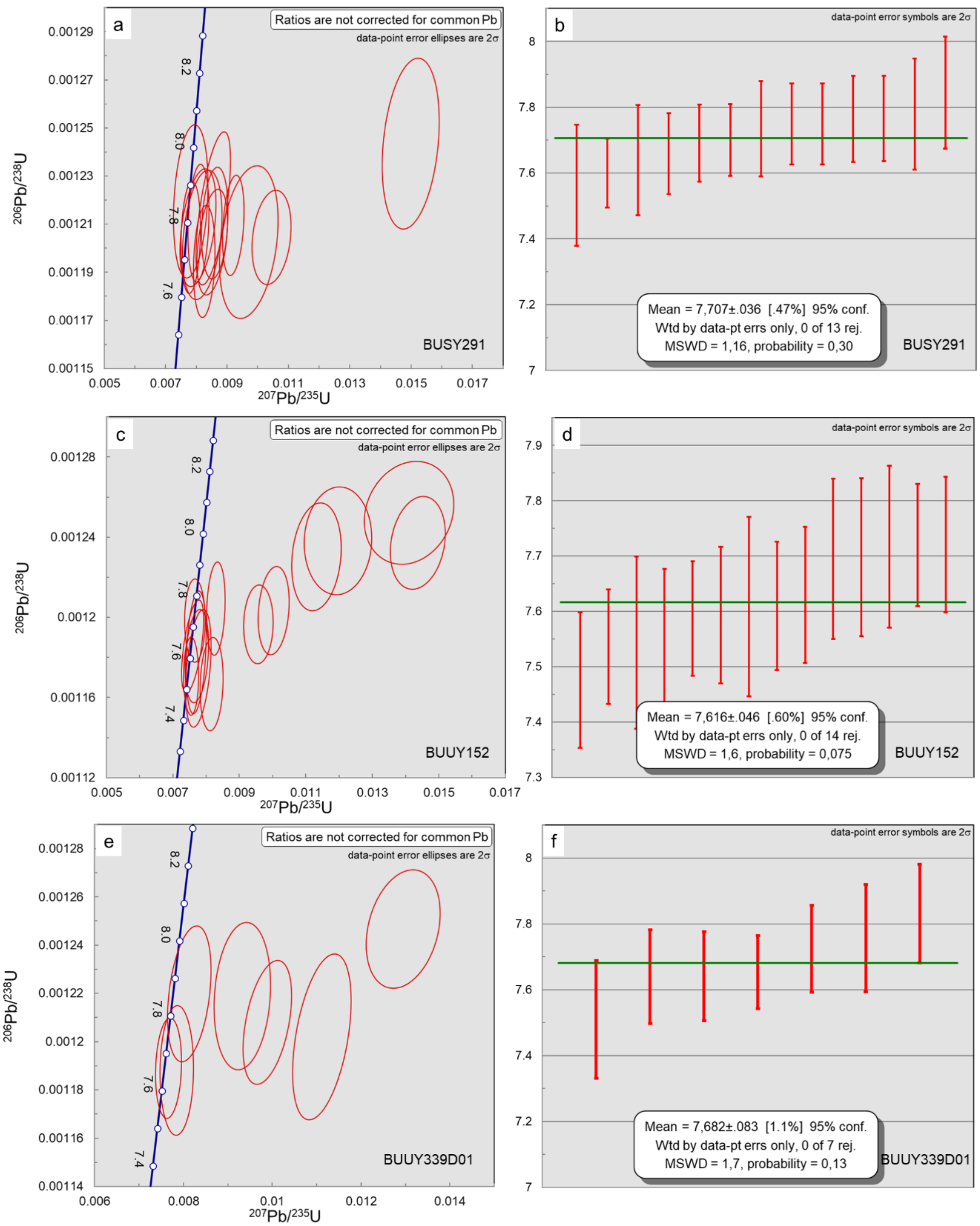

Figure 61. Zircon U-Pb Concordia plots (a, c, e) and weighted mean $^{206}Pb/^{238}U$ ages (b, d, f) for the BIC rocks.

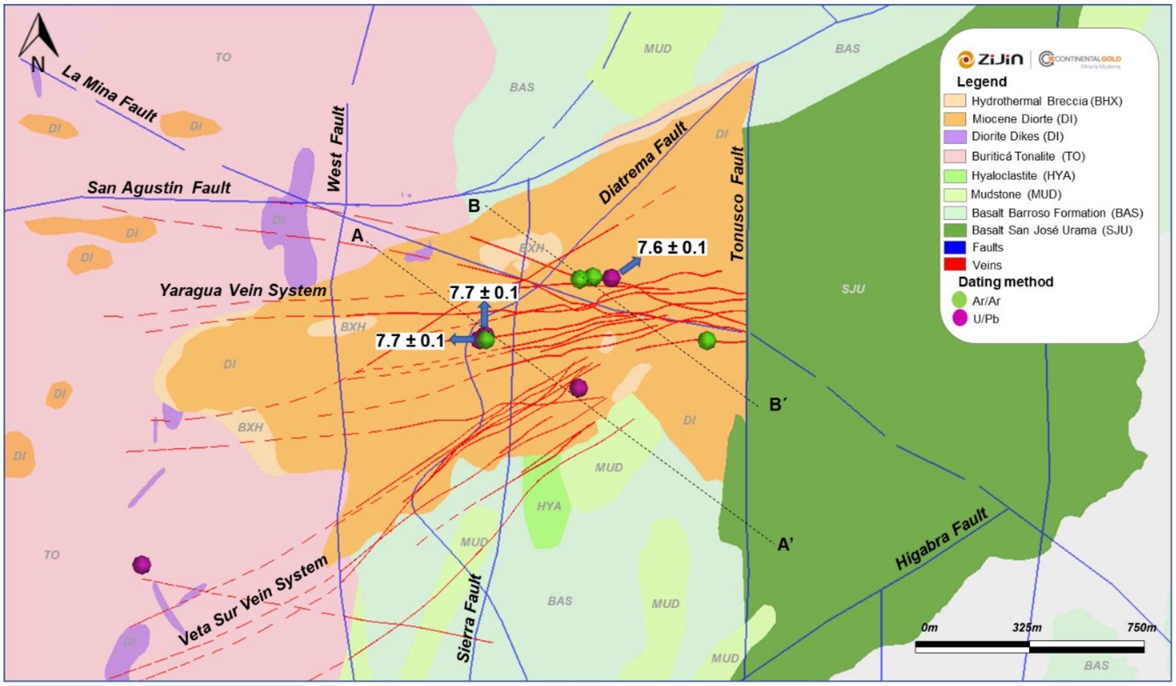

Figure 62. Plan view of Buriticá gold deposit constraining the age results.

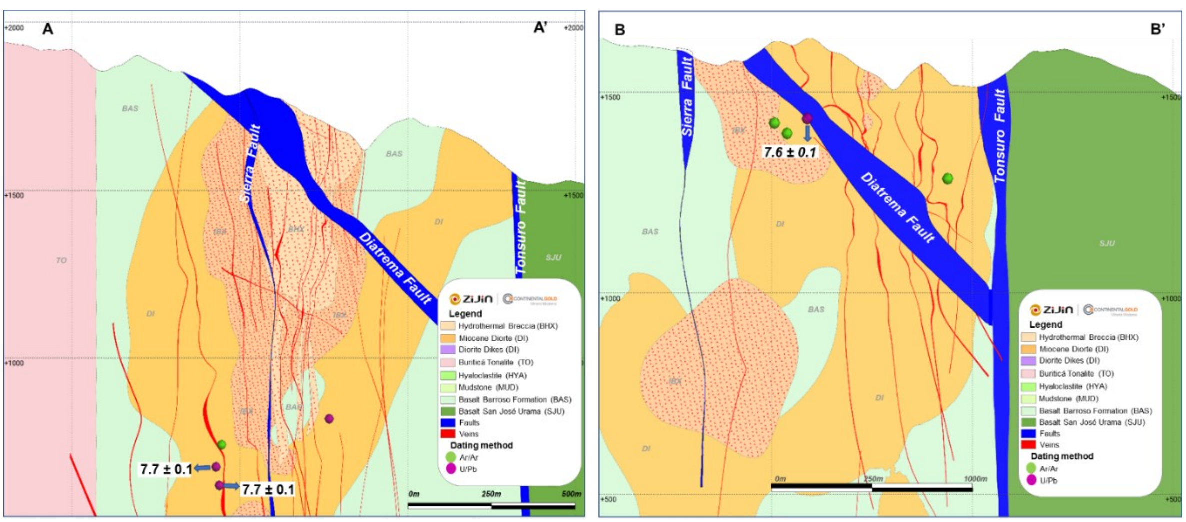

Figure 63. Simplified cross section of geology and location of geochronology ages at Buriticá deposit.

6. Discussion

6.1. Permeability development at the deposits-scale - Roles of faults in the development of permeability

Formation of all types of hydrothermal ore systems is principally ruled by permeability, which is in turn controlled by deformation style, intensity, and duration, plus temperature-pressure gradients, and fluid buoyancy. Permeability in the Buriticá gold deposit played a critical role for fluid precipitation, from source to site of deposition. The principal permeability pathways were represented by the main faults (i.e., Tonusco Fault, Diatrema Fault, Sierra Fault, La Mina Fault), which were also responsible for the formation and control of the deposit-scale architecture, which in turn also controlled low-order architecture that constrained alteration and mineralization.

For both volumes of mineralized rock hosting the Veta Sur and Yaraguá systems, host-rock competence was also a key feature in function of permeability. The deposition of hydrothermal minerals was both reduced and triggered by the formation and breaching of impermeable barriers (aquacludes) (Figure 55, 56). Therefore, deposition of mineralization was localized at the intersection of the feeder structure and the impermeable barriers, which resulted in high-grade zones with variable geometries depending on the structure involved and its spatial distribution (Figure 59). Relatively larger-scale tectonic structures are important for permeability enhancement through active faults, as inherited properties including structural and stratigraphic frameworks become key for strain localization.

At the deposit-scale, the central part of Diatrema Fault shows that the western mineralization of the Yaraguá system straddles the fault (Figure 55), suggesting that permeability was higher in this zone than that for the mineralization occurring further up-dip. This results from the fluid being able to locally access the permeable hanging-wall rocks of the Diatrema Fault. Additionally, intersection of the Sierra Fault with the western portion of the Yaraguá vein system and Diatrema Fault at depth, also controlled the deposition of mineralization (Figure 56, 59). The Sierra Fault and La Mina Fault controlled the emplacement of magmatic-hydrothermal breccias, which are closely implicated in the pathways and deposition of mineralization in the Veta Sur system (Figure 30).

Formation and evolution of the mineralized structures from Yaraguá and Veta Sur systems originated under a NNW-SSE extensional environment in which veins have in turn been overprinted by deformation, transforming them into shear veins. The composite characteristic of the veins is due to an event of progressive deformation during a single cycle where multiple permeability-fluid flow cycles occurred, due to fault failure and continually promoted during earthquake after-shock events that enhanced permeability (Figure 39). Attributed deformation was influenced by the collision of the Panama-Chocó block and Nazca plate subduction (Jaramillo et al., 2019).

The larger and first-order veins at the Buriticá gold deposit play the role of the main structures that the relatively thinner second-order veins diverge from (Figure 35, 36). Examples include the Murcielagos and Cassandra veins in which the smaller veins splay off these larger and thicker veins, rather than truncating each other. Variations in the strike orientations of first-order veins were a direct control on the generation of favorable opening sites during fault failure and movement (i.e., Cassandra jog), the latter occurring at all scales. Thickness of the main veins varies along strike and up and down dip as a product of transient sites of limited fault opening that tapped permeability-controlled flow, the reason for the erratic fluid pathways morphologies that link distal sites at depth principally (Figure 36-a, 59).

Vein system morphology indicates the geometry of the host structures and can be extrapolated to larger scales, with morphologies ranging from braided to subparallel sheeted structures to those that bifurcate with asymmetric geometries. Interconnection of these structures and their opening were the controlling parameters for permeability enhancement to occur, resulting in a wide range of possibilities to contain continuous zones of strike- and dip-extensive mineralization. Exceptions for the latter are the first-order veins including San Antonio, Murcielagos, Centena. Hence, the principal mineralized structures display variations in Au grade, indicating that these shoots have finite dimensions but repeat along strike or up and down dip (Figure 41-a, 54, 55).

Mineral deposition and transient permeability relationships were functions of the fluid flux accommodated by the different structures at several scales. The relatively more dilational portions of the mineralized structures defined the sites of enhanced permeability zones that became ore shoots when localized at structural intersections (i.e., Tonusco and Diatrema Faults intersection, single main veins intersection at development-scale) (Figure 55).

Physical properties of the host rocks were key factors in the relationship between vein systems and alteration, which show a variation in the degree of development. Competent massive bodies (BIC) were easily fractured and accommodated more shortening strain than adjacent units with lithological layering (Barroso Formation) (Figure 35). The BIC is an example of a competent body in which fracture permeability links back to faults and shears that acted as fluids pathways, and in which mineralization occurs in fractures related to low mean stress sites that sourced fluids from adjacent shear zones. The incompetent and layered lithologies, such as the Barroso Formation, tended to accommodate shearing strain along bedding and fine-grained phyllosilicates-rich layers. Therefore, rigid, and competent rock units are more likely to host mineralization, localized adjacent to or within the layered sequences (Figure 35-a, b).

Fault damage zones of the different mineralized structures were important permeability-controlling factors at the Buriticá gold deposit. Sheeted veins arrays, and alteration halos of lower-order mineralized structures define a critical zone for mineral deposition and represent a volumetrically larger amount of host-rock available for mineralizing fluids than only the first-order structure (Figure 35-c, d). Consequently, the permeability framework at the deposit-scale has been controlled and favored by major faults and their related damage zones (Table 2). It is the interaction between these large-scale and long-lived structures that is the key parameter for permeability enhancement processes that finally controlled and sponsored deposition of mineralization under variable stress field conditions.

The orientations of the structures and the prevailing principal stresses were important for controlling the sense of movement accommodated by the structures. This, in turn, produced zones of extension and contraction along structures, resulting in variable propensities for host-rock fracturing, development of extensional sites, controls on the location of linking structures, transient development of low mean stress sites, and the ultimate control on the location of shoot geometries within tabular mineralized structures. Furthermore, resolving the kinematics on differently oriented structures allows inferences for movement senses on ones where kinematic indicators are yet to be defined, such as unmined or poorly drilled volumes. This enhances the predictability of models for mineralization when undertaking ongoing exploration.

6.2. Controls on high-grade accumulation zones

Once the mineralized structures are recognized as faults, several geometric arrays can form to localize mineralization (Cox, 2020). The structural history of these arrays has been characterized from exposures in mining development. The different strands of the major faults have accommodated complex movement histories, representing variable magnitudes and senses of movement, in which correlation to individual mineralized events is commonly difficult to evaluate. As noted previously, mineralization at all scales in the Buriticá gold deposit is in function of fault-controlled permeability. As such, mosaics of faults with long deformation histories exhibit strong controls on fluid movement and hydrothermal mineral deposition. Principally, it is the population of steeply dipping N - S striking faults that are the crucial ones for acting as mineralizing fluid pathways (Figure 26, 55) (Table 2). These long-lived faults have interacted multiple times with different oriented faults that comprise moderate to gentle dipping structures, playing the role of linkage and finally localizing mineralization (Table 2). A similar situation also occurs, with the intersections with NW-SE striking faults (Figure 54, 55).

In addition to the intersection between the principal faults, their associated damage zones generated large and irregularly shaped volumes of rock available for mineralizing fluids to deposit. These variable shaped zones are internally termed LPM/BMZ (Low Porphyry Mineralization / Broad Mineralized Zone), display high vein density, several orientations with a sheeted vein pattern, stockwork-like array, all stages mineral infill, and pervasive sericite alteration (Figure 26, 39-g, 55).

The moderately east dipping Diatrema Fault is defined as a braided structure rather than single plane and is represented by several subparallel splays. This has been transformed into an impermeable barrier-zone due to deposition of hydrothermal minerals, creating an obstacle for mineralizing fluids to flow through. Gouge material has acted as impermeable zones where found with considerable thickness, and has not fractured during fault failure, instead reducing any permeability enhancement process. Relatively thinner gouge-rich zones were likely to be traversed by mineralizing fluids, but this locally deposited minerals such carbonate and quartz and thus imped the fluid flow as well (Figure 39-h). Locally, mineralizing fluids crossed one strand of the fault only to be impeded by the next one. The different conditions described above also served to compartmentalize mineralization at the Buriticá gold deposit.

At the development-scale, a dextral sense of movement was accommodated by structures at low angles to the first-order veins, representing the current vein geometries of Buriticá gold deposit (Figure 36-a). Second- and third-order structures are linking splays/relays between the first-order structures. Mostly, hanging-wall-up movements on the host structures are the responsible for the second-order vein formation. The formation of jogs in the principal veins at Buriticá, is a function of the movement senses accommodated by the host structures, being both dilational and contractional at the mine-scale (Figure 36). The Cassandra vein shows a contractional jog resulting from dextral movement sense on bounding faults, which promoted hydrothermal breccia emplacement and higher permeability, and which is characterized by enhanced Au grade values (Figure 36-c).

The structural architecture of Buriticá consists of a mosaic of major faults that have had episodic movements and opening in the seismogenic zone, leading to the possibility for a fault-valve system (e.g., Sibson, 2019). During this process, the faults behave as impermeable zones during the interseismic period but are able to generate permeable pathways for fluid flow after post-failure events. The Tonusco Fault and Diatrema Fault display evidence for acting as both impermeable seals and permeable channelways (Figure 27, 28) (Table 2).

6.3. Fault architecture and igneous intrusion relationships

The fault populations at Buriticá are responsible for controlling the emplacement of igneous bodies, including all units within the BIC. Cretaceous mylonitic structures define the oldest and most important contributors to the deposit-scale structural architecture and mylonites are identified in all the faults (Figure 27, 29). These ductile deformed rocks are now remnants within brittle continuous zones, adjacent to the main faults (Figure 28). This deformation regime relationship is evidence for the primary identifiable structural framework at Buriticá being established as a system of high-strain structures generated at depths greater than ~6 km, with subsequent progressive uplift and overprinting. Mylonites usually form at greater depths, but porphyry intrusion promoted ongoing ductile fabric formation along pre-existing mylonites due to increase in the geothermal gradient, fluids and development of phyllosilicate-rich mineral assemblages. Overall, the evolution of the mylonites through to the brittle permeability network seen today is considered to represent a protracted progressive event.

To the east, the Tonusco Fault shows a large and deep control for the dioritic body that hosts the Yaraguá veins. The Tonusco Fault and adjacent strands have resulted in structural interleaving the diorites and basalt from San Jose de Urama and BIC. Hydrothermal breccias with tabular- to pipe-shaped morphologies are localized and controlled by the Sierra Fault that are controlled by, and define, the intersection line with other faults (Figure 30, 55, 59-f). The intersection line and its plunge define the body shapes principally at depth and localize mineralization below the Diatrema Fault (Figure 55). The NW-SE to WNE-ESE trending La Mina Fault, hosts some mineral occurrences in the district and represents a transfer fault produced during a protracted deformation history related to terrane accretion processes. Outcrops displaying this relationship are found in La Mina creek where hydrothermal breccias are bounded and crosscut by sheeted W-E faults (Figure 30). The Cretaceous Buriticá Tonalite to the west and Santa Fe Tonalite to the south are bounded by subparallel faults farther from the current mine development, but still indicate the deformation history and control during and post intrusions, as Buriticá gold deposit architecture is extrapolated in a larger scale.

Geochronological data indicates emplacement of these rock formations is consistent with the Buriticá fault architecture. Diorites yielded U/Pb ages on zircon of 7.7 ± 0.1 Ma and 7.6 ± 0.1 Ma, and contrast with data from Lesage (2011), who reported an Ar/Ar age for hydrothermal alteration at 7.74 ± 0.08 Ma on sericite, are consistent with the timing of magmatism. Intrusion of the entire BIC units aided in coeval uplift and deformation of the Barroso Formation, generating a large antiform, now eroded, its axial plane striking NNE-SSW with west- and east-dipping limbs peripheral to the BIC (Figure 34). In addition, Veta Sur systems records the complete suite of temperature pathfinders (Au-Ag-Zn-Pb-Sb-Bi-Cu-Mo) distribution while the Yaraguá system just displays the low temperature one (Au-Ag-Bi-Te-Sb) (Figure 59). The Cu/Zn ratio used for the determination of feeders displayed higher values of Cu at greater depths in the Veta Sur system than the Yaraguá system, indicating a better preservation in the hanging wall of Diatrema Fault (Figure 59-h). So, the latter plus the crosscutting relationship of Diatrema Fault with some of the Yaraguá veins support accommodation of east-side-up movement of this fault. Aerne & Kretz (2014) estimated pressure conditions of 500 bar for vein formation in which rock overburden would have been of 1.85 km, this results in ± 1 km of eroded material since deposit formation compared to present day topography. Diatrema Fault sense of movement is consistent with this statement.

All the described and mentioned faults contribute to the pervasive N-S regional structural setting, including the Diatrema Fault and its splays at the mine-scale. These less thick but similarly oriented splays can be considered as members of the same fault set, with abundant subparallel brittle structures hosting the same fault-fill crossing the country rock in between the strands (Figure 28). Consequently, the Diatrema Fault and its subparallel bifurcations represent splays off the Tonusco Fault at depth as a result of strain accommodation features from the Tonusco Fault and Sierra Fault to the west. Mineralization, alteration, orientation and kinematic characteristics of Diatrema Fault and related splays reflects the impermeability of these structures and that they do belong to the same deformation suite.

The Tonusco Fault is the eastern most bounding structure at Buriticá, comprising a braided pattern of fault strands separated by lower strain blocks with local N-S orientations (Figure

26, 27). The numerous anastomosing shears have undergone movement and multiple reactivations over time, generating access for mineralizing fluids during the life of this fault (i.e., LPM-302) (Figure 27, 39-g).

The single and progressive deformation event for which Buriticá structural architecture is attributed for, can be observed at all scales. Local reactivated faults cut across the mineralized and vertical veins, creating mutual cross-cutting relationships associated with later events (Figure 37-d). So, syn-mineral and post-mineral deformation has played a role for deposit formation (Table 2).

6.4. Ongoing exploration implications

When considering the large area of the Middle Cauca belt and known gold districts such Marmato, La Colosa, Nuevo Chaquiro, the definition of the Buriticá structural framework allows for a specific and practical procedure to follow in regional-scale exploration programs (Figure 64). Host rock units seem important controlling factors for deposit formation, but the structural context and calc-alkaline magmatic suite sources (Combia Formation) are major contributors. A combination of these will identify an area as prospective and should be considered for examination. The nearest evidence of this is the Abriaqui project (Fenix Gold Corp) to the west of Giraldo town, where the main features including vein characteristics, orientations of structures, and host rocks, (Arrubla-Arango & Silva-Sánchez, 2021), remain similar and is in general framed within a fault setting analogous to Buriticá. Other occurrences along and beside the N-S Cauca Romeral fault zone represent good examples of mineralization and deformation processes that involved near- and far-field stresses (Figure 64). This can be resolved with detailed assessment of structural geology.

Combia Formation and Amagá Fm are useful geologic unit markers to visualize a range-scale distribution, crustal deformation and evolution of the Middle Cauca belt, hence giving information about prospective areas with similar geologic-structural settings (Figure 64).

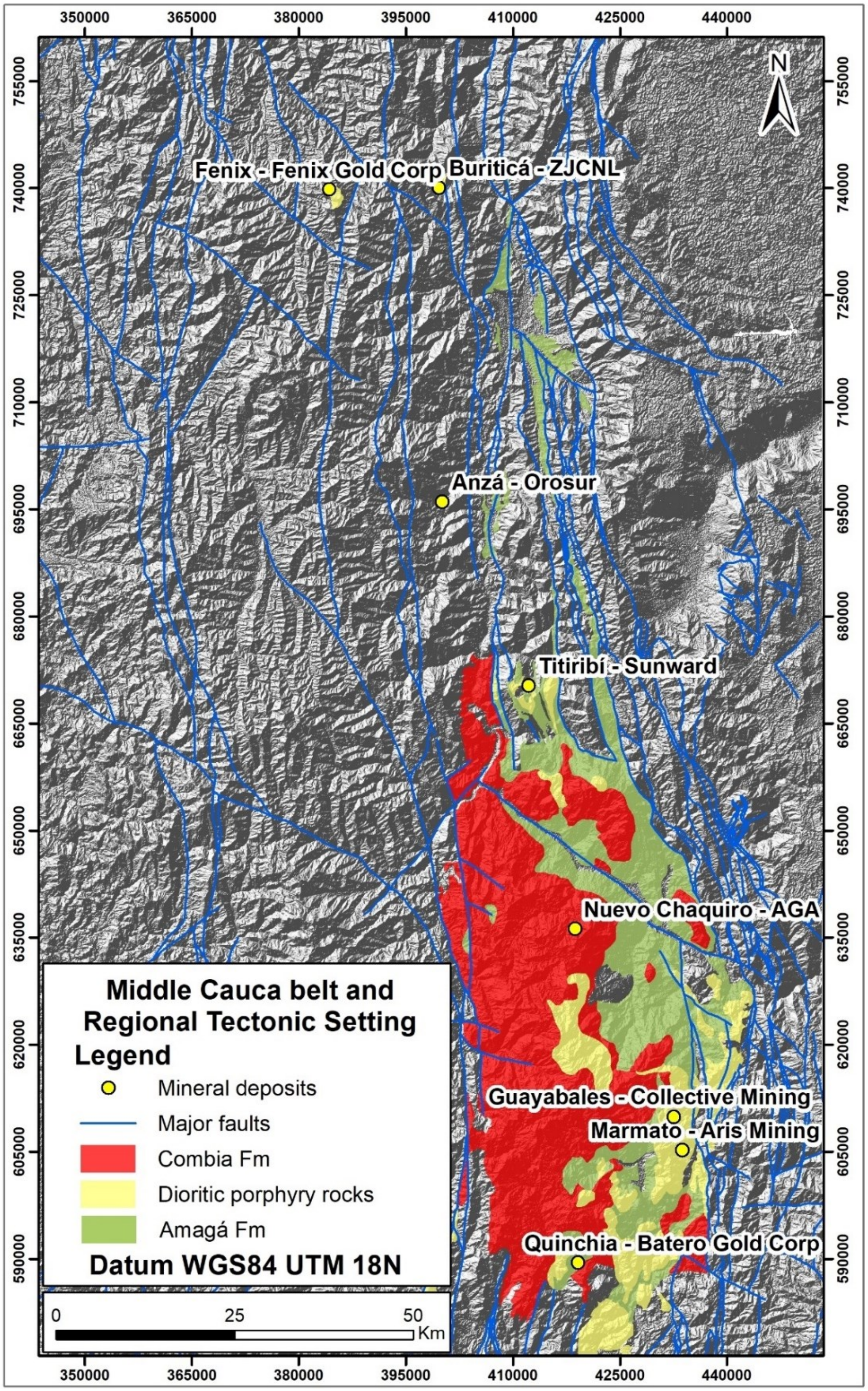

Figure 64. Regional-scale architecture showing major faults, Miocene intrusive units and the spatial relationship to significant Au-Cu deposits. Geology taken from the SGC, 2020. WGS 84 18 N projection and 30 m Digital Elevation Model.

At Buriticá, recent results from district-scale, exploration indicate that targets including Perseus, Medusa, Poseidon and Orion, are attributed to mineral occurrences in which predominantly parameters such lithogeochemistry, geophysics and structural geology were the most important features for localizing mineralization. At the mine-scale, this results in the addition of mineral resources because mineralization controls are well distinguished during wall-face mapping and sampling, core logging, surface, and underground cartography. In support of that, deep holes planned to test the strike and depth extensions of both vein systems have recently reported high-grade intersections at 0 m.a.s.l and 300 m.a.s.l for Veta Sur and Yaraguá systems, respectively. The latter results in a total vertical extension of 1 – 1.5 km (Figure 65).

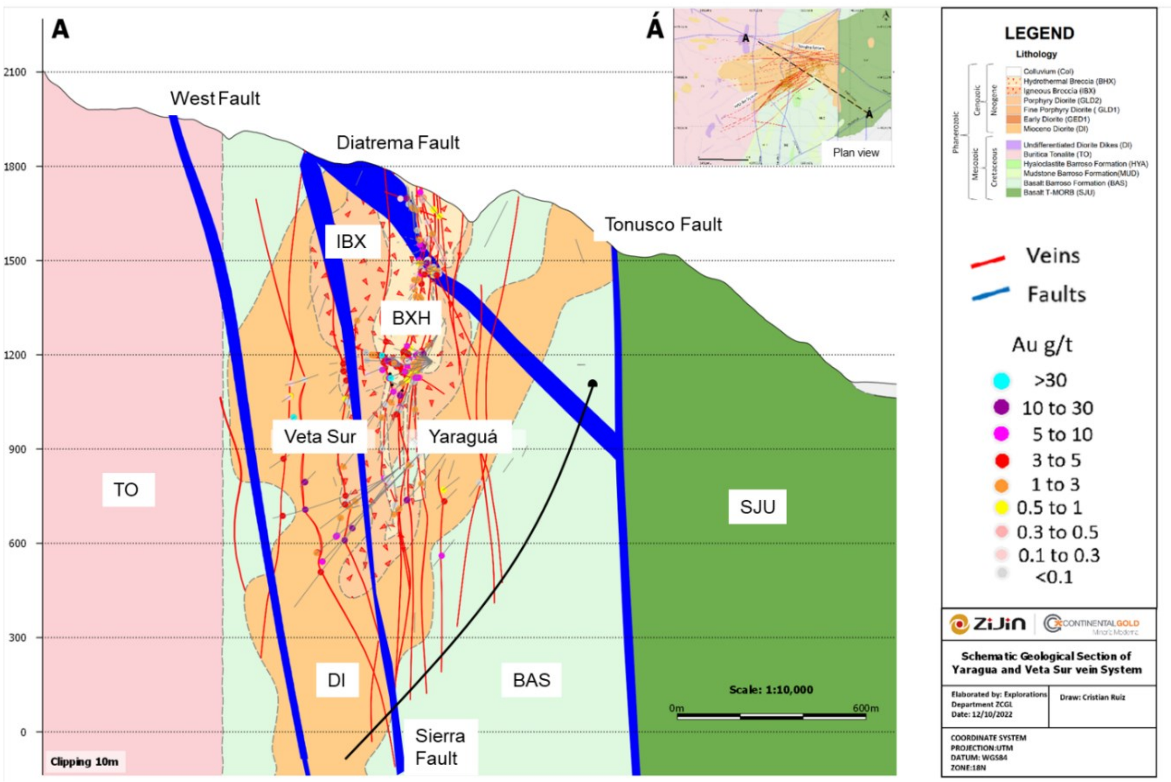

Figure 65. Exploration drill program undertaken in 2019 with the aim of testing the continuity of the Veta Sur and Yaraguá systems, and porphyry intrusive bodies. Black line represents the drillholes.

6.5. Litho-geochemistry insights

Assessment of geochemical characteristics provides important facts about magma genesis, tectonic environment, and hydrothermal processes. This information indicates that BIC rocks formed in a magmatic arc environment with calc-alkaline affinity. This is consistent with the 7.7 ± 0.1 Ma U/Pb age constraint that puts Buriticá gold deposit within the Miocene-aged igneous bodies related to subduction arc magmatism (Figure 45, 46, 47). Jaramillo et al., (2019) discriminated the calk-alkaline geochemical affinity for porphyry and adakite-signal rocks of the Combia volcanic complex, in a segment located close to Nuevo Chaquiro and Marmato deposits.

The geochemistry of the Barroso Formation, Buriticá Tonalite and San José de Urama are well discriminated by using immobile elements. La Vs Ce diagram clearly separates the BIC rocks from the other hosting units (Figure 42). Also, basaltic rocks from eastern San José de Urama are well differentiated from the basalts of the Barroso Formation through the Ni and Cr content (Figure 44). This is a key feature, given that east of Tonusco Fault there is no evidence of mineralization. It is notable that the geochemical assessment involved in this work, when compared to the La Colosa Porphyry gold (Naranjo et al., 2018), display strong similarities for both deposits including geochemical signature and tectono-magmatic discrimination.

The Buriticá gold deposit shows several intensities and stages of hydrothermal alteration (propylitic, potassic and sericite) (Figure 48, 49). Most significantly, gold-related hydrothermal alteration is sericite, particularly where it is controlled by the mineralized structures and overprints all lithologies and other alterations (Figure 35-d, 48-g). Consequently, there is a proportional relationship between K content, sericite alteration intensity and Au grade. In Figure 50, moderate to strong sericite alteration roughly ranges from 50 – 95% K, 5 – 20% Na and 10 – 30% Ca. In the ternary graph, the alteration fields annotated as “Moderate” and “Strong” represents the zone where higher Au grades values occur, consistent when field observations and assays are constraint (Figure 51). An additional field of “Sericite + Carbonates” is related to a high content of Ca, which is related to the typical carbonate-quartz rich fluid that the Buriticá gold deposit was formed from, specially the stage 2 (Lesage, 2011). Microthermometry and LA-ICP-MS analysis in fluid inclusions resulted in moderate saline fluids, boiling as precipitation driver and 450 °C brines that developed feldspar-destructive sericite alteration (Aerne & Kretz, 2014).

Sericite alteration displays a tight relationship with K-rich minerals such muscovite and illite, the latter identified through XRD analysis (Figure 60). Figure 52 displays the sericite alteration intensities in contrast with different mineral nodes, indicating the gradual formation of K minerals as sericite intensity and Au grade increase. The trend from least altered toward most altered displays a combination of the older porphyry Cu related hydrothermal biotite (potassic) plus weak onset of chlorite-sericite (Fe-Mg rich white mica). As K/Al molar ratio data reached molar ratios greater than 0.6 to 0.8 molar K/Al, this also comprises biotite and not just sericite (Figure 52). 0.3 to 0.2 molar K/Al identifies the overprinting sericite alteration (> 300 °C) followed by illite-kaolinite alteration (± 200 °C) that was additionally recognized through XRD (Figure 60). A similar configuration occurs when pyrite and anhydrite minerals are compared with sericite alteration. Despite both being observed in the deposit, it is pyrite that is associated with the strong sericite alteration and high Au grade (Figure 53-a). Anhydrite is the structurally deepest type of alteration associated with the potassic alteration assemblage minerals, however it does not display any genetic relationship with Au grade. These variable temperature alteration types, their mineral assemblages and crosscutting relationships display a typical behavior within a porphyry Cu deposit, evidenced as multiple body intrusions within the BIC and emplaced under the control of inherited penetrative faults and changing field stresses.

Metal zonation at Buriticá deposit is lateral and vertical, and in function of faults and hosting rocks (Figure 59). Au and Ag mimic the same pattern since these are the principal commodities whereas base metals like Zn are located mostly above Diatrema Fault and in the Yaraguá vein system. Tonusco and Sierra Faults played the roles as fluid pathways, demonstrated by both strong sericite alteration intensity down-dip and the K distribution (Figure 55, 59-f). Barroso Formation and Buriticá Tonalite located to the west, mark a contrast due to differences with the fluid-to-rock ratio properties during mineralization events, but still showed evidence of vein continuity to the west. Importantly, Tonusco Fault indicates the limit for mineralizing volumes to the east. High temperature and porphyry-associated elements including Cu, Mo and the Cu/Zn ratio increase with depth and more likely in the BIC than the Barroso Formation. Overall characteristics of Buriticá gold deposit involve low- to intermediate-sulphidation and porphyry Cu styles, suggesting an hybrid model between both. Also, the occurrence of Buriticá magmatism and Combia Formation along major strike-slip faults parallel to the arc support porphyry environments (Richards et al., 2001).

Geochemical distributions of the different units, metal zonation, hydrothermal alterations and vein systems at the deposit-scale help differentiate the structural architecture and overprinting relationships (Figure 54, 55, 58, 59, 66). Consequently, geochemistry is a practical tool for exploration programs and targeting.

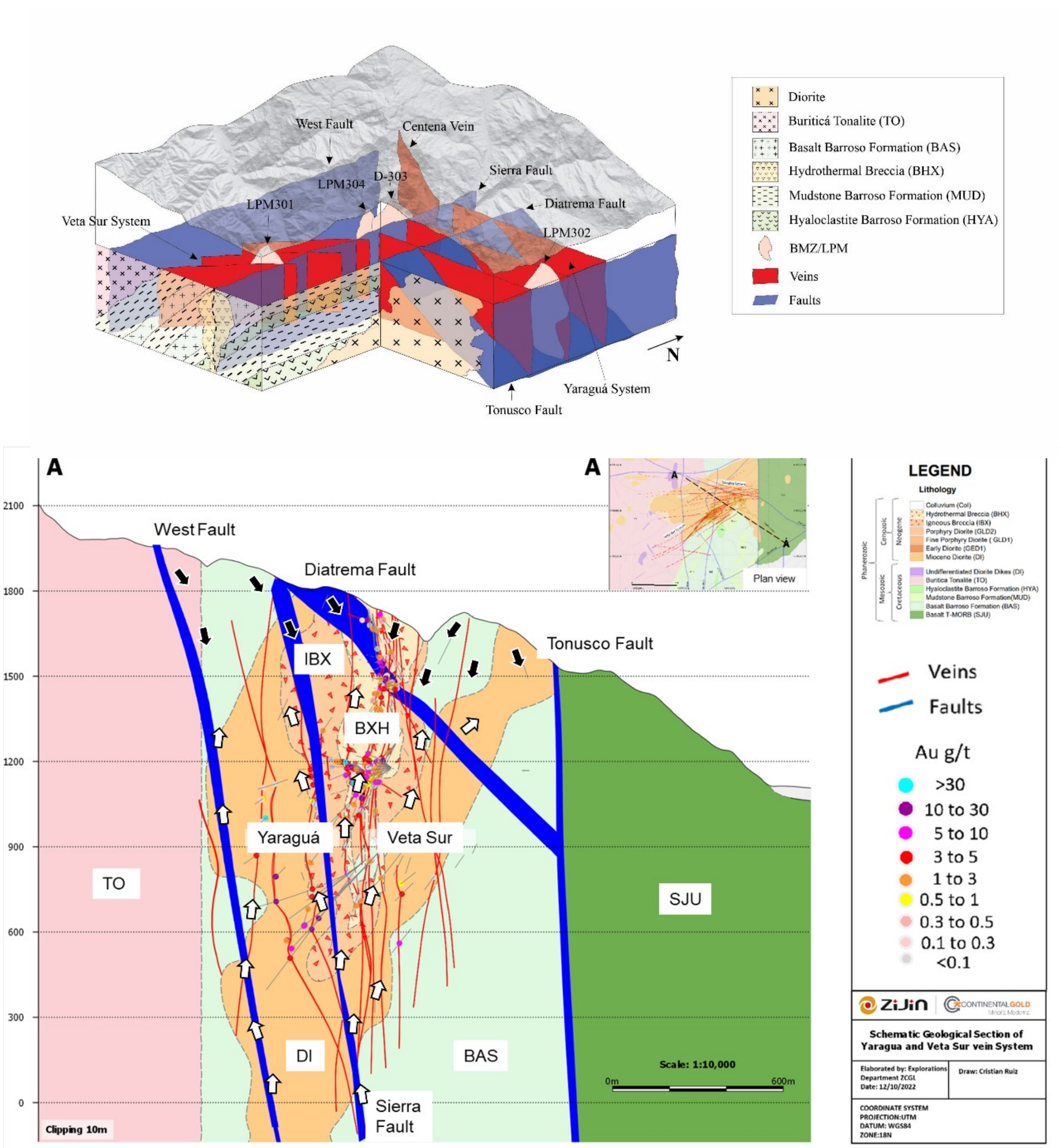

Figure 66. 2D and 3D models of the Buriticá gold deposit with different rock formations, fault architecture, mineralized volumes and fluid pathways at district-scale. White and black arrows indicate flow direction of brines and meteoric waters, respectively.

7. Conclusions

The structural architecture of Buriticá gold deposit consists of a series of early-formed mylonite zones belonging to principal faults (i.e., Tonusco Fault, Diatrema Fault, Sierra Fault, La Mina Fault). These faults now comprise a suite of cataclasite-hosting structures with widths greater than several meters. Volumes of host-rock between these major brittle deformed zones are traversed by populations of minor deformation structures and are commonly centimetric or less. Mineralized structures are grouped into Yaraguá and Veta Sur vein systems, nearly vertical and extensional originated structures with brittle deformation dominating the latest stages of formation. These veins initiated as sulphide-bearing structures that localized later vein formation and subsequent post-mineralization carbonate-rich events resulted in the formation of composite veins. The latter is associated with deformation controls for the last mineralizing events (Stage 3) recorded at all scales in which geometric relationships between the different order structures suggest a single progressive deformation event for Buriticá.

In terms of mineralized structures, Buriticá gold deposit comprises fault-shear hosted veins that have sulphide-related mineralization. These are intermediate temperature veins associated with a degassing porphyry Cu intrusive center. The latter comprises the “Stage 0”, which manifests as A- and B-type veins at depth. Buriticá mineralized structures are typical late porphyry-type veins which cut an older breccia centered porphyry Au-Cu center that contains only low grades of Cu and Au. Multiple movements have been accommodated along the host structures during the deformation history and have been critical for the formation of different vein stages and associated permeability enhancement processes. Recognition of veins as faults becomes key for assessing the kinematics of these structures, and effectively predicting where mineralization is localized. Additionally, the dextral shear sense of veins controlled the formation of ore shoots and higher-grade accumulation zones (i.e., Cassandra jog).

The structural framework is defined by N-S and NW-SE trending and steeply dipping faults that have been crucial for the formation and emplacement of mineralization. These large-scale and first order structures such as the Tonusco Fault, represent sharp boundaries at the deposit-scale and a major control at the regional-scale. A dextral sense of shear was accommodated over a protracted deformation history, consistent with the regional tectonic setting along the Cauca-Romeral fault system. Localization of mineralization against the western most side of the Tonusco Fault indicates: 1) this structure was a critical fluid pathway (at least the western strand), and that ongoing deformation has dismembered early-deposited mineralization during subsequent movements. 2) Linkage relationships between the Sierra Fault, Diatrema Fault and Tonusco Fault, are products of the accommodation of east-side-down movement. The possible exception is the juxtaposition of the San Jose de Urama unit on the eastern side of Tonusco Fault, which may be a product of opposite kinematics. Overall, the Tonusco Fault has accommodated a protracted movement history comprising several senses of movement hosted by the different anastomosing strands at different times.

The Diatrema Fault is a linking feature with the Tonusco Fault and the Sierra Fault. It shows a spatial relationship with mineralization because the interaction with different oriented structures and movement senses has promoted permeability enhancement frameworks for mineralizing fluids. Subparallel east dipping faults to the Diatrema Fault also occur as a set of stacked inclined features with control over hydrothermal breccia formation, and appear to be coeval with the deposition of mineralization according to the east-side-up movement. Moreover, the regional northwesterly striking faults (i.e., La Mina Fault, Puná Fault) were important for localizing mineralization at the district-scale, specially to the north. In general, the major controlling structures of Buriticá gold deposit are inherited fault zones that formed during early tectonic assembly of the region. These faults had preexisting rheological, structural, and stratigraphic characteristics that played a controlling role for subsequent strain localization and pathways formation. Those orogen-scale Andean tectonic events, including current Nazca plate subduction, also controlled far- and near-field stresses. This included the collision of Panamá-Chocó block, which is responsible for several country-scale faults running NW-SE, such as the Dabeiba-Cañas Gordas (Puná) and Arma Faults.

The BIC belongs to a population of Miocene-aged deposits located along the Middle Cauca belt (e.g., Marmato, La Colosa, Nuevo Chaquiro). This is supported by the U-Pb age obtained during the current study, which indicated magmatic crystallization occurred at 7.7 ± 0.1 Ma. The calc-alkaline affinity confirms the subduction-related magmatism for the hosting intrusive bodies, especially in the Yaraguá system. These intrusive units, including the Barroso Fm, Buriticá Tonalite and San José de Urama, are well differentiated geochemically. This has led to an accurate model of lithologies, which has in turn defined how they are disposed within the structural architecture. All the porphyry-related hydrothermal alteration types occur at the deposit-scale, however the sericite alteration associated with mineralized structures is the most important assemblage for gold mineralization. The 3D spatial distribution of sericite alteration intensity has established that the steeply dipping faults are the plumbing systems that allowed fluid flow through the different rock formations and behaved as impermeable barriers during progressive deformation (Figure 66). Sericite alteration intensity and gold grade indicate a proportional relationship. Despite BIC is part of the intrusive suite, this does not appear to be the source of the fluids but good rheological hosting rocks, since veins remain open at depth and to the west and that the deepest hole reached high-temperature mineral assemblages but is not part of the fluid source body.

Sericite alteration and faults are critical elements in the context of mineralization controls and permeability enhancement processes. Consequently, exploration guidelines for the Buriticá mineralized volume, surrounding prospects, and along Middle Cauca belt, can be carried out by following a pragmatic guide like the one taken in this work.

8. References

Aerne, U., & Kretz, P. (2014). Magmatic-Hydrothermal evolution of the Buriticá carbonate base metal deposit, Antioquia department, Colombia. *Master thesis, Swiss Federal Institute of Technology (ETHZ).*, 52–56.

Álvarez, A. J. (1983). Geología de la cordillera Central y el occidente colombiano y petroquímica de los intrusivos granitoides mesocenozoicos. *Boletín Geológico*.

Álvarez, E., & Gonzáles, H. (1978). Geología y geoquímica del Cuadrángulo I–7 (Urrao). Mapa escala 1:100.000. *Ingeominas, Informe 1761*.

Álvarez, J., Rico, H., Vásquez, H., Hall, R., & Blade, L. (1975). Geological map of the Yarumal Quadrangle (H-8) and part of the Ituango Quadrangle (H-7), Escala 1:100.000. *INGEOMINAS*.

Arancibia, O. N., & Clark, A. H. (1996). Early magnetite-amphibole-plagioclase alteration-mineralization in the Island Copper porphyry copper-gold-molybdenum deposit, British Columbia. *Economic Geology, 91*, 402–438.

Arrubla-Arango, F., & Silva-Sánchez, S. (2021). Geology of the Frontino-Morrogacho Gold Mining District and metallogeny of the El Cerro Igneous Complex. *Boletín Geológico, 48(1)*, 7–47.

Bateman, A. M. (1958). Economic mineral deposits, 2nd ed.: New York, Wiley. 916.

Battles, D. A. (1995). Arc-related sodic hydrothermal alteration in the western United States. *Geology,, 23*, 913–916.

Blenkinsop, T. G. (2008). Relationships between faults, extension factures and. *Journal of Structural Geology, 30*, 622–632.

Cediel, F., Shaw, R. P., & Cáceres, C. (2003). Tectonic Assembly of the Northern Andean Block, The Circum-Gulf of Mexico and the Caribbean: Hydrocarbon habitats, basin formation, and plate tectonics. *AAPG Memoir 79*, 815–848.

Corbett, G. J., & Leach, T. M. (1998). Southwest Pacific gold-copper systems: Structure, alteration and mineralization. *Economic Geology*, 238.

Cowan, E. J. (2020). Deposit-scale structural architecture of the Sigma-Lamaque gold deposit, Canada—insights from a newly proposed 3D method for assessing structural controls from drill hole data. *Mineralium Deposita, 55*, 217–240.

Cox, S. F. (1995). Faulting processes at high fluid pressures: An example of fault-valve behavior from the Wattle Gully fault, Victoria, Australia. *Journal of Geophysical Research, 100*, 841–859.

Cox, S. F. (2005). Coupling between deformation, fluid pressures, and fluid flow in ore-producing hydrothermal environments. *Economic Geology, 100th Anniversary Volume*, 39–75.

Cox, S. F. (2016). Injection-driven swarm seismicity and permeability enhancement: Implications for the dynamics of hydrothermal ore systems in high fluid flux overpressured faulting regimes. *Economic Geology, 111*, 559–587.

Cox, S. F. (2020). The dynamics of permeability enhancement and fluid flow in overpressured, fracture-controlled hydrothermal systems. *Reviews in Economic Geology, 21*, 25–82.

Cox, S. F., Braun, J., & Knackstedt, M. A. (2001). Principles of structural control on permeability and fluid flow in hydrothermal systems. *Reviews in Economic Geology, 14*, 1–24.

Cox, S. F., Wall, V. J., Etheridge, M. A., & Potter, T. F. (1991). Deformational and metamorphic processes in the formation of mesothermal vein-hosted gold depositsdeposits—examples from the Lachlan fold belt in central Victoria, Australia. *Ore Geology Reviews, 6*, 391–423.

Curewitz, D., & Karson, J. A. (1997). Structural settings of hydrothermal outflow: Fracture permeability maintained by fault propagation and interaction. *Journal of Volcanology and Geothermal Research, 79*, 1459–1468.

Dilles, J. H. (1987). Petrology of the Yerington batholith, Nevada: Evidence for evolution of porphyry copper ore fluids. *Economic Geology, 82*, 1750–1789.

Dilles, J. H., & Einaudi, M. T. (1992). Wall-rock alteration and hydrothermal flow paths about the Ann-Mason porphyry copper deposit, Nevada—a 6–km vertical reconstruction. *Economic Geology, 87*, 1963–2001.

Dilles, J. H., & Proffett, J. M. (1995). Metallogenesis of the Yerington batholith, Nevada. *Arizona Geological Society Digest 20*, 306–315.

Dilles, J. H., Einaudi, M. T., Proffett, J., & Barton, M. D. (2000a). Overview of the Yerington porphyry copper district: Magmatic to nonmagmatic sources of hydrothermal fluids: Their flow paths and alteration effects on rocks and Cu-Mo-Fe-Au ores. *Society of Economic Geologists Guidebook Series, 32*, 55–66.

Ego, F., Sébrier, M., & Yepes, H. (1995). Is the Cauca-Patia and Romeral Fault System left or rightlateral? *22*, 33–36.

Einaudi, M. T. (1977b). Environment of ore deposition at Cerro de Pasco, Peru. *Economic Geology, 72*, 893–924.

Einaudi, M. T. (1982a). Description of skarns associated with porphyry copper plutons, southwestern North America, in Titley, S.R. ed. Advances in geology of the porphyry copper deposits, southwestern North America. *Tucson, University of Arizona Press*, 139–183.

Einaudi, M. T., Hedenquist, J. W., & Inan, E. E. (2003). Sulfidation state of fluids in active and extinct hydrothermal systems: Transitions from porphyry to epithermal environments. *Society of Economic Geologists Special Publication*, 285–313.

Emmons, W. H. (1927). Relations of the disseminated copper ore in porphyry to igneous intrusives. *American Institute of Mining and Metallurgical Engineers Transactions, 75*, 797–815.

Etayo-Serna, F., González, H., & Álvarez, E. (1980). Mid–Albian ammonites from northern Western Cordillera, Colombia, S.A. *Geología Norandina, 2*, 25–30.

Faulds, J. E., & Hinze, N. H. (2015). Favorable tectonic settings of geothermal systems in the Great Basin region, western USA: Proxies for discovering blind geothermal systems. *World Geothermal Congress, Melbourne, Australia*, 1–6.

Feininger, T., Barrero, D., & Castro, N. (1972). Geología de Antioquia y Caldas (subzona JIB). *Ingeominas, Bol. Geol., 20*(2), 173.

Fleming, A. W., Handley, G. A., Williams, K. L., Hills, A. L., & Corbett, G. J. (1986). The Porgera gold deposit, Papua New Guinea. *Economic Geology, 81*(3), 660–680.

Fournier, R. O. (1999). Hydrothermal processes related to movement of fluid from plastic into brittle rock in the magmatic-epithermal environment. *Economic Geology, 94*, 1193–1211.

Garson, M. S., & Mitchell, A. H. (1981). Chapter 27 Precambrian Ore Deposits and Plate Tectonics. *Developments in Precambrian Geology, 4*, 689–731.

Geoestudios-Ingeominas. (2005). Complementación geológica, geoquímica y geofísica de la parte occidental de las planchas 130 Santa Fé de Antioquia y 146 Medellín Occidental. Escala 1:100,000: INGEOMINAS. *Informe técnino*.

Gerya, T. V., Stern, R. J., Baes, M. S., & Whattam, S. A. (2015). Plate tectonics on the Earth triggered by plume-induced subduction initiation. *Nature, 527*, 221–225.

Göbel, V., & Stibane, F. (1979). K/Ar hornblende ages of tonalite plutons, Cordillera Occidental, Colombia. *Publicaciones Especiales Geología*(19), 1–2.

Gonzáles, H., & Londoño, A. (1998). Edades K/Ar en algunos plutones del Graben del Cauca y norte de la Cordillera Occidental. *Rev. Geol. Col*, 117–131.

González, H., Restrepo, J. J., Toussaint, J. F., & Linares, E. (1976). Edad radiométrica K-Ar del Batolito de Sabanalarga. *Publicación Especial de Geología, 8. Departamento de Ciencias de la Tierra, Facultad de Ciencias, Universidad Ciencias de la Tierra, Facultad de Ciencias, Universidad Nacional de Colombia, Medellín*.

Greene, A. R., Scoates, J., Weis, D., Katvala, E. C., Israel, S., & Nixon, G. T. (2010). The architecture of oceanic plateaus revealed by the volcanic stratigraphy of the accreted Wrangellia oceanic plateau. *Geosphere, 6*, 47–73.

Guiral-Vega, J. S., Rincón-Gamero, J. J., & Ordoñez-Carmona, O. (2015). Geología de la porción sur del Batolito de Sabanalarga. Implicaciones para la teoría de terrenos al occidente de Colombia. *Boletín de Ciencias de la Tierra*.

Guiral-Vega, J. S., Rincon-Ramero, J. J., & Ordóñez-Carmona, O. (2015). Geology of the southern part of Sabanalarga Batholith: Implications for terrane theory in the west of Colombia. *Boletin de Ciencias de la Tierra*(38), 41–48.

Gustafson, L. B. (1978). Some major factors of porphyry copper genesis. *Economic Geology, 73*, 600–607.

Gustafson, L. B., & Hunt, J. P. (1975). The porphyry copper deposit at El Salvador, Chile. *Economic Geology, 70*(5), 857–912.

Gustafson, L. B., & Quiroga, J. (1995). Patterns of mineralization and alteration below the porphyry copper orebody at El Salvador, Chile. *Economic Geology, 90*, 2–16.

Hemley, J. J., & Hunt, J. P. (1992). Hydrothermal ore-forming processes in the light of studies in rock-buffered systems: II. Some general geologic applications. *Economic Geology, 87*, 23–43.

Hill, D. P., & Prejean, S. (2005). Magmatic unrest beneath Mammoth Mountain, California. *Journal of Volcanology and Geothermal Research, 146*, 257–283.

Houston, R. A. (2001). Geology and structural history of the Butte district, Montana. *Unpublished M.S. thesis, Corvallis, Oregon State University*, 45.

Jaramillo, J. S., Cardona, A., Monsalve, G., Valencia, V., & León, S. (2019). Petrogenesis of the late Miocene Combia Volcanic complex, northwestern Colombian Andes: Tectonic implication of short term and compositionally heterogeneous arc magmatism. *LITHOS*, 194–210. doi:https://doi.org/10.1016/j.lithos.2019.02.017

Jensen, E. P., & Barton, M. D. (2000). Gold deposits related to alkaline magmatism. *Reviews in Economic Geology, 13*, 279–314.

Kerr, A. C., & Tarney, J. (2005). Tectonic evolution of the Caribbean and northwestern South America: The case for accretion of two Late Cretaceous oceanic plateaus. *Geology, 33*, 269–272.

Kerr, A. C., Tarney, J., Marriner, G. F., Nivia, A., & Saunders, A. D. (1997). The Caribbean-Colombian Cretaceous Igneous Province: The internal anatomy of an oceanic plateau. *American Geophysical Union Books*, 123–144.

Lawn, B. (1993). Fracture of brittle solids, 2nd ed. *Cambridge University Press*, 378.

Leal-Mejia, H. (2011). Phanerozoic gold metallogeny in the colombian andes: a tectonic-magmatic approach. *Anglogold Ashanti*.

Leal-Mejía, H., Shaw, R., & Melgarejo, J. C. (2019). Spatial-Temporal Migration of Granitoid Magmatism and the Phanerozoic Tectono-Magmatic Evolution of the Colombian Andes. *Geology and Tectonics of Northwestern South America*.

Leckenby, R. J., Sanderson, D. J., & Lonergan, L. (2005). Estimating flow heterogeneity in natural fracture systems. *Journal of Volcanology and Geothermal Research*, 116–129.

León, S., Cardona, A., Jaramillo, J. S., Zapata, S., & Avellaneda-Jiménez, D. S. (2019). Comment on "Origin of pre-Mesozoic xenocrystic zircons in Cretaceous sub-volcanic rocks of the northern Andes (Colombia): Paleogeographic implications for the region" by Cetina et al. (2019). *Journal of South American Earth Sciences*.

Lesage, G. (2011). Geochronology, Petrography, Geochemical Constraints and Fluid Characterization of the Buriticá Gold Deposit, Antioquia Department, Colombia. *Master thesis, University of Alberta*, 75.

Lindsay, D. D., Zentilli, M., & Rojas de la Rivera, J. (1995). Evolution of an active ductile to brittle shear system controlling mineralization at the Chuquicamata porphyry copper deposit, northern Chile. *International Geology Review, 37*, 945–958.

Lowell, J. D., & Guilbert, J. M. (1970). Lateral and vertical alteration-mineralization zoning in porphyry ore deposits. *Economic Geology, 65*, 373–408.

Marín-Cerón, M., Leal-Mejía, H., Bernet, M., & Mesa-García, J. (2019). Late Cenozoic to Modern-Day Volcanism in the Northern Andes: A Geochronological, Petrographical, and Geochemical Review. *Geology and Tectonics of Northwestern South America*, 603–648.

McCourt, W. J., Aspden, J. A., & Brook, M. (1984). New geological and geochronological data from the Colombian Andes: continental growth by multiple accretion. *Journal of the Geological Society, 141*, 831–845.

McGrath, A. G., & Davison, I. (1995). Damage zone geometry at fault tips. *Journal of Structural Geology, 17*, 1011–1024.

McInnes, B. I., Farley, K. A., Sillitoe, R. H., & Kohn, B. P. (1999). Application of apatite (U-Th)/He thermochronometry to the determination of the sense and amount of vertical fault displacement at the Chuquicamata porphyry copper deposit, Chile. *Economic Geology, 94*, 937–947.

Mejía, M., & Salazar, G. (1989). Memoria explicativa de la Geología de la Plancha 114 (Dabeiba) y parte W de la 115 (Toledo). Escala 1:100.000. *INGEOMINAS*, 111.

Meyer, C. (1981). Ore-forming processes in geologic history. *Economic Geology, 75TH ANNIVERSARY VOLUME*, 6-41.

Meyer, C., & Hemley, J. J. (1967). Wall rock alteration, in Barnes, H.L., ed., Geochemistry of hydrothermal ore deposits: New York, Holt, Rinehart, and Winston . 166–235.

Meyer, C., Shea, E. P., Goddard, C. C., Jr., & staff, a. (1968). Ore deposits at Butte, Montana, in Ridge, J.D., ed., Ore deposits of the United States, 1933–1967 (Graton-Sales Volume). *New York, American Institute of Mining, Metallurgical, and Petroleum Engineers, 2*, 1373–1416.

Moreno-Sanchez, M., & Pardo-Trujillo, A. (2003). Stratigraphical and Sedimentological Constraints on Western Colombia: Implications on the Evolution of the Caribbean Plate. *AAPG Special Volumes*, 891–924.

Munroe, S. M. (1995). The Porgera gold deposit, Papua New Guinea: The influence of structure and tectonic setting on hydrothermal fluid flow and mineralisation at a convergent margin. *PACRIM '95 Conference, Australasian Institute of Mining and Metallurgy, Auckland, New Zealand*, 413–416.

Naney, M. T. (1983). Phase equilibria of rock-forming ferromagnesian silicates in granitic systems. *American Journal of Science, 283*, 993–1033.

Naranjo, A.; Horner, J.; Jahoda, R.; Diamond, L.; Castro, A.; Uribe, A.; Perez, C.; Paz, H.; Mejia, C.; Weil, J. (2017). La Colosa Au Porphyry Deposit, Colombia: Mineralization Styles, Structural Controls, and Age Constraints. *Economic Geology, 113*, 553–578.

Nguyen, P. T., Cox, S. F., Powell, C. M., & H. L. (1998). Fault-valve behaviour in optimally oriented shear zones at Revenge gold mine, Kambalda, Western Australia. *Journal of Structural Geology, 20*, 1625–1640.

Nivia, A. (1996). The Bolivar mafic-ultramafic complex, SW Colombia: the base of an obducted oceanic plateau. *Journal of South American Earth Sciences, 9*(1-2), 59–68.

Nivia, A., & Gómez-Tapias, J. (2015). Consideraciones acerca del modelo geológico evolutivo del Occidente Colombiano (Colombia). *Conference: X Congreso Colombiano de Geología*.

Nivia, A., Gómez-Tapias, J., Jiménez-Mejía, D., & Mora-Penagos, M. (2005). Mapa Geológico de Colombia a escala 1:1 000 000 versión 2005. *Conference: X Congreso Colombiano de Geología*.

Ordóñez-Carmona, O., & Pimentel, M. (2002). Rb–Sr and Sm–Nd isotopic study of the Puquıí complex, Colombian Andes. *Journal of South American Earth Sciences, 15*(2), 173–182.

Peterson, E. C., & Mavrogenes, J. A. (2014). Linking high-grade gold mineralization to earthquake-induced fault-valve processes in the Porgera gold deposit, Papua New Guinea. *The Geological Society of America, 42*(5), 383–386.

Pindell, J. L. (2009). Tectonic evolution of the Gulf of Mexico, Caribbean and northern South America in the mantle reference frame: an update. *Geological Society, London, Special Publications, 328*, 1–55.

Ramsey, J. M. (2004). Hybrid fracture and the transition. *Nature, 428*, 63–65.

Reches, Z., & Lockner, D. A. (1994). Nucleation and growth of faults in brittle rocks. *Journal of Geophysical Research, 99*, 18159–18173.

Redmond, P. B., Einaudi, M. T., Inan, E. E., Landtwing, M. R., & Heinrich, C. A. (2004). Copper deposition by fluid cooling in intrusion-centered systems: New insights from the Bingham porphyry ore deposit, Utah. *Geology, 32*, 217–220.

Reid, R. R., & Caddey, S. W. (1975). Primary refraction control of ore shoots, with examples from Coeur d'Alene district, Idaho. *Economic Geology, 70*, 1050–1061.

Restrepo, J. J., & Toussaint, J. F. (1987). Cuencas de traccion sinistrales en la falla de minas del Sistema Cauca-Romeral, en las cercanias de Medellin, Colombia. *31*.

Restrepo, J. J., Ordóñez-Carmona, O., Marterns, U., & Correa-Martinez, A. M. (2009). Terrenos, complejos y provincias en la Cordillera Central de Colombia. *Revista de Planeación y Desarrollo*, 49–56.

Richards, J. P. (1990). Petrology and geochemistry of alkalic intrusives at the Porgera gold deposit, Papua New Guinea. *Journal of Geochemical Exploration, 35*(1-5), 141–199.

Richards, J. P. (1992). Magmatic-epithermal transitions in alkalic systems: Porgera gold deposit, Papua New Guinea. *Economic Geology*.

Richards, J. P. (1992). Magmatic-epithermal transitions in alkalic systems: Porgera gold deposit, Papua New Guinea. *Geology, 20*(6), 547–550.

Richards, J. P., Boyce, A. J., & Pringle, M. S. (2001). Geologic evolution of the Escondida area, northern Chile: A model for spatial and temporal localization of porphyry Cu mineralization. *Economic Geology, 96*, 271–305.

Richards, J. P., Bray, C. J., Channer, D. M., & Spooner, E. T. (1997). Fluid chemistry and processes at the Porgera gold deposit, Papua New Guinea. *Mineralium Deposita, 32*, 119–132.

Richards, J. P., McCulloch, M. T., W., C. B., & Robert, K. (1991). Sources of metals in the Porgera gold deposit, Papua New Guinea: evidence from alteration, isotope, and noble metal geochemistry. *Geochimica et Cosmochimica Acta, 55*(2), 565–580.

Robert, F., & Poulsen, K. H. (2001). Structural controls on veins in gold. *Reviews in Economic Geology, 14*, 111–156.

Rodriguez, C., & Warden, A. J. (1993). Overview of some Colombian gold deposits and their development potential. *Mineral. Deposita 28*, 47–57.

Rodríguez, G., & Arango, M. (2013). Barroso Formation: a Tholeiitic volcanic arc and San Jose de Urama diabases: a T-MORB Type accretionary prism in the northern segment of Western Cordillera of Colombia. *Boletin, 33*, 17–38.

Rodríguez, G., & Zapata, G. (2012). Basalto de El Botón, volcanismo mioceno de afinidad shoshonítica en el noreste de la Cordillera Occidental de Colombia.

Rodríguez, G., & Zapata, G. (2012). Características del plutonismo Mioceno superior en el segmento Norte de la Cordillera Occidental e implicaciones tectónicas en el modelo geológico del Noroccidente Colombiano. *Boletin de Ciencias de La Tierra, 31*, 522.

Rodríguez, G., Zapata, G., & Gómez, J. F. (2012). Plancha Geológica 114, Dabeiba ,Antioquia. *Servicio geológico colombiano*.

Rodríguez–García, G., Correa–Martínez, A. M., Zapata–García, G., Arango–Mejía, M. I., Obando–Erazo, G., Zapata–Villada, J. P., & Bermúdez, J. G. (2020). Diverse Jurassic Magmatic Arcs of the Colombian Andes: Constraints from Petrography, Geochronology, and Geochemistry. *The Geology of Colombia, Volume 2 Mesozoic. Servicio Geológico Colombiano, Publicaciones Geológicas Especiales 36*, 117–170.

Rodríguez–García, G., Correa–Martínez, A., Zapata–García, G., Arango–Mejía, M. I., Obando–Erazo, G., Zapata–Villada, J. P., & Bermúdez, J. G. (2020). Diverse Jurassic Magmatic Arcs of the Colombian

Andes: Constraints from Petrography, Geochronology, and Geochemistry. *he Geology of Colombia, Volume 2 Mesozoic. Servicio Geológico Colombiano, Publicaciones Geológicas Especiales 36*, 117–170.

Ronacher, E., Richards, J. P., & Johnston, M. D. (2000). Evidence for fluid phase separation in high-grade ore zones at the Porgera gold deposit, Papua New Guinea. *Mineralium Deposita, 35*, 683–688.

Ronacher, E., Richards, J. P., Reed, M. H., Bray, C. J., Spooner, E. T., & Adams, P. D. (2004). Characteristics and evolution of the hydrothermal fluid in the North zone high-grade area, Porgera gold deposit, Papua New Guinea. *Economic Geology, 99*(5), 843–867.

Rowland, J. V., & Simmons, S. F. (2012). Hydrologic, magmatic, and tectonic controls on hydrothermal flow, Taupo volcanic zone, New Zealand: Implications for the formation of epithermal vein deposits. *Economic Geology, 107*, 427–457.

Rusk, B. G. (2002). Scanning electron microscope-cathodoluminescence analysis of quartz reveals complex growth histories in veins from the Butte porphyry copper deposit, Montana. *Geology, 30*, 727–730.

Seedorff, E., & Einaudi, M. T. (2004a). Henderson porphyry molybdenum system, Colorado I. Sequence and abundance of hydrothermal mineral assemblages, flow paths of evolving fluids, and evolutionary style. *Economic Geology, 99*, 3–37.

Seedorff, E., Dilles, J., & Proffett, J. (2005). Porphyry Deposits: Characteristics and Origin of Hypogene Features. *Economic Geology, 100th Anniversary Volume*, 251–298.

SEG. (2020). Applied structural geology of ore-forming hydrothermal systems. *Reviews in Economic Geology, 21*, 25–82.

Selby, D., Nesbitt, B. E., Muehlenbachs, K., & Prochaska, W. (2000). Hydrothermal alteration and fluid chemistry of the Endako porphyry molybdenum deposit, British Columbia. *Economic Geology, 95*, 183–202.

Shapiro, S. A. (2015). Fluid-induced seismicity. *Cambridge, Cambridge University*, 276.

Shelly, D. R., Hill, D. P., Massin, F., Farrell, J., Smith, R. B., & Taira, T. (2013a). A fluid-driven earthquake swarm on the margin of the Yellowstone caldera. *Journal of Geophysical Research, 118*, 4872–4886.

Shelly, D. R., Moran, S. C., & Thelen, W. A. (2013b). Evidence for fluid-triggered slip in the 2009 Mount Rainier, Washington, earthquake swarm. *Geophysical Research Letters, 40*, 1506–1512.

Shelly, D. R., Taira, T., Prejean, S. G., Hill, D. P., & Dreger, D. S. (2015). Fluid faulting interactions: Fracture mesh and fault-valve behavior in the February 2014 Mammoth Mountain, California, earthquake swarm. *Geophysical Research Letters, 42*, 5803–5812.

Sheppard, S. M., Nielsen, R. L., & Taylor, H. P. (1971). Hydrogen and oxygen isotope ratios in minerals from porphyry copper deposits. *Economic Geology, 66*, 515–542.

Sibson, R. H. (1981). Fluid flow accompanying faulting: Field evidence and models, in Simpson, D.W., and Richards, P.G, eds., Earthquake prediction: An international review. *Maurice Ewing series, 4*, 593–603.

Sibson, R. H. (1989). Earthquake faulting as a structural process. *Journal of Structural, 11*, 1–14.

Sibson, R. H. (1996). Structural permeability of fluid-driven fault-fracture meshes. *Journal of Structural Geology, 18*, 1031–1042.

Sibson, R. H. (2001). Seismogenic framework for ore deposition. *Reviews in Economic Geology, 14*, 25–50.

Sibson, R. H. (2003). Thickness of the seismic slip zone. *Bulletin of the Seismological Society of America, 93*, 1169–1178.

Sibson, R. H. (2019). Arterial faults and their role in mineralizing systems. *Geoscience Frontiers, 10*(6), 2093–2100. doi://doi.org/10.1016/j.gsf.2019.01.007.

Sillitoe, R. H. (1972). A plate tectonic model for the origin of porphyry copper deposits. *Economic Geology, 67*, 184–197.

Sillitoe, R. H. (1976). Andean mineralization: A model for the metallogeny of convergent plate margins. *Geological Association of Canada Special Paper 14*, 59–100.

Sillitoe, R. H. (1985). Ore-related breccias in volcanoplutonic arcs. *Economic Geology, 80*, 1467–1514.

Sillitoe, R. H. (1994). Erosion and collapse of volcanoes: Causes of telescoping in intrusion-centered ore deposits. *Geology, 22*, 945–948.

Sillitoe, R. H. (2000). Gold-rich porphyry deposits: Descriptive and genetic models and their role in exploration and discovery. *Reviews in Economic Geology, 13*, 315–345.

Sillitoe, R. H. (2008). Major gold deposits and belts of the North and South American Cordillera: Distribution, tectonomagmatic settings, and metallogenic considerations. *Economic Geology and the Bulletin of the Society of Economic Geologists, 103*, 663–687.

Sillitoe, R. H. (2010). Porphyry Copper Systems. *Economic Geology*(105), 3–41. doi:http://dx.doi.org/10.2113/gsecongeo.105.1.3

Sillitoe, R. H., & Hedenquist, J. W. (2003). Linkages between volcanotectonic settings, ore-fluid compositions, and epithermal precious metal deposits. *Socitety of Economic Geology*.

Sillitoe, R. H., Jaramillo, L., Damon, P. E., Shafiqullah, M., & Escovar, R. (1982). Setting, characteristics, and age of the Andean porphyry copper belt in Colombia. *Economic Geology*, 1837–1850.

Skewes, M. A. (1996). Late Miocene mineralized breccias in the Andes of central Chile: Sr- and Nd-isotopic evidence for multiple magmatic sources. *Society of Economic Geologists Special Publication 5*, 33–41.

Spikings, R., Cochrane, R., Villagomez, D., Lelij, R. V., Vallejo, C., Winkler, W., & Beate, B. (2015). The geological history of northwestern South America: from Pangaea to the early collision of the Caribbean Large Igneous Province (290–75 Ma). *Gondwana Research*, 95–139.

Staude, J. -M., & Barton, M. D. (2001). Jurassic to Holocene tectonics magmatism, and metallogeny of northwestern Mexico. *Geological Society of America Bulletin, 113*, 1357–1374.

Sterling, M. W., Wesnousky, S. G., & Shimazaki, K. (1996). Fault trace complexity, cumulative slip, and the shape of the magnitude-frequency distribution for strike-slip faults. *Geophysical Journal International, 124*, 833–868.

Stoffregen, R. E. (1987). Genesis of acid-sulfate alteration and Au-Cu-Ag mineralization at Summitville, Colorado. *Economic Geology*, 1575–1591.

Suppe, J. (1983). Geometry and kinematics of fault-bend folding. *American Journal of Science, 283*, 684–721.

Taboada, A.; Rivera, L. A.; Fuenzalida, A.; Cisternas, A.; Philip, H.; Bijwaard, H.; Olaya, J.; Rivera, C. (2000). Geodynamics of the northern Andes: Subductions and intracontinental deformation (Colombia). *Tectonics, 19*(5), 787–813.

Titley, S. R. (1966). Preface, in Titley, S.R., and Hicks, C.L., eds., Geology of the porphyry copper deposits, southwestern North America. *Tucson, University of Arizona Press*, ix-x.

Titley, S. R. (1982b). The style and progress of mineralization and alteration in porphyry systems, in Titley, S.R., ed. Advances in geology of the porphyry. *Tucson, Arizona, University of Arizona Press*, 93–116.

Titley, S. R. (1997). 1997 Jackling Lecture: Porphyry copper geology: A late century. *Mining Engineering, 49*, 57–63.

Tomlinson, A. J., & Blanco, N. (1997a). Structural evolution and displacement history of the West fault system, Precordillera, Chile: Part 1 Synmineral history. *Congreso Geológico Chileno, 8th, Antofagasta, Actas, 3*, 1873–1877.

Tomlinson, A. J., Dilles, J. H., & Maksaev, V. (2001). Application of apatite (U-Th)/He thermochronometry to the determination of the sense and amount of vertical fault displacement at the Chuquicamata porphyry copper deposit, Chile—a discussion. *Economic Geology, 96*, 1307–1309.

Toussaint, J. F., & Restrepo, J. J. (1988). Terranes and Continental Accretion in the Colombian Andes. *11*, 189–193.

Toussaint, J. F., & Restrepo, J. J. (1990). Cronología de las acreciones de terrenos alóctonos en los Andes colombianos. *Universidad Nacional de Colombia, Facultad de Ciencias*.

Toussaint, J. F., & Restrepo, J. J. (1994). The Colombian Andes During Cretaceous Times. *Cretaceous Tectonics of the Ande. Earth Evolution Sciences*, 61–100.

Ulrich, T., & Heinrich, C. A. (2001). Geology and alteration geochemistry of the porphyry Cu-Au deposit at Bajo de la Alumbrera, Argentina. *Economic Geology, 96*, 1719–1742.

Vinasco, C. (2019). The Romeral Shear Zone. *Geology and Tectonics of Northwestern South America. Frontiers in Earth Sciences. Springer, Cham.*

Vinasco, C., & Cordani, U. (2012). Reactivation episodes of the Romeral fault system in the Northwestern part of Central Andes, Colombia, through 39Ar-40Ar and K-Ar results. *Boletín de Ciencias de la Tierra*.

Vinasco, C., Cordani, U., & Vasconcelos, P. (2001). 40Ar/39Ar dates in the Central Cordillera of Colombia: Evidence for an upper triassic regional tecnomagmatic event. *South American symposium on isotope geology*.

Walsh, J. J., Torremans, K., Güven, J., Kyne, R., Conneally, J., & Bonson, C. (2018). Fault-controlled fluid flow within extensional basins and its implications for sedimentary rock-hosted mineral deposits. *Society of Economic Geologists, Inc. SEG Special Publications*(21), 237–269. doi:10.5382/sp.21.11; 33 p.

Walsh, J. J., Watterson, J., Bailey, W. R., & Childs, C. (1999). Fault relays, bends, and branch lines. *Journal of Structural Geology, 21*, 1019–1026.

Weber, M., Cardona, A., Valencia, V., & Altenberger, U. (2011). Geochemistry and Geochronology of the Guajira Eclogites, northern Colombia: evidence of a metamorphosed primitive Cretaceous Caribbean Island-arc. *Geologica Acta: an international earth science journal*.

Weber, M., Gómez-Tapias, J., Cardona, A., Duarte, E., Pardo-Trujillo, A., & Valencia, V. A. (2015). Geochemistry of the Santa Fé Batholith and Buriticá Tonalite in NW Colombia – Evidence of subduction initiation beneath the Colombian Caribbean Plateau. *62*, 257–274.

Wesnousky, S. G. (1988). Seismological and structural evolution of strike-slip faults. *Nature, 335*, 340–342.

White, D., Musacchio, G., Helmstaedt, H., Harrap, R., Thurston, P., Velden, A. v., & Hall, K. (2003). Images of a lower-crustal oceanic slab: Direct evidence for tectonic accretion in the Archean western Superior province. *Geology, 311*, 997–1000.

Williams, S. A., & Forrester, J. D. (1995). Characteristics of porphyry copper deposits. *Arizona Geological Society Digest 20*, 21–34.

Wilson, J. W., Kesler, S. E., Cloke, P. L., & Kelly, W. C. (1980). Fluid inclusion geochemistry of the Granisle and Bell porphyry copper deposits, British Columbia. *Economic Geology, 75*, 45–61.

Yielding, G. (2016). The geometry of branch lines. *Geological Society of London, Special Publication 439*.

Yukutake, Y., Ito, H., Honda, R., Harada, M., Tanada, T., & Yoshida, A. (2011). Fluid-induced swarm earthquake sequence revealed by precisely determined hypocentres and focal mechanisms in the 2009 activity at Hakone volcano, Japan. *Journal of Geophysical Research, 116*.

Zapata-Villada, J., Restrepo, J., Cardona-Molina, A., & Martens, U. (2017). Geoquímica y geocronología de las rocas volcánicas básicas y el Gabro de Altamira, Cordillera Occidental (Colombia): Registro de ambientes de Plateau y arco oceánico superpuestos durante el cretácico. *Boletín de Geología, 39*(2), 13–30.

Appendix

Appendix 1. Petrography samples, locations and descriptions.

WSG84 18N projection.

Samples	Observations	X	Y	Z
BUUY152	155.20	399916.507	741354.535	1434.89
BUUY249D01	350.75	399818.305	741013.976	828.172
BUUY339D01	338.20	399514.972	741166.96	677.478
BUUY455	31.80	399720.476	740924.85	1468.91
BUUY455	285.50	399744.845	741141.928	1341.07
GBUS003	681.10	398476.837	740477.812	1729.49
SA_01	GA 9617 E	400136.822	741307.681	1409.350
SA_02	BUUY295, Sample 515576	400185.495	741305.72	870.609
SA_03	BUUY291D03, Sample 525930	399506.271	741198.416	553.140
CTN_01	SG 9610 E	399959.519	741363.838	1507.000
CTN_02	SG 9608 E	399947.656	741371.185	1497.700
CASSANDRA	GA_9339 E	399839.432	741126.84	1165.440
NEMESIS-2	GA 9351 W	400044.31	739728.409	1166.963
MU_01	GA 9843 W	400101.527	741215.056	1372.025
MU_02	BUUY249D01, Sample 475578	399792.099	741097.844	697.013
MU_03	BUSY367D03, Sample 497460,	399775.24	741096.504	236.687
NEMESIS	GA_9168W	399366.379	740735.558	1239.7

Sample: BUUY152 – 155.20

Rock	Porphyritic diorite
Texture	Hypocrystalline
Grain size (um)	< 10 - 1000
General texture	Porphyritic, fine-grained crystals with allotriomorphic shape

Mineralogy

Mineral	**Percentage**	**Size (um)**	**Texture**
Lithologic			
Quartz	0.7	40	Disseminated
Plagioclase	54.6	200 - 1000	Disseminated
Hornblende	9.3	100 - 700	Disseminated
Matrix	4.6	< 10	Matrix
Zircon	0.3	5 - 20	Inclusion
Alteration			
Actinolite	5	10 - 50	Selective replacement in hornblende
Epidote	1.7	30 - 150	Selective replacement in mafics
Calcite	11.6	10 - 40	Selective replacement in plagioclase
Chlorite	2	< 10 - 20	Selective replacement in hornblende
Sericite	3	< 10 - 20	Selective replacement in plagioclase
Sphene	1	10 - 20	Selective replacement in hornblende
Rutile	0.7	10	Selective replacement in mafics
Clay	1.7	< 5	Selective replacement in plagioclase
Mineralization			
Pyrite	3	20 - 500	Disseminated
Pyrrhotite	0.7	10 - 20	Inclusion
Chalcopyrite	0.3	10 - 50	Disseminated and inclusion

Observations

Mineralization is mainly disseminated pyrite and as veinlets in which part of the matrix is recognized. Chalcopyrite is associated with zones of epidote and actinolite.

Sample: BUUY249D01 – 350.75

Rock	Pyroxene diorite
Texture	Holocrystalline
Grain size (um)	< 10 - 2000
General texture	Phaneritic, fine-grained crystals with allotriomorphic shape

Mineralogy

Mineral	**Percentage**	**Size (um)**	**Texture**
Lithologic			
Plagioclase	70.6	20 - 1000	Disseminated
Quartz	0.3	100	Disseminated
K Feldspar	0.3	10 - 40	Disseminated
Clinopyroxene	4.2	30 - 450	Disseminated
Hornblende	7.2	10 - 80	Disseminated
Biotite	8.9	10 - 200	Disseminated
Zircon	0.3	< 10	Inclusion
Apatite	0.3	< 10 - 20	Inclusion
Alteration			
Chlorite	0.6	10 - 20	Selective replacement in biotite
Rutile	1.1	10	Selective replacement in mafics
Mineralization			
Magnetite	5.5	100 - 400	Disseminated
Pyrrhotite	0.3	< 10 - 20	Disseminated and inclusion
Chalcopyrite	0.6	< 10	Disseminated and inclusion

Observations

Mineralization is related to the presence of disseminated chalcopyrite in the middle, particularly of biotites accumulations. Some inclusions of pyrrhotite and chalcopyrite are often recognized in magnetite as inclusions which follow crystallographic planes. Magnetite concentrations also occur amid biotite and mafic clusters.

Sample: BUUY339D01 – 338.20

Rock	Pyroxene diorite
Texture	Holocrystalline
Grain size (um)	< 10 - 2000
General texture	Phaneritic, fine-grained crystals with allotriomorphic shape

Mineralogy

Mineral	**Percentage**	**Size (um)**	**Texture**
Lithologic			
Plagioclase	54	100 - 2000	Disseminated
K Feldspar	0.5	20 - 80	Disseminated
Quartz	0.8	30 - 100	Disseminated
Clinopyroxene	8.5	100 - 600	Disseminated
Hornblende	1.8	200 - 500	Disseminated
Biotite	9.3	10 - 50	Disseminated
Zircon	0.5	10	Inclusion
Apatite	0.8	20	Inclusion
Alteration			
Actinolite	7.2	10 - 30	Selective replacement in hornblende
Epidote	0.5	20 - 50	Selective replacement in pyroxene
Secondary biotite	0.3	< 10	Selective replacement in hornblende
Chlorite	0.8	< 10	Selective replacement in biotite
Sphene	1	30	Selective replacement in biotite
Calcite	0.5	10 - 40	Selective replacement in plagioclase
Rutile	0.3	< 10	Selective replacement in mafics
Mineralization			
Magnetite	6.5	30 - 250	Disseminated and hydrothermal
Pyrite	1	10 - 50	Disseminated and infill
Pyrrhotite	0.3	10	Disseminated and inclusion
Chalcopyrite	1.3	10 - 30	Disseminated and inclusion
Observations			

Intrusive igneous rock of dioritic composition with slightly hydrothermal alteration. The texture is phaneritic with specific poikilitic texture associated with the presence of plagioclase inclusions in hornblende and augite. Hydrothermal alteration is associated with the transformation of primary minerals such as hornblende, into actinolite and epidote. Due to their size, shape and the presence of apatite and zircon inclusions, a large part of the biotites correspond to primary varieties. Secondary biotite is recognized in low proportion in almost trace amounts. Mineralization is fundamentally related to the occurrence of disseminated pyrite which grows from primary magnetite. There are varieties of magmatic magnetite with a regular polygonal shape, and hydrothermal differentiated by the presence of chalcopyrite inclusions. In the middle-lower part of the sample, hornblende appears aligned as a microvein around with a halo of pyrite, actinolite and epidote.

Sample: BUUY455 – 31.80

Rock	Hyaloclastite
Texture	Hypocrystalline
Grain size (um)	< 10 - 7000
General texture	Brecciated, fine-grained crystals

Mineralogy

Mineral	**Percentage**	**Size (um)**	**Texture**
Lithologic			
Plagioclase	1.8	100 - 300	Disseminated
Quartz	0.4	10 - 50	Disseminated
Matrix	45.7	< 10	Matrix
Volcanic clasts	8.3	120 - 7000	Clasts
Pyroclastic clasts	3.6	200 - 5000	Clasts
Zircon	0.2	< 10	Inclusion
Apatite	0.2	< 10	Inclusion
Alteration			
Secondary Bt	16.8	< 10 - 40	Selective replacement in mafics
Albite	1.6	20 - 50	Selective replacement in mafics
Sericite	3.1	< 10	Selective replacement in plagioclase
Chlorite	4.5	< 10	Selective replacement in biotite
Epidote	0.7	10 -200	Selective replacement in biotite
Calcite	0.9	10 - 50	Selective replacement in plagioclase
Rutile	0.7	< 10	Selective replacement in mafics
Clay	2.2	< 10	Selective replacement in matrix
Mineralization			
Magnetite	6.1	20 - 140	Disseminated
Pyrite	1.8	10 -300	Disseminated and infill
Pyrrhotite	0.2	< 10 - 20	Disseminated and inclusion
Chalcopyrite	0.4	< 10 - 60	Disseminated and inclusion

Observations

Chalcopyrite in this sample is associated with the presence of secondary biotite and chlorite. The small size of the crystals of this sulphide is possibly also associated with the small flakes of secondary biotite. Pyrite is observed scattered and in microveins. Magnetite is particularly abundant in the clasts, so it is estimated to be primary. Magnetite related to alteration is generally associated with secondary biotite.

Sample: BUUY455 – 285.50

Rock	Hydrothermal breccia
Texture	Hypocrystalline
Grain size (um)	< 10 - 1000
General texture	Brecciated, fine-grained crystals

Mineralogy

Mineral	**Percentage**	**Size (um)**	**Texture**
Lithologic			
Quartz	0.5	20 - 80	Disseminated
Plagioclase	1	100 - 300	Disseminated
Matrix	18.2	< 10	Matrix
Zircon	0.3	< 10	Inclusion
Alteration			
Sericite	57.9	< 10 - 40	Selective replacement in plagioclase
Quartz	7.3	< 10 - 60	Selective replacement in matrix
Calcite	0.8	10 - 30	Selective replacement in plagioclase
Chlorite	1	< 10 - 20	Selective replacement in biotite
Rutile	2.6	< 5 - 20	Selective replacement in mafics
Mineralization			
Pyrite	9.1	30 - 1500	Disseminated
Galena	0.5	< 10	Inclusion
Pyrrhotite	0.3	10 - 30	Inclusion
Chalcopyrite	0.5	20 - 500	Disseminated and inclusion

Observations

Pyrite mineralization is related to the sericitization process where it is scattered and often forming some clusters. There are some inclusions of galena, pyrrhotite and chalcopyrite within pyrite.

Sample: GBUS003 – 681.10

Rock	Porphyritic quartzdiorite
Texture	Hypocrystalline
Grain size (um)	< 10 - 1000
General texture	Porphyritic, fine-grained crystals

Mineralogy

Mineral	**Percentage**	**Size (um)**	**Texture**
Lithologic			
Quartz	0.6	30 - 100	Disseminated
Plagioclase	4.8	20 - 1000	Disseminated
Hornblende	5.1	40 -800	Disseminated
Matrix	68.2	< 10	Matrix
Zircon	0.3	< 5	Inclusion
Alteration			
Sericite	1	< 10	Selective replacement in plagioclase
Calcite	3.5	10 - 20	Selective replacement in plagioclase
Chlorite	1.3	< 10	Selective replacement in hornblende
Rutile	1.3	< 10 - 20	Selective replacement in mafics
Mineralization			
Pyrite	11.6	10 - 1000	Disseminated
Pyrrhotite	0.3	10 - 30	Inclusion
Chalcopyrite	1.9	10 - 200	Disseminated and inclusion

Observations

Pyrite is scattered in the matrix that is altered to sericite, carbonates and chlorite. Inside some scattered crystals of pyrite, there are some inclusions of chalcopyrite and pyrrhotite. Chalcopyrite is also scattered in altered mafic clusters.

Appendix 2. XRD data

Diffractograms for samples analyzed through XRD.

Face sample location (WSG84 18N projection): X: 399575.351 - Y: 740901.035 - Z: 1437.217

Sample 1.

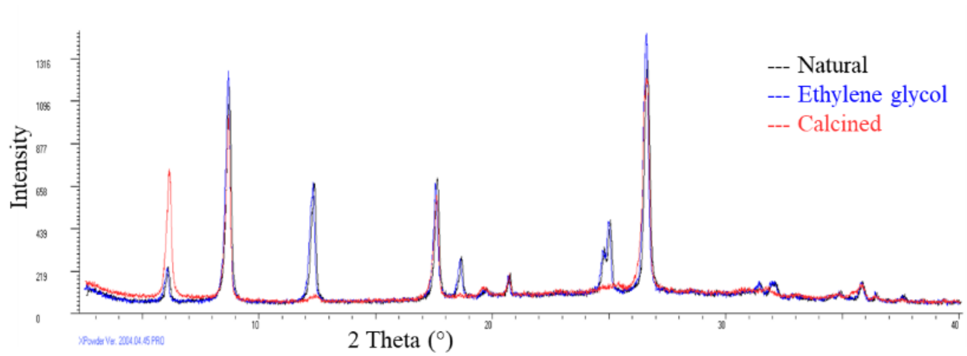

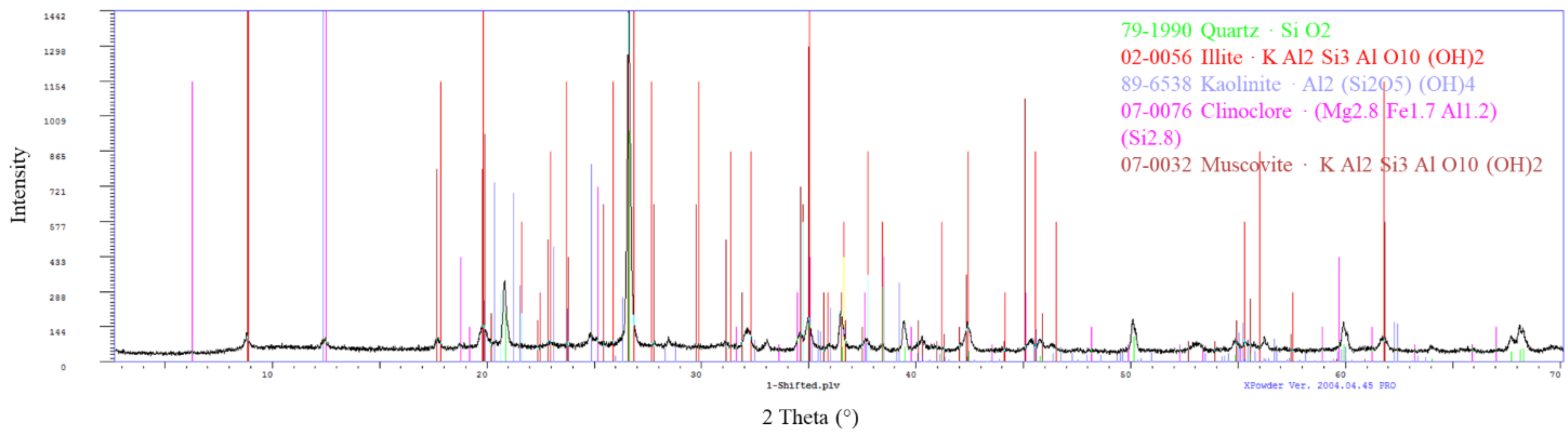

Sample 2.

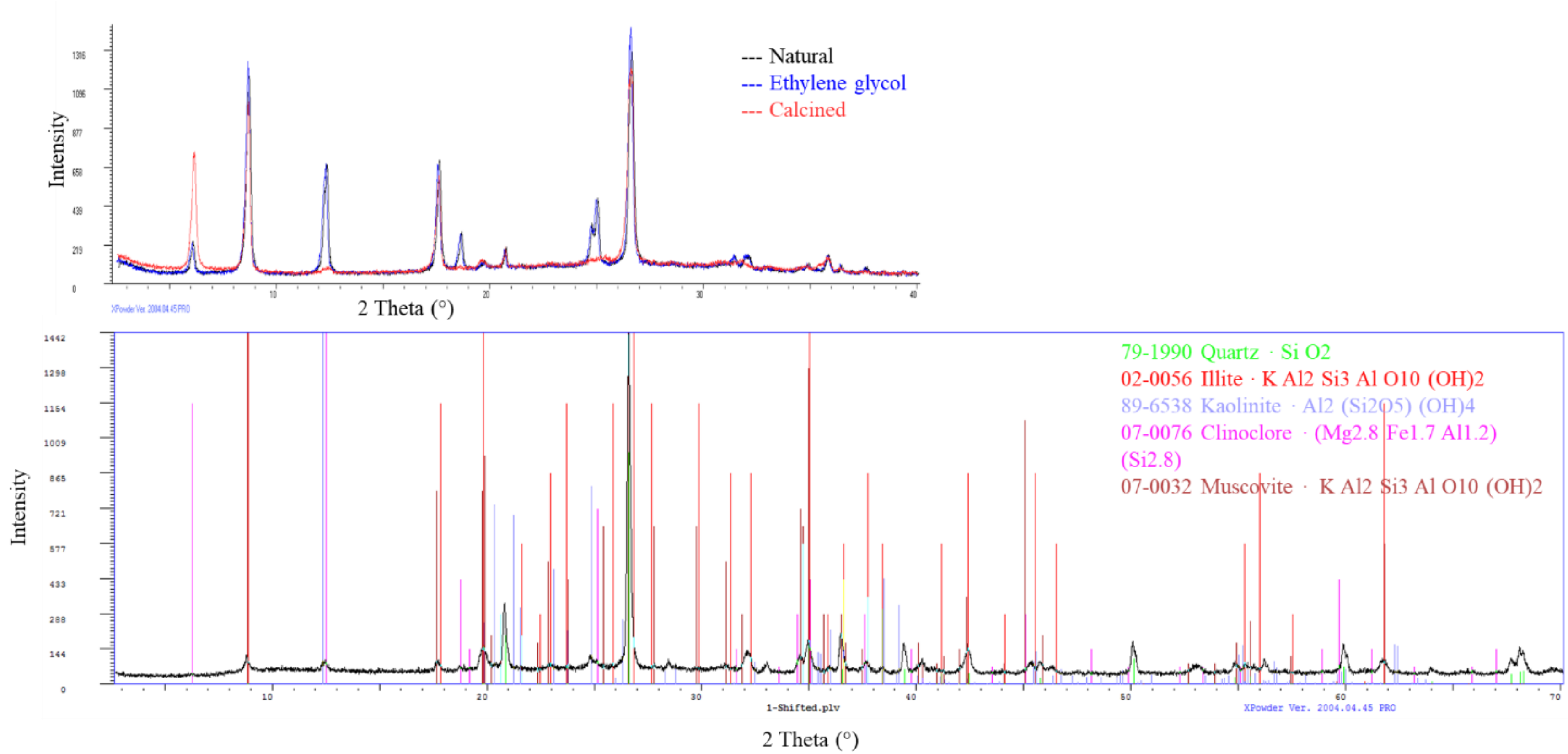
Intensity
--- Natural
--- Ethylene glycol
--- Calcined
2 Theta (°)
1442
1298
1154
1009
865
721
577
433
288
144
0
Intensity
79-1990 Quartz · Si O2
02-0056 Illite · K Al2 Si3 Al O10 (OH)2
89-6538 Kaolinite · Al2 (Si2O5) (OH)4
07-0076 Clinoclore · (Mg2.8 Fe1.7 Al1.2) (Si2.8)
07-0032 Muscovite · K Al2 Si3 Al O10 (OH)2
10
20
30
40
50
60
70
1-Shifted.plv
XPowder Ver. 2004.04.45 PRO
2 Theta (°)

Sample 3.

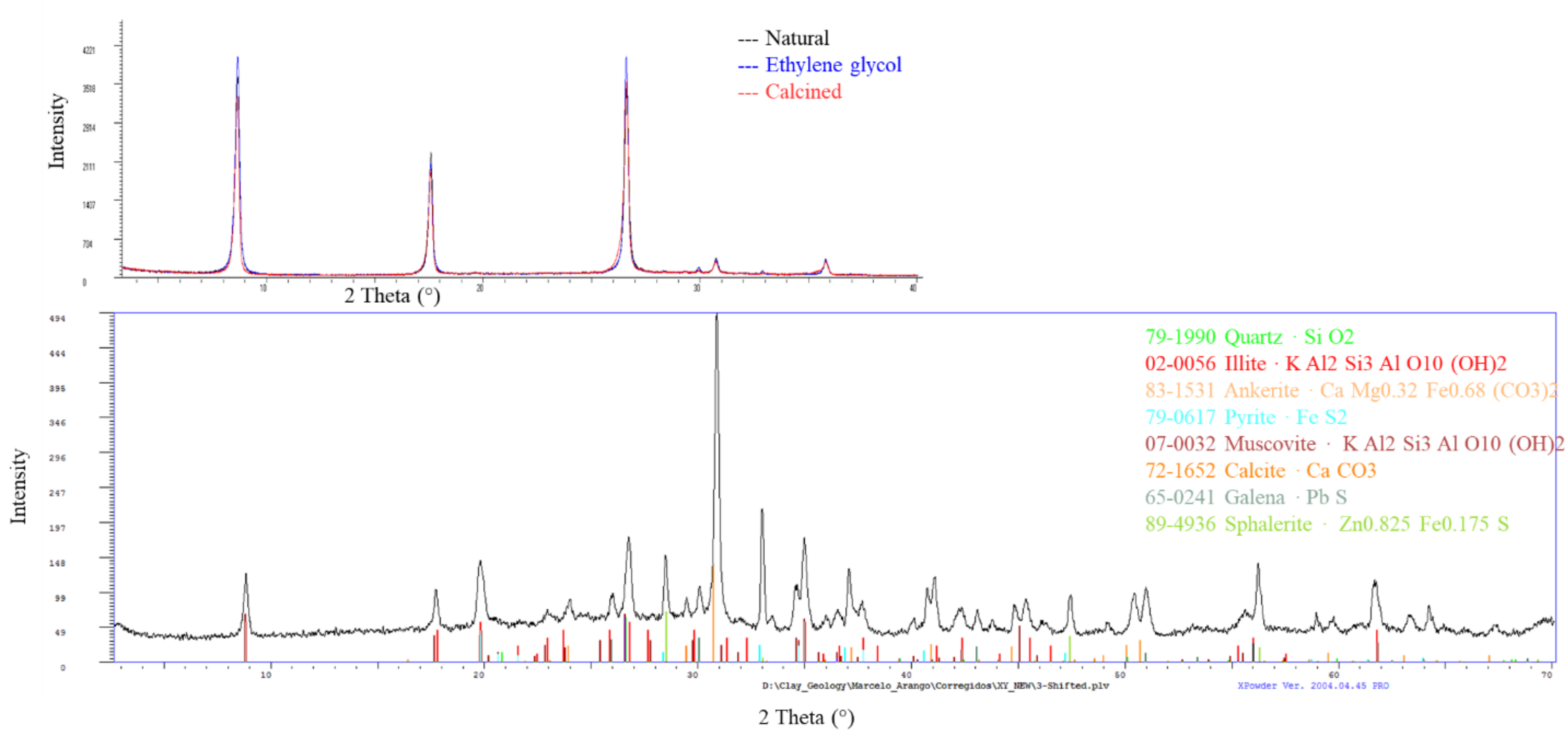
--- Natural
--- Ethylene glycol
--- Calcined
Intensity
2 Theta (°)
79-1990 Quartz · Si O2
02-0056 Illite · K Al2 Si3 Al O10 (OH)2
83-1531 Ankerite · Ca Mg0.32 Fe0.68 (CO3)2
79-0617 Pyrite · Fe S2
07-0032 Muscovite · K Al2 Si3 Al O10 (OH)2
72-1652 Calcite · Ca CO3
65-0241 Galena · Pb S
89-4936 Sphalerite · Zn0.825 Fe0.175 S
494
444
395
346
296
247
197
148
99
49
0
10
20
30
40
50
60
70
D:\Clay_Geology\Marcelo_Arango\Corregidos\XY_NEW\3-Shifted.plv
XPowder Ver. 2004.04.45 PRO
Intensity
2 Theta (°)

Sample 4.

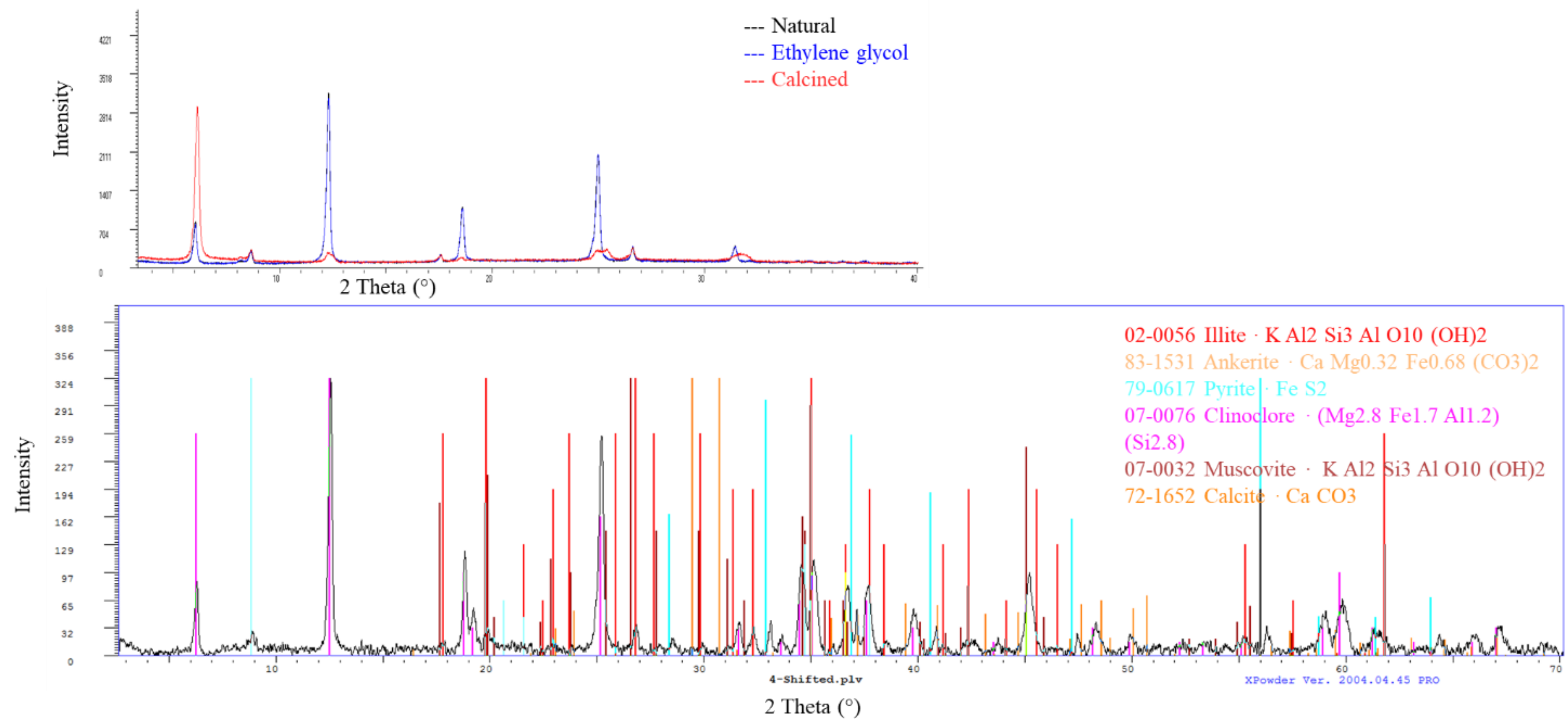
--- Natural
--- Ethylene glycol
--- Calcined
Intensity
2 Theta (°)
02-0056 Illite · K Al2 Si3 Al O10 (OH)2
83-1531 Ankerite · Ca Mg0.32 Fe0.68 (CO3)2
79-0617 Pyrite · Fe S2
07-0076 Clinoclore · (Mg2.8 Fe1.7 Al1.2) (Si2.8)
07-0032 Muscovite · K Al2 Si3 Al O10 (OH)2
72-1652 Calcite · Ca CO3
Intensity
4-Shifted.plv
XPowder Ver. 2004.04.45 PRO
2 Theta (°)

Sample 5.

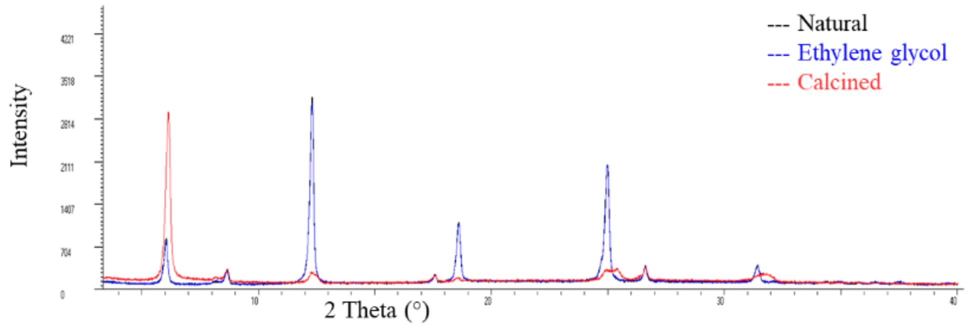
--- Natural
--- Ethylene glycol
--- Calcined
Intensity
2 Theta (°)

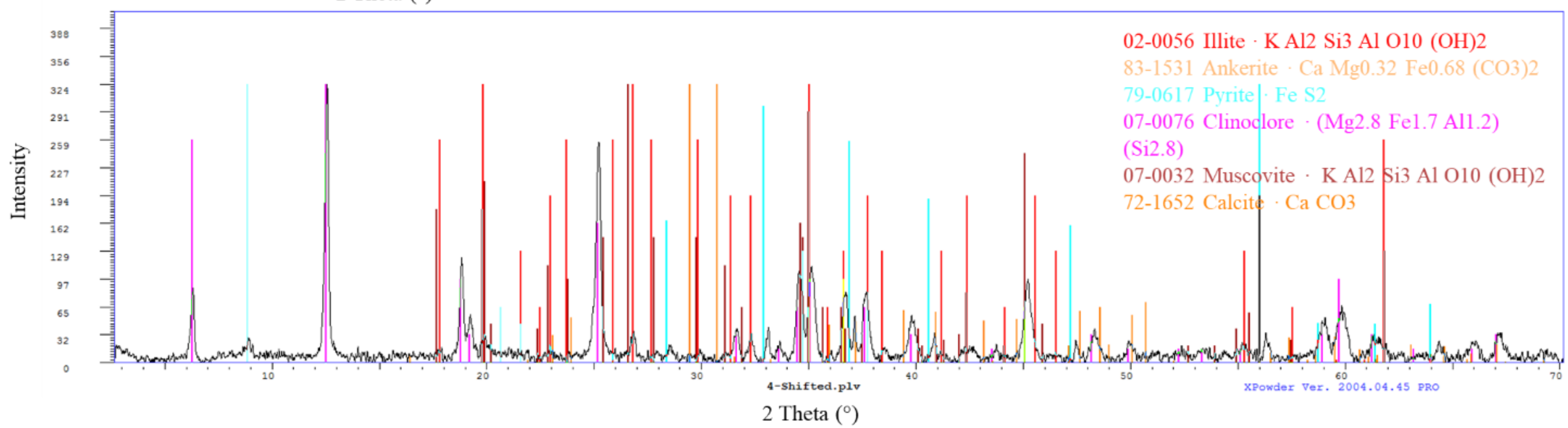
02-0056 Illite · K Al2 Si3 Al O10 (OH)2
83-1531 Ankerite · Ca Mg0.32 Fe0.68 (CO3)2
79-0617 Pyrite · Fe S2
07-0076 Clinoclore · (Mg2.8 Fe1.7 Al1.2) (Si2.8)
07-0032 Muscovite · K Al2 Si3 Al O10 (OH)2
72-1652 Calcite · Ca CO3
Intensity
4-Shifted.plv
XPowder Ver. 2004.04.45 PRO
2 Theta (°)

Appendix 3. Geochronological data

Related information with the dated samples, including coordinates, ratios, ages, MSWD. Al well as graphic material such concordia plots, weighted mean age diagrams and backscattered/cathodoluminescence (BSC/CL) images of zircon grains.

Sample	Label	mFrom	mTo	X	Y	Z
BUSY291	2	1269.55	1275.5	399575.441	741191.786	623.003
BUUY152	4	155.2	161.15	399916.507	741354.535	1434.892
BUUY339D01	5	338.2	344.4	399514.972	741166.960	677.478

Sample:	**BUUY-152**																		
				RATIOS							**AGES [Ma]**						**Age - Common Pb correction (e)**		
N° spot	**U [ppm] a**	**Pb [ppm] a**	**Th [ppm] a**	**$^{207}Pb/^{235}U^{b}$**	**2 s^{d}**	**$^{206}Pb/^{238}U^{b}$**	**2 s^{d}**	**rho^{c}**	**$^{207}Pb/^{206}Pb^{b}$**	**2 s^{d}**	**$^{207}Pb/^{235}U$**	**2 s**	**$^{206}Pb/^{238}U$**	**2 s**	**$^{207}Pb/^{206}Pb$**	**2 s**	**$^{206}Pb/^{238}U$**	**2 s**	**$^{207}Pb/^{206}Pb$ común**
BUUY-152_15	883	17	1030	0.00816	0.00028	0.00117	0.00002	0.12395	0.05030	0.00140	8.3	0.3	7.5	0.1	220.0	67.0	**7.5**	**0.1**	**0.80316**
BUUY-152_4	1533	27	1738	0.00755	0.00018	0.00117	0.00002	0.00304	0.04680	0.00110	7.6	0.2	7.5	0.1	36.0	51.0	**7.5**	**0.1**	**0.80316**
BUUY-152_14	912	19	1253	0.00777	0.00031	0.00117	0.00002	0.38275	0.04860	0.00250	7.9	0.3	7.6	0.2	130.0	110.0	**7.5**	**0.2**	**0.80316**
BUUY-152_6	1239	39	1818	0.01437	0.00068	0.00124	0.00002	0.19660	0.08580	0.00380	14.5	0.7	8.0	0.1	1344.0	82.0	**7.6**	**0.1**	**0.80319**
BUUY-152_9	1174	32	1857	0.00957	0.00036	0.00120	0.00002	0.05141	0.05810	0.00210	9.7	0.4	7.7	0.1	552.0	83.0	**7.6**	**0.1**	**0.80317**
BUUY-152_13	1245	31	1784	0.00773	0.00029	0.00118	0.00002	0.25902	0.04750	0.00180	7.8	0.3	7.6	0.1	82.0	78.0	**7.6**	**0.1**	**0.80317**
BUUY-152_18	1240	41	2479	0.00770	0.00025	0.00118	0.00003	0.27208	0.04720	0.00180	7.8	0.3	7.6	0.2	66.0	79.0	**7.6**	**0.2**	**0.80317**
BUUY-152_24	1938	44	2985	0.01003	0.00038	0.00120	0.00002	0.19443	0.06020	0.00220	10.1	0.4	7.8	0.1	618.0	74.0	**7.6**	**0.1**	**0.80318**
BUUY-152_12	743	13	783	0.00760	0.00027	0.00119	0.00002	0.57800	0.04700	0.00130	7.7	0.3	7.6	0.1	47.0	58.0	**7.6**	**0.1**	**0.80317**
BUUY-152_23	1038	43	2041	0.01410	0.00110	0.00125	0.00002	0.16256	0.08110	0.00610	14.2	1.1	8.1	0.1	1230.0	160.0	**7.7**	**0.1**	**0.80319**
BUUY-152_17	868	21	974	0.01132	0.00061	0.00123	0.00002	0.16429	0.06800	0.00370	11.4	0.6	7.9	0.1	840.0	110.0	**7.7**	**0.1**	**0.80319**
BUUY-152_2	300	7	333	0.01197	0.00083	0.00124	0.00002	0.04658	0.07090	0.00490	12.1	0.8	8.0	0.1	940.0	160.0	**7.7**	**0.1**	**0.80319**
BUUY-152_7	1606	36	2229	0.00766	0.00025	0.00120	0.00002	0.00326	0.04630	0.00150	7.7	0.3	7.7	0.1	12.0	64.0	**7.7**	**0.1**	**0.80317**
BUUY-152_21	1795	63	4037	0.00829	0.00023	0.00120	0.00002	0.17718	0.05000	0.00150	8.4	0.2	7.8	0.1	187.0	68.0	**7.7**	**0.1**	**0.80318**

Number of shots used in this age: 14. Weighted average age: 7.6 ± 0.1 [0.1%] Ma

MSWD: 1.6


BUUY152
100 μm

Sample:	**BUUY-339D01**																		
				RATIOS							**AGES [Ma]**						**Age - Common Pb correction (e)**		
N° spot	**U [ppm][a]**	**Pb [ppm][a]**	**Th [ppm][a]**	**$^{207}Pb/^{235}U$[b]**	**2 s[d]**	**$^{206}Pb/^{238}U$[b]**	**2 s[d]**	**rho[c]**	**$^{207}Pb/^{206}Pb$[b]**	**2 s[d]**	**$^{207}Pb/^{235}U$**	**2 s**	**$^{206}Pb/^{238}U$**	**2 s**	**$^{207}Pb/^{206}Pb$**	**2 s**	**$^{206}Pb/^{238}U$**	**2 s**	**$^{207}Pb/^{206}Pb$ común**
BUUY-339D01_11	433	10	560	0.01112	0.00054	0.00120	0.00003	0.43381	0.06910	0.00350	11.2	0.5	7.7	0.2	890.0	100.0	**7.5**	**0.2**	**0.80318**
BUUY-339D01_18	347	7	458	0.00785	0.00031	0.00119	0.00002	0.03916	0.04760	0.00190	7.9	0.3	7.7	0.1	60.0	92.0	**7.6**	**0.1**	**0.80317**
BUUY-339D01_12	388	11	614	0.00989	0.00045	0.00121	0.00002	0.42868	0.05990	0.00250	10.0	0.5	7.8	0.1	594.0	96.0	**7.6**	**0.1**	**0.80318**
BUUY-339D01_22	533	10	645	0.00766	0.00024	0.00119	0.00002	0.12327	0.04690	0.00150	7.8	0.2	7.7	0.1	58.0	65.0	**7.7**	**0.1**	**0.80317**
BUUY-339D01_16	376	10	482	0.01295	0.00068	0.00125	0.00002	0.26577	0.07510	0.00430	13.1	0.7	8.0	0.1	1040.0	120.0	**7.7**	**0.1**	**0.80319**
BUUY-339D01_5	266	4	210	0.00932	0.00052	0.00122	0.00003	0.14998	0.05540	0.00330	9.4	0.5	7.9	0.2	410.0	130.0	**7.8**	**0.2**	**0.80318**
BUUY-339D01_4	255	4	188	0.00813	0.00040	0.00122	0.00002	0.34126	0.04890	0.00250	8.2	0.4	7.9	0.2	140.0	100.0	**7.8**	**0.1**	**0.80318**

Number of shots used in this age: 7. Weighted average age: 7.7 ± 0.1 [1.1%] Ma

MSWD: 1.7

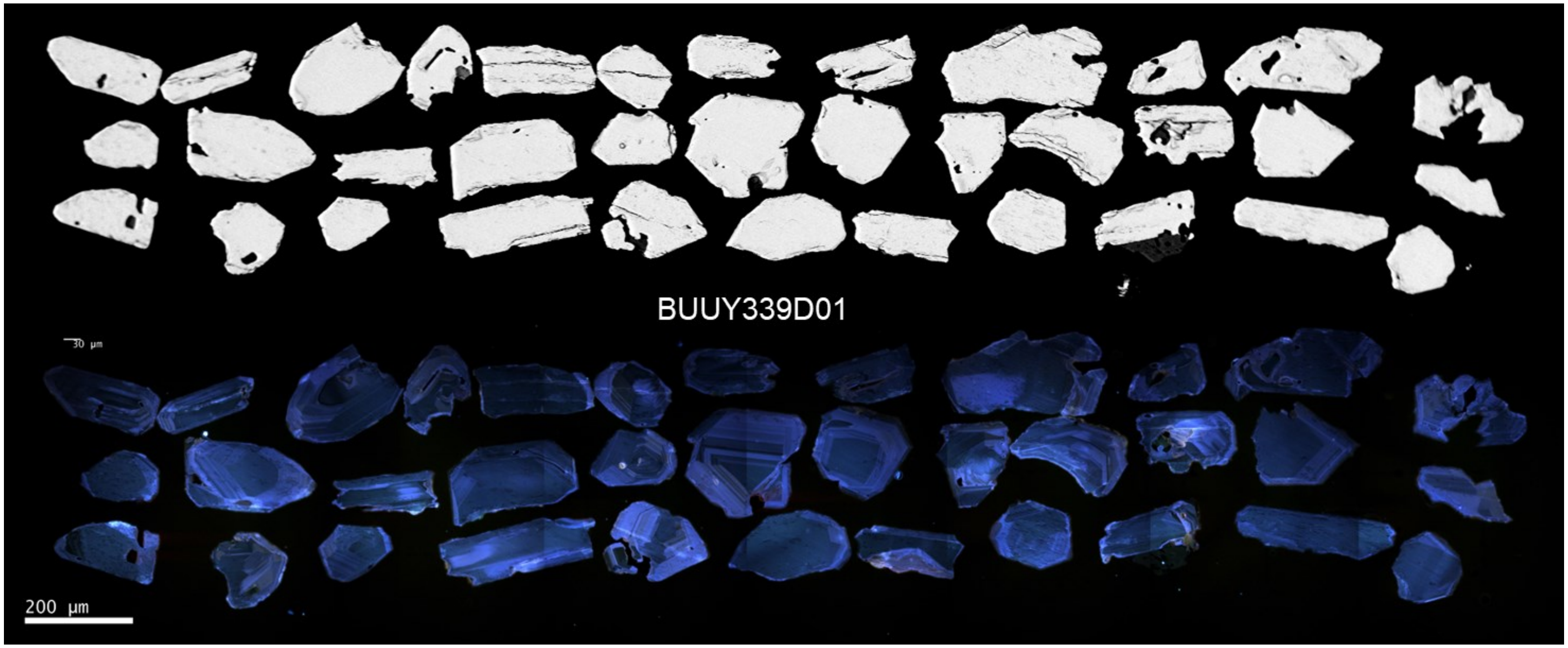
BUUY339D01
30 µm
200 µm

Sample:	BUSY-291			RATIOS							AGES [Ma]						Age - Common Pb correction (e)		
N° spot	U [ppm] [a]	Pb [ppm] [a]	Th [ppm] [a]	$^{207}Pb/^{235}U$ [b]	2 s [d]	$^{206}Pb/^{238}U$ [b]	2 s [d]	rho [c]	$^{207}Pb/^{206}Pb$ [b]	2 s [d]	$^{207}Pb/^{235}U$	2 s	$^{206}Pb/^{238}U$	2 s	$^{207}Pb/^{206}Pb$	2 s	$^{206}Pb/^{238}U$	2 s	$^{207}Pb/^{206}Pb$ común
BUSY-291_7	288	8	308	0.014991	0.000760	0.001243	0.000029	0.258430	0.088500	0.004900	15.1	0.76	8.0	0.19	1370	100	**7.6**	**0.2**	**0.80319**
BUSY-291_21	393	10	513	0.010453	0.000520	0.001205	0.000016	0.226230	0.061800	0.002800	10.6	0.52	7.8	0.1	670	100	**7.6**	**0.1**	**0.80318**
BUSY-291_17	671	16	857	0.009705	0.000780	0.001203	0.000026	0.284780	0.056800	0.002800	9.8	0.79	7.7	0.17	470	110	**7.6**	**0.2**	**0.80318**
BUSY-291_23	663	13	793	0.008259	0.000290	0.001195	0.000019	0.170930	0.049900	0.001700	8.3	0.3	7.7	0.13	184	73	**7.7**	**0.1**	**0.80317**
BUSY-291_14	697	17	987	0.008518	0.000410	0.001203	0.000018	0.391960	0.051700	0.002200	8.6	0.41	7.7	0.12	250	88	**7.7**	**0.1**	**0.80318**
BUSY-291_13	701	25	1421	0.009206	0.000290	0.001210	0.000017	0.280180	0.055100	0.001600	9.3	0.29	7.8	0.11	410	66	**7.7**	**0.1**	**0.80318**
BUSY-291_11	274	4	234	0.008189	0.000530	0.001206	0.000022	0.309290	0.049300	0.003100	8.3	0.54	7.8	0.14	160	130	**7.7**	**0.1**	**0.80318**
BUSY-291_18	507	10	619	0.007820	0.000260	0.001205	0.000019	0.153370	0.047300	0.001500	7.9	0.26	7.8	0.12	72	64	**7.7**	**0.1**	**0.80318**
BUSY-291_1	605	21	1258	0.008598	0.000350	0.001211	0.000019	0.210540	0.051000	0.002100	8.7	0.35	7.8	0.13	232	93	**7.7**	**0.1**	**0.80318**
BUSY-291_20	500	12	636	0.008059	0.000480	0.001209	0.000020	0.403850	0.048300	0.002600	8.1	0.48	7.8	0.13	130	110	**7.8**	**0.1**	**0.80318**
BUSY-291_9	682	11	674	0.008069	0.000280	0.001211	0.000020	0.197370	0.049400	0.001500	8.2	0.29	7.8	0.13	163	67	**7.8**	**0.1**	**0.80318**

BUSY-291_4	597	19	1108	0.008558	0.000460	0.001217	0.000026	0.629880	0.051800	0.002800	8.7	0.46	7.8	0.17	250	110	**7.8**	**0.2**	**0.80318**
BUSY-291_3	383	7	418	0.007810	0.000460	0.001219	0.000026	0.230160	0.047400	0.003200	7.9	0.46	7.9	0.17	80	130	**7.8**	**0.2**	**0.80318**

Number of shots used in this age: 13. Weighted average age: 7.7 ± 0.1 [0.5%] Ma

MSWD: 1.2

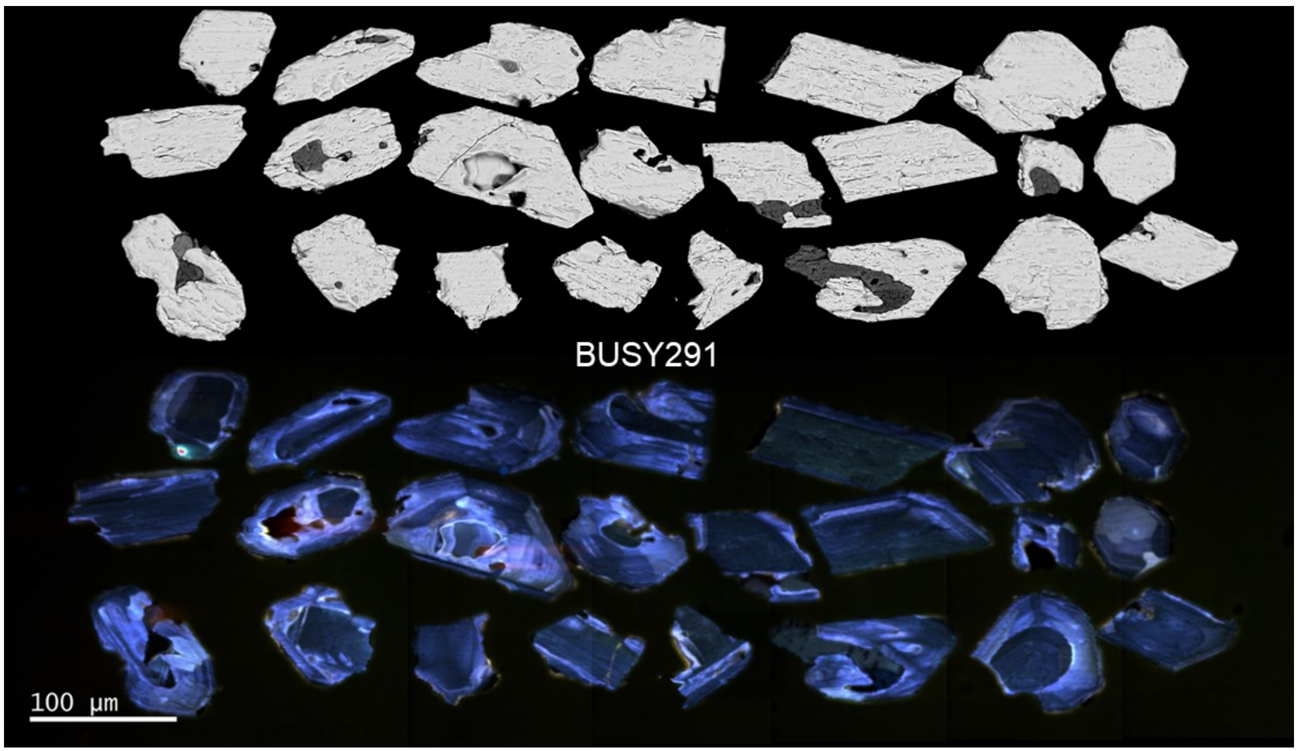

Appendix 4. Mapping

Maps of ore galleries viewing in plan, to wall drifts and face. Additionally, field book notes with mapping details both at surface and underground.

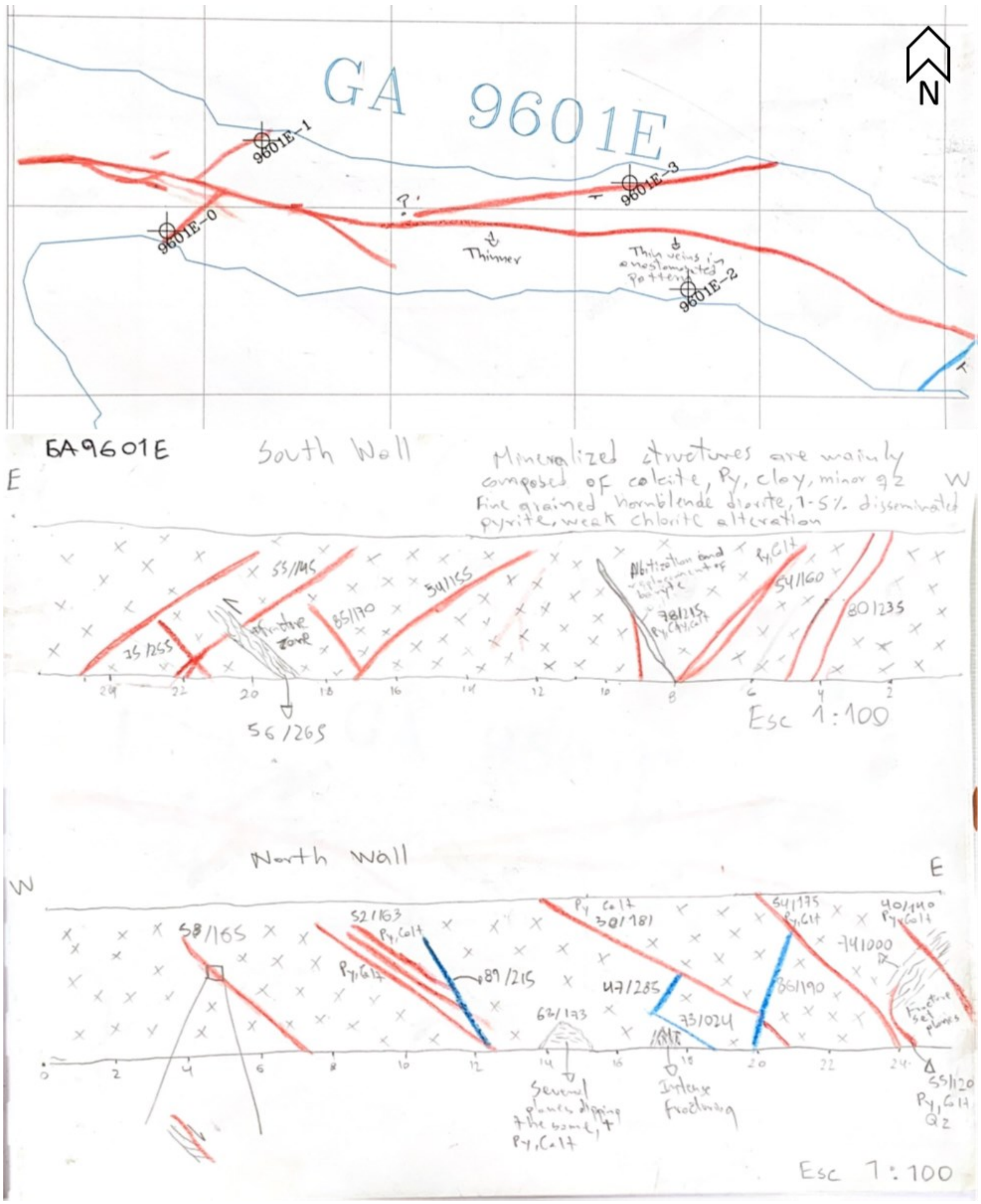

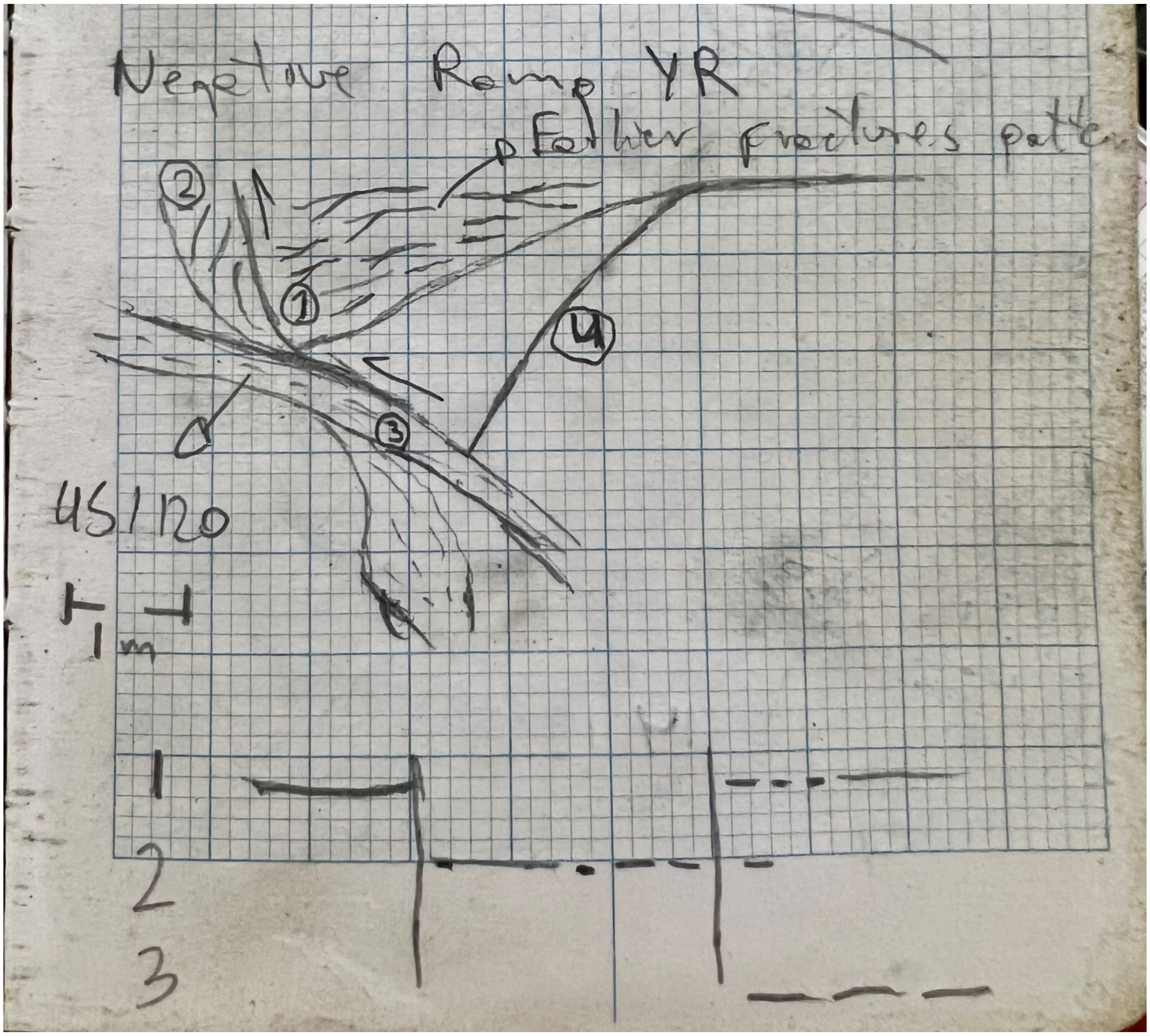
Negative Ramp YR
Feather fractures patt
2
1
4
3
45/120
1m
1
2
3

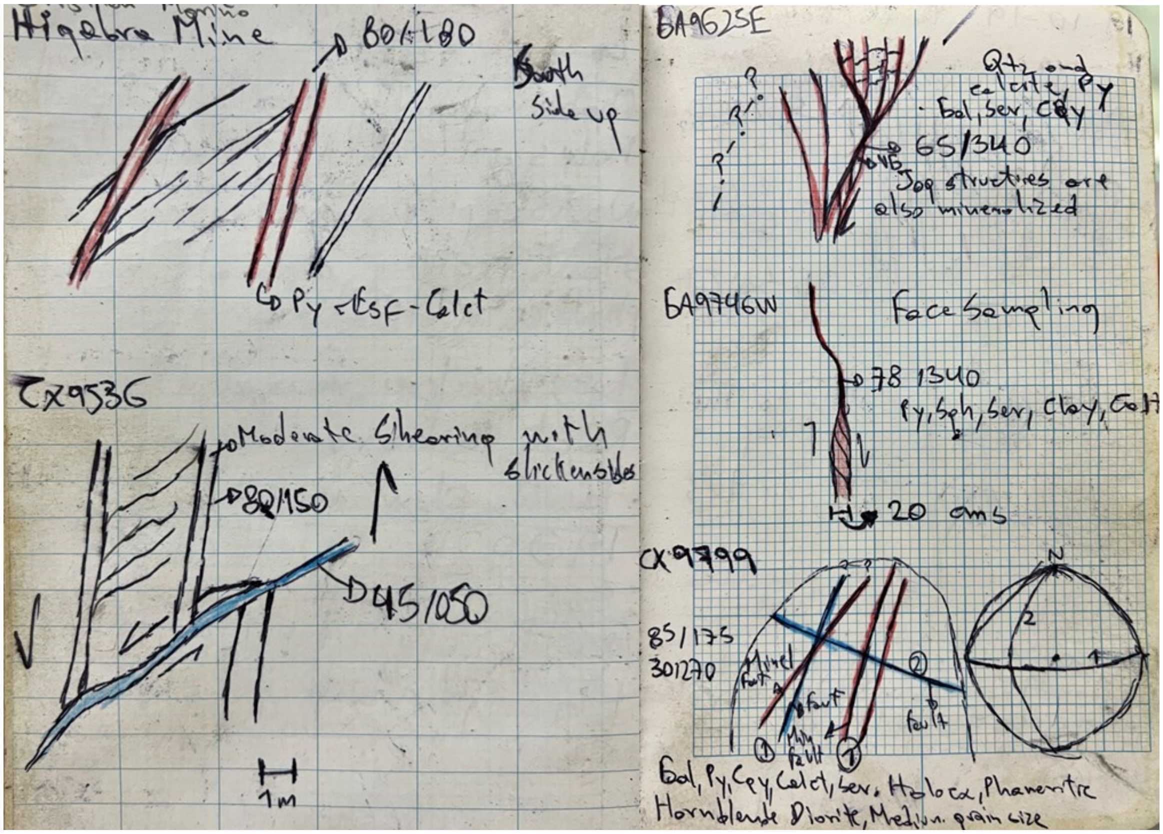
Higabra Mine
80/180
South
Side up
Cp Py Esf - Calct
CX9536
Moderate Shearing with
slickensides
80/150
45/050
1m
6A9625E
Qtz and
calcite, Py
Gal, Ser, Clay
65/340
Jog structures are
also mineralized
6A9746W
Face Sampling
78/340
Py, Sph, Ser, Clay, Calt
20 cms
CX9799
85/175
30/270
Mixed fault
fault
Main fault
fault
Gal, Py, Cpy, Calct, Ser. Holocx, Phaneritic
Hornblende Diorite, Medium grain size

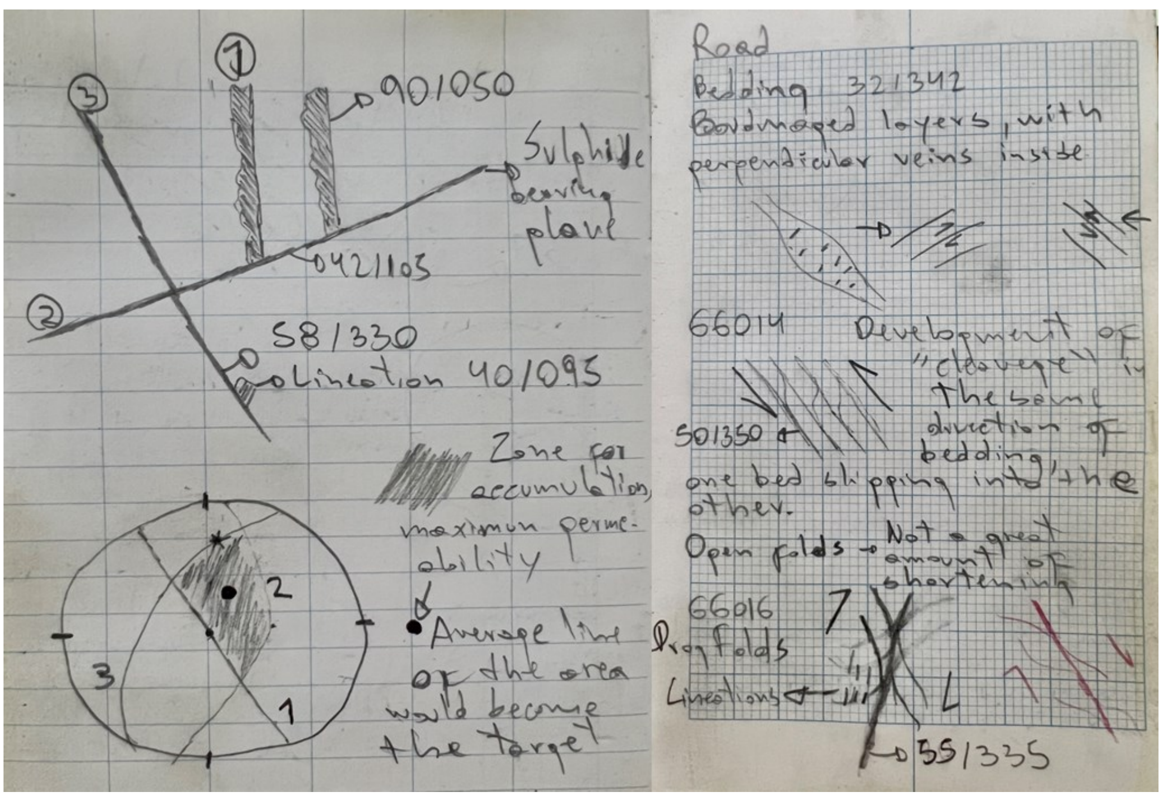
90/050
Sulphide
bearing
plane
042/103
58/330
Lineation 40/095
Zone for
accumulation,
maximum perme-
ability
Average line
of the area
would become
the target
Road
Bedding 32/342
Boudinaged layers, with
perpendicular veins inside
66014
Development of
"cleavage" in
the same
direction of
bedding,
50/350
one bed slipping into the
other.
Open folds
Not a great
amount of
shortening
66016
Drag folds
Lineations
35/335

Appendix 5. Oriented drillcore data

Tables with structural data measurements obtained from oriented drillcore data, classified by structure type.

Faults:

Dip	Dip Dir	Dip	Dip Dir	Dip	Dip Dir	Dip	Dip Dir	Dip	Dip Dir	Dip	Dip Dir	Dip	Dip Dir	Dip	Dip Dir	Dip	Dip Dir	Dip	Dip Dir
45	145	60	334	79	135	65	250	57	95	46	150	50	220	34	90	50	215	60	10
45	125	65	350	72	330	30	310	89	50	46	150	50	160	65	90	45	210	60	360
48	140	65	124	45	245	43	310	38	20	10	145	70	330	40	270	45	60	65	150
40	205	70	0	78	230	56	15	60	110	10	145	64	350	45	330	70	35	87	20
85	285	60	325	60	240	63	165	6	170	50	160	55	350	60	125	45	210	75	180
40	150	69	293	63	110	88	160	4	300	50	160	75	215	45	30	75	40	84	210
58	320	71	60	55	350	40	320	20	150	53	300	85	230	45	15	80	290	75	340
83	240	71	60	45	15	71	120	60	220	73	265	80	5	45	335	35	290	86	270
78	200	33	34	45	340	32	200	68	220	73	200	57	25	55	170	65	205	88	40
48	255	25	100	65	180	42	250	66	225	36	280	40	110	75	300	35	20	80	0
25	230	54	160	85	265	70	265	38	70	48	250	65	227	60	220	45	20	65	190
52	195	48	157	50	230	48	300	45	150	61	170	85	220	60	220	80	255	55	130
75	200	67	325	38	50	14	235	30	130	48	210	39	213	40	220	45	20	85	5
62	225	35	315	63	210	78	232	50	50	48	210	75	38	50	195	50	235	45	180
46	210	54	32	70	260	70	240	63	40	40	190	69	239	45	220	35	100	80	20
88	210	62	140	82	300	50	290	86	110	25	236	40	209	75	300	75	220	65	150
75	70	57	185	66	190	65	105	46	300	89	180	38	65	20	20	45	0	50	45
83	355	40	165	60	120	82	330	64	110	70	180	65	250	35	210	60	0	25	280
80	232	64	210	63	40	75	250	88	170	63	350	70	55	20	210	60	0	62	92
32	145	70	220	86	110	45	25	49	178	70	140	63	65	25	210	85	30	65	211
71	294	32	145	68	295	57	320	84	280	65	205	64	325	30	240	80	20	26	114
51	39																		

Fractures:

Dip	Dip Dir	Dip	Dip Dir	Dip	Dip Dir	Dip	Dip Dir	Dip	Dip Dir	Dip	Dip Dir	Dip	Dip Dir	Dip	Dip Dir	Dip	Dip Dir	Dip	Dip Dir
20	40	38	155	65	150	87	140	64	70	60	222	55	170	82	315	40	90	35	200
79	170	88	355	61	350	30	350	75	320	50	270	55	255	50	180	60	90	70	135
80	35	84	67	61	175	40	115	44	150	84	225	80	360	50	180	55	350	30	140
80	25	80	155	54	195	70	40	66	110	80	270	75	5	40	275	68	70	85	200
55	15	71	345	73	195	39	210	65	310	43	0	75	30	15	170	30	185	75	215
85	25	52	187	73	220	70	50	84	220	65	65	60	40	70	340	75	355	45	220
30	160	62	190	76	170	71	130	75	310	90	320	35	5	40	60	75	345	70	195
46	190	85	62	75	90	60	80	46	200	90	270	50	328	70	190	70	40	60	210
76	125	65	20	80	120	40	270	35	280	72	250	65	255	25	240	60	225	30	150
65	10	89	140	80	180	43	260	65	340	81	75	25	145	35	60	40	310	75	25
80	42	42	275	70	230	85	110	71	135	70	340	30	280	80	70	85	20	85	65
90	40	87	95	85	270	46	325	80	260	86	0	52	100	45	150	70	35	50	170
85	160	66	350	54	100	60	245	80	110	85	200	52	90	70	155	85	55	80	55
76	220	68	70	66	14	57	295	71	30	83	245	52	150	80	335	70	75	85	50
76	227	85	215	30	81	57	25	63	295	70	40	85	340	85	125	70	230	45	75
67	145	75	10	84	175	46	160	55	190	67	25	86	310	55	230	80	240	25	10
85	85	87	5	20	95	57	225	45	30	85	340	55	60	70	150	45	180	80	150
49	113	84	5	26	280	30	55	56	100	75	300	50	45	80	125	55	135	55	310
43	308	74	161	44	100	66	130	46	55	68	242	65	340	85	160	25	250	55	295
67	185	67	240	45	90	79	160	86	270	55	105	87	360	80	160	40	160	5	95
80	126	80	250	71	120	76	90	50	195	36	63	57	275	77	225	60	65	70	200
49	115	80	175	60	340	40	70	51	270	75	230	35	75	80	160	85	50	80	110
65	214	61	350	45	60	75	330	30	340	55	345	43	55	70	180	85	40	40	350
40	95	75	185	85	15	76	250	70	290	43	297	70	135	75	205	40	135	80	290
20	90	72	295	56	330	80	120	40	160	68	225	87	70	55	200	80	30	70	270
60	140	47	125	73	22	80	160	35	50	50	235	50	345	50	245	85	30	65	20
69	5	79	270	74	298	42	5	66	95	60	215	45	175	30	220	80	195	55	80
34	340	85	0	88	305	77	340	82	210	50	72	40	60	80	150	55	20	83	65
89	264	15	335	49	135	85	255	54	255	30	40	65	90	80	170	60	60	80	90
47	4	72	165	82	150	36	80	51	260	20	115	70	10	15	105	85	10	65	130

Fractures:

76	340	66	170	74	155	42	100	32	140	60	225	70	170	75	220	85	45	35	220
59	204	40	90	63	55	40	50	73	350	70	205	80	345	35	320	80	130	85	270
43	330	71	140	65	265	82	278	76	322	55	40	55	350	65	325	80	20	80	145
35	45	75	235	26	95	55	84	77	240	70	235	80	225	86	330	80	0	45	205
84	300	80	230	66	270	34	190	74	325	24	67	40	15	52	205	65	55	70	205
46	95	85	245	80	270	90	50	70	165	86	221	50	10	80	245	60	210	80	225
75	240	60	310	74	20	54	180	75	270	79	54	50	345	88	105	80	60	60	0
81	96	72	355	55	75	60	340	76	240	89	126	60	350	70	175	35	125	80	90
49	310	75	285	56	180	40	55	65	0	82	174	82	325	50	150	70	5	65	110
87	90	55	320	68	105	52	190	29	0	72	149	80	20	60	220	55	315	60	220
48	205	65	0	55	155	60	225	87	0	60	226	70	210	80	190	45	70	50	120
74	165	70	250	76	155	77	95	81	325	60	25	80	180	65	350	40	50	80	300
54	185	35	230	55	285	55	310	48	70	54	20	55	250	42	225	70	55	75	210
54	260	70	230	43	110	25	175	68	20	85	210	85	210	75	220	85	300	65	155
81	320	55	90	20	140	60	155	78	325	30	25	70	210	86	195	45	50	50	145
77	10	63	227	54	135	65	140	84	310	32	95	35	230	76	100	50	210	70	170
50	140	63	55	56	100	69	130	48	70	55	80	70	320	45	220	80	255	65	15
46	155	63	150	90	80	75	90	80	60	55	110	80	240	60	210	70	220	75	40
43	140	51	255	66	130	55	40	70	195	45	340	60	235	35	125	85	210	75	0
70	72	55	215	65	165	89	90	75	120	80	10	45	220	55	20	50	200	80	200
79	300	67	230	43	200	54	170	76	325	52	5	80	190	70	5	70	340	88	210
72	150	62	240	60	355	41	120	86	40	65	70	70	220	65	270	50	175	80	65
80	330	46	145	89	220	60	225	82	54	65	80	55	245	50	5	55	195	85	50
68	295	75	30	70	240	67	330	52	135	65	95	80	310	70	95	50	350	60	45
80	110	80	130	42	275	76	295	70	180	65	330	75	15	70	215	50	310	50	45
79	170	78	200	65	230	60	357	69	335	75	225	50	180	55	200	65	355	50	45
20	120	35	335	52	50	60	220	49	220	85	220	70	10	60	320	80	335	54	30
50	310	57	70																

Dikes:

Dip	Dip Dir	Dip	Dip Dir	Dip	Dip Dir	Dip	Dip Dir	Dip	Dip Dir	Dip	Dip Dir	Dip	Dip Dir	Dip	Dip Dir	Dip	Dip Dir	Dip	Dip Dir
60	240	88	56	60	25	85	180	28	235	70	265	70	95	55	355	60	230	84	70
80	60	84	229	68	230	80	235	65	270	68	210	65	325	80	35	70	205	85	222
85	240	89	154	65	300	60	50	85	250	45	200	45	310	76	253	85	75	57	200
44	150	75	247	55	75	64	260	57	240	75	55	60	310	80	20	71	170	75	180
81	165	59	321	73	170	68	275	67	260	61	250	85	120	85	105	76	250	68	230

Contacts:

Dip	Dip Dir	Dip	Dip Dir	Dip	Dip Dir	Dip	Dip Dir	Dip	Dip Dir	Dip	Dip Dir	Dip	Dip Dir	Dip	Dip Dir	Dip	Dip Dir	Dip	Dip Dir
75	113	47	19	66	74	15	249	30	298	72	309	57	218	55	44	40	278	78	37
32	17	28	274	84	337	88	48	56	309	30	274	36	275	56	238	88	202	83	65
80	212	77	181	46	236	68	114	57	46	74	313	58	201	86	176	69	204	83	63
55	244	33	79	59	258	74	359	75	351	62	51	0	332	27	77	41	258	90	227
67	16	65	163	85	161	61	271	57	313	63	343	82	169	49	209	42	136	35	250
68	230	66	79	86	163	46	5	40	315	20	94	16	201	77	133	81	124	88	194
84	75	84	199	74	341	83	55	34	120	75	177	32	210	33	120	11	208	79	194
84	199	89	209	80	234														

Bedding:

Dip	Dip Dir	Dip	Dip Dir	Dip	Dip Dir	Dip	Dip Dir	Dip	Dip Dir	Dip	Dip Dir	Dip	Dip Dir	Dip	Dip Dir	Dip	Dip Dir	Dip	Dip Dir
31	1	53	144	50	354	16	60	84	270	57	300	25	340	45	125	22	45	45	340
58	77	57	276	67	323	70	270	30	305	55	285	59	70	22	125	72	80	80	40
54	89	66	331	47	318	51	30	38	245	24	135	16	290	77	340	66	35	15	30

36	100	31	313	15	317	37	334	46	280	65	80	4	105	44	45	87	140	40	10
63	90	45	301	54	319	20	0	24	250	45	245	46	250	36	105	48	320	40	315
83	112	49	309	52	281	28	230	35	150	56	260	22	255	34	215	58	305	82	205
86	55	65	23	41	270	19	45	67	240	76	240	52	25	61	50	12	350	40	50
62	150	51	313	43	298	79	80	54	100	35	150	45	20	70	60	30	5	50	85
87	241	34	318	10	233	51	250	35	125	24	250	30	65	35	300	40	5	65	295
85	281	54	319	85	113	40	65	37	245	22	350	50	50	70	0	20	30		

Veins:

Dip	Dip Dir	Dip	Dip Dir	Dip	Dip Dir	Dip	Dip Dir	Dip	Dip Dir	Dip	Dip Dir	Dip	Dip Dir	Dip	Dip Dir	Dip	Dip Dir	Dip	Dip Dir
70	300	49	18	80	25	45	211	65	275	31	120	40	335	70	330	86	76	48	58
40	180	15	325	33	292	61	212	33	53	28	179	75	329	52	134	69	290	32	110
75	230	88	127	38	147	25	0	31	244	24	165	78	347	87	313	88	137	75	137
80	305	79	98	76	157	16	11	48	87	38	253	58	348	81	141	21	175	87	156
65	230	79	98	87	113	35	24	57	89	38	253	68	240	84	125	59	174	42	80
85	305	90	279	65	114	73	179	62	57	71	160	40	100	78	150	90	306	68	165
80	100	52	240	83	296	58	174	64	29	30	145	61	314	63	133	34	178	30	173
55	200	90	145	79	166	3	325	74	38	79	177	88	348	36	117	30	184	87	5
86	295	63	83	29	230	2	145	23	41	45	141	86	169	69	146	75	306	82	30
80	125	82	71	65	216	49	186	42	165	81	213	80	355	54	128	63	176	17	80
10	210	60	74	76	315	52	152	24	230	45	159	66	1	36	117	30	166	53	38
88	275	41	174	61	152	8	245	81	99	48	226	56	331	49	127	53	176	53	38
65	165	35	88	67	161	87	89	59	123	33	233	76	15	64	155	66	77	38	119
62	240	76	310	45	145	48	204	76	315	30	219	83	199	54	149	75	306	89	31
88	200	71	170	82	324	58	117	78	227	37	236	64	318	53	132	57	163	66	194
65	35	45	105	60	124	56	132	83	292	50	251	70	359	37	137	40	161	49	161
65	30	56	191	46	159	72	146	67	74	50	251	66	1	55	148	50	157	27	80
70	210	32	273	44	267	72	146	63	259	33	151	61	334	55	140	35	163	38	70
83	245	51	123	78	111	62	153	12	171	63	170	36	168	49	146	49	171	17	80
70	150	82	71	61	275	42	156	68	100	45	141	79	11	58	133	82	91	7	80

Veins:

5	10	54	95	54	121	69	206	51	100	71	120	68	235	57	136	55	160	52	129
80	110	62	196	56	135	86	128	64	16	50	189	82	7	43	140	54	152	33	110
83	15	60	83	47	159	50	66	66	217	59	196	59	348	56	138	78	132	43	130
85	25	35	109	78	182	3	327	77	35	51	94	66	135	47	84	82	158	45	53
73	160	73	65	43	191	30	77	27	74	68	169	74	348	59	127	59	155	48	155
85	30	42	129	49	146	30	103	85	119	61	264	31	339	60	142	29	152	57	49
80	120	75	69	88	160	32	327	23	161	63	170	41	340	84	178	24	152	47	80
85	25	20	217	75	208	38	313	82	158	52	189	76	357	48	146	24	152	58	200
50	120	75	137	36	213	18	306	79	126	77	148	58	312	79	342	71	115	61	223
64	165	75	86	43	161	39	355	77	291	61	161	65	300	41	97	65	216	55	193
80	300	65	58	64	179	52	266	89	299	78	157	69	324	60	71	63	162	75	19
74	245	83	165	71	134	12	327	79	126	59	179	63	277	54	66	54	152	85	192
65	210	38	155	20	353	3	147	61	265	29	263	63	295	79	328	49	152	58	84
84	320	69	62	40	173	23	309	77	104	43	141	54	355	75	188	44	152	82	30
72	25	30	125	77	159	39	257	81	116	25	192	68	160	59	132	76	285	38	70
60	40	37	91	61	139	4	197	83	113	66	195	73	19	52	87	62	169	68	267
35	55	25	14	56	137	58	72	86	110	79	231	50	147	62	200	83	148	38	42
50	115	48	160	65	142	74	264	88	290	55	219	43	210	57	83	54	152	67	154
80	285	90	279	9	225	71	76	90	113	70	212	33	171	54	103	1	332	41	139
80	250	54	74	30	231	34	210	86	296	45	218	37	163	42	90	74	89	22	135
78	330	77	82	24	149	23	63	90	113	73	212	37	136	53	120	73	10	27	80
70	215	49	154	57	118	29	295	28	13	44	120	68	16	32	112	58	32	38	314
85	210	70	145	88	210	68	250	62	162	48	269	60	152	81	96	56	332	66	194
80	120	77	100	31	335	26	224	83	352	72	168	83	1	75	126	25	170	76	153
85	210	10	154	46	148	87	323	48	254	67	276	37	136	30	134	30	184	24	101
43	25	39	217	69	236	26	54	37	151	71	288	32	211	87	291	78	111	41	139
50	240	28	1	46	187	11	267	57	74	52	136	84	356	72	191	40	161	39	151
40	190	56	191	52	87	14	133	77	218	71	248	59	152	38	73	66	159	78	60
80	30	51	201	30	231	34	237	84	143	76	138	78	166	66	100	51	332	51	129
29	130	80	325	34	269	34	237	70	128	40	191	86	33	45	84	19	152	82	312
20	105	84	97	56	199	30	48	56	153	58	171	74	327	68	174	64	296	50	135

Veins:

25	140	90	325	84	142	42	246	76	232	62	306	72	150	72	163	89	342	42	132
30	110	62	196	82	339	29	360	85	302	69	130	69	139	77	172	26	112	74	226
45	260	19	13	64	246	15	252	87	140	61	328	63	130	38	90	37	173	44	108
22	30	46	9	69	236	37	327	49	213	61	228	55	109	43	83	73	89	48	149
85	110	7	163	84	150	32	14	46	138	65	212	58	35	70	131	14	152	49	114
67	210	85	292	70	4	8	291	73	215	61	161	73	327	40	129	14	152	74	132
44	110	42	353	80	3	7	328	12	125	72	221	73	327	35	144	20	47	48	150
71	205	59	133	73	259	11	209	56	278	53	235	59	15	75	358	49	203	82	131
65	210	21	135	47	149	20	287	85	29	64	229	82	315	44	142	29	230	58	137
35	350	50	35	69	202	8	291	81	32	49	218	87	314	63	173	64	281	86	302
60	225	20	145	89	43	5	194	87	211	53	211	69	298	70	189	38	187	26	99
58	52	19	187	87	194	12	185	70	21	84	176	68	16	52	182	48	216	75	331
71	230	55	34	52	156	8	243	34	31	45	211	74	7	82	73	10	85	36	105
83	20	45	14	78	114	8	207	51	6	83	167	47	163	82	136	54	283	80	241
73	100	20	314	85	197	44	22	74	204	80	157	70	3	14	124	14	152	74	226
70	235	23	29	80	153	20	160	86	212	70	222	79	169	70	169	78	172	85	46
88	295	23	29	52	110	43	37	78	217	69	160	26	116	45	225	83	358	50	136
57	27	78	95	61	128	47	265	83	5	54	136	83	1	21	206	81	171	85	10
87	220	44	156	85	181	49	207	78	207	50	270	50	147	85	184	47	186	78	163
62	75	41	116	80	145	27	209	83	35	56	125	89	154	75	94	76	298	83	260
85	225	30	165	41	175	55	258	82	210	55	212	88	159	40	123	38	187	87	80
80	260	41	175	65	178	51	331	56	278	52	127	86	325	87	291	76	262	81	37
64	130	20	325	59	183	21	141	90	323	61	123	76	332	53	134	52	176	74	29
47	140	18	349	59	114	42	250	76	135	71	168	34	107	79	270	6	332	66	23
85	150	75	152	11	175	48	358	54	8	72	168	88	144	5	126	38	73	76	238
71	214	56	263	72	215	54	152	44	172	55	219	82	326	29	146	37	173	86	149
49	130	80	149	89	139	32	348	87	146	59	133	82	326	86	321	78	172	73	123
54	150	41	205	43	185	42	55	87	313	62	142	85	23	76	202	53	167	85	324
80	205	20	330	46	163	28	93	47	18	66	140	87	330	51	126	79	166	81	185
72	185	85	149	59	237	50	294	39	14	57	144	26	210	14	306	84	22	62	198
54	140	74	156	84	217	62	218	52	280	75	249	85	337	69	117	70	14	83	100

Veins:

65	230	80	223	84	333	36	347	79	132	62	237	77	344	90	230	80	2	18	99
67	235	49	106	78	223	6	114	6	74	63	317	71	331	29	306	84	191	33	313
45	310	81	306	74	33	83	272	72	119	21	248	90	168	72	162	88	13	48	286
59	170	38	230	85	181	19	98	80	116	41	238	43	49	25	353	13	106	36	209
74	210	45	254	38	248	19	16	31	69	44	224	84	173	79	259	65	171	34	246
63	74	55	256	52	137	12	97	63	133	61	284	79	22	74	256	79	14	40	293
82	50	56	108	49	228	4	153	58	123	70	277	88	353	69	30	85	6	89	186
43	335	86	175	21	176	11	181	43	46	51	243	69	171	9	306	86	18	4	212
51	40	70	155	35	147	19	98	50	93	27	339	74	337	65	119	66	183	54	81
84	126	42	87	47	100	26	45	76	135	65	247	73	177	78	354	73	215	75	142
77	214	42	87	87	194	48	143	72	125	40	197	61	95	80	191	57	228	79	140
75	150	53	92	89	307	38	75	76	149	61	285	84	349	37	233	69	161	30	318
76	80	21	347	23	98	38	99	68	115	39	332	57	117	51	195	78	172	39	251
20	170	43	325	81	286	31	87	19	268	33	279	48	164	10	169	90	189	80	188
44	60	55	256	55	125	31	87	66	74	49	336	57	344	8	307	88	205	28	208
64	277	27	125	57	273	34	35	80	9	17	41	72	344	86	338	73	209	41	210
82	125	35	234	43	137	89	191	44	147	21	56	73	337	56	83	73	209	26	123
80	140	23	188	60	169	54	148	16	287	77	137	84	184	34	28	72	209	22	40
27	120	40	310	88	158	77	355	25	175	66	140	69	181	33	307	72	204	12	146
84	165	39	287	86	26	60	264	55	30	79	156	82	12	21	4	72	204	73	76
45	305	52	260	62	163	84	4	70	284	71	148	69	298	61	87	56	210	72	109
55	245	53	261	78	102	38	209	57	138	88	344	88	184	61	74	80	2	57	266
45	200	56	28	90	141	54	84	85	67	71	118	85	182	85	339	89	189	45	224
75	25	69	44	61	198	38	100	76	271	45	267	48	164	29	78	67	339	43	134
67	145	51	266	90	159	56	323	39	84	88	343	69	335	74	290	83	191	19	135
89	290	85	184	68	317	53	310	58	46	71	340	85	350	52	124	73	215	10	158
36	255	87	91	76	323	86	108	40	150	40	345	70	293	62	168	87	201	86	145
35	160	65	198	89	173	76	324	87	212	56	102	58	6	63	159	78	198	62	153
74	190	40	355	80	225	34	36	25	301	51	325	75	179	65	186	64	210	48	71
74	190	70	28	87	145	58	119	55	51	86	3	81	0	35	77	78	198	61	77
47	195	42	350	80	131	46	335	55	51	44	310	81	0	60	108	86	18	51	163

Veins:

80	195	25	50	78	105	38	306	55	51	35	197	58	35	86	331	85	196	90	9
89	150	25	50	84	329	77	314	28	184	57	349	90	358	29	69	89	189	52	157
60	240	69	29	86	137	23	74	43	87	90	313	64	196	22	70	52	190	15	227
89	150	58	39	70	239	89	117	71	73	83	301	88	109	65	70	35	194	44	178
66	55	57	59	89	250	84	146	26	66	88	323	64	204	82	170	41	181	73	236
46	222	30	355	56	136	27	81	39	126	26	234	59	175	6	308	71	125	61	254
55	290	33	52	45	330	66	335	46	102	42	231	53	210	41	340	38	152	43	350
86	115	27	23	57	10	21	130	79	49	39	332	77	275	88	135	23	152	81	309
80	15	50	150	76	209	84	155	1	73	44	224	34	359	37	25	28	152	38	348
14	265	88	167	83	200	66	335	6	73	38	229	87	13	18	278	29	231	86	103
24	187	54	248	87	203	74	155	76	73	23	69	88	358	11	309	64	210	70	274
20	122	65	238	61	187	28	9	6	211	54	134	69	29	77	176	64	199	76	256
35	140	44	156	79	198	47	1	36	76	37	112	81	203	62	342	42	200	34	86
30	125	30	317	66	198	15	168	27	85	45	139	88	324	45	199	33	178	54	352
42	135	47	165	16	247	60	127	21	199	78	301	80	21	38	54	28	152	70	276
25	135	36	326	87	11	12	100	23	164	73	321	84	186	59	191	64	210	49	66
6	190	58	189	76	58	16	138	58	123	77	35	82	183	80	207	65	216	90	117
14	140	48	272	54	154	38	48	64	180	45	97	62	164	0	309	48	209	33	231
50	5	85	204	76	202	62	134	71	339	49	314	57	167	88	280	18	151	80	238
45	230	43	173	86	5	61	34	88	112	5	156	57	161	72	98	32	202	66	268
24	175	61	178	55	142	46	336	49	46	81	128	84	17	15	129	40	207	53	22
65	171	79	161	39	127	46	336	34	11	64	189	74	19	72	291	22	203	59	320
80	185	28	3	58	253	46	336	32	167	35	212	71	11	72	291	29	185	62	190
25	195	49	19	75	218	47	1	49	159	70	260	73	19	85	287	13	151	53	331
79	210	10	307	80	175	15	100	65	81	73	110	66	7	82	294	3	151	89	88
48	45	52	179	39	231	72	132	27	88	52	128	78	10	84	97	18	151	16	36
89	210	42	214	20	179	48	28	48	137	36	172	46	144	80	100	18	151	87	196
85	215	38	2	17	112	55	156	42	102	28	69	83	193	83	342	7	331	74	219
84	100	53	17	21	141	66	100	73	48	70	161	84	183	61	130	81	156	64	333
47	120	38	20	32	151	5	337	74	214	19	237	52	125	55	79	48	171	38	169
85	170	22	77	32	248	80	83	63	119	8	283	65	333	53	155	73	141	58	148

Veins:

59	107	60	32	80	160	16	212	36	236	20	211	87	44	59	115	65	221	43	351
26	105	15	90	84	189	56	38	58	123	68	111	74	327	76	157	48	210	44	349
77	198	21	118	75	218	47	43	65	297	66	152	72	94	73	161	86	144	34	84
51	150	88	167	74	190	73	173	21	355	49	158	85	13	34	101	7	151	40	345
55	270	69	90	85	170	65	158	83	163	25	26	87	194	84	155	34	194	61	258
52	180	57	90	64	244	35	97	65	285	68	152	88	214	84	141	41	200	80	276
80	210	43	173	36	180	49	300	66	144	22	58	70	4	72	196	30	212	81	320
68	245	35	172	65	159	6	123	60	142	28	69	88	204	59	191	19	231	86	235
88	0	48	160	62	190	42	61	62	162	83	317	86	331	69	166	12	151	48	107
60	90	46	166	81	206	65	338	81	311	84	21	73	191	52	217	29	243	74	317
60	230	76	118	65	186	64	144	78	151	84	21	37	164	79	335	88	205	54	238
60	10	72	103	88	19	42	61	83	142	4	20	80	156	88	331	56	205	76	189
63	65	84	276	53	230	7	23	69	155	67	191	73	213	88	311	84	80	69	194
85	175	28	88	85	150	65	338	66	144	32	301	81	204	69	166	84	196	89	315
60	200	87	205	68	190	65	338	73	138	73	183	71	228	89	167	41	200	67	189
75	274	87	209	22	58	65	338	84	119	32	90	77	275	77	166	40	181	69	237
36	227	77	299	75	187	45	338	69	127	26	114	71	223	71	2	51	191	71	225
44	180	27	208	63	14	65	339	31	117	83	358	36	114	64	183	49	197	62	325
82	170	88	198	61	26	65	339	41	213	79	1	12	111	88	176	22	151	29	29
85	90	85	314	62	158	65	339	30	137	51	71	25	321	88	150	30	212	55	305
85	155	47	185	74	4	65	339	31	314	51	71	63	338	88	176	38	240	80	36
70	320	60	244	89	73	64	59	62	178	69	350	58	158	70	329	2	151	82	318
35	190	32	153	30	326	34	40	84	86	50	58	71	223	87	170	27	151	85	311
55	140	88	299	32	330	65	129	78	179	39	73	71	223	87	143	7	151	43	179
75	320	24	102	61	341	22	60	35	244	76	357	59	108	82	354	2	151	89	104
45	40	84	265	63	118	28	13	30	348	73	27	90	324	83	137	63	194	60	12
75	310	86	344	57	15	22	60	84	109	74	20	71	132	87	187	83	293	53	41
60	190	24	49	47	330	82	358	73	115	84	15	87	8	87	187	48	237	51	106
75	40	85	337	83	359	65	339	58	101	66	1	85	189	89	204	86	200	90	277
85	90	41	145	82	125	65	339	70	77	76	357	89	24	63	178	84	107	69	282
85	20	31	204	60	330	7	294	80	227	84	15	88	204	66	170	66	131	81	177

Veins:

40	245	11	135	60	330	86	329	61	206	84	15	81	322	90	177	77	137	86	120
49	205	47	43	65	338	65	339	43	59	86	194	82	194	69	147	43	193	84	306
53	315	58	38	81	136	65	339	79	98	84	15	89	149	79	151	40	181	76	249
65	30	66	32	58	157	65	339	26	275	79	1	85	154	63	356	87	205	59	320
85	350	29	114	60	152	22	280	5	253	81	158	65	211	77	145	38	78	85	329
20	250	80	25	67	151	64	152	67	273	55	57	88	13	86	15	40	169	33	208
10	260	69	78	48	323	51	55	46	15	84	351	63	221	39	73	67	166	11	159
70	200	87	89	69	170	68	57	70	93	79	1	10	164	83	123	64	216	8	146
85	10	22	213	57	170	64	60	79	206	79	1	41	187	87	119	65	306	37	325
85	35	27	67	73	161	6	195	86	131	87	356	84	295	83	143	79	267	48	140
77	235	38	8	57	280	81	300	39	52	87	356	74	308	39	200	61	303	11	138
56	5	84	278	45	77	53	209	43	59	84	20	86	325	57	138	69	182	59	176
60	230	13	114	87	128	67	92	5	253	43	133	74	340	71	212	61	150	88	264
80	310	19	121	82	10	64	152	72	57	79	20	83	343	20	133	79	137	50	169
80	50	21	150	54	322	86	330	55	117	79	346	52	203	51	144	39	93	62	158
76	190	33	1	78	341	35	99	55	96	90	182	49	208	77	156	71	317	16	345
75	195	42	353	78	341	89	292	45	343	32	90	55	137	72	180	79	170	74	299
78	190	46	347	78	2	60	131	20	266	86	194	70	138	36	166	51	151	48	223
77	220	41	353	69	158	50	160	76	112	84	15	70	326	43	105	61	154	19	208
67	244	75	52	51	87	77	266	73	31	74	17	82	137	87	341	76	151	25	2
54	240	43	360	74	73	47	274	61	57	84	15	87	203	27	145	39	181	75	242
85	180	74	304	53	85	73	264	32	301	87	356	57	28	45	120	39	181	43	305
75	225	74	67	63	315	26	249	60	70	78	185	65	22	27	145	39	181	68	301
70	234	40	339	78	79	59	75	54	67	38	123	70	19	37	166	57	187	20	178
85	170	71	303	88	186	35	100	10	253	73	316	74	357	64	11	36	151	38	169
74	120	51	343	73	14	57	108	22	199	48	92	70	0	32	201	36	150	89	202
75	200	79	319	74	4	71	100	23	341	45	72	62	14	46	121	41	158	13	329
40	260	30	341	74	120	83	143	60	79	38	123	87	323	60	139	47	210	39	288
79	245	29	324	62	3	83	177	65	73	38	123	73	52	88	118	56	192	51	217
50	230	30	341	81	20	83	143	80	95	79	39	65	253	75	1	54	122	75	195
64	300	30	342	54	360	43	35	70	283	35	200	82	167	59	129	88	169	37	302

Veins:

48	210	25	334	11	313	42	89	57	109	84	230	79	340	75	1	84	172	54	237
82	200	32	154	9	158	89	178	52	126	86	194	87	151	34	86	85	183	52	311
80	195	41	343	65	125	82	134	83	287	54	83	84	319	85	185	64	159	27	160
82	205	62	153	51	107	70	129	65	73	15	20	19	261	85	84	70	204	13	236
79	200	34	357	71	93	59	125	89	358	76	357	19	246	63	218	59	60	25	331
50	80	67	214	79	88	54	127	46	16	84	15	19	261	86	342	82	308	61	189
70	20	64	229	82	52	79	107	57	109	67	159	76	191	88	176	89	330	51	217
80	5	75	324	47	133	64	146	57	52	76	357	22	197	78	315	69	171	85	242
35	150	30	338	85	36	65	340	75	253	46	116	16	177	87	135	75	171	80	279
64	230	53	15	57	52	55	160	56	87	79	39	44	357	84	120	62	163	50	272
74	235	65	81	28	232	80	195	68	60	68	325	1	177	48	105	83	275	84	233
35	63	88	189	54	323	65	340	63	146	58	94	90	183	69	62	78	99	10	300
86	200	70	107	49	354	67	183	54	132	80	55	84	184	46	121	62	170	46	11
78	240	68	124	80	67	26	34	55	50	38	354	86	177	75	1	50	175	89	236
76	230	38	90	85	100	46	261	71	55	52	70	69	219	82	345	48	104	53	150
70	120	60	138	85	100	22	62	46	87	84	161	64	247	83	354	1	150	43	304
85	0	41	237	88	289	15	160	63	132	28	359	70	3	87	351	81	320	57	259
33	240	54	172	39	360	71	101	19	42	40	313	74	357	78	347	86	21	34	210
46	180	78	194	90	268	51	136	55	169	43	9	63	139	74	350	14	112	31	258
82	150	0	144	57	52	65	341	50	53	80	346	53	197	70	353	21	37	47	259
80	220	10	324	45	348	76	77	5	73	84	342	65	156	77	151	50	175	88	79
70	250	44	210	87	52	55	243	52	126	66	311	74	140	90	168	76	279	64	79
50	340	85	148	70	347	55	255	39	346	66	89	66	322	78	292	65	171	83	214
60	255	30	144	72	322	46	73	53	358	78	76	87	344	75	108	75	108	78	216
65	25	45	283	58	339	5	161	40	356	43	352	9	259	52	178	55	320	40	173
80	25	49	157	68	325	56	42	70	211	59	23	75	319	81	8	52	22	21	143
85	320	80	152	44	305	65	341	84	60	74	33	74	337	78	315	86	128	75	241
86	12	35	324	51	306	65	341	33	221	52	44	85	127	57	202	39	171	57	158
88	2	42	53	85	195	35	161	35	73	10	23	64	247	81	127	32	146	51	205
65	185	67	214	18	245	65	341	15	173	72	319	61	329	82	345	74	38	85	325
87	192	20	118	78	232	90	341	74	291	23	110	85	144	67	168	79	44	40	159

Veins:

70	15	53	187	68	232	85	161	88	221	88	15	56	249	73	315	86	29	52	299
71	130	35	324	78	237	55	161	60	55	81	209	16	177	68	160	67	138	8	9
60	128	47	40	77	330	56	203	60	55	19	79	85	128	75	331	21	187	78	302
88	165	35	128	85	270	60	341	25	73	85	3	1	177	57	99	36	187	80	347
45	175	83	296	85	214	40	298	39	203	67	50	40	127	86	165	70	31	36	353
87	105	60	184	84	90	85	341	53	65	88	183	88	196	78	338	36	187	48	6
85	215	46	166	78	233	50	265	35	253	85	21	34	357	79	158	26	187	81	209
88	210	68	165	89	27	84	292	36	79	82	193	44	329	86	351	18	269	36	166
63	335	42	183	89	13	64	261	41	59	88	41	78	310	52	217	82	200	56	263
83	320	67	168	77	278	50	265	51	98	85	203	84	357	55	74	68	133	50	99
88	65	52	178	43	233	71	221	61	105	54	9	27	128	51	64	26	187	14	72
72	180	74	203	86	19	55	256	89	135	87	195	71	124	77	52	41	148	83	288
40	20	35	161	86	296	15	342	70	313	79	327	69	209	31	246	26	187	83	233
56	140	83	183	89	27	49	20	86	138	86	199	56	177	77	52	35	221	68	234
52	270	47	298	89	78	85	162	15	253	51	214	88	202	77	52	6	187	63	300
76	115	40	165	73	238	90	342	0	253	34	47	73	357	33	122	27	220	16	149
24	230	54	247	79	103	85	342	15	253	87	346	81	19	59	71	35	207	34	128
69	105	32	73	83	95	65	342	32	61	9	294	90	350	17	284	11	187	90	220
24	225	49	18	74	75	65	162	56	109	80	203	65	151	63	238	79	330	75	278
66	135	29	82	48	288	65	162	82	283	76	240	64	140	77	116	55	18	61	290
26	245	65	82	70	254	85	162	81	302	44	346	27	177	86	75	82	32	38	118
45	215	16	183	61	344	85	342	65	253	80	198	78	357	51	159	66	143	90	63
58	200	48	131	83	185	45	162	72	88	60	35	69	145	3	104	55	269	56	259
43	210	44	103	22	233	85	342	32	48	74	346	57	162	64	306	55	269	86	215
40	215	8	226	35	166	70	162	80	227	90	53	75	125	73	82	53	124	90	93
43	200	38	135	88	10	85	162	65	23	63	157	82	12	14	105	36	187	6	269
25	265	20	150	44	160	85	162	55	59	28	108	61	329	18	138	46	187	46	251
40	20	43	170	77	85	85	342	46	15	63	55	73	337	40	236	38	215	40	332
57	150	45	147	88	360	45	162	12	102	80	200	55	111	88	220	36	187	53	136
87	160	21	138	42	142	85	342	45	314	56	65	84	149	63	142	82	116	21	111
70	170	81	339	72	246	80	162	72	57	51	77	75	48	72	255	23	146	24	6

Veins:

47	60	69	100	48	165	85	162	77	239	82	13	74	3	48	211	46	272	36	261
55	330	36	131	57	159	65	162	63	51	79	19	70	325	42	220	16	187	34	87
75	270	49	204	48	166	65	162	9	195	62	340	80	182	38	215	45	130	54	342
22	205	40	325	54	117	75	162	35	73	51	214	79	43	31	285	76	47	28	357
55	270	56	109	53	156	80	162	25	329	87	55	79	30	45	225	45	137	60	342
59	290	38	264	51	140	85	162	62	327	86	10	71	56	76	258	6	187	32	171
15	20	79	157	6	236	55	162	66	242	72	13	80	2	33	41	81	304	26	225
10	70	89	133	53	80	75	162	61	87	72	2	61	6	71	256	70	252	71	227
28	210	36	278	84	49	45	162	44	298	85	56	80	357	30	100	28	280	82	229
46	355	48	132	19	323	85	162	38	126	75	32	44	205	80	260	27	258	66	318
63	180	66	226	73	43	65	162	86	252	29	320	40	177	48	211	30	238	61	316
19	95	71	218	74	44	55	162	83	109	20	23	58	326	27	161	84	7	51	262
58	150	48	161	70	51	85	162	30	118	85	151	74	103	76	30	30	161	2	312
75	352	46	208	43	87	70	162	54	72	87	4	68	90	76	30	19	120	36	164
80	160	51	38	66	130	65	163	49	71	51	50	50	357	79	185	53	43	35	149
88	260	16	184	80	89	85	162	88	211	64	32	82	111	51	96	10	300	20	209
57	305	25	326	64	141	65	162	87	55	54	45	46	146	88	244	11	187	23	150
72	200	80	138	77	302	55	162	62	206	55	90	85	253	59	88	37	242	19	158
88	40	72	168	43	162	52	138	27	273	39	6	84	74	80	239	49	157	19	193
75	25	84	129	79	81	65	342	71	21	70	288	26	141	55	203	53	257	73	218
78	150	23	7	35	292	46	100	83	108	58	177	50	319	45	206	53	43	50	271
37	55	27	23	68	37	59	127	83	85	73	79	33	222	53	181	36	268	20	101
43	45	54	249	31	183	65	342	20	5	47	121	90	193	38	215	86	268	31	170
70	215	30	326	54	352	65	342	39	160	74	69	84	52	44	85	75	21	86	208
78	170	20	337	45	8	55	92	33	45	90	247	87	158	46	100	76	327	23	184
88	182	30	317	42	339	53	114	42	317	58	260	59	267	71	257	34	222	24	152
70	155	31	301	87	9	75	163	72	144	47	121	53	165	66	254	25	187	7	245
78	240	59	215	58	13	85	163	86	252	75	188	74	52	89	44	77	147	21	143
76	230	36	14	25	101	90	343	68	18	47	121	77	185	85	232	76	205	61	304
70	120	33	359	5	241	90	343	4	72	57	121	58	159	45	107	45	7	67	289
33	240	35	270	62	153	90	343	12	318	83	128	90	207	65	157	82	161	42	355

Veins:

46	180	62	183	10	241	85	343	83	327	83	128	71	29	59	148	82	161	85	66
88	225	23	7	34	207	85	163	88	293	64	150	78	22	40	168	85	187	64	277
81	245	23	7	68	146	85	163	65	99	83	181	76	34	75	259	88	215	51	194
60	190	32	8	46	317	85	163	4	72	65	348	74	251	75	287	75	7	35	57
80	200	41	206	49	153	65	343	54	199	82	171	55	244	87	208	70	360	25	4
60	230	17	32	83	32	65	163	39	34	82	171	83	27	57	157	60	165	27	119
80	50	17	32	83	288	55	163	32	16	77	121	66	66	28	32	71	145	54	278
75	210	15	70	70	232	65	163	33	108	54	11	75	70	79	251	80	187	50	229
30	40	85	326	78	291	85	163	29	106	71	26	83	19	55	107	37	132	43	318
70	20	53	93	89	20	50	163	4	72	30	331	66	46	79	240	82	168	46	161
80	5	12	252	24	196	42	259	18	281	64	149	71	193	85	288	68	127	89	84
35	150	51	180	86	258	81	163	61	48	44	166	86	203	90	288	40	147	71	176
85	0	87	92	80	6	86	163	39	10	82	288	88	201	33	63	75	7	43	294
85	0	19	104	68	353	51	163	10	305	80	292	72	188	74	327	38	171	48	342
86	50	78	196	62	153	76	163	27	5	75	131	66	22	10	108	15	187	58	208
54	310	15	203	86	23	86	163	59	330	32	150	51	8	46	165	52	142	49	82
31	95	20	218	73	272	86	163	71	257	75	131	89	184	38	63	38	171	47	297
85	90	70	51	49	44	86	163	79	158	57	2	80	179	30	108	15	187	17	123
28	60	26	189	86	209	71	163	85	105	81	140	87	16	75	338	25	187	47	298
78	240	83	167	52	346	71	163	41	141	73	162	78	190	90	288	64	154	48	320
62	160	47	105	43	306	64	343	28	150	65	348	76	203	69	99	51	163	55	178
21	260	33	205	25	4	50	158	53	356	78	146	30	177	81	108	56	191	88	306
47	48	48	76	37	295	14	343	34	100	78	151	66	179	79	335	35	187	38	314
85	290	64	61	61	41	18	297	74	41	78	90	62	234	79	335	49	33	40	197
60	260	69	69	23	72	71	104	21	349	73	89	63	221	46	80	71	343	60	330
54	290	87	121	29	90	4	343	78	284	57	2	70	177	62	197	26	202	8	225
44	0	51	25	18	77	84	343	79	69	88	40	48	226	50	39	27	115	69	312
74	290	64	61	88	86	30	68	71	56	74	172	43	234	46	51	27	104	71	267
58	290	53	199	77	205	76	196	74	188	62	142	74	219	84	343	33	166	5	328
83	155	79	162	89	259	75	214	37	348	80	356	77	333	30	76	37	98	83	63
40	320	45	37	82	100	55	233	38	165	60	132	75	200	28	56	50	7	75	309

Veins:

69	195	30	116	68	84	35	297	74	91	77	286	81	197	61	141	58	142	14	61
34	330	76	174	72	151	38	269	71	161	74	100	32	271	68	133	48	174	27	160
84	70	40	27	68	300	84	343	64	150	77	110	18	143	88	157	36	351	29	268
82	72	23	47	27	245	66	163	86	148	68	36	12	187	84	289	44	116	75	245
47	300	62	25	47	245	66	163	60	62	49	87	22	187	34	46	49	342	70	242
60	225	54	56	54	283	46	163	78	155	68	343	88	168	33	65	87	357	61	305
55	230	31	344	83	162	84	343	64	150	77	100	81	157	80	43	54	155	47	186
47	205	77	318	55	101	66	163	90	276	90	247	88	232	14	29	31	198	38	169
64	235	59	133	27	244	86	163	74	153	78	151	22	187	1	109	59	130	65	274
55	190	73	227	37	111	76	163	36	55	25	166	61	166	4	289	59	154	44	168
55	170	77	8	78	107	51	163	6	303	84	278	33	151	69	205	75	187	50	246
65	180	20	328	2	244	56	163	89	169	80	75	7	187	28	45	49	157	38	313
75	235	82	221	49	203	51	163	76	163	47	97	74	164	88	237	44	130	44	276
56	180	47	199	83	148	76	163	80	165	61	135	67	244	61	77	56	166	53	322
86	180	80	337	41	50	76	163	36	55	67	117	74	16	59	193	10	129	18	28
40	200	42	210	59	339	46	163	82	186	36	120	90	175	84	234	10	129	59	321
48	230	33	186	39	51	89	343	77	173	58	177	22	187	90	47	74	134	56	259
62	90	42	11	51	57	76	163	64	176	34	300	72	227	29	67	30	187	31	111
70	195	58	29	69	45	46	163	72	171	73	79	72	227	83	265	30	187	63	236
80	50	73	68	62	350	61	163	83	322	85	125	81	217	34	153	79	340	24	72
46	235	38	105	90	88	66	163	64	176	58	112	66	348	48	89	75	187	9	102
60	185	49	69	84	314	55	163	44	56	80	161	72	187	74	250	46	101	47	236
70	185	49	69	76	295	85	163	74	154	74	172	31	242	77	79	25	187	4	326
40	200	61	59	60	246	50	163	35	160	84	186	65	117	46	30	45	187	15	106
54	200	67	48	60	33	75	163	71	161	50	176	76	168	24	72	17	214	9	80
60	215	59	66	35	301	75	163	33	62	67	162	74	35	86	116	70	319	54	355
52	205	90	92	5	66	55	163	72	171	74	177	81	166	84	64	29	214	65	243
30	190	41	99	57	283	85	163	81	147	73	157	23	111	64	289	58	232	81	296
44	210	35	329	52	48	85	343	9	123	90	136	7	188	90	171	17	214	81	267
48	220	58	29	20	246	70	163	10	211	73	301	78	8	83	178	46	178	66	250
54	170	45	25	35	325	65	163	16	357	83	60	7	188	83	192	47	224	68	292

Veins:

46	235	57	62	69	344	55	163	32	152	44	93	65	258	83	192	10	246	56	257
45	230	20	329	55	234	85	343	56	191	82	140	65	258	44	67	45	187	82	291
50	210	34	69	87	46	80	163	22	77	57	189	79	203	7	110	35	187	51	265
10	260	69	138	70	217	75	163	75	333	52	334	54	279	22	49	55	187	62	289
80	225	54	77	85	240	59	248	28	57	69	281	86	338	22	49	55	187	11	188
52	167	54	58	86	61	50	107	46	206	84	278	73	136	47	166	53	220	30	100
33	270	70	65	80	306	42	116	25	342	89	296	82	137	43	105	52	226	30	103
15	245	70	65	84	55	55	163	71	84	62	224	78	333	12	110	48	156	64	281
45	230	47	44	80	56	76	163	64	69	85	308	18	78	42	19	58	238	17	154
62	20	82	85	75	19	84	343	63	79	86	121	70	267	7	110	34	187	46	262
42	55	73	69	75	239	66	163	78	115	88	275	34	176	2	110	90	254	66	264
50	110	69	82	76	37	76	163	68	116	57	46	18	8	69	134	88	182	20	195
42	180	71	76	62	270	81	163	66	102	89	113	12	188	81	324	53	187	63	235
35	350	24	80	15	9	10	59	34	85	84	301	9	81	34	101	21	141	29	354
80	100	68	60	42	1	83	32	57	137	69	281	86	338	44	138	38	187	37	6
60	240	49	70	60	237	56	163	69	93	73	152	16	94	56	154	69	253	59	198
42	180	64	75	39	16	46	162	64	123	66	315	78	0	83	345	87	221	74	301
74	245	21	340	11	68	13	41	56	191	89	142	15	332	78	338	87	325	82	229
60	255	56	92	34	328	85	145	56	191	84	297	55	163	8	110	43	128	51	265
60	80	81	319	83	179	30	69	78	155	85	331	82	193	77	317	69	253	82	33
50	230	32	354	39	153	51	96	20	258	44	137	61	166	72	330	66	242	84	340
80	160	65	86	73	209	63	342	25	342	73	162	8	8	82	335	28	187	68	235
55	65	56	81	87	314	30	204	48	172	62	264	89	152	33	110	38	187	68	146
45	295	64	96	83	331	52	162	56	180	79	136	85	163	62	164	43	187	38	156
25	300	10	64	27	319	43	117	69	189	84	301	87	185	63	38	43	215	73	302
56	280	51	74	63	249	88	163	14	184	54	296	8	8	56	126	43	246	45	246
24	210	90	103	82	178	39	88	24	193	65	254	67	131	87	342	43	187	51	314
45	295	56	44	75	11	30	253	46	206	48	107	44	96	81	68	85	246	50	339
45	25	3	250	18	160	13	47	85	167	84	254	9	79	33	110	34	196	11	159
65	295	46	66	74	93	77	147	86	199	23	142	23	8	62	290	54	315	72	168
60	10	68	103	46	101	68	163	82	186	81	171	12	188	64	155	32	223	28	122

Veins:

35	260	82	212	85	15	63	163	42	215	81	146	68	8	87	24	25	58	27	202
80	5	68	61	86	126	58	163	68	178	89	128	32	105	81	335	43	192	24	78
45	280	55	112	88	175	68	163	78	155	86	160	83	326	89	159	55	270	70	175
70	285	52	54	54	207	58	163	89	169	86	311	82	137	85	156	66	131	59	344
30	270	20	258	24	207	58	163	22	168	74	141	72	122	79	307	49	170	27	189
60	270	49	158	43	318	68	163	49	236	81	172	18	8	87	169	54	181	53	281
60	190	15	228	63	82	88	164	88	158	88	313	85	22	90	330	40	152	41	259
20	180	71	339	80	11	88	163	47	162	51	72	67	131	74	309	46	173	76	188
70	210	45	127	76	355	34	82	46	206	51	102	51	129	85	333	71	235	9	102
55	310	56	25	71	20	41	42	86	148	51	93	80	352	73	67	88	187	63	184
28	310	76	339	76	28	34	16	78	155	66	315	18	8	50	71	89	237	49	155
65	290	32	110	76	327	61	344	76	163	49	59	2	188	32	22	35	110	46	334
30	300	46	53	55	109	87	181	37	178	51	170	8	8	83	346	31	210	81	268
80	270	23	132	70	314	32	0	71	144	81	282	77	168	51	99	35	217	59	198
70	280	34	229	55	329	83	130	69	123	66	121	73	330	31	72	90	37	30	100
50	330	29	329	75	324	61	344	60	148	73	117	7	188	77	318	69	33	9	76
45	175	56	19	46	114	87	147	51	303	87	149	22	188	89	321	80	74	15	15
80	290	83	353	47	91	57	196	66	143	62	317	31	114	62	302	89	255	25	106
60	295	17	53	59	9	61	344	62	156	71	313	31	114	89	330	18	108	52	286
60	150	42	58	67	85	61	344	68	136	82	177	89	1	83	145	89	255	6	27
30	260	70	36	81	92	84	164	68	168	26	18	49	355	41	138	88	49	18	31
30	155	47	24	74	348	79	164	71	161	22	293	50	107	89	330	88	326	15	310
85	185	48	356	78	346	61	344	64	150	79	305	16	129	85	333	23	66	65	331
60	220	41	13	66	270	74	164	62	156	89	33	3	8	80	326	87	251	66	266
75	95	47	45	72	98	85	120	66	159	43	76	3	8	77	339	65	36	49	242
45	220	18	6	49	149	71	142	52	69	44	56	8	8	15	200	70	116	5	119
80	170	46	10	46	147	69	164	52	69	46	217	24	276	85	130	14	155	14	287
30	155	15	25	64	150	58	176	52	58	56	357	2	188	78	308	9	80	52	233
55	240	57	63	71	307	81	344	64	59	39	107	83	8	80	326	14	155	55	226
55	240	51	183	39	39	89	164	50	355	40	86	34	96	90	63	86	168	13	212
55	240	40	29	82	357	79	164	31	49	22	111	43	171	76	318	19	165	13	188
80	30	25	52	77	358	86	344	27	284	30	335	81	198	74	310	26	108	24	89

Veins:

80	200	48	189	63	6	44	231	24	52	40	129	77	222	72	331	14	155	49	243
35	265	45	40	85	198	83	325	76	163	88	9	74	175	86	344	33	178	66	263
30	250	56	103	78	90	57	70	87	140	34	56	85	22	87	170	43	240	56	259
70	290	59	144	78	90	84	14	73	137	20	129	44	163	64	143	57	345	38	314
55	220	40	14	89	84	41	58	71	161	68	60	38	117	80	163	68	97	44	241
45	210	87	17	86	342	59	168	60	148	32	69	81	226	80	326	54	58	14	74
50	190	67	209	89	330	88	127	53	94	38	91	47	113	81	336	46	155	44	241
40	10	85	180	45	200	87	229	86	148	44	123	88	8	86	314	58	246	66	264
35	10	45	25	55	146	87	229	77	173	85	159	33	152	76	318	51	221	58	311
75	190	49	36	52	157	55	64	59	82	61	302	53	123	87	148	38	211	70	244
75	195	31	338	46	140	66	137	87	140	17	127	73	240	83	145	86	343	71	256
85	225	38	360	84	311	64	239	83	322	52	232	65	117	81	316	38	211	69	299
30	250	67	50	84	332	69	157	64	150	32	118	72	122	76	329	23	204	66	259
40	225	88	167	76	326	82	73	64	150	79	313	85	229	52	138	53	209	15	54
75	285	25	152	80	323	75	219	22	282	20	139	62	188	86	157	42	216	52	346
40	25	47	255	79	324	89	13	62	157	85	339	65	98	77	300	43	177	4	102
75	0	54	100	60	124	78	1	71	161	57	288	2	188	87	139	45	201	20	103
60	105	37	251	69	129	46	322	71	161	86	330	73	148	21	292	79	197	74	301
75	325	41	345	84	343	29	316	64	150	41	150	12	188	84	57	8	7	21	15
55	180	31	339	82	168	83	253	5	24	80	322	53	252	87	125	50	134	69	283
80	330	43	124	69	348	78	258	82	139	80	322	72	122	81	316	88	49	17	7
35	10	60	110	86	169	73	249	24	193	79	155	72	188	87	139	52	260	84	205
15	315	52	107	69	348	82	150	87	140	76	330	56	205	54	163	41	158	16	11
40	60	46	11	78	177	90	115	21	303	15	175	51	129	74	156	59	251	21	18
50	70	33	3	83	198	90	115	21	303	29	150	57	188	85	47	37	281	5	328
46	35	70	192	80	167	87	70	57	154	19	150	55	163	89	142	65	244	6	331
50	210	52	166	89	319	68	296	69	152	70	19	61	209	1	115	52	260	57	326
70	230	73	185	79	334	64	264	39	197	65	337	26	89	33	128	42	248	20	161
80	170	69	157	66	145	69	263	59	164	24	150	36	286	60	94	42	248	16	11
75	200	84	209	68	141	72	278	64	176	75	322	31	261	81	146	43	141	23	322
40	210	88	100	85	246	69	285	73	192	80	140	64	136	54	141	32	187	16	347
40	90	84	116	74	218	43	190	85	167	44	75	38	149	89	302	52	260	4	50

Veins:

75	330	68	105	78	238	66	232	83	157	86	131	75	117	62	30	43	141	52	149
75	360	83	307	79	217	77	230	74	154	79	23	53	149	78	131	26	108	70	273
80	80	54	241	44	42	64	220	64	49	24	150	82	136	85	149	51	187	63	184
70	145	13	16	81	19	71	233	78	139	24	150	64	161	73	168	23	171	36	151
70	260	10	66	59	124	67	264	79	123	44	150	77	153	69	177	84	215	59	175
70	240	32	190	87	180	85	146	32	287	30	200	29	204	81	94	62	50	77	228
75	245	20	122	88	1	82	142	74	92	45	137	50	135	32	116	53	166	10	4
85	215	35	11	86	165	61	230	69	123	34	150	48	155	31	42	69	7	32	349
85	215	29	151	55	121	61	230	78	139	65	297	77	168	77	151	37	144	37	227
75	215	64	151	76	355	73	282	44	168	77	54	78	7	67	160	37	144	78	317
75	215	5	59	55	318	58	144	24	193	21	88	64	161	62	163	39	151	89	77
65	200	31	348	84	169	77	302	71	303	78	355	58	151	50	169	70	236	36	353
60	210	52	194	88	342	46	349	12	90	80	346	55	257	66	147	27	245	53	281
75	200	68	239	55	184	44	13	59	41	67	27	78	7	79	24	76	250	4	46
75	200	60	126	48	7	87	73	25	167	34	150	12	187	81	138	52	343	61	268
20	0	89	138	46	127	68	142	58	4	68	60	2	187	62	137	68	231	6	24
80	20	73	93	41	180	65	138	60	173	81	338	77	152	32	116	44	148	37	340
40	55	52	87	76	327	89	125	71	161	75	279	82	182	60	158	76	310	45	2
65	10	43	198	42	28	18	253	86	149	85	313	77	152	43	156	32	178	65	176
25	320	36	35	68	310	39	34	21	303	80	33	69	152	48	142	37	282	71	265
70	240	31	340	72	329	81	109	21	303	30	99	87	328	49	162	34	170	79	79
85	215	5	243	47	327	79	262	78	139	22	110	24	136	82	146	34	170	4	115
15	350	1	151	87	161	89	124	40	93	83	304	89	1	48	156	83	145	72	178
80	20	83	308	25	265	82	73	78	139	73	314	72	122	56	166	51	187	19	1
75	185	71	321	66	21	78	253	49	132	64	293	81	165	53	155	26	187	70	175
60	250	42	60	84	3	62	357	86	303	86	330	81	165	77	117	31	187	55	179
40	280	42	60	66	42	49	162	72	101	39	265	43	241	61	138	37	144	42	8
80	250	48	165	61	15	78	253	64	129	30	99	43	241	68	130	37	163	54	123
80	20	60	91	51	58	87	307	41	347	25	74	2	187	55	129	34	156	35	202
85	65	44	85	27	343	82	73	88	106	75	346	67	230	55	129	37	163	30	131
70	180	44	6	77	178	37	304	81	98	75	21	82	136	53	79	11	187	15	350
88	155	38	42	80	12	84	244	84	89	63	69	89	1	45	108	65	221	80	122

Veins:

65	50	16	345	79	4	90	31	65	60	27	186	22	187	73	156	28	258	51	263
82	5	30	15	65	352	70	62	20	49	56	324	62	140	64	98	75	240	73	340
65	320	32	22	77	356	71	273	74	92	46	231	22	187	81	155	40	185	11	1
80	220	89	143	81	92	77	291	20	303	82	169	85	212	57	21	86	174	52	134
50	270	73	93	86	150	78	280	37	22	74	11	32	187	84	311	70	177	22	354
45	310	63	139	90	321	81	119	59	163	42	206	79	234	79	164	63	214	78	351
85	165	83	288	81	325	82	4	36	138	65	344	46	169	76	161	24	193	86	336
25	30	56	34	81	325	83	253	62	157	37	226	43	170	86	337	34	193	68	349
40	280	80	124	59	327	58	58	88	106	47	43	24	238	67	148	28	117	64	241
80	250	90	310	45	60	82	300	86	68	20	281	75	24	52	105	54	138	73	351
10	190	33	5	65	352	73	282	24	192	62	358	53	149	62	71	77	323	85	337
45	340	5	332	82	354	28	253	32	162	55	271	81	182	90	334	53	222	83	342
80	20	12	95	86	150	20	227	73	75	17	37	73	148	80	165	29	193	40	174
80	20	5	332	50	345	34	357	41	84	43	150	43	133	72	298	63	256	89	190
55	65	48	359	78	199	36	157	41	84	43	17	76	168	82	148	37	268	72	187
45	125	51	44	74	230	71	68	40	244	54	75	89	14	62	203	57	224	90	202
60	275	29	111	77	62	71	273	90	123	88	16	18	7	62	203	79	348	63	182
65	280	24	83	86	47	73	42	90	123	72	50	79	172	88	118	42	178	71	185
75	320	59	58	68	59	74	136	59	163	75	345	66	156	56	143	35	183	72	215
10	5	33	103	74	349	35	43	59	29	51	359	86	338	69	132	58	224	78	187
10	210	16	134	57	29	74	136	54	20	72	39	13	7	44	171	53	222	56	266
55	345	40	32	82	29	86	220	51	48	34	54	77	192	53	150	52	173	79	200
35	335	48	113	59	317	81	28	50	23	54	282	79	202	70	197	38	212	19	148
50	290	39	132	49	51	62	343	74	334	13	150	82	187	86	160	55	240	19	72
50	290	56	54	86	269	81	119	68	169	37	74	27	187	85	328	69	310	56	163
55	295	36	138	77	91	77	303	73	181	39	46	28	7	80	179	44	156	61	334
60	310	11	134	67	344	80	18	90	123	26	150	18	7	75	149	90	332	84	197
79	158	87	113	54	352	77	303	86	200	76	314	23	7	52	113	68	159	83	213
70	123	77	73	40	15	80	129	77	100	77	2	87	187	49	17	43	159	78	237
53	123	70	75	61	56	74	136	51	198	33	150	25	211	85	328	87	156	88	73
56	190	87	315	42	337	42	171	49	172	10	231	33	152	83	129	47	338	50	280
57	148	17	112	87	13	49	163	72	145	76	345	75	24	81	322	69	186	60	251

Veins:

83	158	48	140	59	270	62	149	81	166	84	295	58	8	68	25	73	158	62	295
82	144	63	56	89	324	29	47	64	80	53	262	43	148	85	320	87	350	52	262
35	89	15	153	90	143	62	149	60	83	27	285	36	170	81	341	79	348	87	41
69	172	36	138	35	339	62	44	69	130	55	50	37	242	88	326	50	76	36	133
34	185	59	144	64	3	53	27	77	147	13	150	39	157	80	331	88	228	79	179
83	159	12	46	73	23	49	180	83	140	53	273	84	229	87	286	79	167	46	126
32	151	55	153	47	44	46	350	60	83	7	330	90	20	84	170	54	164	81	211
50	191	6	2	76	54	51	308	60	74	39	61	2	188	84	329	74	176	89	243
64	171	31	81	33	13	33	310	52	70	14	242	85	230	75	158	51	173	87	258
48	154	34	31	40	1	53	185	81	313	68	36	52	156	67	157	50	82	78	188
59	168	39	10	60	320	65	153	20	303	66	343	38	149	81	166	81	163	64	195
33	161	47	112	76	8	69	157	85	351	54	224	89	224	80	154	66	320	76	235
76	195	38	11	33	331	69	157	35	87	57	248	70	215	73	146	89	351	75	192
84	164	65	61	77	341	62	70	55	86	64	254	70	215	75	158	84	165	68	207
17	100	27	1	50	8	69	264	47	41	88	140	73	227	80	154	89	167	83	174
52	173	49	144	68	18	8	254	20	304	55	249	88	207	73	139	61	217	78	48
89	150	32	108	86	174	72	213	16	163	65	253	84	15	41	84	89	243	70	181
89	150	7	24	86	337	43	191	43	332	76	278	72	188	45	68	86	27	81	202
63	123	38	4	85	347	64	264	35	304	72	298	74	359	83	352	84	37	70	224
70	122	63	138	79	24	53	185	0	304	2	149	69	17	39	60	29	158	52	219
61	204	20	148	81	202	45	176	72	145	16	65	87	28	80	323	62	360	75	168
88	259	40	333	79	172	59	347	12	337	38	57	78	8	77	143	65	201	18	13
44	13	21	355	40	330	77	204	88	141	46	245	80	352	56	83	54	158	80	210
89	345	73	95	86	212	55	8	55	86	87	307	87	347	68	175	86	27	63	205
80	316	73	95	73	312	67	19	43	332	60	128	17	188	72	154	50	166	29	163
71	318	56	43	54	301	30	165	19	256	69	333	32	232	83	158	52	329	76	26
41	166	44	88	63	44	69	172	75	93	80	283	54	96	69	150	86	208	81	207
51	306	52	59	63	129	37	203	70	124	76	262	43	227	81	166	52	329	59	2
59	340	48	83	50	173	86	288	90	350	14	333	25	211	67	157	46	301	74	228
80	151	17	79	82	7	87	278	87	98	49	52	2	188	88	153	60	234	74	231
74	346	51	32	76	160	76	22	65	151	17	145	70	215	64	141	56	146	57	347
77	325	30	325	78	48	76	127	77	344	7	253	12	188	72	154	66	151	51	334

Veins:

26	157	47	112	86	6	8	254	38	91	67	150	86	338	56	156	71	150	82	260
51	112	38	68	82	163	37	288	38	167	54	180	72	188	71	198	52	144	46	289
79	346	43	117	85	153	49	3	87	189	25	225	36	88	69	150	71	334	34	64
32	143	55	104	90	166	73	284	24	192	59	208	56	138	46	157	79	239	35	149
53	333	36	318	89	357	64	23	75	93	26	188	86	37	58	96	73	5	58	203
34	188	56	108	58	1	8	254	58	18	63	177	68	201	81	180	80	193	69	310
47	178	12	48	55	355	28	296	68	144	58	184	62	221	42	139	80	351	62	312
63	22	40	334	75	32	14	96	75	155	42	192	76	231	55	151	67	195	67	212
19	207	24	72	84	175	56	319	27	1	54	161	85	199	46	164	87	343	90	273
86	174	56	56	90	167	37	221	20	196	65	192	88	8	64	184	79	357	78	244
86	169	29	91	85	165	77	117	35	203	54	189	60	159	70	300	55	158	49	236
81	175	41	18	56	10	88	97	26	323	56	187	85	22	85	294	66	133	81	216
79	337	20	154	69	347	49	163	30	304	68	205	86	37	80	154	27	317	74	348
79	337	10	75	55	28	43	152	40	304	76	185	62	234	80	154	86	1	66	167
83	36	35	327	60	38	42	171	45	263	85	163	25	164	62	136	83	274	76	202
71	31	41	50	89	156	78	108	84	108	65	182	73	148	70	97	71	255	52	215
60	301	23	294	87	338	55	156	62	246	89	19	70	152	80	139	52	51	84	136
71	57	45	46	90	167	55	173	78	175	76	172	64	161	83	135	64	43	61	40
12	137	35	66	43	330	84	186	22	209	44	165	77	187	85	150	52	144	87	14
84	345	31	106	39	1	50	35	83	276	49	238	39	81	79	323	70	306	74	293
46	165	42	4	82	76	61	86	52	145	7	144	31	133	82	167	52	134	71	309
50	77	48	9	60	286	29	275	65	125	18	324	16	110	87	327	59	287	51	91
85	62	59	93	53	330	75	151	86	48	57	144	2	188	83	330	46	167	80	243
54	56	73	134	63	94	29	191	60	165	72	144	2	188	87	337	46	149	69	318
84	51	81	114	55	44	73	285	60	165	18	324	12	188	78	333	48	141	78	247
67	54	54	86	71	19	83	263	66	152	32	145	77	188	83	330	35	158	66	229
51	209	54	128	87	195	32	293	85	353	77	144	72	253	78	144	35	106	61	324
86	32	79	141	79	18	82	39	79	109	3	200	73	227	86	116	57	169	61	327
86	32	50	131	81	1	46	158	49	305	77	144	60	127	79	301	75	280	81	219
82	7	81	128	22	133	47	141	78	175	56	153	57	284	66	121	87	158	70	242
38	194	45	133	73	3	55	157	39	305	29	210	58	151	80	112	55	158	90	243
85	48	79	141	84	25	69	158	39	305	76	154	85	199	33	93	48	175	68	204

Veins:

83	305	51	134	76	354	46	158	66	125	15	293	74	164	84	301	80	4	80	259
83	306	30	157	86	33	55	173	82	177	54	16	65	258	89	295	77	348	89	260
83	41	75	126	60	354	86	231	72	163	46	172	70	267	84	295	45	125	71	262
38	16	25	266	36	294	89	98	70	138	64	161	47	286	84	295	68	168	86	254
54	221	32	294	73	346	18	42	39	135	77	182	24	276	89	301	72	165	55	332
86	166	15	342	58	16	85	222	60	165	64	161	82	188	79	294	51	165	83	199
46	166	88	117	63	0	82	145	33	32	38	324	58	164	74	301	64	297	73	211
53	234	42	118	82	351	63	113	87	150	77	169	55	258	89	88	55	158	81	251
79	268	82	303	61	334	51	131	79	140	77	169	46	255	65	271	73	270	82	250
84	337	41	128	68	47	89	98	14	305	71	170	53	123	58	301	55	158	76	300
77	145	22	73	29	278	14	76	71	125	77	169	85	212	55	97	22	218	79	235
60	107	71	115	46	350	26	256	23	347	52	162	2	187	71	151	65	338	64	214
24	96	56	79	65	76	72	134	14	305	54	170	48	148	62	63	58	169	55	157
63	37	77	117	60	39	71	297	45	319	62	144	80	23	63	204	89	161	82	218
81	126	34	140	76	104	67	35	57	171	88	4	86	37	66	53	70	171	75	207
61	14	42	109	56	100	63	47	56	192	39	242	72	227	79	79	55	338	85	193
67	278	36	42	89	167	38	47	87	180	76	151	76	231	53	72	64	171	77	243
80	346	44	71	66	6	87	125	76	325	12	70	43	155	61	68	65	338	79	237
84	215	45	150	63	360	59	117	65	316	23	214	58	151	41	79	50	77	64	312
85	346	53	42	76	173	87	47	75	295	61	179	85	212	65	343	52	309	89	235
85	355	44	92	69	20	59	76	49	27	67	145	78	7	59	145	69	322	70	210
75	166	37	124	56	151	84	290	60	114	88	169	33	151	85	4	83	274	75	224
75	346	15	83	85	166	40	207	61	131	90	178	85	154	88	163	73	350	83	35
85	166	43	58	58	165	5	256	6	125	59	242	18	7	88	67	79	102	35	319
35	166	58	140	58	165	40	207	26	108	82	171	82	187	60	104	61	54	49	351
84	4	49	58	69	47	72	148	48	56	80	159	74	200	22	86	63	48	85	63
19	260	58	52	57	101	63	136	80	110	85	160	73	239	54	103	68	314	66	261
78	55	80	112	59	4	71	121	14	243	90	178	73	239	89	182	73	350	89	34
42	251	36	59	85	177	84	83	41	276	6	145	71	26	54	162	79	4	56	265
86	148	63	124	81	175	15	76	15	197	66	145	79	173	61	150	48	317	86	226
37	115	66	100	83	87	87	125	34	306	72	167	69	327	65	358	62	325	56	255
49	94	70	148	68	182	86	149	28	227	88	182	65	336	72	306	70	178	47	175

Veins:

41	87	29	338	61	335	59	94	27	247	15	111	88	7	48	130	87	351	90	41
75	347	40	346	73	184	63	98	43	202	66	145	29	325	83	122	72	50	59	7
89	337	78	135	59	65	41	191	90	270	61	145	68	201	90	92	65	332	69	281
25	167	86	128	73	72	74	125	85	109	75	158	81	209	63	178	63	179	70	274
35	122	60	130	53	87	81	96	82	84	90	161	8	7	86	181	87	198	69	173
33	120	34	54	57	81	62	122	78	306	65	171	72	226	72	306	61	162	56	162
63	310	57	112	78	85	80	110	77	336	72	167	12	187	61	314	83	177	61	229
34	127	20	117	82	238	66	127	87	72	56	145	8	7	43	139	81	187	46	319
64	358	88	137	82	109	84	113	78	306	66	145	18	7	52	334	87	122	89	82
21	147	33	338	60	117	38	328	27	51	46	145	77	152	24	162	86	188	57	218
82	208	50	149	56	113	88	289	69	203	61	145	85	315	34	162	77	348	68	213
64	285	7	34	49	74	75	296	74	185	70	157	90	354	61	300	87	198	46	111
85	166	18	119	83	244	48	13	44	293	83	167	88	28	61	300	80	203	71	102
85	166	16	121	52	129	84	113	90	271	76	144	74	218	65	358	55	108	70	345
80	166	16	121	88	10	74	125	40	85	55	231	78	42	63	353	84	338	65	243
85	346	15	124	72	189	89	308	49	69	57	176	83	344	82	337	48	203	87	206
85	166	26	7	59	129	82	132	44	321	85	160	78	7	39	162	66	348	64	239
85	166	26	117	77	191	87	125	87	83	24	257	44	95	70	169	67	182	49	322
70	346	71	121	78	186	74	125	54	179	52	199	81	312	70	155	64	338	52	354
85	166	63	125	80	51	87	125	81	95	36	170	49	141	89	122	70	228	17	181
85	346	42	7	88	159	82	132	38	44	66	144	83	325	89	182	84	167	65	248
85	166	84	142	59	5	60	146	32	58	46	189	37	132	72	335	75	344	78	254
85	346	67	79	81	28	63	136	10	199	9	324	32	187	69	165	89	228	11	159
85	346	43	11	81	28	72	113	40	57	30	44	71	349	76	146	64	338	65	246
85	346	27	106	78	186	69	145	49	294	56	247	12	187	89	342	90	177	84	237
80	346	5	81	68	124	60	146	30	43	86	144	12	187	59	133	79	4	58	186
85	346	40	138	71	138	63	3	64	43	36	73	90	354	81	180	69	333	53	329
85	346	5	81	81	48	69	355	45	63	4	324	25	163	71	153	45	327	77	51
75	347	32	268	69	320	50	125	60	144	69	185	24	136	78	335	71	329	80	247
75	347	21	154	57	340	69	9	74	80	53	180	43	155	89	187	45	327	83	208
85	359	29	339	67	9	69	9	38	113	53	189	44	133	47	143	84	349	86	224
72	319	30	74	84	168	69	9	87	127	45	163	43	148	72	150	79	4	39	188

Veins:

85	347	45	105	42	8	88	299	8	307	73	198	22	187	86	312	60	88	80	187
65	300	25	93	51	122	14	159	36	339	64	174	37	141	84	160	44	215	57	314
75	347	89	293	78	107	23	55	66	75	28	4	66	347	52	272	57	187	44	157
86	348	84	143	59	19	68	90	61	58	56	144	37	132	68	203	60	331	52	301
52	86	37	10	82	78	73	62	31	166	61	144	44	133	73	18	56	163	81	295
84	167	44	36	73	75	78	26	52	13	76	151	37	141	67	133	65	144	9	102
36	133	47	56	82	121	58	66	53	308	56	144	30	123	79	123	46	158	84	218
72	345	29	339	67	136	83	189	74	149	76	144	17	129	66	110	38	202	53	310
58	100	39	347	86	71	62	63	82	128	61	144	7	187	56	26	75	13	84	68
73	333	25	359	76	67	70	10	83	170	76	144	12	187	56	26	56	163	76	260
24	323	36	143	77	187	88	126	79	105	66	150	2	187	79	9	64	179	58	346
12	54	39	118	74	350	29	258	90	291	46	144	12	187	79	144	36	157	57	22
55	355	71	160	84	287	83	160	77	121	51	144	86	46	43	100	74	337	47	332
44	86	74	112	79	97	73	42	39	10	81	343	31	114	58	47	84	6	45	10
56	158	70	82	88	149	87	299	71	146	89	324	90	354	71	152	79	325	75	247
57	169	31	160	74	330	32	170	75	348	69	173	44	133	51	135	65	346	47	332
33	95	30	63	79	98	72	33	18	6	8	182	37	241	77	152	89	2	48	316
52	100	12	30	52	166	74	297	16	308	11	284	83	30	61	36	82	47	73	251
83	343	40	25	43	86	31	78	28	328	51	218	37	133	49	162	82	182	62	309
57	101	80	93	66	51	83	147	74	105	62	166	22	155	41	180	64	338	61	237
63	201	49	26	64	5	86	136	74	105	46	171	78	7	79	159	76	346	49	45
89	296	25	31	52	270	82	133	87	160	69	324	61	29	84	133	74	180	47	304
50	211	87	105	78	328	59	269	70	159	59	159	19	144	81	314	76	168	33	339
72	279	35	29	70	94	6	78	56	153	76	144	17	130	80	352	72	163	52	252
54	89	54	90	70	84	86	137	78	326	19	324	38	141	81	175	74	341	52	340
54	136	87	298	83	171	41	19	82	158	89	178	82	30	72	346	74	173	36	338
86	107	65	98	57	144	68	258	71	110	61	149	48	148	54	327	66	154	69	265
75	297	49	102	68	126	90	16	78	156	76	344	61	209	40	150	89	172	53	237
49	135	32	14	77	121	57	14	69	151	36	275	39	167	64	219	84	172	55	337
73	260	61	101	48	39	55	326	19	128	81	343	74	156	79	162	84	172	69	266
90	145	65	87	83	357	86	323	88	139	86	152	13	187	77	172	84	172	88	331
90	296	61	121	30	318	87	78	79	165	21	173	8	187	54	327	81	157	70	216

Veins:

76	230	35	29	67	209	87	150	79	346	17	202	71	215	81	156	53	168	17	167
84	345	90	125	76	190	59	162	63	162	84	163	49	226	34	162	58	201	65	327
34	334	67	85	83	327	2	78	26	308	27	201	50	135	86	57	42	120	47	345
49	339	73	93	83	327	3	258	70	160	46	144	7	7	67	15	86	331	79	204
32	205	78	111	78	318	31	258	74	151	86	152	39	149	50	1	57	151	73	207
50	148	78	111	82	316	69	288	67	165	86	144	24	175	80	157	74	173	68	209
16	174	67	91	89	32	86	216	63	162	51	226	28	187	52	334	89	133	71	214
89	345	76	86	83	327	76	17	67	165	24	32	2	7	81	325	75	148	76	197
84	136	61	91	85	320	86	216	19	179	21	247	38	133	90	87	83	148	66	205
65	212	47	79	82	161	74	267	3	18	59	191	50	136	36	342	71	177	69	195
44	136	88	135	72	241	52	284	55	44	89	332	38	133	89	122	88	7	51	187
52	171	79	142	77	240	47	286	80	149	71	144	52	129	61	342	73	152	76	299
72	352	78	90	72	311	90	196	70	160	84	159	31	134	79	327	40	350	40	237
58	349	32	15	84	247	90	182	69	188	74	324	12	7	68	28	77	146	56	212
66	273	7	42	74	323	18	258	78	185	86	346	83	187	74	332	39	331	37	228
76	317	41	10	77	355	59	105	65	184	49	157	42	103	84	154	79	171	8	325
49	4	42	48	90	358	76	153	75	177	89	325	24	126	87	172	75	344	57	179
67	356	82	119	86	176	62	350	59	167	57	194	80	312	52	179	87	187	61	312
85	5	44	23	87	186	87	78	78	185	79	198	86	133	40	39	87	345	48	54
71	1	73	123	85	340	83	59	63	171	46	145	65	239	31	342	83	355	76	295
54	148	73	123	73	180	90	117	86	309	23	280	40	149	77	140	74	13	17	311
45	111	34	341	79	193	17	78	76	159	23	280	46	170	90	112	71	357	26	332
54	136	19	341	53	303	85	114	63	152	76	145	60	198	90	112	65	137	74	308
76	316	70	116	28	162	85	273	9	129	83	168	52	232	32	307	84	117	75	190
49	138	53	46	86	187	85	91	66	157	29	212	33	297	66	338	50	174	67	325
50	271	37	4	73	8	59	98	70	160	81	184	36	20	54	103	60	350	68	332
60	194	39	280	73	87	10	37	76	338	44	164	75	151	42	331	86	268	70	315
71	335	14	326	77	80	85	114	73	103	44	208	40	275	73	109	88	338	43	141
74	208	90	144	73	223	70	311	77	145	69	325	49	284	73	109	84	341	85	323
53	140	70	148	78	223	86	300	71	146	14	325	86	151	77	124	87	37	81	215
62	207	19	329	90	239	88	310	89	129	50	155	62	117	87	2	90	172	74	179
80	349	86	309	66	332	64	33	63	171	61	205	49	134	60	345	76	167	57	317

Veins:

86	113	29	359	74	325	24	235	67	175	43	183	66	169	55	162	89	357	88	326
24	143	32	16	32	10	37	1	59	159	18	254	53	199	75	175	81	353	76	200
53	291	19	342	42	44	83	23	59	159	42	176	25	327	88	357	46	138	79	219
83	359	61	156	46	53	70	24	60	168	32	271	81	321	87	2	88	351	54	289
55	163	29	276	72	44	77	294	75	172	84	164	66	130	81	278	50	141	60	182
37	231	39	342	31	119	69	300	50	238	56	147	37	242	80	360	43	147	27	102
25	171	41	312	54	9	20	230	63	149	6	147	82	125	90	177	42	157	82	255
65	26	85	128	50	155	8	329	81	300	78	168	20	263	90	177	66	129	38	260
50	7	86	319	39	308	49	91	54	182	86	147	52	172	81	339	75	179	29	26
50	26	69	331	70	305	8	186	66	309	66	153	56	144	80	360	65	178	32	331
63	16	75	322	86	293	8	186	77	184	55	158	56	344	88	357	83	155	76	2
31	357	12	289	76	276	54	245	83	159	52	147	89	310	89	352	90	352	63	155
80	296	54	147	54	18	12	78	67	166	83	170	62	176	87	2	60	169	86	141
60	195	78	342	81	59	22	3	71	147	61	226	49	48	74	36	70	227	63	141
59	49	78	122	71	343	20	230	27	43	74	167	57	92	41	203	90	341	65	207
45	163	89	140	67	115	41	189	66	158	56	249	56	144	73	41	64	38	16	298
88	356	76	151	65	348	41	136	52	91	62	169	62	156	71	335	18	321	80	9
39	190	84	124	78	349	41	136	87	161	69	198	62	106	85	334	62	337	80	191
44	150	76	131	37	78	70	145	79	347	62	241	81	132	75	329	81	149	78	42
76	318	82	298	58	358	41	136	68	155	81	178	62	106	42	291	46	359	90	65
76	309	74	332	76	26	23	165	4	129	57	144	58	81	84	335	72	341	55	296
34	117	78	139	84	190	78	231	74	155	87	155	43	89	67	208	79	322	76	63
24	122	79	332	24	271	37	155	65	150	50	259	46	188	39	162	89	12	42	267
65	293	38	342	36	259	56	234	74	155	83	328	14	28	44	162	89	357	78	57
62	277	32	123	38	266	24	234	88	275	7	148	82	125	29	162	49	39	80	175
59	228	22	153	84	204	22	138	67	145	22	148	42	29	49	161	61	135	59	276
54	150	36	64	87	242	41	136	84	129	81	178	45	161	49	161	71	193	90	138
73	18	20	140	13	263	55	136	69	129	76	161	14	4	74	288	59	138	56	202
66	336	78	91	27	132	62	166	89	129	76	161	2	297	89	196	75	184	60	262
66	252	34	59	18	286	55	136	69	153	72	174	72	15	81	221	78	191	52	283
67	256	28	342	48	332	81	120	37	97	25	180	35	182	64	218	69	198	49	286
36	306	56	152	59	76	37	52	65	150	85	346	37	180	64	218	85	166	13	143

Veins:

53	138	78	139	58	118	82	302	54	148	25	228	27	190	75	188	71	205	72	346
76	309	90	316	10	226	59	127	63	96	23	204	84	65	49	161	42	209	37	112
88	356	29	333	31	77	73	113	70	153	45	27	36	240	81	221	78	191	71	156
89	148	35	31	46	48	69	118	83	336	13	100	88	52	73	193	82	170	65	206
71	336	43	342	68	19	73	113	85	310	45	157	44	10	72	45	74	206	75	33
67	358	36	64	41	70	87	78	60	130	45	27	71	130	81	107	89	335	74	16
86	7	33	342	64	5	49	118	69	353	45	177	43	230	68	27	33	276	76	118
85	348	8	91	42	17	70	204	60	134	89	284	35	81	75	29	90	204	86	35
51	176	38	21	71	133	68	216	62	148	72	212	54	158	70	66	58	116	87	348
74	34	76	318	52	2	59	127	49	147	32	5	42	97	72	5	57	124	90	65
65	216	47	60	89	244	64	123	24	105	90	2	69	276	72	45	62	326	65	208
41	204	49	303	72	10	80	241	78	287	45	27	64	81	77	200	56	134	70	30
36	314	35	136	60	41	77	139	72	90	36	2	23	155	82	206	71	121	50	269
85	292	48	289	54	20	42	169	68	59	40	164	44	10	54	161	71	204	76	53
54	289	16	302	67	354	28	71	68	59	19	24	30	58	82	41	84	123	81	50
14	167	75	244	55	357	8	333	69	59	3	329	52	127	34	161	69	122	25	302
70	333	73	243	26	125	8	78	83	71	42	231	88	73	57	194	86	287	85	9
90	311	19	7	44	55	18	39	73	67	86	164	59	95	69	354	83	113	5	352
15	106	18	331	54	78	87	236	70	279	84	346	23	117	81	226	75	289	85	194
24	157	82	163	37	46	89	30	43	356	84	346	78	113	68	27	60	153	49	115
48	277	17	55	20	284	15	170	44	85	13	56	84	315	87	345	71	193	33	119
15	180	48	38	78	30	75	63	76	271	76	136	50	290	81	221	88	257	38	156
45	237	41	314	72	18	22	138	56	173	62	242	48	277	72	220	51	123	84	236
20	166	18	344	32	341	27	186	70	82	36	59	29	135	53	199	40	151	70	268
15	166	52	237	52	23	37	104	77	196	59	212	17	297	86	327	68	170	78	75
15	166	22	276	80	329	73	208	65	151	63	216	79	167	58	209	51	115	75	11
51	312	83	286	36	36	45	120	70	153	67	220	76	234	89	221	48	126	65	172
42	255	89	139	68	118	55	173	73	155	13	242	46	105	72	45	54	120	79	212
70	338	81	150	70	350	55	173	75	156	61	227	42	297	81	216	89	342	78	164
74	331	25	314	75	293	15	347	66	170	42	196	27	112	67	207	88	177	79	189
75	349	30	146	83	70	24	234	72	148	48	208	32	155	89	221	45	112	85	164
68	325	89	328	85	79	54	54	80	262	42	196	84	25	82	211	66	208	65	208

Veins:

89	2	48	345	69	261	86	217	63	156	36	239	75	13	60	190	71	46	86	176
36	180	33	329	51	49	84	243	80	310	36	59	45	180	56	194	51	114	80	158
49	336	38	345	56	49	41	136	71	180	45	357	17	284	60	82	54	119	57	222
40	166	50	319	51	49	55	41	21	39	76	241	51	201	83	292	51	122	75	211
36	330	64	187	61	348	15	170	43	69	14	2	32	359	81	102	51	341	85	28
45	165	51	332	51	25	35	129	72	170	24	162	51	33	69	2	82	1	80	167
3	245	75	108	59	61	8	78	73	102	58	180	83	356	32	50	78	5	65	237
24	327	62	106	81	49	47	180	65	310	89	3	29	112	82	282	44	218	24	163
82	156	50	108	66	45	85	290	65	104	39	182	47	65	80	81	79	174	82	145
77	327	47	85	61	49	14	295	69	310	42	196	17	70	83	292	80	57	66	204
69	350	65	93	80	354	19	288	74	310	37	38	20	82	49	29	57	359	87	349
72	329	53	64	45	6	8	337	78	287	54	80	43	119	90	91	81	319	31	253
80	340	13	165	61	42	34	341	83	289	86	164	59	95	61	341	66	231	60	262
74	354	14	315	76	102	79	275	84	285	47	329	76	151	71	341	53	273	74	342
48	335	65	93	57	75	42	169	41	171	64	308	18	323	57	34	62	119	61	225
82	156	31	127	75	61	54	190	80	167	82	330	34	90	69	321	76	149	80	12
54	343	3	346	64	75	76	222	74	281	73	175	22	275	55	215	58	350	39	221
59	341	57	270	67	50	37	154	66	151	78	143	49	137	72	130	61	12	75	208
74	347	35	192	72	1	70	145	79	187	13	241	80	325	51	233	59	290	60	196
88	5	26	285	81	87	24	234	41	161	67	139	87	306	76	123	59	160	86	6
39	252	47	133	24	183	17	259	60	178	68	150	17	70	70	236	78	212	85	13
40	317	57	171	50	106	20	199	78	175	42	68	35	43	61	230	71	186	33	157
69	53	82	134	90	9	27	259	81	200	40	1	74	338	71	226	52	321	61	168
78	338	47	133	24	277	90	229	66	186	44	271	30	260	21	189	63	190	89	17
45	97	18	132	89	238	60	236	37	145	48	209	45	247	71	231	86	91	58	221
58	341	72	194	67	106	78	40	40	191	74	311	23	325	67	32	54	172	77	163
32	37	79	189	75	335	58	194	76	183	61	228	21	344	47	130	75	282	70	240
36	11	21	100	70	62	89	197	38	162	58	181	34	263	68	161	70	272	87	41
43	195	58	111	88	74	88	79	43	169	48	209	76	24	81	211	43	3	48	257
60	322	74	188	45	95	75	197	49	187	67	161	83	85	42	139	68	121	54	135
58	359	30	84	52	334	72	219	56	174	31	293	55	66	60	28	79	171	63	267
52	3	33	119	49	304	56	136	84	131	61	228	56	0	80	242	34	111	86	7

Veins:

74	2	88	122	49	304	32	97	71	204	30	248	46	143	79	20	88	150	42	277
70	347	58	144	78	204	77	232	67	200	30	248	87	165	77	24	62	195	70	29
84	314	63	166	57	9	86	281	11	131	14	196	69	143	89	212	85	151	64	164
77	297	78	166	68	343	82	54	56	200	88	347	82	173	59	190	62	171	58	279
85	344	84	142	32	269	8	18	47	143	82	181	69	192	89	212	54	172	71	268
79	315	86	132	46	328	72	193	51	133	83	102	19	148	73	210	38	307	61	248
47	6	71	180	84	353	72	219	68	200	13	62	34	227	32	342	87	10	86	62
47	6	70	186	72	139	77	211	67	186	36	331	38	232	75	205	23	141	59	210
49	352	78	166	83	135	63	214	45	176	41	174	25	233	37	11	38	141	39	106
45	304	68	166	62	52	89	197	72	181	43	181	64	230	80	221	59	212	87	220
67	8	57	176	67	32	79	79	89	319	64	259	43	173	27	342	78	70	47	258
59	360	78	167	23	232	11	259	69	311	87	136	65	227	63	219	79	65	66	175
39	348	89	141	72	191	58	17	42	116	84	285	87	229	69	186	87	272	23	221
31	171	86	133	57	52	39	357	74	311	9	151	89	117	60	82	73	145	84	22
61	168	83	125	90	20	47	127	71	131	44	15	84	125	81	206	38	141	70	25
87	205	76	152	81	6	86	236	76	131	75	280	35	43	66	208	69	81	18	122
37	43	58	145	65	254	49	46	89	311	66	247	8	247	88	157	85	91	67	227
63	340	84	309	38	232	77	127	81	131	60	213	17	324	78	163	69	75	45	237
73	339	11	73	45	189	79	84	81	131	62	244	69	114	42	317	78	91	64	122
79	342	14	53	77	194	29	72	74	156	90	241	36	289	82	277	60	82	36	154
87	3	35	91	73	13	77	127	32	32	66	105	69	91	38	162	61	87	75	186
88	354	88	301	57	22	76	286	73	352	88	144	80	67	49	118	54	277	87	259
22	174	53	167	88	17	68	142	76	132	90	241	55	149	71	97	87	338	68	139
33	342	74	129	88	13	49	162	86	320	82	340	21	297	84	292	68	316	88	320
38	340	66	115	87	193	17	30	69	312	79	9	83	101	67	32	84	110	81	302
59	261	76	181	76	27	70	119	89	319	60	214	89	271	56	18	78	90	82	147
48	12	71	180	86	163	45	9	80	144	74	204	36	22	86	307	54	171	87	180
47	27	54	255	77	12	35	88	39	40	63	194	26	128	74	349	86	201	68	359
48	12	70	187	47	73	10	317	67	77	31	79	80	90	52	342	78	176	36	165
52	16	85	129	78	191	19	197	88	336	88	298	11	297	75	289	25	161	72	70
64	14	89	311	77	299	12	46	62	346	79	115	29	354	51	360	65	200	76	354
33	83	51	178	84	153	23	358	77	350	78	313	30	13	33	194	51	320	57	328

Veins:

66	23	71	150	48	191	59	237	83	338	4	151	59	152	54	138	79	221	90	358
68	354	40	126	89	228	29	22	68	86	79	294	53	104	63	9	44	140	69	190
56	329	71	180	75	149	76	212	31	190	34	202	35	296	69	125	34	140	41	176
58	359	78	167	78	53	59	211	56	164	6	332	5	116	80	66	59	140	72	16
59	336	43	195	77	221	49	106	36	48	66	275	36	99	88	202	47	157	49	351
17	193	43	139	79	35	76	95	52	54	85	129	36	44	45	40	60	174	29	139
34	343	50	110	51	241	42	54	79	321	88	193	49	21	84	31	72	37	26	226
76	11	62	178	88	324	12	46	44	169	83	181	51	350	73	342	38	334	66	56
58	359	72	196	79	190	83	122	54	169	78	46	68	167	37	189	42	161	50	112
73	268	52	143	21	126	27	184	44	154	49	60	61	178	80	217	88	276	69	31
69	348	23	176	89	153	35	224	90	327	26	15	61	95	65	209	27	184	89	189
66	326	11	235	74	329	30	2	51	164	54	84	40	116	80	107	58	157	46	14
12	21	46	220	88	157	68	87	35	163	62	272	10	116	88	102	47	157	67	325
12	99	31	274	55	289	22	285	22	123	88	204	59	171	63	47	42	161	83	159
89	299	31	312	67	66	18	291	63	312	83	211	28	130	53	138	69	69	85	153
84	300	19	267	50	112	8	171	55	312	21	23	29	132	82	273	78	200	52	106
87	309	16	100	46	122	48	66	72	83	88	27	49	75	57	162	47	169	85	153
45	326	82	175	55	128	76	233	61	71	67	82	59	81	54	350	44	140	24	236
67	299	78	168	56	10	71	220	37	23	86	175	65	141	51	123	50	71	52	106
75	322	63	168	39	190	31	260	49	43	75	195	68	168	80	247	40	100	24	236
88	337	40	146	34	190	65	137	64	291	76	269	15	116	32	162	71	320	66	152
18	190	52	159	87	218	32	241	73	163	36	168	86	92	27	162	85	180	66	152
72	182	38	202	80	26	29	148	73	283	88	137	64	127	66	37	24	87	77	229
88	356	63	72	87	218	9	80	77	274	74	127	0	116	82	192	29	140	77	229
74	355	50	111	85	208	40	85	63	312	71	121	85	124	79	91	63	169	52	122
59	28	59	324	55	128	81	260	85	218	78	166	34	72	75	39	29	140	76	138
81	168	68	194	34	174	30	32	47	66	74	178	30	118	32	162	47	157	52	122
39	345	23	172	87	71	61	99	27	155	64	219	20	146	64	9	50	165	76	138
76	324	52	282	59	118	89	73	81	276	82	351	30	116	83	41	50	165	55	215
71	26	70	123	81	18	36	22	32	312	21	26	22	130	82	51	82	357	55	215
58	52	6	226	46	216	63	281	46	89	84	202	10	117	27	162	71	90	86	134
74	348	86	184	28	347	27	305	59	77	82	351	52	153	67	162	44	140	86	134

Veins:

64	348	66	116	81	43	36	137	66	313	85	146	64	155	37	162	86	90	79	156
73	188	52	192	64	258	67	3	80	334	80	342	72	171	79	168	24	140	80	157
73	57	68	81	86	259	54	80	53	133	44	124	63	146	25	246	38	165	81	158
71	10	65	187	76	81	67	290	82	63	74	293	46	81	87	342	44	140	81	159
72	2	88	1	48	348	88	67	50	77	35	131	37	82	57	185	39	140	64	177
57	1	69	92	48	150	79	50	59	77	82	351	42	31	76	174	88	359	64	177
81	49	70	148	81	43	64	63	61	74	77	220	76	163	86	299	32	201	85	357
61	4	77	199	79	199	76	286	68	133	79	210	50	137	40	149	47	157	68	72
63	71	14	55	84	194	71	146	38	243	50	121	36	23	13	4	47	157	85	357
39	133	79	97	80	170	76	212	17	313	72	136	70	16	22	184	58	305	68	72
87	153	26	106	81	43	84	49	21	338	61	77	25	296	8	161	66	301	40	111
61	307	35	93	89	189	80	290	74	332	80	190	42	128	41	165	66	301	40	111
80	24	73	168	80	149	27	252	17	313	40	138	46	152	47	178	35	153	89	317
73	51	54	117	81	9	39	358	62	58	54	101	59	143	13	135	55	134	84	100
87	161	11	102	88	342	36	345	62	73	87	216	39	18	76	195	50	180	75	162
81	34	79	129	86	9	58	121	70	169	49	262	63	59	28	123	79	200	85	162
78	309	47	293	76	336	65	154	79	330	42	74	50	50	44	227	44	140	60	162
78	342	83	210	90	176	15	181	85	347	65	19	49	76	33	175	70	351	75	163
73	343	79	119	44	196	85	96	62	73	75	325	19	209	49	123	39	140	87	325
72	330	83	210	89	189	71	284	76	2	79	210	43	126	22	258	24	140	60	165
78	334	44	62	81	357	33	352	62	313	70	334	76	154	18	4	44	140	60	167
88	330	41	200	56	0	6	253	89	155	85	326	46	132	27	223	48	157	28	326
86	326	59	191	36	159	88	199	78	175	74	294	68	167	28	211	64	187	30	190
43	268	30	109	36	159	77	87	72	272	78	12	33	81	80	21	39	164	18	89
70	84	56	120	53	345	22	230	82	321	75	179	68	167	51	117	45	131	20	8
72	3	72	182	65	355	83	236	67	313	87	300	76	154	71	173	50	147	20	124
82	168	84	193	50	267	62	166	87	313	89	113	36	209	66	177	56	170	20	110
51	304	21	206	78	138	16	254	15	84	87	300	60	160	88	357	86	190	22	100
88	131	78	169	71	41	88	237	53	72	78	296	68	167	75	22	70	178	4	152
75	352	79	8	74	29	88	308	87	147	81	85	22	175	70	251	43	160	44	126
83	348	83	169	86	213	81	263	85	154	31	124	90	304	77	179	84	19	74	210
87	335	81	184	85	151	37	141	81	339	87	8	85	116	46	135	48	157	75	162

Veins:

83	348	84	193	72	54	83	104	80	277	75	231	58	131	77	123	45	140	75	162
75	307	78	169	55	128	44	193	77	285	49	64	81	166	69	144	59	157	65	162
82	177	88	169	41	161	88	59	89	249	88	186	72	62	66	163	61	174	85	162
70	347	40	100	87	131	81	144	89	281	49	46	49	157	53	132	59	157	75	162
80	347	54	136	80	149	54	142	73	84	75	180	76	153	78	355	31	156	65	162
87	186	56	92	51	125	15	117	66	92	39	161	82	356	73	188	40	66	65	162
76	168	81	321	47	156	71	24	72	260	24	197	76	315	59	149	80	261	65	162
43	322	89	6	48	150	30	12	63	96	23	251	68	134	73	164	83	341	55	162
58	241	85	194	85	356	27	320	73	84	24	197	34	296	76	136	40	179	85	163
88	0	51	132	53	152	62	48	61	87	67	161	73	136	60	164	74	340	75	162
39	347	39	118	70	320	19	354	70	76	9	146	76	116	84	129	79	339	56	163
83	347	27	97	57	343	36	347	31	107	78	159	1	116	39	101	87	343	65	149
73	346	43	123	90	351	48	148	85	279	45	182	73	136	41	52	71	167	11	310
63	340	45	106	86	9	19	354	69	270	58	194	62	138	83	184	88	159	68	163
87	157	49	72	66	9	71	124	71	272	54	165	49	22	82	4	35	87	67	343
87	329	87	349	59	118	57	17	87	119	86	181	68	148	71	117	85	348	59	205
87	166	30	25	46	14	42	354	80	313	77	177	68	202	82	288	71	146	20	198
78	346	82	137	86	9	64	70	77	322	72	174	50	181	60	157	87	338	79	119
82	171	40	20	86	9	62	22	64	313	86	326	27	60	77	162	75	348	88	116
71	172	79	240	86	0	29	22	84	347	88	346	54	152	42	172	56	169	83	291
79	348	68	143	79	316	54	127	76	313	54	165	22	116	40	166	71	167	72	135
73	333	55	81	88	157	61	151	83	297	84	172	50	156	20	64	67	177	70	25
76	178	9	34	78	344	58	147	82	133	66	164	41	102	81	119	56	169	82	292
81	168	88	169	85	175	68	64	83	329	49	171	50	156	25	125	89	179	47	339
87	6	87	349	81	334	89	278	74	332	47	164	54	152	87	236	57	344	35	307
84	347	30	314	83	139	34	219	64	358	58	168	57	165	57	141	54	158	60	136
89	354	79	109	87	323	82	237	85	305	48	220	86	64	52	95	56	162	84	97
45	324	7	350	90	151	86	52	81	321	69	146	77	153	83	19	53	174	72	286
74	1	24	80	64	132	85	186	80	360	72	163	57	156	83	19	48	122	26	341
74	1	39	53	78	344	46	241	84	133	76	11	49	166	37	259	85	348	76	131
64	358	52	97	87	160	42	97	78	304	51	170	85	342	87	242	35	149	88	148
65	349	29	188	83	342	26	114	58	80	59	146	29	50	61	173	68	290	46	63

Veins:

70	11	83	128	84	154	53	187	84	347	75	146	41	102	35	134	66	170	48	101
77	6	79	130	90	151	81	144	71	322	50	161	61	82	31	43	46	314	71	27
72	21	89	195	90	151	80	264	83	120	62	172	53	296	90	135	53	167	68	278
72	5	44	276	52	137	89	117	75	274	59	150	55	31	16	311	66	194	84	198
72	306	80	193	85	332	81	145	89	261	54	152	86	158	71	250	87	79	43	332
80	114	87	204	88	159	21	75	85	313	35	161	54	152	45	149	60	185	57	166
78	309	84	312	87	84	80	39	80	313	78	159	64	173	63	347	51	115	82	148
70	318	77	350	68	218	83	313	74	138	32	168	64	173	34	88	18	264	48	150
83	347	89	333	46	119	19	49	68	142	45	159	69	157	45	156	80	120	25	146
88	349	44	142	71	143	43	193	64	140	79	183	70	75	41	166	79	283	82	55
83	346	14	58	55	100	89	152	65	150	35	205	69	135	80	329	79	59	40	183
88	346	79	210	65	197	87	310	71	169	39	162	84	93	74	140	80	104	42	62
88	346	80	147	90	96	77	294	87	181	48	220	74	38	77	109	43	287	80	153
88	347	87	136	79	102	81	6	57	153	49	146	80	46	73	268	37	94	64	133
83	347	79	120	74	57	81	6	65	226	81	326	72	179	15	269	85	291	69	156
56	31	82	155	74	57	58	19	74	181	24	267	64	8	19	183	76	296	81	203
65	342	62	131	84	61	83	256	79	198	15	138	47	123	39	208	76	284	86	212
84	325	65	137	55	88	82	76	86	205	8	196	61	38	89	225	87	84	29	254
87	140	66	128	55	88	89	107	86	320	28	219	47	159	20	169	85	170	27	137
75	339	54	119	85	6	77	217	89	290	24	198	30	20	8	127	85	109	76	343
87	327	43	306	72	87	68	256	86	112	53	154	76	86	83	216	85	281	45	182
58	348	36	266	50	85	80	273	31	133	29	188	32	339	60	231	41	279	84	297
78	349	77	140	26	54	87	310	60	64	19	195	23	63	83	172	69	96	82	57
83	345	73	141	38	71	39	37	67	92	19	211	59	165	73	345	75	110	45	101
88	344	80	147	40	186	90	240	56	118	77	196	49	25	29	115	73	111	47	114
83	344	89	333	34	78	88	53	49	153	61	223	43	16	42	95	65	136	27	5
87	164	73	163	72	87	84	247	27	197	81	199	48	42	31	211	86	180	14	139
68	40	26	108	50	109	54	88	58	171	83	176	31	44	74	164	67	177	63	166
78	341	89	333	50	109	78	256	68	92	79	146	3	117	60	149	51	329	74	154
58	38	82	155	49	146	65	101	76	123	22	165	23	117	38	275	40	101	59	163
56	31	65	97	50	61	88	256	45	232	63	189	73	143	29	115	64	176	68	77
69	288	38	186	31	71	75	237	52	187	63	155	78	124	39	102	86	180	16	163

Veins:

52	37	84	27	16	17	73	226	35	204	19	146	87	169	39	168	28	112	82	85
67	54	71	215	46	92	83	230	4	313	58	169	64	149	71	243	31	124	23	307
69	60	21	133	25	5	69	159	16	133	69	169	88	125	77	168	35	146	87	334
83	135	83	178	68	107	80	132	84	161	88	161	78	283	66	227	70	205	75	267
86	145	89	196	63	93	88	138	68	313	65	167	81	170	15	268	56	149	39	323
69	42	77	200	82	246	86	310	39	162	68	157	84	91	77	16	40	134	13	40
73	7	80	193	73	121	82	230	9	17	10	204	36	7	48	129	71	195	74	182
88	331	79	210	14	130	22	76	82	269	72	175	78	174	60	135	61	174	72	143
71	323	51	133	70	186	87	69	84	134	71	178	83	167	33	126	73	179	71	309
58	20	73	170	81	91	78	256	86	134	38	204	74	152	42	127	72	184	85	335
86	305	39	119	90	275	87	232	90	321	65	167	74	152	45	113	69	178	76	149
74	356	73	170	50	186	81	48	60	147	15	189	83	310	65	215	62	181	90	130
79	139	62	159	42	54	70	236	49	161	86	169	85	140	16	162	76	185	60	160
59	83	82	159	70	131	71	65	75	264	62	172	75	137	0	3	36	153	70	153
51	64	70	150	76	89	68	145	89	148	85	6	64	167	84	238	57	34	76	164
64	344	81	19	56	125	90	224	71	333	62	172	54	186	80	153	67	177	84	160
74	344	63	170	59	115	86	62	45	36	59	154	89	318	36	143	60	49	77	174
90	346	79	10	85	195	88	256	28	197	86	182	84	143	73	345	67	177	52	209
50	342	62	209	52	211	70	236	79	267	54	149	89	155	43	120	50	180	43	158
35	178	47	128	72	87	75	152	76	352	48	188	41	141	15	249	83	185	63	133
65	16	77	350	25	5	90	24	34	195	84	146	47	124	86	153	59	179	24	292
70	320	79	144	65	242	75	138	77	210	80	171	79	154	83	141	57	295	62	330
65	51	36	75	27	77	41	121	60	67	75	190	67	155	36	143	68	189	81	86
83	2	73	142	78	123	84	240	37	58	88	161	42	165	17	231	50	172	84	185
73	36	45	233	44	226	78	110	55	77	71	164	72	106	38	110	69	183	39	170
41	26	85	146	79	58	74	36	42	70	52	158	89	155	36	135	78	180	89	198
48	55	35	23	49	224	79	95	42	44	56	181	83	157	26	49	88	205	84	343
87	351	49	74	57	161	84	240	77	60	73	193	81	160	77	168	47	177	86	352
72	349	49	267	38	84	78	247	68	315	69	206	88	331	72	170	57	185	34	139
89	124	62	132	42	116	62	256	20	13	37	179	82	289	35	179	85	14	17	38
49	272	81	19	61	162	32	174	69	54	54	199	83	157	60	3	83	185	18	317
86	152	47	295	47	211	52	153	54	24	71	196	83	157	61	352	49	255	39	325

Veins:

40	94	83	171	78	124	84	240	51	89	79	193	82	147	28	138	64	188	71	11
77	10	82	155	16	19	28	236	73	287	75	223	82	147	47	143	63	193	64	346
85	167	88	334	65	186	80	95	90	277	88	347	85	140	47	223	44	173	27	151
75	349	73	177	12	59	62	256	65	194	74	172	85	153	0	183	51	188	19	201
78	327	83	171	53	25	65	141	86	250	77	360	70	149	58	226	69	296	83	257
85	208	25	159	56	49	72	256	66	90	74	152	84	319	30	107	79	185	81	242
53	318	63	165	22	31	68	225	52	155	61	327	82	177	44	246	80	2	46	272
74	28	14	60	22	126	86	232	70	112	84	147	83	167	61	231	81	110	73	342
88	124	87	137	23	58	67	262	80	187	70	9	79	164	66	139	55	360	76	326
81	334	59	216	16	19	67	267	65	78	88	162	65	158	37	205	41	91	50	111
89	133	60	109	16	19	67	288	75	63	81	327	85	173	10	183	71	194	71	147
68	349	83	171	30	87	42	172	78	166	71	327	78	174	43	128	89	219	70	148
87	169	38	186	10	116	77	265	42	46	84	186	61	163	23	129	25	89	76	82
26	335	59	193	16	19	67	288	58	199	72	175	49	143	50	157	82	304	72	115
67	354	50	93	23	149	85	291	40	246	46	218	89	145	30	127	80	2	69	158
77	351	12	72	29	52	76	295	70	96	49	223	84	319	37	223	51	71	85	162
78	181	23	195	22	58	69	277	35	87	83	168	77	157	63	131	41	101	73	174
86	79	48	166	39	35	35	180	66	59	72	181	63	160	36	127	89	349	85	344
88	172	64	181	47	43	80	303	51	250	88	169	69	177	84	194	87	348	88	175
41	202	71	76	27	79	87	90	49	342	47	202	63	151	54	164	73	313	81	325
72	352	27	82	9	54	72	266	54	242	49	177	83	166	57	159	86	169	73	175
72	319	73	267	52	137	81	282	15	60	43	269	83	315	90	357	79	184	15	104
37	347	58	297	27	79	69	277	64	342	78	171	88	133	87	164	80	351	10	146
36	85	69	167	70	56	20	7	69	221	78	171	81	151	46	164	65	338	58	123
78	309	69	167	18	142	71	227	37	241	19	197	88	129	55	152	86	4	49	54
66	336	29	141	16	20	83	240	62	251	81	175	84	321	35	155	65	319	59	106
30	264	42	188	16	19	42	171	52	237	68	152	19	338	75	253	89	149	60	149
69	9	87	334	67	75	68	236	22	228	58	210	19	338	78	257	75	323	60	149
72	258	22	248	29	119	71	227	79	348	66	297	81	302	90	170	76	326	63	184
52	24	32	149	61	234	20	144	51	267	84	137	73	275	76	179	84	18	61	149
75	310	48	182	66	165	73	238	33	18	89	78	80	164	76	179	89	349	61	149
58	335	40	191	37	158	76	257	88	331	69	275	74	322	46	129	81	333	51	149

Veins:

59	293	47	265	37	158	35	71	84	195	83	2	37	93	83	210	49	269	77	138
85	350	52	187	66	166	69	159	62	152	63	227	42	79	90	170	82	130	79	157
75	351	83	303	61	165	76	347	55	263	11	146	81	340	80	173	85	317	88	72
60	316	37	157	35	172	84	325	39	18	55	181	88	352	49	137	85	336	58	211
80	292	64	224	61	165	74	125	32	262	60	169	86	153	72	340	86	114	77	138
85	297	75	209	63	165	69	9	68	354	60	169	30	22	84	10	83	79	69	131
86	171	39	165	57	49	52	169	36	254	72	223	86	163	86	33	80	99	87	195
55	310	47	265	17	77	76	153	53	257	74	204	67	154	52	97	88	79	71	212
86	169	51	197	68	121	55	173	44	245	51	174	75	182	72	47	87	94	67	212
75	351	48	183	18	141	80	35	59	108	77	185	29	337	81	205	88	143	57	211
84	172	88	357	27	78	69	159	55	264	89	198	19	338	88	228	89	136	77	212
84	172	49	237	61	142	41	190	54	260	64	119	24	54	82	186	84	291	16	187
86	355	58	206	51	137	16	224	36	273	33	103	69	152	47	109	89	136	30	223
83	196	41	8	77	125	24	257	70	315	69	148	71	149	20	3	84	309	88	125
51	263	36	142	70	145	80	156	77	176	39	89	71	149	71	21	80	293	71	120
74	190	51	31	13	31	89	107	56	13	73	220	73	155	89	167	75	284	77	214
52	335	41	77	6	131	85	90	43	189	77	185	65	157	90	350	81	114	35	182
49	144	81	202	54	176	70	145	78	191	77	185	71	167	81	344	85	319	75	178
86	311	39	127	70	145	74	113	40	64	66	243	71	167	83	3	81	137	52	166
29	356	36	143	33	124	66	155	23	289	56	115	78	44	78	359	88	311	65	180
88	149	42	58	49	43	86	91	60	70	78	181	63	160	74	350	82	312	48	259
81	44	28	210	54	176	86	192	66	297	76	352	66	22	81	205	90	305	29	125
54	77	47	127	54	176	85	33	58	354	82	214	80	154	79	351	53	252	55	228
73	244	14	323	53	188	69	38	61	319	84	170	79	127	88	301	85	129	76	222
59	60	53	72	54	176	89	127	53	272	64	236	75	170	70	193	85	129	41	210
41	191	76	210	43	175	83	203	62	283	16	201	89	110	56	165	31	147	39	155
55	217	19	323	18	74	34	176	47	256	45	140	67	187	56	171	72	126	52	165
23	329	33	288	51	138	66	1	27	181	35	126	43	146	58	159	88	306	61	162
86	197	19	323	23	170	72	323	30	121	31	359	58	165	51	176	84	101	46	211
13	234	24	323	76	60	49	355	44	134	59	156	81	54	81	344	87	126	65	187
21	140	37	256	18	73	23	162	57	154	48	9	29	233	83	3	86	139	57	263
26	283	16	143	64	235	45	149	87	278	55	241	58	83	47	180	30	219	44	225

Veins:

18	328	71	169	69	233	79	109	77	281	12	55	50	157	21	304	70	223	33	227
58	89	30	66	51	54	84	134	54	136	48	103	89	355	36	166	79	266	68	308
13	148	11	143	63	248	83	112	75	275	85	192	26	163	78	338	83	306	61	161
68	148	41	94	10	101	15	259	70	259	64	175	78	236	83	340	72	126	44	225
24	296	9	323	56	67	63	118	69	257	86	217	82	322	87	188	47	126	21	257
23	123	23	188	44	55	30	79	81	293	81	356	80	224	88	201	87	126	54	227
36	132	47	127	28	77	89	210	80	314	65	109	35	128	15	326	77	159	46	211
56	130	81	103	45	135	62	98	58	193	72	124	85	235	85	197	87	126	30	214
25	167	47	203	12	190	79	69	45	51	84	196	44	80	82	183	88	306	42	132
26	283	15	108	41	248	57	55	42	176	89	126	36	87	23	107	68	317	53	235
90	300	45	232	81	63	69	114	58	217	41	180	13	45	87	183	43	293	66	307
17	183	34	125	64	306	87	298	82	169	80	158	32	227	78	3	36	150	59	112
74	113	14	323	68	304	77	114	63	29	37	61	32	19	86	194	41	176	73	131
90	300	4	323	71	49	51	138	63	189	39	157	9	217	78	3	68	194	84	21
13	351	36	143	2	190	59	121	58	345	88	145	32	214	85	207	68	205	86	339
62	190	62	49	67	111	75	122	32	181	78	177	87	106	80	18	63	180	84	171
61	124	60	64	81	96	61	126	55	207	69	148	75	353	60	160	72	127	76	192
32	115	28	2	31	191	67	123	57	167	69	155	14	138	89	167	62	170	76	357
52	225	64	127	56	191	72	145	53	187	69	176	68	137	67	183	44	258	78	185
52	73	45	337	68	148	60	160	82	161	58	145	50	127	65	175	31	133	88	173
55	82	87	255	37	46	65	150	47	147	77	185	80	331	88	201	56	82	84	15
90	358	72	79	64	76	88	98	57	171	79	154	64	359	85	197	64	51	73	353
13	329	87	255	41	135	82	109	38	339	69	176	60	358	48	144	76	65	40	36
37	149	73	259	21	193	16	4	58	334	52	98	45	102	85	17	28	306	78	4
19	99	37	13	51	193	40	1	42	166	79	154	32	154	55	158	25	149	78	4
41	108	30	305	51	193	65	279	52	168	80	162	73	231	56	165	77	134	64	150
16	132	49	49	76	130	69	278	57	158	74	169	68	171	52	151	87	126	64	150
29	125	23	99	72	28	81	302	57	160	78	146	20	45	38	137	87	127	44	166
57	70	86	341	68	149	66	315	58	306	73	147	36	70	89	124	56	115	88	275
41	264	70	218	50	114	86	121	62	177	69	148	72	326	38	137	74	150	51	139
26	98	37	30	76	130	68	110	55	207	84	154	73	117	72	117	82	118	74	137
8	329	34	170	67	126	82	267	48	338	74	155	63	117	45	158	76	138	38	48

Veins:

41	191	21	115	31	87	87	112	33	195	80	158	72	338	59	159	74	192	80	130
50	29	35	127	50	114	86	148	28	344	69	155	50	188	63	184	77	127	85	321
64	149	55	259	58	120	71	45	35	11	70	159	26	174	57	179	88	307	69	28
47	222	30	129	51	194	85	289	41	212	16	144	32	164	38	129	84	326	40	108
35	207	11	284	58	170	90	125	48	332	83	178	83	117	41	153	77	199	48	179
42	174	29	324	63	173	76	295	61	318	83	178	51	76	39	145	85	167	40	169
37	100	24	324	61	196	6	260	52	178	78	177	23	20	49	151	88	173	54	189
63	182	84	46	68	152	35	86	71	85	69	148	42	232	89	18	57	127	73	179
38	82	90	280	63	113	75	80	48	143	83	146	16	224	44	144	47	128	28	200
53	53	41	26	41	153	82	94	52	177	73	114	23	48	50	164	82	79	3	324
42	57	40	140	18	41	55	260	38	140	85	162	19	130	30	152	69	89	72	151
80	48	24	324	12	126	21	42	52	171	77	185	11	182	31	166	57	134	28	324
67	174	51	32	55	159	89	279	52	181	38	172	22	94	37	155	78	308	62	149
67	185	51	62	84	50	66	92	30	26	67	182	78	142	83	152	90	326	27	166
81	163	59	208	68	152	74	90	34	198	77	185	50	143	82	160	37	125	73	198
63	182	81	95	41	122	80	330	43	241	73	104	78	142	56	158	42	105	71	145
71	171	86	307	1	196	52	298	87	175	10	108	82	129	56	158	51	98	71	151
71	171	62	238	24	157	32	72	37	152	59	168	84	117	51	131	85	88	86	144
64	146	75	194	33	112	42	99	52	151	61	222	34	190	44	144	30	85	64	174
71	188	77	285	37	118	60	63	48	332	54	253	58	135	51	131	37	128	30	233
50	162	41	96	63	151	28	124	43	357	61	102	39	178	39	251	33	89	60	223
84	172	89	209	50	104	73	127	41	270	77	139	62	138	47	164	90	326	77	191
78	202	19	54	26	197	69	135	53	145	89	153	50	128	32	130	36	134	11	144
40	308	34	324	51	92	59	128	46	209	86	356	46	138	65	131	77	128	84	160
52	140	30	306	10	102	52	117	50	278	70	162	51	135	54	145	57	128	81	144
50	159	78	353	63	175	74	144	16	0	37	138	33	200	23	152	66	82	90	4
73	170	64	62	1	198	59	128	56	210	79	170	26	207	20	165	72	187	71	192
11	79	43	248	62	127	65	101	52	158	39	141	63	145	23	152	46	137	84	325
51	105	85	356	67	130	42	115	53	146	37	216	89	348	89	137	57	128	39	243
37	338	74	324	53	173	38	180	58	115	84	314	27	161	8	86	57	128	42	210
44	188	34	252	29	39	76	87	35	124	84	128	89	179	39	138	57	128	74	167
47	194	81	152	59	150	57	347	22	174	38	76	71	297	49	151	87	128	90	2

Veins:

78	172	89	316	49	23	60	33	70	106	81	332	57	81	18	129	83	308	86	164
81	161	49	324	35	352	76	353	62	171	64	119	84	107	82	355	83	308	2	329
82	157	64	87	59	12	51	299	48	256	38	119	64	124	32	131	67	128	39	182
83	150	89	36	84	227	34	54	32	151	82	259	39	30	75	151	32	128	27	10
15	122	45	225	1	199	41	8	73	250	5	251	78	129	35	148	42	132	48	208
81	176	45	234	53	350	68	82	48	272	15	162	62	139	87	215	47	128	84	313
19	44	69	32	89	27	53	207	87	4	10	245	85	139	59	24	47	128	89	276
66	175	68	8	62	38	35	66	22	247	10	342	85	139	83	220	77	129	73	176
55	193	85	129	48	58	90	333	66	14	32	273	83	130	66	156	37	129	77	138
70	199	42	354	80	36	53	80	85	131	30	342	87	312	83	348	57	129	1	331
74	3	83	109	84	345	23	114	34	297	5	342	74	56	73	209	77	129	6	332
33	339	77	107	78	34	71	196	47	288	37	216	72	153	75	166	68	50	63	195
23	343	49	324	15	142	67	101	38	345	45	66	75	147	90	182	77	161	0	332
55	262	45	22	47	159	46	173	50	295	34	82	78	65	65	195	66	114	87	288
67	193	12	124	38	293	33	221	30	26	36	228	69	139	16	205	57	63	35	105
71	196	74	67	60	259	65	168	36	326	59	244	71	134	16	205	78	308	53	153
27	322	32	199	57	36	79	246	32	292	59	244	44	167	88	158	77	128	74	146
87	331	88	120	47	253	29	216	52	303	54	134	21	182	5	182	52	129	84	146
87	176	84	316	88	246	29	122	42	304	85	342	80	150	57	206	67	128	63	188
73	203	28	118	42	357	28	80	43	310	10	342	67	141	15	182	61	186	58	158
69	208	39	325	86	247	28	239	27	157	84	154	59	151	47	158	88	129	82	189
57	181	84	218	90	246	46	348	34	297	81	154	48	159	57	158	20	242	48	153
68	185	59	26	56	42	48	80	42	25	78	146	52	171	63	168	83	129	48	153
45	168	63	278	76	60	43	329	58	26	87	324	86	150	64	246	88	129	65	146
41	173	82	95	80	82	60	63	26	0	80	342	50	84	61	135	75	153	86	182
39	193	75	339	76	275	59	39	65	18	82	323	52	171	72	313	78	130	72	202
58	234	86	186	55	86	17	351	27	332	86	136	40	56	65	215	68	186	27	175
75	85	80	240	78	92	21	323	47	114	72	321	41	3	75	6	70	168	86	169
52	42	54	161	59	274	77	261	24	290	80	342	49	104	78	195	88	130	60	204
14	253	23	326	51	266	82	261	40	265	80	342	80	122	46	87	55	177	19	177
30	166	56	247	57	334	56	310	54	192	79	194	79	128	89	60	34	212	56	169
14	30	19	59	45	337	67	289	44	312	0	342	74	127	69	2	51	206	69	148

Veins:

38	80	70	289	87	75	59	294	76	278	87	324	63	128	70	40	78	130	39	89
62	181	78	40	58	38	86	119	12	186	87	324	72	153	89	2	78	130	69	169
71	186	32	132	39	325	71	261	29	28	81	32	85	169	74	2	78	130	81	352
21	344	89	10	60	261	54	237	63	346	59	244	70	137	72	195	59	170	70	162
54	104	22	326	70	50	67	233	41	233	77	185	42	146	67	134	52	184	78	143
20	286	46	244	77	241	76	237	54	19	89	171	57	153	54	38	64	130	79	154
49	44	54	162	54	353	51	261	61	229	44	127	70	137	45	190	69	130	84	170
86	88	78	183	52	307	46	261	63	340	76	202	51	17	61	191	61	149	41	328
48	252	39	114	65	329	16	107	55	84	78	177	84	107	79	33	55	153	33	103
30	57	62	13	81	106	19	25	29	101	75	342	66	54	87	10	82	147	90	158
82	113	50	169	39	53	57	272	42	305	38	76	50	84	75	312	47	144	36	147
85	113	58	177	40	93	67	125	67	231	73	104	88	166	64	336	56	198	69	155
76	48	58	57	65	74	35	126	58	76	61	222	68	142	72	337	77	181	68	145
77	346	49	162	45	327	17	10	50	67	40	282	17	99	81	2	41	158	41	211
42	102	49	54	44	317	88	293	39	13	82	110	21	53	38	228	44	130	69	176
57	207	78	110	87	327	84	297	78	166	31	325	83	331	58	313	57	148	67	182
80	105	37	35	32	168	73	22	81	53	33	15	63	162	85	326	48	170	79	154
76	98	38	147	36	171	78	30	34	297	86	118	77	315	49	342	48	170	39	89
83	312	38	147	60	34	46	350	36	287	68	250	44	67	81	111	74	161	90	162
85	112	43	145	81	321	18	294	49	291	64	88	27	53	54	38	69	130	80	162
76	234	38	147	89	211	81	104	58	43	69	96	49	144	55	187	59	130	52	98
66	204	38	147	69	202	64	115	70	143	45	118	83	350	77	39	56	187	88	360
89	150	38	147	90	40	62	133	80	17	65	189	54	155	81	357	55	168	39	183
56	93	28	147	82	22	36	126	52	171	77	244	77	358	84	35	52	184	78	146
52	141	53	118	69	123	68	13	74	58	5	162	17	135	67	46	42	104	56	139
44	321	75	18	62	333	84	225	19	195	41	57	37	19	46	171	79	122	63	128
75	180	47	104	50	335	48	129	26	341	25	342	15	315	38	48	51	206	41	113
11	231	77	322	50	345	49	116	83	135	36	295	65	146	88	5	44	186	48	103
29	171	20	109	70	68	62	246	29	115	69	155	84	242	77	345	78	115	88	73
48	174	36	114	62	20	40	51	62	336	54	253	20	87	40	181	76	310	10	162
62	58	70	97	90	220	73	322	53	78	58	145	75	128	90	161	67	151	69	37
51	296	36	114	52	96	77	107	30	333	83	178	29	99	71	145	58	250	20	235

Veins:

27	78	36	114	57	327	79	291	86	40	64	168	80	347	71	157	65	157	10	162
22	43	72	84	51	47	40	51	69	346	58	145	74	26	83	45	48	222	40	41
65	233	42	327	72	23	64	138	71	4	33	15	55	22	54	143	62	164	20	89
29	171	51	83	82	341	87	119	61	231	60	342	84	352	46	171	69	197	35	115
33	179	26	164	63	119	34	152	22	27	40	342	23	207	64	181	67	190	33	221
33	247	60	210	64	4	28	214	39	141	31	90	79	176	82	354	64	183	75	131
77	323	31	221	88	49	21	196	43	74	82	65	88	349	68	340	59	171	87	324
85	130	23	154	66	23	17	167	69	326	78	280	60	186	44	120	73	165	87	324
80	130	68	142	77	302	88	294	69	326	69	106	35	353	70	4	60	180	39	89
41	199	67	137	31	320	81	104	86	5	20	54	69	171	75	3	56	177	90	162
89	326	36	181	74	31	34	10	81	9	78	223	52	92	73	122	64	183	15	84
76	141	54	103	88	250	73	245	74	345	64	175	69	171	80	29	52	184	15	84
79	199	17	327	89	307	43	57	58	28	35	198	72	153	85	30	48	170	60	137
80	130	8	147	32	295	80	136	27	343	34	82	76	315	66	232	51	164	30	74
30	122	19	158	88	319	79	172	39	312	82	236	67	61	86	201	62	164	16	201
71	148	26	117	78	314	77	54	47	43	80	342	80	183	83	311	43	156	20	89
90	150	37	258	83	322	71	135	70	301	64	88	57	147	45	171	65	194	19	104
31	136	65	163	66	333	86	306	46	338	50	62	64	176	72	25	64	183	0	342
84	330	67	158	41	68	73	277	63	266	0	342	66	160	86	31	33	190	69	176
79	81	57	155	19	285	81	254	61	49	31	111	84	163	65	214	73	189	42	71
78	191	57	155	53	98	75	144	44	49	34	82	46	61	50	189	46	214	86	233
27	31	57	155	80	214	83	140	56	355	45	206	53	20	39	181	77	181	72	97
65	103	52	154	82	253	83	140	73	337	53	46	82	173	40	193	38	164	28	102
69	329	68	142	32	222	85	107	73	337	33	67	82	263	50	189	60	180	82	150
67	205	42	161	87	178	76	336	84	175	84	10	66	167	49	181	56	198	89	278
41	162	18	79	88	188	55	91	87	157	60	342	48	240	43	204	59	171	55	130
75	168	52	168	74	348	26	141	79	185	89	9	64	128	51	110	52	184	51	158
71	117	38	147	90	359	58	146	52	103	30	342	63	163	30	198	78	191	28	340
89	321	39	115	44	311	67	125	76	5	60	342	63	163	55	188	66	180	84	108
84	103	23	93	44	53	41	26	66	306	60	342	71	177	64	181	53	159	65	164
77	265	62	157	50	357	42	191	53	304	38	119	69	164	52	165	20	204	51	107
47	283	48	143	57	358	48	129	71	331	41	26	74	195	44	181	68	144	26	103

Veins:

38	73	24	160	74	185	84	323	87	13	60	342	35	188	80	328	44	197	68	151
26	350	24	160	32	63	49	136	61	19	50	62	65	330	70	333	60	131	82	144
71	141	24	160	41	56	58	294	87	15	19	104	88	349	64	238	56	153	85	163
31	269	29	155	39	50	79	350	86	214	13	130	69	327	82	344	69	120	81	16
57	227	68	142	87	332	70	211	90	30	69	148	71	137	85	342	69	120	40	335
45	195	68	142	66	7	84	198	43	29	48	201	79	306	72	358	58	145	49	338
27	183	17	328	38	324	73	214	31	47	64	119	85	169	82	297	68	144	28	151
48	69	75	167	71	198	28	130	87	10	10	79	80	326	59	201	57	148	85	357
84	125	89	348	85	181	10	322	80	26	28	182	89	156	85	184	67	151	73	344
88	64	52	156	78	198	26	164	35	76	10	245	87	3	69	181	31	69	84	178
88	350	85	170	36	192	73	39	23	174	21	152	70	128	49	173	56	154	24	286
53	99	48	152	72	198	86	66	63	60	16	123	79	225	70	188	56	153	42	164
70	332	41	154	76	198	61	5	58	326	15	84	80	183	56	167	67	167	72	164
84	21	77	135	74	8	42	33	76	355	32	33	88	166	74	178	77	181	67	359
81	303	56	136	83	245	51	249	46	16	13	194	58	153	82	344	57	148	73	19
31	53	52	138	73	249	50	261	88	194	72	200	58	167	77	6	55	156	86	164
19	229	62	138	82	226	36	352	78	191	22	248	62	150	37	31	21	289	74	357
56	34	62	138	82	226	86	95	81	354	40	41	49	145	39	307	28	255	54	357
85	185	45	119	49	69	49	39	77	53	17	257	65	81	82	351	28	255	74	337
75	209	76	131	45	297	70	311	87	0	43	136	56	115	71	85	50	131	83	12
36	146	42	84	77	218	87	319	5	305	48	221	37	123	66	334	62	164	87	158
61	198	38	98	87	52	88	13	57	324	68	208	85	153	66	334	57	151	85	1
74	159	52	41	81	145	54	45	41	79	47	132	89	147	67	311	47	146	25	319
81	142	4	31	76	145	87	30	32	69	78	269	85	153	69	314	70	172	74	164
71	146	59	187	60	176	46	107	38	82	47	245	50	144	63	323	51	164	38	117
81	142	68	192	86	145	75	35	28	140	44	96	73	307	89	124	60	171	12	187
48	268	19	137	89	163	57	21	51	61	72	184	83	306	44	154	72	169	25	164
32	181	53	145	50	223	89	277	25	218	36	29	23	71	60	154	84	165	2	187
86	142	73	142	13	195	88	51	89	196	19	104	10	157	39	154	60	171	85	212
35	188	89	2	70	160	5	261	9	160	34	242	54	280	72	317	48	170	85	212
34	190	50	161	85	153	67	222	30	217	20	89	70	51	35	139	77	181	67	230
53	251	59	167	66	145	30	71	88	191	70	342	23	71	89	214	65	158	80	197

Veins:

59	99	73	142	76	145	87	337	23	186	88	145	35	76	71	334	45	175	85	22
90	309	53	155	56	151	41	26	11	231	52	215	61	109	75	353	65	183	53	149
29	80	55	183	81	145	64	70	28	28	54	190	15	210	75	11	59	213	31	113
84	122	58	179	85	153	88	110	36	63	59	244	37	264	82	346	63	164	18	187
89	159	58	179	76	145	63	97	8	259	78	146	33	113	83	357	64	45	59	95
82	298	27	237	66	145	68	148	59	129	86	86	64	104	89	119	38	141	72	130
78	293	60	165	88	357	57	140	25	29	69	106	22	90	65	310	51	206	24	109
89	276	39	181	61	176	71	253	26	266	51	128	72	298	63	323	51	164	47	65
80	96	39	181	86	145	70	311	51	119	10	342	35	76	82	330	62	149	69	123
68	85	45	210	89	163	73	277	21	288	24	23	28	342	56	81	56	198	47	47
66	68	41	197	83	100	83	22	22	28	33	15	74	316	66	334	68	176	74	117
43	43	58	179	50	223	75	78	86	57	30	74	86	301	63	345	61	191	39	150
61	66	50	259	57	119	81	58	67	51	40	342	75	158	34	147	12	344	50	96
51	49	55	200	13	195	74	58	57	12	32	291	63	179	79	136	30	311	72	82
89	255	35	21	70	160	73	122	37	111	59	80	67	172	84	154	31	328	37	133
40	55	43	162	85	153	71	118	11	48	82	99	76	168	84	326	60	171	86	116
85	83	34	144	66	145	64	70	15	55	60	342	86	301	83	352	59	142	44	125
78	92	52	139	76	145	68	148	72	10	27	38	78	151	89	329	33	112	53	132
65	240	67	175	56	151	15	81	20	348	60	342	88	284	66	329	32	241	64	145
52	109	39	157	86	153	58	146	18	21	51	237	83	338	45	164	59	213	64	173
19	136	50	197	66	145	84	297	77	53	45	38	21	349	61	328	69	86	77	153
47	162	52	158	88	357	0	261	38	83	38	277	78	91	45	312	60	213	82	155
41	300	39	64	83	100	75	144	67	9	38	177	87	358	69	195	49	230	28	61
33	235	82	338	57	119	63	303	69	29	17	316	75	84	35	140	60	125	72	338
71	149	87	357	33	28	84	225	27	146	88	112	80	161	22	180	57	178	85	353
57	188	17	329	25	343	68	148	52	60	5	112	68	172	88	348	49	170	90	150
76	169	13	128	30	15	82	93	75	209	43	76	74	128	48	202	48	149	84	319
88	163	12	83	68	167	67	289	61	358	68	112	67	154	61	328	65	184	77	157
83	298	24	131	76	145	89	86	84	342	30	203	72	166	74	173	16	122	60	156
83	160	55	184	87	99	25	112	46	15	38	112	72	166	78	326	82	90	36	180
87	146	47	167	38	24	76	254	78	311	64	37	62	138	78	326	46	132	25	73
88	125	48	174	76	145	63	241	89	323	37	67	76	178	44	312	59	149	51	156

Veins:

89	198	29	86	86	145	90	315	47	293	58	71	86	347	82	310	57	154	85	351
66	333	37	90	50	115	86	95	21	318	31	120	81	170	89	329	23	269	59	111
48	114	34	107	25	344	36	126	46	315	47	51	85	163	83	347	55	160	16	135
52	189	24	96	30	16	34	134	74	313	62	112	41	187	77	327	71	134	57	167
85	121	53	1	90	2	84	47	31	289	85	57	86	121	45	181	66	184	83	162
71	306	19	67	19	325	17	106	66	77	47	152	64	334	42	322	64	165	61	149
58	125	19	67	68	167	78	149	46	119	43	148	86	347	23	309	73	170	35	188
88	163	27	132	42	63	54	122	56	137	34	140	61	165	36	304	82	174	48	144
89	164	49	164	36	145	38	44	44	176	76	18	64	301	86	158	65	205	54	133
61	117	78	177	76	145	80	282	50	312	37	147	80	151	72	317	80	178	69	171
81	351	22	127	66	175	70	153	81	15	58	153	76	29	25	299	61	172	73	132
70	184	24	42	31	148	54	237	43	150	80	165	76	29	60	99	14	249	84	171
82	205	29	107	87	99	88	294	35	169	58	195	77	352	43	176	78	155	84	163
85	355	40	93	38	24	80	26	66	13	86	340	32	355	58	40	53	165	57	181
90	133	58	69	76	145	87	355	76	18	70	151	52	66	32	318	58	154	82	181
85	331	45	227	86	145	84	115	51	25	64	157	87	9	79	171	87	354	80	160
89	154	45	246	50	115	83	212	56	10	36	56	62	214	75	175	64	165	76	179
71	194	32	163	89	334	90	206	31	155	73	81	48	197	79	356	82	217	82	8
89	151	28	181	61	145	86	216	50	353	37	354	59	147	85	358	76	225	79	324
87	129	29	97	86	154	86	216	3	73	8	112	81	151	89	174	65	205	79	324
82	142	87	182	90	2	83	22	39	352	55	44	52	24	82	173	15	160	79	324
81	227	30	213	19	325	83	212	56	13	9	90	65	141	87	158	68	315	78	321
80	331	31	172	80	198	68	243	34	122	43	45	79	156	46	169	43	180	77	319
64	99	29	182	42	63	40	111	48	148	24	159	58	208	76	192	37	134	82	332
40	139	43	136	36	145	90	206	12	104	24	185	40	128	84	154	45	157	87	150
85	142	31	107	75	196	77	54	47	155	14	177	40	151	86	320	47	129	85	130
59	170	27	168	66	175	79	231	16	119	11	76	47	147	61	28	45	157	78	145
66	166	25	134	31	149	80	261	37	152	65	150	34	78	73	32	40	123	77	148
88	159	58	102	89	334	78	13	45	210	82	332	57	55	76	170	37	131	74	306
33	124	31	173	78	170	75	17	29	63	16	141	59	168	59	287	42	130	75	158
83	134	4	150	88	358	67	125	25	215	33	163	68	343	44	159	86	166	68	172
70	135	1	330	86	154	67	54	35	207	55	172	60	150	89	329	45	157	72	165

Veins:

89	129	7	204	35	204	60	261	76	360	59	63	70	125	89	359	30	192	89	301
27	88	27	133	68	224	87	119	84	183	79	157	55	37	89	184	25	196	63	145
72	180	21	113	83	190	61	271	89	183	68	181	45	34	71	145	83	12	63	162
74	188	47	143	80	199	60	121	79	198	84	333	68	157	83	178	62	172	52	98
54	202	35	135	71	205	56	272	7	334	88	160	76	163	81	2	57	122	11	120
82	322	19	69	56	146	71	253	82	219	86	353	59	167	68	272	17	312	61	160
82	205	62	176	48	110	85	280	72	37	8	294	39	72	78	187	35	169	71	163
74	114	59	171	75	197	42	151	19	36	77	114	19	198	78	171	45	196	78	173
64	207	35	166	63	221	30	81	73	190	77	114	81	317	89	354	28	104	73	150
83	126	35	166	90	3	74	65	87	209	45	240	50	137	87	179	88	245	53	72
47	100	38	167	71	146	64	138	67	200	37	114	14	300	54	116	81	117	90	350
59	153	29	194	52	122	49	142	74	186	26	198	79	176	40	129	60	175	54	145
62	209	34	221	78	171	69	130	77	38	67	172	85	291	35	147	74	143	51	128
87	119	37	219	88	358	67	125	80	228	40	130	89	196	55	151	75	307	45	118
83	104	64	130	35	204	64	138	87	235	56	160	84	357	61	165	77	33	49	178
79	351	40	217	76	138	74	163	46	131	43	184	78	113	86	359	45	132	82	100
49	153	26	14	68	224	38	118	50	57	51	170	90	169	31	104	55	127	74	149
73	200	42	166	83	190	73	22	29	78	13	295	75	180	84	348	82	153	85	190
73	200	9	151	76	146	67	233	62	342	36	80	63	149	71	338	85	136	82	360
66	166	6	331	71	205	42	191	15	133	21	53	27	323	78	319	54	139	82	145
73	222	48	226	56	146	25	112	78	187	58	157	68	312	68	323	55	121	54	307
62	209	47	194	48	110	61	157	78	358	36	150	66	110	75	175	45	127	80	5
87	163	84	285	79	326	17	167	78	19	47	65	53	167	58	137	65	127	45	170
87	163	37	315	63	222	76	167	58	29	42	238	77	313	51	142	85	127	34	220
73	68	71	89	64	125	58	294	33	118	41	88	87	323	73	343	41	150	51	149
86	313	24	151	89	3	88	71	36	136	37	115	72	130	89	124	74	307	49	230
50	228	39	77	76	146	68	148	10	356	30	157	53	134	75	169	84	307	90	310
86	196	16	331	80	129	84	297	24	79	47	142	68	116	75	354	86	127	80	168
87	142	57	35	71	146	25	49	83	336	43	162	72	129	77	1	85	316	69	313
88	159	24	151	52	122	49	172	30	288	43	47	82	127	69	354	84	307	87	145
61	164	11	331	76	138	45	167	34	142	58	90	87	332	28	295	84	307	85	152
81	184	10	180	76	146	36	171	45	104	68	194	53	147	83	280	86	127	13	100

Veins:

54	192	19	141	79	325	42	162	79	168	25	57	73	143	89	4	46	127	68	151
88	159	6	331	76	145	44	150	64	75	81	41	74	143	89	194	74	307	76	175
72	199	6	54	80	129	78	237	64	29	47	111	72	156	82	204	36	127	68	132
82	79	39	152	46	258	31	331	86	202	87	125	82	158	75	354	76	127	49	125
76	332	39	152	80	6	56	319	26	56	46	242	87	177	70	160	46	127	45	119
56	188	39	152	55	27	40	126	46	78	68	146	82	158	51	332	76	127	63	147
70	184	36	176	46	258	84	138	16	110	62	116	62	154	83	311	30	123	59	132
69	149	64	156	23	105	86	100	39	18	79	123	16	323	61	334	54	109	81	107
50	137	49	148	33	248	70	151	57	91	46	136	63	182	80	301	56	127	45	113
60	142	80	173	81	123	62	170	43	89	53	210	41	211	74	345	74	307	69	102
69	156	21	332	48	169	84	117	12	349	49	145	65	215	86	334	65	113	55	137
44	133	48	159	23	105	74	75	14	69	50	149	71	355	76	147	39	100	86	331
71	167	43	156	75	132	13	327	3	130	56	236	80	193	51	279	74	308	59	163
68	142	49	168	33	248	35	149	66	323	61	207	78	173	83	120	89	351	74	72
55	142	62	178	82	123	87	359	17	177	59	251	61	160	78	188	90	279	75	272
65	115	86	90	48	170	74	82	68	302	24	252	87	314	52	44	69	343	36	130
79	174	42	162	75	133	90	281	76	70	57	135	77	333	41	122	69	289	47	149
43	116	19	332	81	140	83	108	54	334	46	136	69	170	28	354	79	122	38	161
83	121	62	178	53	110	60	156	80	340	42	140	53	72	67	25	55	129	66	174
35	142	75	190	48	170	60	156	75	28	48	140	39	293	76	354	75	215	31	137
54	170	75	186	46	168	68	162	79	33	20	315	38	276	71	26	27	141	37	121
79	96	39	148	53	110	80	125	52	14	59	141	41	104	80	69	55	207	65	136
77	123	24	127	48	170	67	127	75	31	73	196	90	350	59	126	42	141	86	130
34	264	42	252	74	172	43	86	79	83	85	192	78	174	58	302	67	98	73	338
33	38	85	175	55	173	46	138	49	329	65	220	66	177	53	116	70	162	82	161
32	253	80	360	69	171	62	145	51	50	48	141	87	315	47	123	37	177	71	275
34	142	34	203	46	169	89	231	65	29	32	228	87	178	51	127	49	187	27	135
81	312	33	166	74	172	40	126	89	359	66	158	84	186	79	281	70	151	32	25
78	126	36	230	55	174	33	204	64	353	29	338	86	333	81	214	73	242	42	220
13	110	42	224	69	171	88	110	64	17	12	260	64	120	67	42	55	207	65	360
60	117	34	203	75	165	64	115	48	345	56	121	76	87	85	145	56	219	82	323
83	308	56	166	84	175	85	77	55	45	71	158	86	316	72	287	38	205	54	183

Veins:

89	295	41	208	89	176	43	132	85	211	89	338	30	1	77	355	73	16	76	127
86	116	42	233	77	221	74	155	76	193	49	145	16	324	78	296	68	7	85	148
45	142	39	152	53	173	42	162	86	199	77	131	80	184	67	296	78	257	66	85
65	169	85	175	66	163	29	315	69	20	78	181	83	287	84	19	89	23	54	160
64	111	34	152	75	98	42	196	80	211	28	106	80	353	49	146	44	5	48	156
47	225	30	248	85	167	42	351	87	8	30	355	59	139	80	318	84	113	77	11
55	168	29	152	75	165	83	3	56	353	52	84	90	350	67	353	73	78	57	100
58	195	37	150	84	175	51	203	86	199	49	59	71	324	70	162	79	171	50	197
68	159	68	163	89	176	82	316	86	115	46	137	63	347	72	334	73	77	33	42
54	213	27	239	77	222	24	351	45	107	51	158	61	359	62	307	45	105	45	68
71	80	18	273	53	173	36	343	63	172	20	117	82	129	60	309	87	253	68	46
81	312	37	193	66	164	43	181	46	327	32	109	46	82	76	354	76	99	78	162
89	151	77	86	75	99	89	131	46	342	14	187	47	35	84	4	52	194	54	144
60	71	26	16	85	167	25	257	54	67	30	320	42	9	55	173	77	295	70	137
78	178	18	32	43	105	13	182	83	87	83	6	52	31	35	210	81	79	81	11
88	313	82	123	51	96	60	77	90	92	51	244	87	257	70	229	72	130	74	176
88	4	64	138	68	181	72	23	74	78	76	158	88	179	53	124	84	169	83	31
46	100	36	177	77	143	25	257	83	82	32	12	33	17	83	322	88	103	69	321
39	145	44	33	82	117	42	351	90	92	61	198	56	29	35	279	50	165	85	307
82	90	73	352	82	117	81	27	63	344	78	108	63	184	70	191	55	206	68	120
87	264	18	32	82	117	63	135	68	261	80	126	67	113	33	120	77	224	79	133
74	135	85	130	65	115	82	353	52	315	89	347	36	239	76	354	77	166	63	104
30	142	15	260	62	107	81	292	49	259	81	166	86	186	79	126	85	162	84	342
38	153	49	61	80	99	21	56	71	307	86	166	78	82	83	347	69	321	66	156
86	207	73	165	70	129	25	243	54	246	74	216	90	86	67	353	64	172	76	198
37	155	67	84	82	143	81	195	70	266	74	216	12	244	64	188	56	213	40	248
72	180	48	147	57	145	44	56	43	242	86	114	57	209	70	2	64	172	54	285
72	180	27	67	19	309	64	74	74	254	42	129	76	302	82	13	79	268	84	150
72	164	39	60	68	181	80	275	80	202	44	133	49	200	68	154	56	63	83	159
74	111	58	146	77	144	28	303	42	318	38	142	53	40	77	336	64	126	69	135
87	187	33	168	82	117	48	346	82	1	61	152	65	79	89	99	74	301	68	173
87	164	21	190	82	117	24	325	52	315	53	56	11	93	75	5	60	312	46	129

Veins:

80	322	19	154	82	117	85	11	77	280	42	129	65	184	79	13	71	172	29	205
43	153	4	154	65	115	55	150	56	307	88	132	60	200	64	159	82	306	85	29
89	254	55	70	62	108	67	175	90	61	20	198	89	30	67	330	66	336	65	13
52	89	56	120	80	99	86	261	80	62	23	200	78	192	83	135	60	312	88	199
54	252	30	60	70	129	89	97	84	351	14	187	69	148	71	136	63	135	59	154
80	170	30	124	82	143	50	83	80	340	32	304	62	183	75	230	77	346	84	7
49	221	54	88	57	146	85	252	89	77	32	304	80	174	68	177	63	183	69	212
58	185	84	117	19	309	80	94	54	322	20	228	75	142	58	40	64	109	64	172
45	61	24	208	45	170	57	138	65	251	54	173	61	142	47	212	88	275	86	333
69	132	74	131	72	200	88	204	43	267	27	199	73	120	81	189	77	187	83	356
52	173	84	206	68	86	58	93	12	307	50	133	50	129	50	21	1	141	64	172
59	153	71	207	33	349	63	80	34	184	42	187	76	172	50	59	49	187	52	157
84	83	76	176	50	253	77	283	50	180	71	158	19	170	68	139	71	199	57	152
56	85	88	172	48	102	31	38	55	175	88	132	89	18	72	129	74	340	55	139
55	63	85	337	63	42	90	9	70	334	44	223	81	201	60	251	40	190	44	144
67	121	66	213	45	170	88	218	84	156	65	146	59	109	84	348	63	200	86	341
71	74	70	337	72	201	53	109	65	335	81	151	54	152	81	105	50	180	59	146
87	285	86	180	83	351	37	177	82	168	39	126	70	324	41	310	56	182	24	182
89	142	10	158	68	86	76	71	88	357	45	125	54	152	85	353	21	85	72	11
71	80	40	158	32	349	80	50	58	157	46	155	84	173	70	32	81	164	21	198
64	148	87	354	50	254	20	220	52	193	68	179	66	321	77	204	83	185	64	156
52	185	50	338	48	103	86	151	82	342	52	232	46	213	75	28	63	195	89	150
85	98	87	12	63	43	46	91	86	172	86	150	65	204	66	311	49	187	76	44
59	133	10	338	83	352	74	81	53	174	89	338	54	170	21	88	13	8	90	156
30	54	12	18	2	333	88	323	89	167	61	228	36	182	83	311	68	178	68	35
60	202	30	251	26	235	60	346	24	146	36	142	53	303	27	109	68	178	71	25
79	153	0	158	2	333	58	175	38	182	48	47	63	336	55	350	60	166	89	166
71	85	59	205	77	138	69	158	80	332	75	144	68	338	47	123	80	105	61	192
41	191	30	278	26	235	56	88	86	337	89	339	75	170	77	322	47	194	52	165
68	155	89	338	77	139	64	122	84	326	59	142	70	174	73	299	61	160	54	174
86	116	71	353	45	44	69	116	83	117	84	339	78	88	83	120	87	194	39	154
47	112	25	293	33	172	46	93	21	145	40	278	80	42	68	196	18	168	36	140

Veins:

39	214	41	158	76	178	67	272	47	172	40	88	68	119	82	270	18	168	82	330
67	135	81	321	89	155	51	146	78	172	51	73	78	165	87	4	63	126	87	337
39	226	90	331	45	44	46	163	44	185	46	116	41	160	69	344	27	176	74	167
78	231	89	174	33	172	54	101	89	116	54	69	77	331	62	46	31	194	41	195
84	190	85	166	76	178	60	92	86	286	58	264	30	170	71	53	27	176	83	173
33	148	24	339	89	155	36	355	76	282	68	247	20	350	89	215	34	163	59	190
44	147	79	343	76	196	57	16	74	161	40	230	82	20	89	220	38	172	50	197
73	84	58	223	52	112	69	158	85	127	76	189	77	150	64	274	88	150	84	14
82	303	85	169	55	118	57	16	26	215	38	106	75	161	86	135	87	159	87	169
73	107	71	232	24	226	80	135	71	289	73	181	80	180	65	5	25	201	84	163
74	111	79	330	58	124	86	107	71	163	56	237	77	330	55	209	15	140	82	352
51	79	68	131	76	196	47	61	59	174	55	169	77	330	81	265	18	169	53	116
52	72	71	319	52	112	71	78	83	204	58	264	74	319	37	335	5	140	70	321
35	105	68	313	55	118	67	119	40	145	20	119	87	342	78	7	26	176	67	91
20	8	82	26	24	226	52	155	55	146	81	159	77	330	66	351	67	355	19	76
52	157	90	175	53	166	62	332	36	170	84	348	89	322	72	335	71	162	80	202
48	181	83	139	49	156	30	165	77	311	76	166	66	329	70	107	41	184	88	159
66	191	76	154	58	125	76	158	65	145	85	357	85	324	26	302	47	194	68	175
32	150	9	340	64	103	76	158	69	149	88	185	70	350	53	95	66	309	72	187
81	227	86	306	39	156	72	154	78	134	51	159	72	339	37	305	83	185	72	318
49	167	67	180	53	167	19	340	71	163	11	206	47	196	37	305	40	191	50	198
87	182	14	340	20	47	45	187	39	125	78	109	40	170	42	335	79	197	19	104
67	30	77	117	49	156	21	165	55	218	74	112	26	1	10	186	9	228	40	142
19	185	67	105	64	103	74	143	24	113	61	148	87	188	57	181	10	140	53	194
84	117	78	94	69	156	88	325	45	208	70	114	69	323	76	22	33	186	58	203
49	179	79	111	55	156	18	30	78	177	73	197	28	35	81	105	47	194	61	162
78	297	76	172	64	156	28	308	81	194	81	167	65	143	52	89	56	219	55	161
45	68	45	263	39	156	19	301	79	179	83	339	79	160	75	298	75	99	76	321
62	176	88	122	49	157	82	59	67	159	67	203	59	86	68	196	15	140	72	178
54	213	36	35	11	337	83	66	56	325	88	185	84	190	81	306	26	177	17	183
64	185	37	342	20	48	38	16	67	189	49	300	77	236	81	3	58	290	23	200
28	163	48	259	31	229	83	66	55	91	75	145	88	189	34	186	84	108	47	165

Veins:

43	168	89	24	69	157	84	263	86	177	57	93	15	170	72	340	39	191	77	167
65	142	68	358	55	157	87	55	73	116	74	91	15	170	80	85	55	207	62	169
78	158	71	221	65	157	42	334	21	163	40	118	63	181	35	99	68	183	30	184
61	179	35	133	50	157	20	284	89	150	82	160	62	177	75	6	49	181	46	165
46	160	28	162	10	337	60	29	74	145	85	176	64	208	37	4	35	140	14	152
66	166	62	237	0	337	45	111	84	145	80	175	69	147	81	100	0	320	39	152
46	160	52	86	31	229	27	287	45	191	83	340	28	130	72	299	10	140	54	152
74	131	56	228	0	337	22	199	71	196	62	160	41	3	72	10	22	119	44	152
17	297	70	126	87	132	18	233	32	46	76	174	76	331	30	172	55	189	44	152
75	197	65	227	87	132	37	246	74	210	84	184	90	338	88	354	54	195	88	157
69	135	3	163	46	136	86	82	40	194	82	167	53	157	56	199	13	181	9	152
69	149	76	32	80	150	87	59	76	190	72	188	41	175	54	179	23	186	4	152
33	83	83	163	79	142	18	190	66	167	81	192	46	178	38	100	28	215	41	255
48	351	65	249	46	137	51	259	77	345	33	340	41	134	79	1	32	186	70	130
3	42	84	359	79	143	58	27	25	97	14	44	36	170	68	174	29	205	31	150
38	150	34	191	30	244	46	58	6	64	66	172	36	170	68	229	38	172	69	166
37	166	10	35	30	73	74	227	13	88	36	258	83	308	58	212	73	71	19	66
52	196	27	96	11	15	77	218	13	66	57	160	82	139	41	153	47	194	76	158
39	69	74	194	59	175	78	346	67	162	30	286	72	302	63	158	21	198	26	157
71	322	16	56	30	244	67	137	65	126	35	237	87	199	55	131	21	83	37	180
18	323	65	214	30	73	82	126	52	169	66	202	89	339	58	130	15	140	86	219
56	163	87	202	52	125	62	247	39	99	54	249	85	190	46	128	30	86	47	111
30	55	78	189	11	15	44	291	43	85	40	128	90	175	61	154	23	186	75	351
62	21	81	108	59	176	25	348	39	99	52	233	88	151	63	141	37	215	51	134
69	77	62	153	52	125	31	140	39	99	66	222	32	138	88	159	28	215	59	175
48	51	51	190	66	152	64	319	35	196	18	340	42	305	51	132	20	198	44	137
71	190	84	112	66	152	72	20	76	103	78	120	78	241	65	140	55	73	48	141
18	323	47	228	71	152	86	221	60	146	72	160	24	350	82	173	29	76	79	351
29	79	65	78	56	237	70	17	70	152	87	160	89	131	56	118	37	73	86	343
84	223	52	274	71	152	84	44	48	155	82	160	80	345	29	186	37	57	87	198
58	11	69	262	75	145	40	294	60	143	46	107	56	17	74	329	42	65	58	146
82	80	56	245	81	151	47	60	88	162	74	228	41	170	62	147	28	65	53	143

Veins:

68	231	84	310	56	237	62	160	78	134	55	145	47	162	41	189	13	99	77	186
30	173	86	336	66	97	75	207	48	105	81	192	56	165	47	171	42	155	40	181
29	207	78	139	75	145	75	207	63	189	38	77	80	327	69	319	19	213	60	174
44	108	49	251	57	159	49	159	61	192	74	139	21	170	82	168	70	87	86	147
55	140	46	246	81	152	85	45	63	189	58	138	30	84	23	181	51	241	49	141
55	140	69	247	66	97	89	302	63	189	50	147	41	170	59	155	19	140	73	184
69	139	84	28	52	31	62	160	75	181	62	166	54	124	75	176	9	140	82	37
40	143	67	123	57	159	54	358	63	189	82	76	30	256	28	218	30	196	81	327
54	40	32	43	52	31	72	237	52	168	70	205	70	125	38	198	83	2	55	164
39	353	22	293	82	160	14	50	65	167	82	160	88	136	89	197	79	140	59	138
70	349	36	83	82	86	83	265	63	189	56	188	73	130	36	150	81	168	60	166
56	185	84	164	23	340	83	230	70	170	52	185	64	132	55	199	75	187	70	154
63	46	87	213	82	160	86	129	56	173	56	133	82	340	48	152	55	183	44	140
45	143	57	136	11	64	16	342	68	183	51	148	65	143	89	27	54	208	58	157
75	143	78	140	83	86	39	295	30	267	51	148	31	177	41	220	67	178	34	140
57	126	56	128	23	340	16	342	47	174	60	130	79	350	28	138	20	200	44	140
82	342	21	246	89	323	60	130	59	154	83	119	22	228	73	182	39	132	40	150
57	126	64	166	62	160	73	21	52	168	87	160	81	165	80	178	63	161	55	190
57	236	84	171	11	65	63	44	60	177	74	139	50	105	33	183	48	181	61	174
89	139	23	205	54	202	67	30	60	177	77	130	30	85	60	189	89	77	64	187
81	337	82	234	62	166	63	25	56	173	62	121	74	15	78	346	64	212	45	140
69	77	18	315	89	323	55	24	52	168	54	109	70	180	32	172	87	81	45	140
75	143	18	197	62	160	16	247	75	223	35	85	59	92	63	175	76	292	55	140
60	214	26	345	54	202	55	33	30	52	87	341	59	92	88	7	56	122	47	163
32	32	87	213	62	166	75	24	80	183	40	58	79	31	58	194	74	125	50	171
62	22	86	352	79	100	54	136	73	210	74	229	69	43	64	178	78	136	42	155
83	347	27	231	79	100	45	56	68	184	47	118	49	340	84	116	81	337	51	164
77	193	16	345	84	213	32	202	59	194	37	341	87	194	71	161	74	307	87	301
41	199	84	158	63	160	20	58	52	169	74	1	83	350	77	130	39	132	76	179
54	53	36	84	57	170	29	88	88	21	18	127	80	343	88	316	61	147	37	160
56	32	65	147	48	160	67	258	33	68	47	118	16	105	77	170	67	97	80	74
68	126	19	283	79	321	56	168	56	173	88	161	32	138	77	141	56	60	84	153

Veins:

76	84	35	268	74	198	53	173	63	189	77	341	88	18	62	24	67	320	57	128
86	67	35	268	69	236	79	31	84	196	70	206	58	134	86	48	84	334	89	345
89	71	75	126	84	213	62	336	71	196	71	106	86	178	83	211	58	156	57	128
58	218	87	116	63	161	3	171	65	167	57	171	87	359	87	329	61	245	67	129
81	273	56	345	57	171	20	58	56	111	3	161	81	14	68	345	59	253	47	128
79	97	1	345	78	164	66	248	81	76	26	223	72	164	89	334	89	356	47	128
37	155	14	79	48	161	58	116	90	146	33	71	62	162	68	230	81	249	56	241
81	228	4	165	79	20	48	126	75	146	77	79	89	7	80	309	65	275	67	129
57	163	89	293	79	322	66	248	60	84	33	71	77	179	82	328	70	300	82	309
47	39	36	246	9	297	46	212	44	100	16	94	49	151	63	191	60	235	88	129
42	52	8	111	74	198	79	199	52	67	68	248	49	151	86	193	67	218	44	175
32	60	38	153	69	237	49	68	10	146	65	128	73	194	60	195	89	32	83	96
87	108	29	131	79	31	70	167	80	298	15	187	60	169	67	203	86	152	68	144
42	52	65	148	62	66	62	160	84	97	2	341	35	169	70	193	80	242	73	145
78	124	56	186	78	165	59	68	37	113	74	199	87	199	48	223	87	78	76	153
83	300	86	337	79	20	87	292	30	84	68	161	45	169	51	196	33	135	62	164
77	61	38	274	75	208	74	151	63	188	88	161	41	179	26	229	80	85	50	164
56	87	45	265	9	296	80	248	10	326	41	130	59	138	47	169	58	261	64	130
59	155	75	196	87	85	62	160	20	136	83	161	88	204	68	170	59	31	68	176
27	51	23	259	78	31	78	149	78	159	78	168	50	170	54	180	87	157	11	310
65	171	75	307	62	66	61	243	68	346	70	96	79	198	65	27	74	251	52	184
44	140	45	137	75	208	81	240	56	111	22	124	85	350	23	182	86	152	76	170
62	76	63	187	87	85	82	266	58	123	6	57	86	156	78	352	58	161	62	164
49	356	24	166	89	162	39	20	9	271	39	110	61	170	61	161	86	280	68	144
40	323	41	136	89	162	72	229	53	136	63	167	66	164	28	157	67	133	69	137
55	169	35	268	78	154	11	42	63	188	38	177	3	350	36	150	80	41	29	172
57	164	38	137	74	162	88	27	79	89	44	178	77	17	46	189	58	155	79	138
38	45	43	122	63	103	65	48	53	115	62	103	81	37	36	150	57	220	59	137
51	69	35	346	76	312	81	48	0	325	44	236	73	13	48	202	83	258	36	146
43	65	25	270	76	342	83	39	56	119	55	120	5	350	38	198	88	98	67	151
57	126	57	101	68	248	82	231	11	172	17	341	62	24	72	140	87	274	51	206
52	342	35	22	78	154	44	310	46	109	74	199	49	85	87	306	85	271	63	164

Veins:

84	178	48	271	80	10	80	72	60	107	45	254	83	331	89	310	49	149	41	160
47	39	16	269	63	104	40	355	75	102	57	227	77	104	81	22	87	70	68	176
49	356	55	280	75	312	75	249	85	299	59	183	60	350	51	133	81	72	65	158
58	100	83	312	76	342	75	249	81	166	44	267	85	194	57	157	20	108	45	152
56	97	79	299	68	248	50	311	69	168	66	223	5	170	56	321	89	32	41	180
64	96	75	197	80	10	90	249	67	74	67	213	80	180	49	127	76	153	39	139
76	298	16	148	60	82	12	288	70	164	50	218	41	107	60	142	84	142	77	181
48	171	28	242	63	114	43	310	50	152	41	202	62	162	67	324	76	71	44	196
60	184	80	160	71	182	25	249	59	224	53	170	81	73	77	327	68	160	86	348
49	118	18	283	60	82	87	215	60	149	58	197	89	38	77	327	20	346	32	112
58	187	54	197	63	114	50	312	65	179	75	140	84	220	78	224	7	81	50	140
79	151	83	20	71	182	15	29	66	346	62	173	80	6	23	193	34	244	49	170
54	115	16	185	72	143	6	345	58	218	83	169	89	131	56	221	83	56	64	165
79	136	72	182	68	287	87	205	63	184	35	107	83	210	21	173	45	108	87	354
73	129	76	228	76	105	65	249	61	149	87	178	82	200	89	231	89	109	65	205
33	203	49	163	81	113	55	346	71	163	79	161	63	63	21	118	81	273	73	211
76	237	55	346	71	98	14	195	83	306	84	214	58	148	11	173	83	265	70	197
20	252	46	109	49	121	87	229	83	306	86	341	77	311	14	135	87	156	65	205
12	251	67	7	5	342	36	292	41	44	84	162	89	193	75	132	74	271	63	312
20	324	72	5	87	325	42	350	15	184	51	219	86	199	85	135	89	32	31	239
5	233	85	346	83	147	30	294	7	24	63	220	82	200	46	12	87	6	61	144
62	35	80	166	85	121	62	160	48	197	74	169	55	32	50	213	83	215	38	108
83	208	64	138	58	98	36	321	61	154	84	162	81	73	53	331	39	8	35	169
38	263	90	174	55	342	30	310	84	166	69	136	90	7	52	207	49	142	42	138
76	104	85	354	90	162	30	310	57	70	67	120	85	350	39	213	84	142	47	140
83	270	52	192	90	162	25	295	40	76	69	136	79	24	47	143	65	194	48	153
83	270	79	142	85	342	48	50	64	123	76	105	85	230	46	193	59	73	30	192
26	187	78	152	80	342	12	208	59	114	60	184	60	170	47	143	82	261	65	127
36	159	45	138	85	162	68	353	58	188	55	203	50	170	88	136	84	142	84	307
29	186	87	2	75	162	21	274	63	46	86	138	15	170	23	193	86	11	89	307
35	144	34	104	85	162	26	317	80	186	75	125	50	170	36	168	49	20	84	307
53	28	70	171	90	162	89	28	77	259	84	120	50	170	81	311	84	188	56	127

Veins:

67	21	76	228	75	162	81	232	36	182	84	120	50	170	29	173	53	99	47	200
71	42	75	167	70	162	81	267	53	166	63	114	68	48	84	31	30	10	67	141
20	324	83	302	90	162	80	236	65	237	71	98	32	29	82	134	89	254	47	206
85	327	72	131	70	188	66	69	90	43	24	76	51	229	68	109	86	287	36	178
48	243	35	167	15	162	89	249	71	120	58	98	82	20	54	185	80	249	29	182
48	236	87	305	55	342	81	63	37	258	71	98	83	215	18	200	87	259	21	197
33	203	42	74	33	76	49	142	42	244	78	148	86	200	59	143	18	81	21	198
58	276	63	240	27	67	45	98	34	208	62	146	82	210	61	175	58	143	13	181
72	106	15	167	89	154	59	58	86	4	83	147	76	216	86	281	25	61	10	140
57	58	40	107	75	156	69	85	52	128	51	134	82	211	1	173	67	281	31	153
52	299	34	104	74	134	88	225	67	265	57	124	81	190	29	235	81	295	10	140
58	263	33	122	64	152	74	220	46	160	71	128	76	231	4	353	51	282	19	212
80	152	20	136	65	163	80	335	51	149	48	214	86	235	45	129	62	42	9	140
60	184	24	205	85	343	54	48	67	142	42	77	62	196	9	89	33	29	54	183
28	30	25	167	75	343	65	264	61	154	80	113	59	184	29	111	78	222	87	202
53	355	15	347	50	163	81	76	50	232	44	117	86	200	38	108	76	246	86	235
74	197	18	282	79	133	78	89	43	222	26	103	57	206	75	316	29	1	77	152
38	347	20	198	65	343	52	164	38	209	47	54	78	185	49	149	86	325	67	154
45	100	17	211	75	343	55	122	45	246	68	112	78	185	56	158	49	245	85	147
56	191	15	167	85	163	50	324	77	158	47	84	24	121	59	185	80	117	75	331
69	78	34	202	69	9	37	283	48	266	51	107	82	69	66	319	57	219	83	212
46	81	57	103	56	31	85	31	48	96	86	297	61	178	55	113	58	155	79	39
64	70	89	325	41	33	49	159	49	149	5	163	77	180	58	143	82	101	86	100
64	218	27	103	46	131	39	47	84	240	72	119	45	170	62	125	68	127	24	183
51	219	63	241	51	139	77	201	71	130	49	67	68	243	31	186	18	81	27	18
58	208	66	89	59	1	47	4	69	130	23	237	78	247	36	152	55	280	24	93
68	221	37	88	68	49	79	150	80	43	40	212	55	152	35	141	59	319	73	180
48	204	9	120	49	304	36	6	81	194	63	124	84	221	79	111	77	286	17	192
90	144	44	93	41	157	49	177	78	203	18	304	51	164	57	215	79	280	76	268
81	169	35	66	86	157	88	316	73	194	62	231	43	152	66	204	53	1	79	75
79	152	14	347	76	167	84	130	75	186	27	67	63	132	29	152	87	202	87	186
80	144	38	123	18	103	84	130	43	197	41	96	59	156	83	91	75	122	24	72

Veins:

78	160	4	347	56	139	84	267	69	220	79	133	59	28	54	40	87	202	24	99
54	356	4	347	66	158	82	251	51	157	79	133	81	196	44	6	63	284	68	300
30	244	40	227	47	43	7	132	47	256	51	146	62	5	53	331	28	81	56	143
53	116	9	214	71	167	46	153	67	169	78	148	82	135	3	331	62	261	72	341
39	287	14	347	53	47	48	177	40	178	81	140	45	101	48	345	37	293	5	189
79	152	76	167	88	47	48	168	74	168	85	163	43	332	59	178	40	16	68	170
39	148	50	236	43	54	11	165	52	148	81	140	21	122	67	192	31	20	69	161
34	340	37	89	76	138	59	157	49	150	88	147	49	195	57	151	89	53	71	263
52	113	23	77	75	113	65	143	31	95	67	145	78	340	87	76	65	288	39	116
74	137	23	146	61	133	48	177	60	154	72	143	49	80	86	80	65	110	89	243
57	127	28	220	75	296	76	213	57	145	69	189	38	252	87	72	81	122	65	188
60	144	38	123	75	128	52	181	63	204	62	86	25	302	68	70	80	117	73	202
27	144	24	348	40	131	83	20	24	221	23	89	57	238	83	254	74	213	38	328
73	130	63	109	39	320	52	181	61	180	58	98	47	71	52	198	69	222	76	195
81	120	30	188	24	205	66	150	58	244	71	103	51	75	48	233	78	252	48	225
65	144	20	198	81	157	55	160	51	250	60	101	53	84	83	91	8	81	86	3
83	144	48	271	61	81	16	251	30	111	7	118	80	159	68	67	60	31	70	242
79	152	45	154	64	348	28	186	39	252	22	102	87	346	57	183	78	163	76	220
64	144	56	166	49	63	49	159	25	241	8	35	46	122	65	276	83	214	63	221
68	127	11	168	25	295	77	238	57	253	22	210	62	140	78	182	76	19	86	224
77	125	17	125	66	153	84	286	67	212	44	165	80	150	77	193	87	41	49	332
57	127	46	111	45	127	62	342	72	195	33	87	14	23	58	77	8	81	31	318
39	147	28	105	32	89	78	234	70	204	20	116	89	164	42	160	68	40	37	311
57	127	80	126	51	81	23	337	51	158	45	163	87	357	62	166	10	152	14	314
59	139	39	140	45	125	71	108	73	213	60	185	63	71	28	331	55	231	21	68
60	73	39	132	45	314	82	141	89	213	73	194	89	199	42	143	39	43	15	242
66	189	57	132	49	347	71	44	77	222	80	202	67	67	43	358	89	53	70	162
3	44	39	140	67	141	90	274	34	106	67	195	60	145	21	151	67	91	85	343
66	168	63	123	66	157	86	137	54	173	45	109	85	172	55	175	67	13	53	210
67	165	68	128	48	83	87	133	71	169	74	153	30	73	52	146	88	202	70	156
17	350	77	129	48	200	87	324	80	213	67	145	77	80	65	308	88	202	47	195
11	118	80	144	9	321	89	304	62	284	79	2	20	77	29	151	87	41	85	351

Veins:

20	347	75	158	56	105	78	124	76	259	86	155	26	85	31	182	83	214	84	314
46	13	88	326	58	112	85	131	19	154	57	180	35	92	75	157	8	81	89	333
15	20	27	59	65	101	75	134	51	249	57	148	35	92	77	177	74	40	57	326
24	5	79	322	72	90	86	138	35	247	52	177	81	169	55	166	67	24	63	327
39	20	42	260	79	116	29	93	79	147	64	155	85	162	44	168	79	299	38	115
5	119	87	317	89	95	75	127	61	283	53	189	32	93	44	106	72	243	82	205
13	64	87	307	45	65	82	128	26	218	51	179	89	154	67	157	54	307	9	341
26	67	88	120	71	127	79	115	65	306	55	141	80	136	59	185	8	80	19	232
17	68	78	322	66	128	84	109	62	211	64	155	86	319	31	152	56	58	66	214
10	134	74	321	21	285	72	130	61	273	74	156	88	327	60	191	80	205	72	306
15	139	83	129	71	151	23	33	65	152	73	176	53	111	61	152	58	154	83	109
61	272	85	133	33	323	41	4	64	275	42	141	86	315	31	121	29	359	80	163
12	86	69	145	69	119	67	268	61	254	86	201	88	327	58	170	76	13	80	26
20	36	77	174	75	217	86	145	74	139	63	177	89	154	85	222	13	80	49	219
11	117	87	176	81	293	63	146	40	146	51	146	83	144	67	170	38	80	70	145
38	154	87	12	84	116	28	284	74	268	86	356	64	148	60	191	41	138	72	136
69	173	80	333	40	351	76	357	17	169	90	163	55	56	44	168	67	143	87	136
3	43	81	145	51	194	61	269	80	195	85	159	31	84	79	111	67	12	81	335
69	78	69	130	63	95	5	252	89	5	89	151	13	303	35	176	54	70	72	135
79	177	44	98	55	164	35	174	79	148	82	1	41	146	85	285	53	75	84	113
58	133	63	138	58	173	80	261	82	157	83	178	49	195	46	152	53	108	80	110
43	66	70	146	62	151	72	159	38	172	88	197	32	222	39	142	50	26	72	324
14	85	81	145	45	77	86	237	27	139	79	193	55	189	39	131	83	23	36	259
14	81	87	177	51	109	28	170	39	155	79	193	83	156	32	165	42	112	54	298
5	52	90	311	31	261	62	162	15	168	89	155	48	158	63	181	35	125	14	343
25	48	90	311	42	283	66	151	79	147	67	224	12	123	73	23	56	57	80	126
49	258	85	186	53	323	85	21	43	169	85	159	44	145	54	175	50	67	87	308
70	60	64	112	47	175	41	186	43	237	90	163	77	129	58	178	34	67	76	313
36	78	64	126	46	53	45	191	57	281	65	198	58	90	72	183	67	29	42	207
12	35	82	128	35	294	18	187	66	187	84	154	63	230	75	285	67	29	85	351
46	5	74	143	53	60	41	186	47	210	89	155	81	151	65	204	67	31	60	172
20	11	81	146	28	323	53	214	81	137	58	98	51	140	45	152	74	39	67	197

Veins:

19	40	86	143	38	47	60	114	24	213	15	176	49	142	43	105	75	29	84	301
11	117	74	143	55	90	53	199	43	275	70	216	65	210	30	86	53	108	77	297
59	227	86	309	79	117	50	240	67	89	50	238	47	104	25	152	58	160	75	155
54	185	82	195	9	356	80	64	34	141	23	89	89	48	58	314	74	29	62	149
48	184	81	182	39	93	51	173	57	263	12	307	42	18	25	152	49	19	52	199
46	186	86	134	27	256	64	167	88	166	15	343	59	150	62	306	59	166	46	145
48	172	86	207	34	338	63	146	89	335	66	65	45	130	89	205	77	8	67	193
58	208	74	206	29	308	57	109	31	190	12	307	28	124	54	299	69	164	65	179
45	189	35	193	82	108	67	136	67	213	11	324	59	139	54	152	45	53	44	160
58	208	70	195	11	77	43	109	40	25	26	3	52	148	48	229	13	124	64	119
13	10	84	189	77	314	75	63	76	187	42	43	65	138	14	152	73	335	79	154
43	223	64	185	41	218	59	157	68	132	16	314	86	163	23	103	22	116	79	154
56	212	71	184	23	18	73	145	89	146	16	357	52	148	86	332	25	124	31	132
58	208	71	139	47	113	66	158	27	209	24	62	55	146	48	88	77	157	67	114
40	205	82	137	52	1	87	153	55	273	41	194	72	132	14	152	53	123	72	114
60	99	54	146	36	114	63	147	79	261	34	53	20	66	68	318	67	148	64	327
62	78	74	135	40	352	83	113	48	260	27	33	57	132	59	314	35	126	24	239
0	325	82	129	35	266	28	13	82	214	20	32	63	154	71	312	76	195	58	143
43	30	56	178	9	292	58	11	52	129	71	98	32	181	87	302	75	190	75	117
66	121	68	122	63	176	48	331	80	118	74	122	74	94	14	152	80	287	82	156
42	45	77	161	47	113	45	32	65	257	72	109	86	154	67	299	27	80	89	120
42	53	87	207	38	325	63	98	55	138	76	125	66	150	82	158	86	10	76	9
27	52	82	146	66	130	15	290	69	258	5	343	81	141	76	285	67	7	69	145
40	55	84	335	86	127	69	353	79	261	76	220	64	142	39	152	59	354	69	95
77	121	62	117	64	280	83	199	61	221	88	129	72	135	74	89	86	151	77	354
84	179	56	113	57	266	77	13	36	149	86	351	78	131	61	276	67	29	81	172
10	145	81	316	42	232	43	24	58	155	82	325	73	125	77	167	84	141	67	134
40	125	77	303	55	349	56	278	61	154	87	230	60	110	30	183	60	35	47	114
68	99	67	101	48	261	35	134	70	179	38	195	83	101	67	177	75	18	46	178
78	108	60	144	77	241	71	112	51	60	39	181	71	140	79	302	39	359	47	146
47	175	77	359	23	231	87	74	71	249	74	317	86	329	86	124	67	7	67	150
44	179	70	147	49	275	58	165	56	189	89	140	53	125	90	306	58	143	76	177

Veins:

40	144	89	321	35	267	84	265	85	233	88	170	51	78	75	167	49	142	47	128
52	91	86	328	12	235	83	19	72	205	17	350	73	130	82	313	66	18	65	158
71	104	81	326	30	294	23	254	52	243	87	350	63	154	73	320	87	5	45	157
40	24	73	191	50	226	90	103	66	121	40	95	81	331	88	137	29	358	90	314
50	280	87	225																